Study of Expansion of Solid Helium-4 into Vacuum

Dissertation
zur Erlangung des Doktorgrades
der Naturwissenschaften

vorgelegt beim Fachbereich Physik
der Johann Wolfgang Goethe-Universität
in Frankfurt am Main

von
Manuel Käsz
aus Idstein

Institut für Kernphysik Frankfurt
Frankfurt am Main, im März 2006

(DF1)

vom Fachbereich Physik der
Johann Wolfgang Goethe-Universität als Dissertation angenommen.

Dekan: Prof. Dr. Wolf Aßmus

1. Gutachter: Prof. Dr. Reinhard Dörner

2. Gutachter: Prof. Dr. Giorgio Benedek

Datum der Disputation:

Abstract

This work gives a detailed introduction into a fully new experimental method to investigate the quantum crystal behavior of solid Helium-4. It has been found that a fascinating new effect occurs in the expansion of solid Helium-4 into a vacuum through pinhole orifices with diameters between 1 and 5 μm.

It is observed that the beam flux intensity shows a periodic behavior for source conditions corresponding to the solid phase of Helium-4. The period is in the range of seconds up to minutes. It shows a strong dependence on temperature and source pressure. The oscillating part of the beam flux intensity amounts several percent of the total flux. This new phenomenon has been studied for temperatures between 2.1 K and 1.3 K and pressures up to 30 bar above the melting pressure. The beam flux intensity has been recorded by the vacuum pressure in a pitot vacuum chamber. The jet velocity in the range of 200 m/sec indicates that surprisingly the beam is a liquid jet, whereas the conditions in the source correspond to the solid state. In this work mainly the behavior of the flux modulation has been studied as a function of pressure and temperature and the influence of the isotope Helium-3. Furthermore geometrical aspects such as the influence of the nozzle diameter d_0 have been investigated.

In order to explain this novel phenomenon a kinetic model based on the injection of excess vacancies into the solid is proposed. According to this model the vacancies are generated at a solid/liquid interface. Forced by drift and diffusion they accumulate at some distance from the orifice, leading to the collapse of the solid. With the subsequent re-injection of vacancies the effect repeats and turns out to be periodical. The reproducibility of the time dependent beam flux intensity is demonstrated for a wide range of temperatures and pressures and gives direct access to values such as the temperature and pressure dependence of the vacancy diffusion coefficient D_v in the range of 10^{-5}cm^2/sec, the recombination time of vacancies with interstitials $\tau_r \approx$ 1-20 sec and the vacancy activation energy $\phi_f \approx$ 20 K. The good agreement with former experimental results by Zuev *et al.* [131] confirms the applicability of the theoretical model.

As a result from the kinetic model the vacancy concentration is increased above the equilibrium vacancy concentration, caused by the injection of excess vacancies. Therefore, the most important discovery is the possibility of generating a non-equilibrium quantum solid. The investigation of this non-equilibrium solid leads to the discovery of a fluid-like regime in the solid phase of Helium-4 at temperatures below T = 1.58 K. The result gives a strong indication for the supersolid state, especially because the fluid-like behavior of the solid can be eliminated with smallest concentrations of Helium-3.

Contents

Chapter 1

Introduction and Motivation

Helium is one of the most fascinating elements, at the latest since in 1937 Kapitza discovered the superfluid flow of liquid Helium-4 [71]. The weak Van-der-Waals interaction causes that at low temperatures the quantum character of the lightest noble gas dominates. Helium is the only element that remains liquid down to absolute zero temperature and herewith it solidifies only at pressures of about 25 bars at temperatures $T < 2$ K. The quantum nature of matter also appears in solids and especially in solid Helium. At low enough temperature the particles wavelength is comparable to the interatomic distance which is also the definition for quantum crystals.

The wave character results in a high mobility of the atoms. This mobility is further enhanced by the presence of lattice defects, such as vacant lattice sites (vacancies). Since the vacancy formation energy is of the order of the thermal energy (≈ 6 K) the vacancy concentration turn out to be about 1-2 percent. At low enough temperature the broad wavelength and tunneling turns vacancies into delocalized entities (vacanions) and the thermally activated diffusion process changes into an quantum mechanical process of phonon controlled quantum diffusion [3, 70]. The intriguing mobility of vacancies in solid Helium is reflected in a vacancy diffusion coefficient in the order of 10^{-5} cm^2/sec which is comparable to particles in liquids [102].

This causes that solid Helium-4 as a so called quantum solid also becomes superfluid, has been fist predicted by Andreev and Lifshitz in the late 1960‘s [3]. Recent experiments show that the so called supersolid state might exist below temperatures $T = 230$ mK [75, 76]. The interpretation of these experiments however is highly controversial. A probable reason for the decades of continuous failures of attempts to observe the supersolid state are contaminations of Helium-3 even in lowest concentrations. For example in NMR experiments Helium-3 is used to study the vacancies mobility. On the other hand the careful crystal growth suppresses lattice defects such as dislocations and vacancies which are assumed to be relevant to form the supersolid.

In the present work a completely new route is taken to address the question of the supersolid phase. It started with a discovery by chance. In 2001 Robert E. Grisenti investigated the first cryogenic microjet of liquid Helium-4 by pressing liquid Helium through a microsized orifice into the vacuum. On a momentous day in October it was

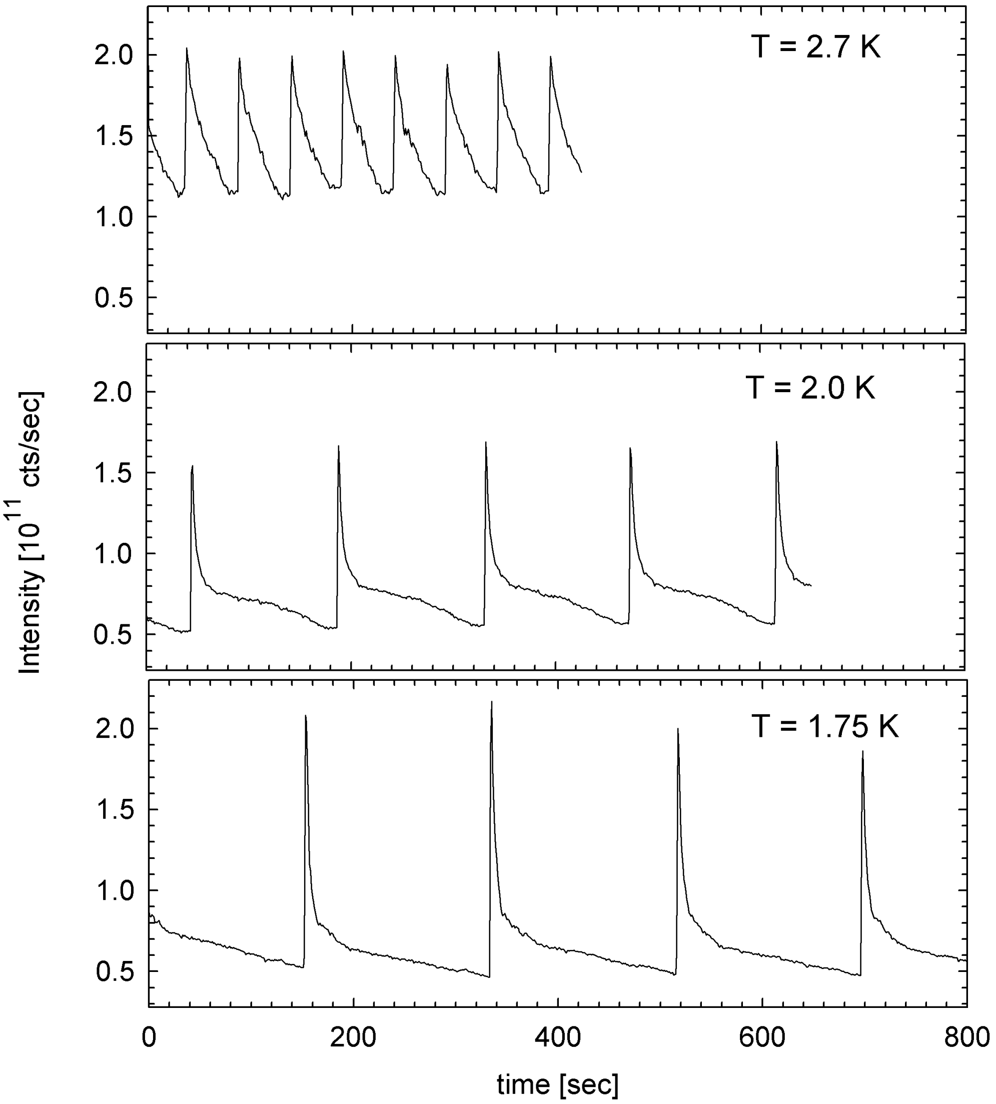

Figure 1.1: The first Geyser oscillations of the beam flux intensity recorded by Grisenti on the day of discovery. The measurements show the time dependent signal at constant source pressure $p_0 \approx 80$ bar and three different temperatures below 2.7 K. The temperature dependence of the period and the change of the periodic curve shape gave the first hint for the discovery of a new physical effect.

at least curiosity that forced him to find out if the orifice freezes up by increasing the pressure in the source tube above the melting pressure.

By observing the vacuum pressure - that is proportional to the beam flux intensity - is was interesting to see that the intensity does not change between the liquid and the solid phase. But it was surprising that suddenly the pressure gauge‘s indicator sometimes dropped down. By measuring the time distance between the drops Grisenti found out that the beam flux intensity oscillates periodically. In figure 1.1 the first oscillations of the beam flux intensity are shown that have been recorded on that day. The period is observed to be in the range of between seconds up to minutes and shows a shape that changes with temperature and pressure. The effect occurs absolute periodically even over hours with an error of below 5 percent, as shown in figure 1.2.

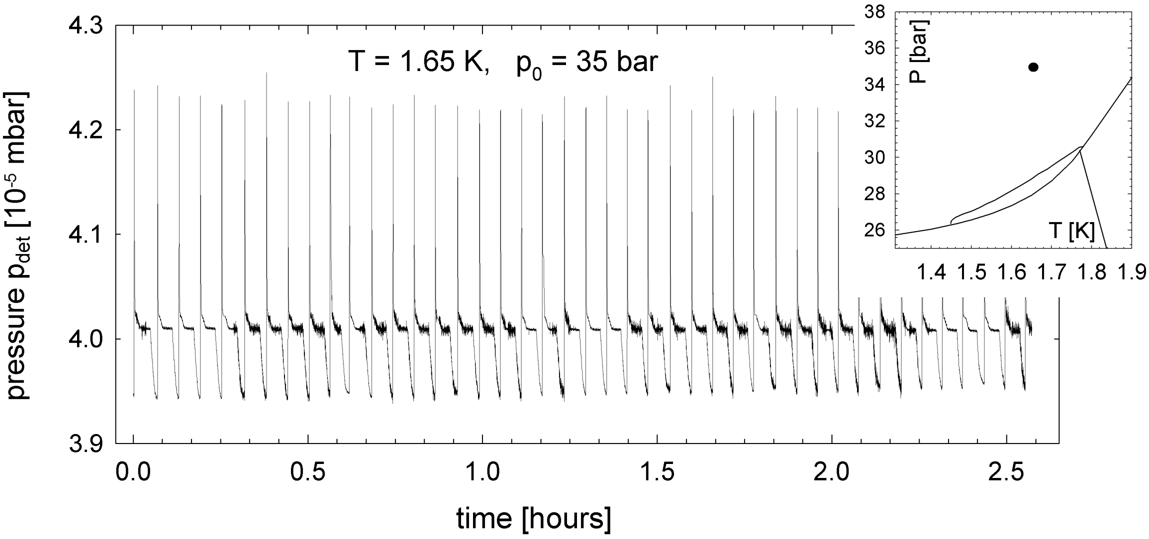

Figure 1.2: Measurement of the vacuum detector pressure p_{det} as a function of time at constant source pressure $p_0 = 35$ bar and constant temperature T = 1.65 Kelvin. The Geyser oscillations of the beam flux intensity occurs absolutely periodically even observed over hours with an average period $\tau = 218 \pm 8$ seconds. The standard deviation is below 4 percent and shows the high accuracy of the periodic effect. Even the curve shape just shows only small deviations.

Seeing the data in a talk of Grisenti it was Franco Dalfovo who suggested that the effect could be related due to vacancies and Giorgio Benedek came up with the idea[1] for a model that explains the oscillations in the beam flux intensity. The next morning the basis was established that explains the oscillations by the injection of vacancies into the solid that leads to a periodic collapse of the crystal. The idea of an oscillatory effect driven by the motion of vacancies which finally cause a collapse of the crystalline structure turns out to be an exciting phenomenon that has to be understood. This early experiment and its tentative explanation layed the ground for the present work

---

[1] Of course! Vacancies!

which gives a systematically study of this Geyser effect and its possible link to the supersolid state.

At the beginning of the work Helium as a solid and its properties as a quantum crystal is presented. Also the aspects of the supersolid state in Helium-4 are illuminated. The oscillations in the beam flux intensity is explained in chapter 3 by the injection of vacancies into the solid at a solid/liquid interface. It will be demonstrated that the periodicity is caused by the collapse of the crystalline structure where the vacancies accumulated. As a final result the mobility of vacancies as a function of time give a theoretical beam flux intensity that reproduces the experimentally observed beam flux intensity. Therefore, the theoretical model gives a direct access to properties of vacancies, like generation and mobility, that has been investigated in several investigations during the last decades [12, 36, 131]. A review of experimental investigations of solid Helium-4 and their results is given in chapter 4.

This work builds the first detailed experimentally investigation of the Geyser effect in solid Helium-4 in a temperature range between 1.3 and 2.1 K and pressures of approximately 30 bars above the melting pressure. The experimental setup for the generation of a cryogenic microjet is explained detailed in chapter 5. The investigation of the period and the curve shape as a function of temperature and source pressure p_0 build the essential element. Furthermore the influence of the isotope Helium-3 and geometry such as the nozzle diameter d_0 is investigated. The experimental results are presented in chapter 6, whereas the detailed analysis of the results is given in chapter 7.

Chapter 2

Introduction to Properties and Specific Features of Solid Helium

Helium as a solid has received much attention from many solid state physicists, because solid Helium is the most fascinating of the so called "quantum crystals". Quantum crystals show some intriguing quantum properties, e.g. extraordinarily increased mobility of atoms. In this introduction Helium as a solid is discussed, explaining the high pressures for solidification and the different crystalline phases in the phase diagram. Furthermore, the introduction discusses solid Helium as a quantum crystal, whereas the terms of quantum crystals and the specific properties are explained first. The quantum properties of solid Helium make it the best candidate to exhibit a new state of matter, the supersolid state. This state was theoretically introduced by Andreev and Lifshitz in 1969 [3]. Ever since, the search for the supersolid state continues. In section 2.4 the theoretical aspect of the supersolid state is presented.

2.1 Solid Helium-4

There are two properties that make Helium remarkable as a solid. As the lightest noble gas, the small atomic mass and the weak Van-der-Vaals binding energy, indicate that the zero-point-motion in liquid and solid Helium is quite high.

In decreasing the temperature Helium at atmospheric pressure remains liquid down to absolute zero temperature, as to be seen in the phase diagram of figure 2.1: At low temperatures Helium becomes solid at pressures of about 25 atmospheres. Solid Helium at low temperatures forms two phases of crystalline order. At temperatures between 1.4 and 1.8 K and pressures close to the melting line Helium forms a bcc[1] crystal structure. At higher pressures solid Helium forms a hcp[2] crystal structure. At higher temperatures $T \approx 15$ K and pressures in the order of magnitude $p = 1000$

---

[1] body-centered cubic

[2] hexagonal closed package

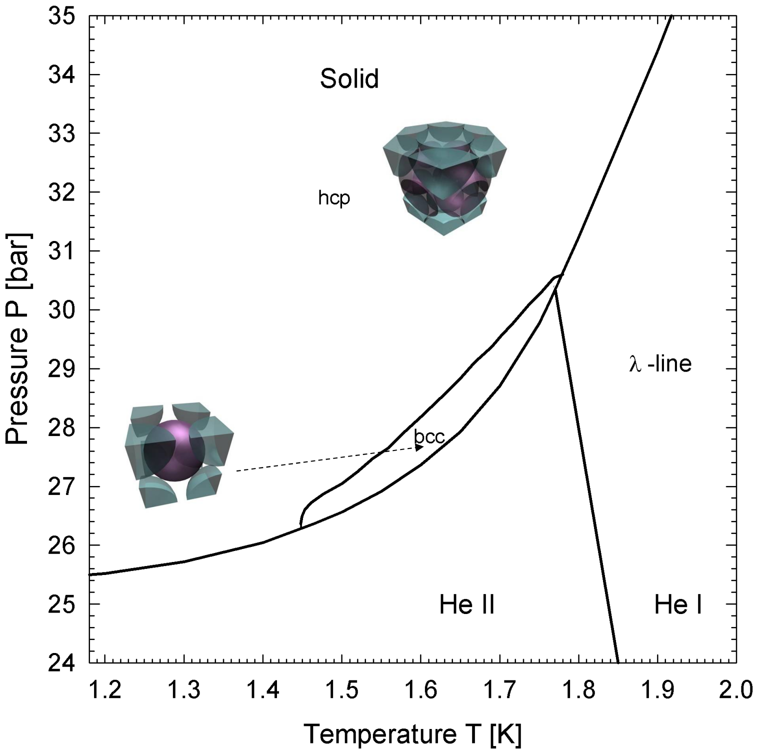

Figure 2.1: Phase diagram of Helium-4:Helium solidifies at pressures above 25 bars. Between temperatures of 1.45 and 1.8 K and pressures close to the melting line solid Helium is bcc ordered. Otherwise the solid assumes a hcp ordered crystal. The inlets showing the bcc and hcp crystals are taken from [28]

atmospheres the third crystalline structure occurs which is fcc[3] ordered (face centered cubic).

The high pressures necessary for solidification is a direct consequence of the high zero-point kinetic energy and the weak Van-der-Waaals interaction. The high kinetic energy is a consequence of the low atomic mass as to be seen by the following arguments [119]. Let V_a be the average atomic volume that is occupied by a single atom in liquid Helium-4, with the radius given by R $\sim$ $V_a^{1/3}$. From the Heisenberg uncertainty principle it follows that the particle has an uncertainty in its momentum $\Delta p \sim h/R$. Thus, the particle zero point energy can be expressed as:

$$E_{kin} = \frac{\Delta p^2}{2m} = \frac{h^2}{2mR^2} = \frac{h^2}{2mV^{2/3}}, \tag{2.1}$$

where m is the particle´s mass. At low pressures the kinetic energy is of the same order as the potential energy. Even though the kinetic energy increases with decreasing

---

[3] face-centered cubic

atomic volume ($E_{kin} \propto 1/V_a^{2/3}$), the potential energy increases much faster (as $E_{pot} \propto V_a^2$ [118]). Therefore, Helium at low temperatures becomes solid at pressures of about 25 atmospheres because with increasing pressure the minimum of the total energy shifts towards smaller atomic volumes and forms a stable lattice.

The high kinetic energy combined with the low potential energy also explains why the small density and the high mobility of Helium atoms in the solid and liquid state that reaches up to the well known superfluid state. Beside the high pressures necessary for solidification the high kinetic energy of Helium causes some more interesting features. This makes Helium to be the most fascinating "quantum crystal".

2.2 Quantum Crystals

In a classical crystal atoms perform vibrations around their strictly defined equilibrium - lattice sites. Thus, crystals are treated as quasi-classical objects. Because of particles belonging to definite lattice sites, and herewith being individualized, the quantum mechanical requirement of indistinguishability for identical particles is not fulfilled [4]. Therefore, the physical properties of most crystals are describable classically.

However, for crystals composed of the light noble gases and molecular Hydrogen the classical description breaks down. The quantum mechanical consideration assigns a broad wavefunction to light particles, like Helium. The overlap of the wavefunction of atoms in neighboring lattice sites allows tunneling of the particles into adjacent lattice sites.

A criterion for such quantum effects in solids is given by the ratio of the amplitude of zero-point vibrations around their lattice site to the lattice parameter. The relative magnitude of quantum-ness in quantum solids is given by the dimensionless parameter of de Boer [32]. The de Boer parameter classifies the so-called quantum crystals by the ratio between the de Broglie wavelength and the lattice parameter $\frac{\lambda_{db}}{a}$ where $\lambda_{dB} = h/p$ is the thermal de Broglie wavelength with momentum $p = \sqrt{2\pi m k_B T}$ and a the interatomic distance. Thus, it follows for the de Boer parameter:

$$\Lambda = \frac{\lambda_{dB}}{a} = \frac{h}{a\sqrt{2\pi m k_B T}}, \tag{2.2}$$

where m is the particle mass, k_B the Boltzmann constant and T the temperature. If the de Broglie wavelength λ is comparable to the interatomic distance a the solid is "highly quantum". From the de Broglie wavelength it follows that the wave character of particles especially enlarges for particles with small mass at low temperatures. Thus, Λ becomes large for the lightest particles with weak interatomic interaction (noble gases) at low temperatures.

The pressure dependence of the parameter Λ comes from the alternative definition of Λ given by Andreev [4], where the de Boer parameter is defined as:

$$\Lambda = \frac{u_0^2}{a^2} = \frac{\hbar}{a}\frac{1}{\sqrt{mE_{pot}}}, \tag{2.3}$$

This definition shows that maximal quantum effects in crystals are expected at low pressures: With increasing pressure the potential energy between two adjacent particles in the lattice (depending on their mutual distance) increases, while the interatomic distance decreases. Finally, Λ changes with the product of $E_{pot}a^2$, so since the energy of interaction of neutral particles (Van-der-Waals potential) changes with the decreasing distance much faster than $1/a^2$, Λ becomes small for higher pressures [4].

The amplitude of the zero point motion in solid Helium is about 30% of the interatomic distance. From the Lindemann melting criterion it follows that a solid should melt if the relation $\langle u\rangle/a \geq 0.1$, where $\langle u\rangle$ is the amplitude of the zero point motion, and a is the interatomic distance. Once more this feature indicates that this kind of solid is not inherently stable [99].

However, as to be seen in the following section, the consequence of the de Boer parameter is the particles mobility inside quantum crystals. Compared to classical crystals the "quantum nature" of atoms in a quantum solid leads to motion by tunneling. The high mobility of particles in a quantum crystal leads to a picture of quantum-mechanically indistinguishability caused by delocalization.

2.2.1 The Role of Vacancies in Quantum Crystals

Inside a crystal the mobility of particles comes from the thermal activation. Classically, point defects in crystals, such as vacancies and impurities, are localized at a definite lattice site that is in the order of the atomic volume. These (quasi-) particles move only occasionally due to a thermally activated diffusion process. Generally, this process occurs if the thermal energy is sufficient to overcome the potential barrier.

In closely packed crystals, e.g. in Helium, tunneling processes and motion via surmounting the potential barrier are difficult because of the absence of enough free volume. It is the reason why vacancies in quantum crystals play a major role: For the motion of atoms it is energetically more favorable to change the lattice site with vacancies than with with neighboring atoms. As a matter of fact, thermally activated motion of atoms in quantum crystals is always due to the existence of thermally acti-

element	Λ
^{3}He	≈ 0.325
^{4}He	≈ 0.282
H_2	≈ 0.17
Ne	≈ 0.061

Table 2.1: Elements with large de Boer parameter [4]

vated vacancies. Vacancies in crystals are always present. This is because the presence of vacancies is due to the increase of entropy. The increase of the entropy occurs because vacancies violate the perfect crystal geometry. The probability for the existence of vacancies even at T = 0 was theoretically proposed by Penrose and Onsaeger in 1956 [96], whereas up till now there has been found no indication for the existence of the so called zero-point-vacancies.

Summarized, one can say that vacancies in quantum solids play a major role because vacancies increase the mobility of particles. As mentioned above, real quantum effects are related to the delocalization of particles, which results in particle mobility. To clarify the importance of vacancies in quantum crystals the following sections will focus on the formation of vacancies and their different kinds of motion.

2.2.2 Vacancy Formation

To create a vacancy a thermally formation energy ϕ_f has to be applied to displace an atom out of its lattice site. The concentration of thermally activated vacancies is given by the Arrhenius expression

$$X_v^0 = exp(-\phi_f/T), \tag{2.4}$$

where ϕ_f is the energy of formation and T is the temperature. In appendix A.1 the exact derivation for the formation energy ϕ_f is presented. The experimental investigation [131, 45] of the formation energy in hcp Helium-4 determined $\phi_f \approx 6 - 8$ K. In the experiment investigated in this work the temperature range is 1.3 K < T < 2.2 K. Thus, the concentration of thermally activated vacancies in this experiment is around $X_v^0 \approx 1 - 2$ percent. For a classical crystal Cu at 1300 K one obtains a vacancy concentration $X_v^0(\text{Cu}) \approx 0.001$ percent at a corresponding formation energy $\phi_f(\text{Cu}) \approx 12000$ K [69].

2.2.3 Motion of Vacancies

Vacancies are able to move in two ways, namely by diffusion and drift. Basically, diffusion of particles is caused by a concentration gradient, whereas drift is a motion driven by a force which is a result of a pressure gradient. In appendix A.2 the process of vacancy motion by diffusion and drift is illustrated more detailed.

Generally, the motion of vacancies by diffusion is associated with a concentration gradient $\Delta X_v^0/\Delta x$. Following the law of Fick [43, 41] one obtains a flux of particles per second through an area [particles/(m^2·sec)]:

$$j_{Diff} = -D_v \frac{\Delta X_v^0}{\Delta x}, \tag{2.5}$$

where D_v means the diffusion coefficient in [m^2/sec], which is related to the vacancies mobility μ by the Einstein relation $D_v = k_B T \mu$. The unit of μ shows the physical meaning of D_v. The mobility μ is defined as the ratio between the vacancies drift velocity u_v and an corresponding applied force F. Thus, D_v is proportional to the vacancy drift velocity u_v. The diffusion coefficient depends on the temperature and on the activation energy ϕ_a:

$$D_v = D_0 \, e^{-\frac{\phi_a}{T}} \tag{2.6}$$

One finds that beside the formation energy ϕ_f an additional energy ϕ_a is necessary for the motion of vacancies. In several experiments, [24, 67, 13, 131] the activation energy ϕ_a of vacancies in solid Helium-4 was determined to be in the range between 15-20 K. The factor D_0 also depends on the temperature and on the activation energy ϕ_a [131]. The corresponding diffusion coefficient was determined to be in the range of 10^{-5} cm^2/sec, which is a value comparable to a liquid.

In quantum crystals the classical process of vacancy diffusion changes at low temperatures. At T $\ll$ T$_\Theta$, where T$_\Theta$ is the Deybe temperature, the process of classical diffusion turns into quantum diffusion. Owing to the large zero-point motion of vacancies tunneling transitions between adjacent lattice sites are expected to occur at significant rates. Defects become delocalized particles, which turn into quasi-particles. They occupy a band of energy states with a band width Δ. The resulting tunneling frequency $\Delta/\hbar$ is in the range of 10^{11} 1/sec. Thus, the mobility of vacancies by diffusion is determined by the energy $\phi_a \pm \Delta$. This quantum diffusion process extremely enhances the mobility of crystal particles. In several studies, e.g. [47], the order of magnitude for the band width Δ in solid Helium-4 was estimated to be $\approx\ 1 - 10$ K.

The process of quantum diffusion occurs with decreasing temperatures, since the de Broglie wavelength increases. With decreasing temperature the diffusion coefficient D_v falls exponentially (classical diffusion). At a certain temperature a minimum of D_v occurs where vacancies are treated as localized defects which obey the process of quantum diffusion. Vacancies are now described as delocalized particles (defectons) [3]. As a result for lowest temperatures the diffusion coefficient increases. Quantum diffusion occurs by the activation of vacancies by phonons [70]

The second mechanism that causes the motion of vacancies is the forced motion by drift. Vacancy motion by drift occurs with the presence of a pressure gradient $\Delta p/\Delta x$. As to be seen in section 3.3.2, vacancies in solid Helium-4 are forced to populate at higher pressures under the influence of a pressure gradient. Vacancy motion by drift will be explained more detailed in section 3.3.2.

2.2.4 Inward Relaxation

As a further effect resulting from the presence of thermal vacancies the crystal properties are affected in such a way that the binding forces between atoms in neighboring lattice sites are lowered. The mechanism is referred to as inward relaxation, as to be seen schematically in figure (figure 2.2). The weak interatomic interaction of noble gas systems affects the repulsion of the neighboring atom caused by the weak atomic binding energy. As to be seen in figure 2.2, the presence of a vacant lattice site increases the particle´s free space and the zero-point oscillation around the equilibrium lattice site broadens. On the one hand the wavefunction of the neighboring atom broadens, and on the other hand the particle is shifted from its equilibrium position towards the vacant lattice site [53]. The increase of the zero-point oscillation causes an increase of the mobility of particles. The weakness of the atomic interaction causes that relative small forces are sufficient to change the crystal structure.

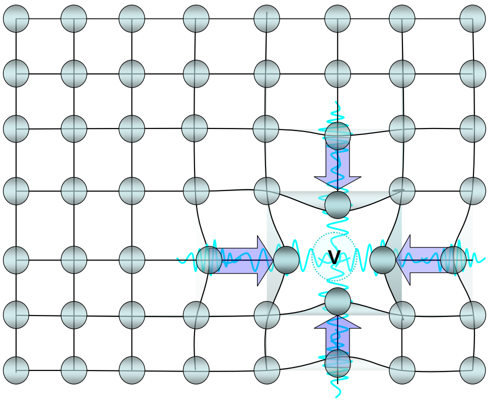

Figure 2.2: Inward relaxation in a crystal. In case of the presence of vacancies the weak atomic interaction of noble gas atoms affects the repulsion of the neighboring atom. Because of the vacant lattice site the zero-point oscillation of atoms around the equilibrium lattice site broadens and the atomic equilibrium lattice site is shifted towards the vacant lattice site.

Deformation of the lattice structure is a quite interesting aspect of quantum crystal systems. Beside plastic deformation, shearing and stress dynamics and compressibility, thermodynamic properties like specific heat belong to the main interesting features of quantum solids.

2.3 Helium as the Most "Quantum" Quantum Crystal

In the small group of quantum crystals Helium is considered to be the most adequate candidate to observe quantum phenomena. This is due to the vacancies formation energy $\phi_f \approx$ 6-8K and activation energy $\phi_a \approx$ 15-20 K which - in the case of solid Helium - are in the range of corresponding temperature T = 1-2 K. Additionally, effort was the investigation of the fundamental properties of quantum solids with smaller de Boer parameter. As to be seen in table 2.1 the most "quantum" element with de Boer parameter smaller than Helium is solid Hydrogen ($\Lambda \approx 0.17$). Experimental results by Zhou *et al.* [130] and Ebner et [39] . al determined the vacancy formation energy to be in the range of $\phi_a \approx$ 91-112 K at temperatures T $\approx$ 10 K. Compared to results obtained for solid Helium, the vacancy concentration of H_2 at T $\approx$ 10 K turns out to be two orders of magnitude below the concentration of thermal vacancies in Helium-4.

The diffusion coefficient D_v of solid Hydrogen was determined to be between $2{\cdot}10^{-6}$ and $1.9 \cdot 10^{-8}$ cm^2/sec [39, 130], which is between one and three orders of magnitude below D_v obtained for Helium. The results for ϕ_a and D_v show that Hydrogen as the element with the second highest de Boer parameter Λ offers a much weaker quantum nature than solid Helium. In table 2.2 experimental results for ϕ_f, X_v^0, ϕ_a and D_v [cm^2/sec] of some quantum crystals with large de Boer parameter are summarized. The data show that the quantum-ness of solid Neon and Argon is much weaker than of Hydrogen. On the one hand this behavior is represented in the thermal equilibrium concentration of vacancies, which is up to five orders of magnitude below the concentration of vacancies. On the other hand, comparing D_v of Helium and Argon the diffusion coefficient D_v drops down even seven orders of magnitude, which is proportional to the vacancies drift velocity. Thus, vacancies in solid Helium move almost 10^7 times faster than in solid Argon.

2.4 Supersolid State of Helium

In 1969 Andreev and Lifshitz [3] proposed a possible new state of matter that should occur in quantum crystals: the “supersolid state“. This new kind of state should show some intriguing features, e.g. a liquid-like behavior of the solid.

The main idea was that the supersolid is a coexistence of a normal solid and a superfluid fraction. The superfluid fraction is a Bose-Einstein condensate of defects, namely vacancies. Since Helium-4 is a boson, the corresponding vacancy is also a boson [17]. Thus, vacancies obey the Bose-Einstein distribution, given by:

$$N_k = \frac{1}{exp(\frac{\epsilon_k - \mu}{k_B T}) - 1}, \tag{2.7}$$

where N_k is the number of particles in each energy state k. Acting as bosons, vacancy

element	Λ	ϕ_f [K]	X_v^0 [%]	ϕ_a [K]	D_v [cm^2/sec]
Helium-4	$\approx$ 0.282	$\approx$ 6-8	$\approx$ 1-2	$\approx$ 15-20	$\approx 10^{-5}$
H_2	$\approx$ 0.17	$\approx 100 \pm 10$	$\approx 5 \cdot 10^{-2}$	$\approx$ 100	$\approx 10^{-6} - 10^{-8}$
Ne	$\approx$0.061	$\approx 239 \pm 10$	$\approx 7 \cdot 10^{-5}$	$\approx 477 \pm 15$	$\approx 8.2 \cdot 10^{-10}$
Ar	$\approx$ 0.019	$\approx 900 \pm 180$	$< 2.5 \cdot 10^{-4}$	$\approx$ 1810-1980 $\pm$ 80	$\approx 4 \cdot 10^{-12}$

Table 2.2: Overview of the vacancies formation energy ϕ_f, activation energy ϕ_a, the equilibrium concentration X_v^0 and the diffusion coefficient D_v for the elements with maximum de Boer parameter. The values for Ne (at T = 25 K) and Ar (at T = 75 K) are taken from [114, 90], except the value of X_v^0(Ar), which is taken from [111]

quasi-particles form at low temperatures a weakly interacting Bose gas. The de Broglie wavelength depends on temperature as follows:

$$\lambda_{db} = \sqrt{\frac{2\pi\hbar^2}{mk_BT}}. \tag{2.8}$$

With decreasing temperature λ_{dB} is of the order of the interatomic spacing. Thus, the particles condense into the lowest energy state. Generally, the temperature for the condensation is given by [42]:

$$T_{BEC} = \frac{2\pi\hbar^2}{mk_B}\left(\frac{N}{2.612 \cdot V}\right)^{2/3} \tag{2.9}$$

At a given atomic volume $V_a \approx 3.5 \cdot 10^{-23}$ cm^{-3} [131] and the vacancy mass obtained by Galli and Reatto [48] to be about 0.35 Helium-4 masses the critical temperature for BEC in solid Helium is approximated to be T$_{BEC}$ $\approx 10.9 \cdot (X_v^0)^{2/3}$. Thus, for a equilibrium vacancy concentration $X_v^0 \approx$ 1-2 percent T$_{BEC}$ is in the order of 1 Kelvin.

At temperatures T $\ll$ T$_{BEC}$ one has Bose-Einstein condensation of the defects with $N_0/N > 0$, where N_0 is the number of particles in the ground state and N the number of all particles. With decreasing temperature the defects accumulate in the ground state and the number of particles N_0 forming the BEC increases. Thus, all particles fall into one single-state k = 0, and the absolute number $N_{k=0}$ becomes equal to the number of all particles N.

This new state would lead to a coexistence of long-range crystalline order and superfluid. Forming Bose-Einstein-condensation each single vacancy has the same wavefunction because the particles motion is absolutely correlated.

As described in section 2.2.4 the presence of vacancies in a crystal lattice affects the neighboring atoms. Thus, the potential barrier becomes smaller. If the number of vacancies in a crystal lattice increases the potential barrier decreases in that way that all vacancies become completely delocalized. Thus, they move freely and frictionless through the crystal. The condition for a supersolid is satisfied when a defect is not localized at any specific lattice site but in a macroscopic region. The superlattice should become unstable and should possess properties according to a liquid. The fraction, which is the Bose-Einstein condensate of defects, is a superfluid in which the vacancies move without any resistance. Together, this superfluid fraction and the "normalsolid" build the two phase system. Together they appear as an ideal fluid.

Therefore, this new kind of state requires defects. In the past the general assumption was that maybe the vacancy equilibrium concentration is too low to observe this kind of state in solid Helium. This is surely the reason why the existence of the supersolid state has yet not been proven at all. Several experiments were proposed to observe the supersolid state. In section 4.3 the different kinds of experiments and their results are presented.

Chapter 3

The Geyser Effect in Solid Helium: A Theoretical Model

In this experiment Helium-4 at pressures and temperatures according to the solid phase was expanded into vacuum through a pinhole orifice of diameter 1-5 μm. Figure 3.1 shows the vacuum detector pressure p_{det} as a function of time for different source pressures and temperatures, that are indicated in the phase diagram. The time dependent pressure p_{det} shows that approximately 1.5 - 10 percent of the beam flux intensity oscillates periodically with a definite period τ_0 in the range of seconds up to several minutes. According to this the pressure p_{det} is separated into an oscillating part p_{det}^{osc} and a background pressure $p_{det,bg}$. The separation is indicated in figure 3.1 by the dashed line in (1).

The theoretical model that is introduced in this chapter explaines the origin of the oscillations in the beam flux intensity under the assumption of the generation of excess[1] vacancies. The process of vacancy generation will be explained first. The theoretical model is separated into the explanation of the oscillatory beam flux and the background signal $p_{det,bg}$.

3.1 Generation of Excess Vacancies

The observed jet flow velocity in the range of 10^2 m/sec indicates that the Helium jet is a liquid beam. The jet velocity u_{exit} is given by

$$u_{exit} = \sqrt{\frac{2p_0}{\rho}}, \tag{3.1}$$

where ρ is the density of liquid Helium. Whereas in this experiment the jet‘s velocity

---

[1] The expression "excess vacancies" comes from the physics of semiconductors. It describes the injection of additional vacancies into the system.

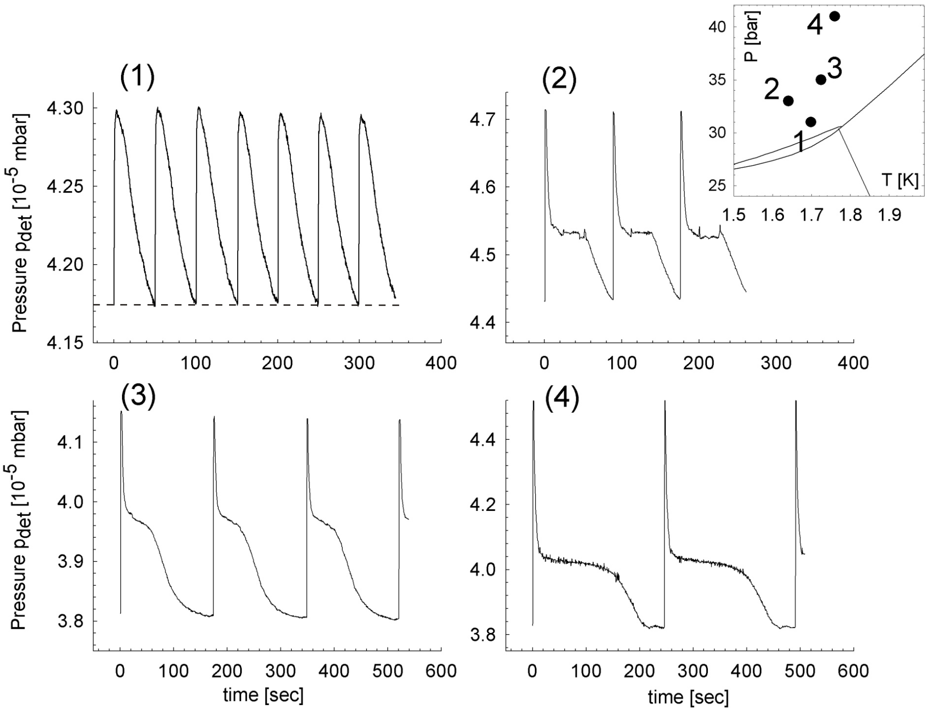

Figure 3.1: Beam flux intensity expressed by the detector pressure p_{det} as a function of time. The beam flux intensity oscillates periodically with a definite period τ_0 in the range of seconds up to several minutes, depending on source pressure and temperature. The inset shows the phase diagram of Helium-4. The points 1-4 indicate the corresponding source pressures p_0 and temperatures T at which the periodic beam flux was investigated. (nozzle diameter: (1) $d_0(\#22) = 2.2$ μm, (2) $d_0(\#20) = 2.07$ μm, (3,4) $d_0(\#17) = 2.28$ μm)

u_{exit} is determined as a function of the vacuum detector pressure p_{det}, as to be seen in section 7.5.

As a result inside the source tube the solid has to become liquid. According to this there must be a solid/liquid interface close to the nozzle, where the pressure corresponds to the melting pressure p_m(T). As to be seen, the decrease of the source pressure p_0 down to p_m is a direct consequence of the generation of excess vacancies. Generally, a thermal activated atom generates a vacancy by jumping out of its former lattice site. The activated atom covers a distance that is given by the mean free path length λ. The direction of the jump is statistically distributed in all directions. For atoms that are close to the solid/liquid interface ($< \lambda/2$) the transition from the solid to the liquid phase is possible.

In figure 3.2 the procedure is illustrated how atoms are crossing the solid/liquid interface due to jumps from the solid into the liquid phase. Atoms that overcome the solid/liquid interface generate a vacancy. Therefore, the interface acts as a source for excess vacancies. The vacancies are generated at a net rate τ_s^{-1} within a surface layer

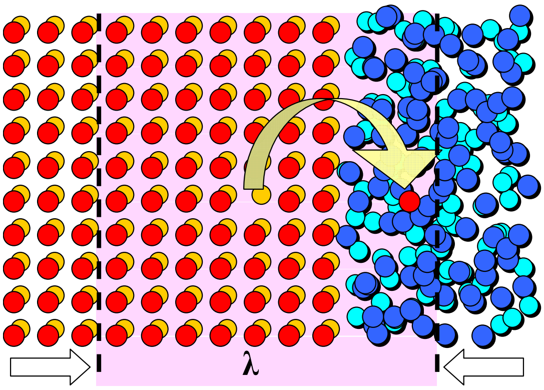

Figure 3.2: Thermally activated atom jumps from solid to liquid phase by leaving a vacancy at its former lattice site. The surface layer thickness λ describes the average mean free path lenght statistically distributed in all directions.

thickness λ that leads to a vacancy surface generation velocity $u_s = \lambda\tau_s^{-1}$. The surface layer thickness λ is shown in figure 3.2. By recombination of atoms returning from the liquid phase and sweeping due to an inward pressure gradient in the region of λ the surface generation velocity reaches equilibrium in a stationary state. Because of the high recombination close to the solid/liquid interface λ gives also the surface depletion layer thickness.

From A.1 it follows that the generation of excess vacancies at the interface strongly depends on the temperature. In entering the liquid phase the atoms are separated from the vacancies. As to be seen in the following sections 3.3.1 and 3.3.2, the vacancies are grasped away from the interface under the influence of a strong pressure gradient and diffusional distribution.

Thermal activated atoms recombine with vacancies after a certain time τ_r. Thus, in thermal equilibrium the rate of vacancy generation and recombination is equal. In this model the velocity of vacancy generation reaches a stationary regime because of recombination with atoms that return from the liquid phase, whereas most atoms leave the nozzle and herewith produce the liquid jet This causes that the recombination time τ_r conspicuously increases, because most interstitial atoms[2] - treated as recombination centers - follow the main flow into the direction of the orifice and support the liquid beam. Additionally, the generation of excess vacancies causes an increase of the vacancy concentration. Thus, the increase of the recombination time τ_r is also a result of the higher vacancy concentration, that will be calculated in section 3.3.4. The increase of the concentration is approximated to be one order of magnitude above the equilibrium concentration. Each vacant lattice site remains much longer vacant because the number of interstitial atoms is much smaler than in equilibrium condition.

---

[2] Interstitial atoms are a defect of the crystal geometry because they do not belong to a definite lattice site and are placed in between

Both effects, the increase of the vacancy concentration and the separation from interstitials cause an increase of the average vacancy lifetime. As to be seen in the following sections the increase of the vacancy concentration is responsible for the background flow and for the oscillatory behavior.

3.2 Melting Process and Background Flow

The explanation for the liquid beam flow through the nozzle is given by a melting process that is caused by the generation of vacancies. The high concentration of vacancies decreases the density of the solid which is related to a decrease of the pressure. This mechanism is presented is this section. Additionally the meaning of the background pressure $p_{det,bg}$ is discussed.

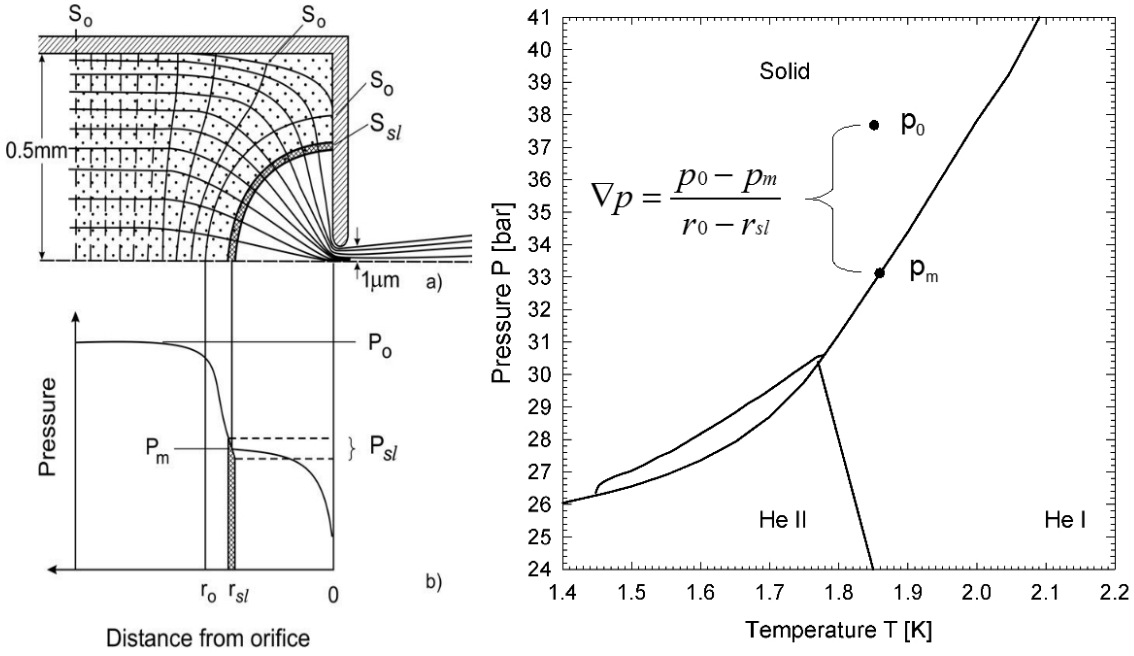

Figure 3.3: Inside the source tube the Helium is solid. Except near the orifice the solid liquifies, where the pressure drops down to almost zero. The lines indicate that the solid cross section S_0 inside the source tube shrinks to the cross section at the solid/liquid interface S_{sl}. The pressure p_0 drops down to p_m caused by dislocation climbing and plastic flow. According to Bernoulli the pressure decreases. The drop of the source pressure indicates a strong pressure gradient inside the system. The phase diagram on the right side shows a representation of the melting pressure p_m at S_{sl} and the pressure p_0 in the solid at S_0. The pressure drop indicates the existence of a pressure gradient close to the nozzle.

In figure 3.3 (left) the schematic of the nozzle head is shown. Inside the source tube the Helium is solid, except close to the orifice it liquifies. The lines indicate that the cross sections S_0, that are isobares with $p = p_0$, inside the source tube shrinks to the cross section at the solid/liquid interface S_{sl}, where the pressure is approximately the melting pressure.

Below the schematic drawing of the nozzle head the pressure is shown as a function of the distance to the orifice. Inside the bulk solid the pressure corresponds to the source pressure p_0. At some distance r_0 from the nozzle exit the pressure drops down from p_0 to p_m. Inside the liquid phase the pressure drops down again according to the Laplace pressure $p_{Lap} = 2\sigma/d_0$. The Laplace pressure gives the pressure inside the liquid filament that results out of the surface tension of the liquid. For $d_0 = 2\mu$m and T = 2 K one obtains for the Laplace pressure $p_{Lap} \approx 3$ mbar.

The constriction of the cross section S_0 is caused by the vacancy motion inside the bulk solid: Atoms move in the direction of the orifice, whereas vacancies propagate into the opposite direction, driven by diffusion and drift. As a consequence vacancies and atoms recombine at edge dislocations and grain boundaries[3].

In figure 3.5 the change of the crystal structure is shown. The recombination of atoms and vacancies at point <R> causes that whole lattice planes are vanishing and the cross section shrinks. This mechanism is known as dislocation climbing. The number atoms that leave the orifice and produce the background pressure $p_{det,bg}$ is assumed to be equal to the number of vacancies that recombine with atoms in the bulk solid Helium to narrow the cross section S_0 down to S_{sl}. These vacancies cause the constant background flow that makes approximately 80 percent of the entire beam flux. Especially near the solid/liquid interface the presence of vacancies causes a decrease

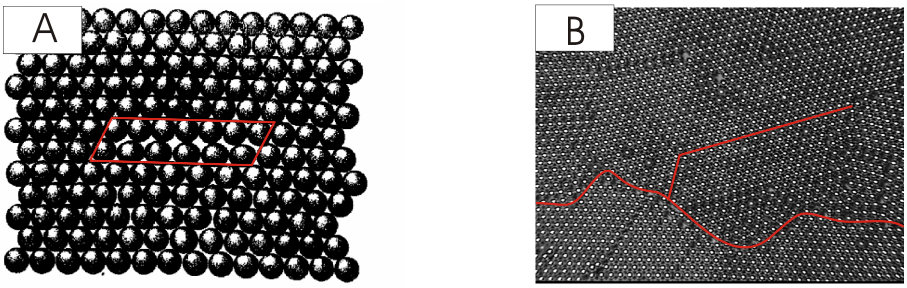

Figure 3.4: Illustration of edge dislocations (A) [40] and grain boundaries (B) [34]. This kind of defect is regarded as the insertion (or removal) of an extra half plane of atoms in the crystal structure. A grain boundary is a defect that separates regions of different crystalline orientations (grains) within a polycrystalline solid [33].

---

[3] In figure 3.4 the defect of the crystal structure is shown, that is caused by Edge dislocations and grain boundaries. Edge dislocations belong to the so called "line defects" of crystalline structures. This kind of defect is regarded as the insertion (or removal) of an extra half plane of atoms in the crystal structure. Grain boundaries are defects of lattice planes. A grain boundary is a defect that separates regions of different crystalline orientations (grains) within a polycrystalline solid [33].

of the density because of inward relaxation and the pressure drops down from p_0 to p_m. To summarize the facts: The model assumes that the high concentration of excess vacancies causes the melting process.

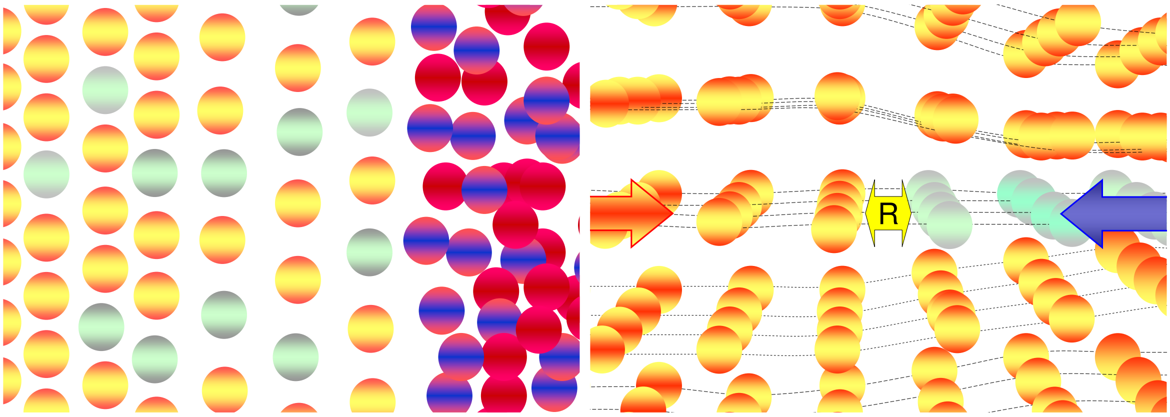

Figure 3.5: Distribution of atoms and vacancies at the solid/liquid interface. The yellow particles indicate atoms, whereas the turqoise particles stand for vacancies. Especially near the solid/liquid interface the presence of vacancies causes a decrease of the density because of inward relaxation. The decrease of the density causes that the pressure drops down from p_0 to p_m. The picture below illustrates dislocation climbing near the solid/liquid interface [34]. Vacancies move from the interface (blue arrow) and recombine with atoms of lattice planes comming from the left (red arrow). At position <R> vacancies and atoms recombine. The whole lattice plane disappears. As a result the cross section shrinks from S_0 down to S_{sl}

The shrinking of the cross section is just possible because in solid Helium the deformation of the crystal is relatively easy. This is related to the weak interatomic binding forces. Under the influence of an external force whole lattice planes are able to slip on each other. This effect is known as "plastic slip motion". Thus, the solid can easily be deformed (plastic deformation). Under continuing external influence the crystal changes its structure permanently. The solid is able to creep. This kind of motion is called "plastic flow" . The effect of plastic flow in Helium is meanwhile well known [99, 117]. Both, the process of plastic flow and the mechanism of dislocation climbing by the presence of excess vacancies allows the constriction of the solid.

3.3 Periodic Pulses

The oscillations showed in figure 3.1 and 3.6 start with a sharp peak at time t = 0 and subsides after a few seconds. The period τ_0 has an accuracy of between 1 and 5 percent, even over hours (figure 1.2). Two main parameters affect the period τ_0 and the curve shape: the source pressure p_0 and temperature T_0. This behavior is investigated in this work. In this theoretical model these oscillations in the beam intensity - the so called "Geyser effect" - are a direct consequence of the injection of excess vacancies into the solid.

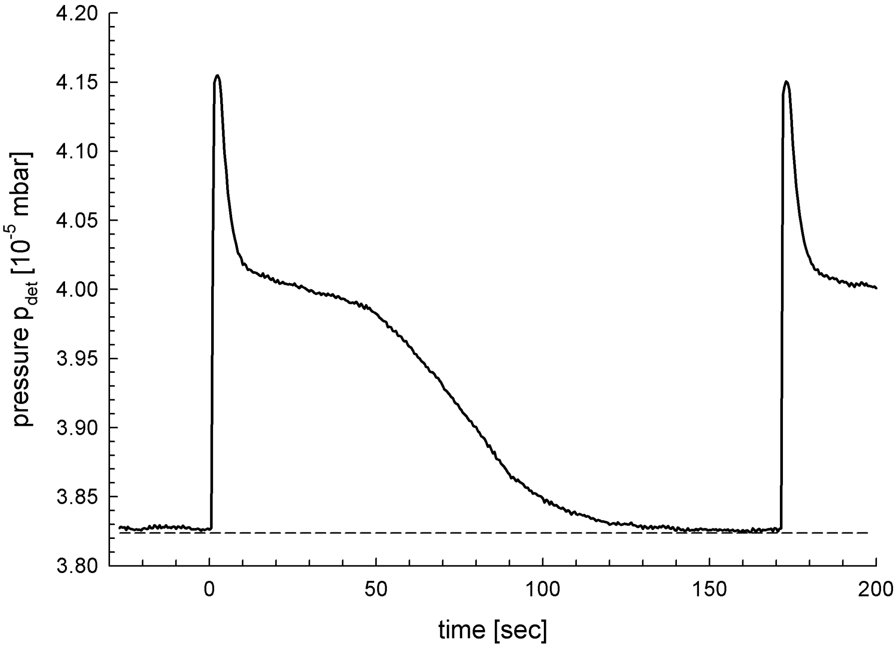

Figure 3.6: Oscillations of the pressure inside the vaccum detector chamber p_{det} at 35 bar and T = 1.725 K. After the sharp peak at t = 0 seconds an attenuated part follows . The period is about 173 seconds. It varies in the range of 1-5 percent. The curve shape strongly depends on the source pressure p_0 and the temperature T_0. The dashed line at $3.83 \cdot 10^{-5}$ mbar is a guide to the eye and marks the separation between the oscillatory part and the background flow. According to the pressure at the top of the peak in relation to the background pressure the oscialltory part is about ≈ 8 percent of the entire flux. (nozzle diameter: $d_0(\#17) = 2.28\ \mu$m)

As mentioned in the previous section the main fraction of excess vacancies recombines with lattice planes. The high concentration of excess vacancies is the reason for the pressure drop and the melting process. A small fraction of vacancies do not recombine with interstitials. These vacancies move freely through the crystal. As a direct result the concentration of vacancies in the bulk solid is increased. The concentration of the excess vacanies X_v^c is about a factor two larger than the equilibrium vacancy concentration X_v^0 .

The periodic behavior results from an interplay of dynamical processes which are vacancy motion, vacancy generation and recombination. In the following these different behaviors of vacancies are described. Finally these three features will be combined.

To demonstrate the model the following sections show time dependent simulations of the vacancy distribution in the nozzle head. In these simulations the distribution of vacancies follows the equations of diffusion and drift, but the model does not represent the original experimental dimensions. For this illustration the following model is

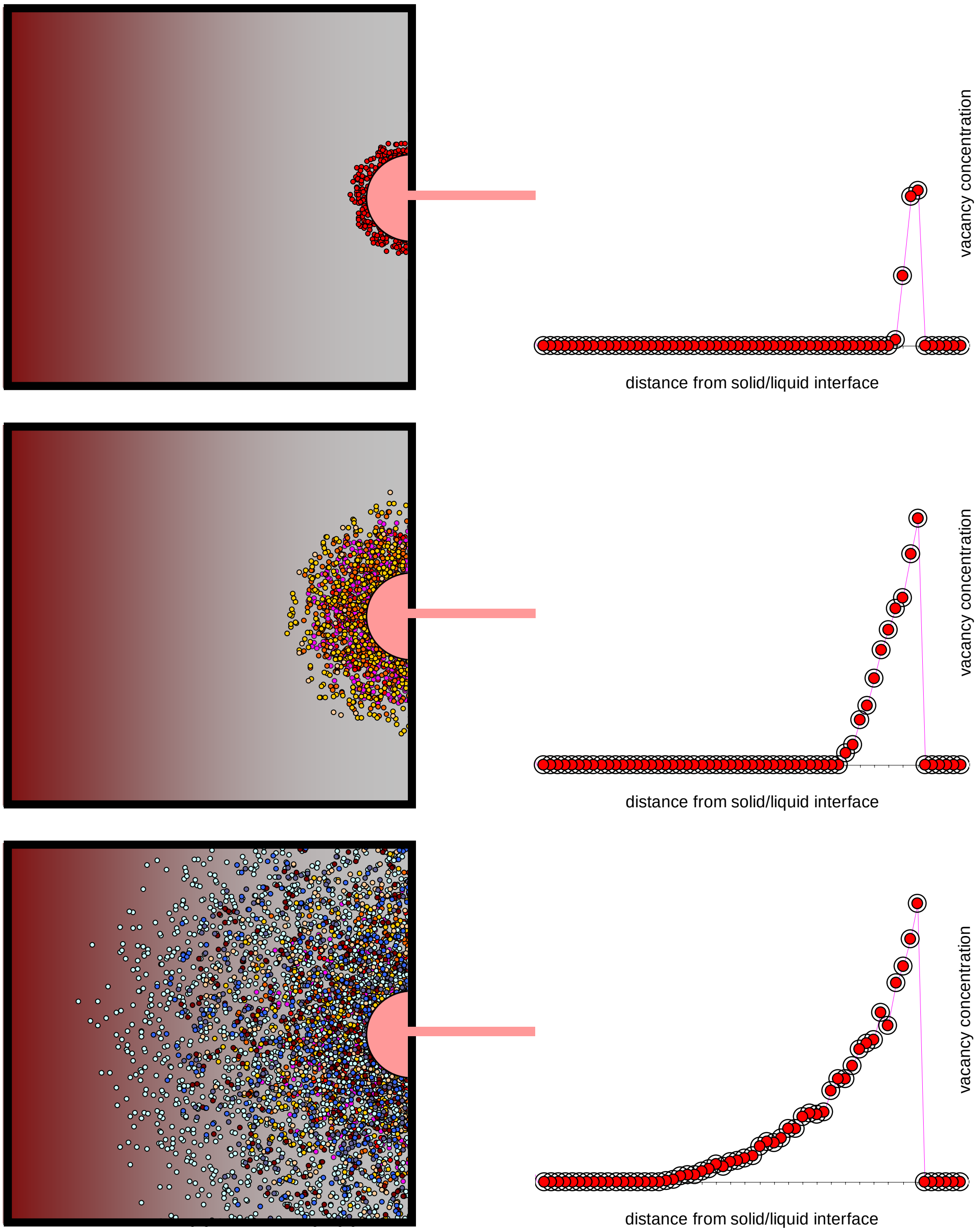

Figure 3.7: Simulation of the distribution of vacancies that move under the influence of diffusion in a non-uniform concentration gradient. On the right side the concentration profile is shown as a function of the distance to the solid/liquid interface. On the top at time t = 0 the vacancy generation at the solid/liquid interface is shown. Here the vacancies build a concentration gradient corresponding to a step function. Later the vacancies move under the laws of non-steady-state diffusion inside the bulk Helium. On the bottom the vacancies are distributed through the crystal. Their concentration increased continuously.

restricted to two dimensions. The behavior of diffusion (fig. 3.7) and drift (fig. 3.8) is shown for three different times, respectively. These times correspond to the beginning and the end of one periodic pulse and one optional time between. In figures 3.10 and 3.11 the simulation of drift and diffusion is summarized. This vacancy distribution is shown for five different times, to make the origin of the periodicity more clearly. All examinations start at a time t = 0, directly after the peak in the periodic signal has occured. The time unit is an arbitrary unit. Additionally to the vacancies distribution the concentration of vacancies is shown as a function of distance to the solid/liquid interface.

First, the distribution of the vacancies under the influence of non-steady-state diffusion is shown. Then the distibution is shown under the influence of drift. Finally, the vacancy distribution is shown as a combination of drift and diffusion.

3.3.1 Diffusion of Vacancies

The process of vacancy diffusion was already discussed in chapter 2.2.3. Thus, the results are just applicated to the present model. The diffusion process of vacancies is caused by a concentration gradient. When the diffusion process begins the concentration as a function of a certain distance build a step function at the solid/liquid interface, as shown in appendix A.2 in figure A.3 and A.2. The time dependent vacancy distribution is given by the second law of Fick [43, 41], which describes a non-steady-state diffusion[4] process:

$$\frac{\partial x_v}{\partial t} = D_v \frac{\partial^2 x_v}{\partial r^2}. \tag{3.2}$$

The vacancy flux is determined by:

$$j_{Diff}(t) = -D_v x_v'(r_{sl}, t), \tag{3.3}$$

where x_v' is the space derivative of the vacancy concentration. At the top of figure 3.7 the simulation of the distribution of vacancies in the nozzle head is shown. The figure shows the vacancy distribution for three different times, corresponding to the beginning (top) , the end (bottom) of the period and one time in between(middle). Additionally, for each time the vacancy concentration is shown as a function of the distance to the solid/liquid interface. According to the dynamic of non-steady-state diffusion the vacancies move inside the bulk Helium as seen in the middle of figure 3.7 and later at a time corresponding to the end of a period. Their concentration increases continuously with time because of the steady generation of vacancies. For each time shown in figure 3.7 the vacancy concentration profile corresponds to classical diffusion related to the second law of Fick.

---

[4] The non-steady-state diffusion describes processes in which the concentration of particles is not constant with time. In this model the non-steady-state diffusion is related to the steady generation of excess vacancies.

3.3.2 Drift of Vacancies

Generally, drift occurs if particles move under the influence of an external force. In the present model this force is given by the strong pressure gradient ∇p, that appears between the cross section S_{sl} and the bulk solid at cross section S_0 where the pressure corresponds to the source pressure p_0, as seen in figure 3.3. In this model the pressure gradient ∇p is assumed to be linear, except in the region of the cross section S_0, as shown in figure 3.3.

In figure 3.3 the phase diagram is also displayed, in which the melting pressure p_m and the source pressure p_0 are shown. Corresponding to the pressure dropdown over a certain distance $l = r_0 - r_{sl}$, the linear pressure gradient ∇p is given by:

$$\nabla p = \frac{p_0 - p_m}{r_0 - r_{sl}} \tag{3.4}$$

This pressure gradient ∇p forces the vacancies to move into the bulk solid Helium. The force is given by [9]:

$$F = -(V^* - V_a)\nabla p, \tag{3.5}$$

where $V_a = 34$ Å^3 is the atomic volume of Helium-4 and $V^* = 0.45\ V_a$ is the isobaric vacancy formation volume [37]. This force that pushes vacancies towards a higher stress has been introduced by Herring in the theory of diffusional creep in polycrystalline materials [68]. This mechanism is known as the "Nabarro-Herring" mechanism. The migration of vacancies climbing a stress gradient is a basic mechanism of the diffusively creep in materials. The Nabarro-Herring mechanism can be applied to the present case because the mobility of vacancies in the high temperature regime that Nabarro‘s experiments were concerned with is comparable to the mobility of vacancies in solid Helium. In solid Helium, at not too high pressure, the mobility of vacancies is orders of magnitude larger than in ordinary solids and is the main reason for plastic deformation even at 1.5 K. Because of their inward relaxation vacancies accumulate in the region of high pressures. The drift flux for vacancies occurs according to:

$$j_{Drift} = u_v x_v(0,t) = -(\mu_v \Delta V \nabla p) \cdot x_v(0,t), \tag{3.6}$$

where u_v is the vacancy drift velocity [cm/s], ΔV is the vacancy volume. The vacancies are forced to move in the same direction as if they are forced to move by diffusion .

In figure 3.8 the drift motion is illustrated for three arbitrary times. Starting at time t = 0 the vacancies are generated at the solid/liquid interface. This situation corresponds to the same conditions at t = 0 as if the vacancies move under the influence of diffusion. At t = 0 the vacancy concentration profile corresponds to a step function.

After a certain time the vacancies move inside the bulk solid Helium under the influence of the pressure gradient, as seen in figure 3.8 (mid). On the right of figure figure 3.8 the vacancy concentration profile illustrates the vacancy density distribution inside

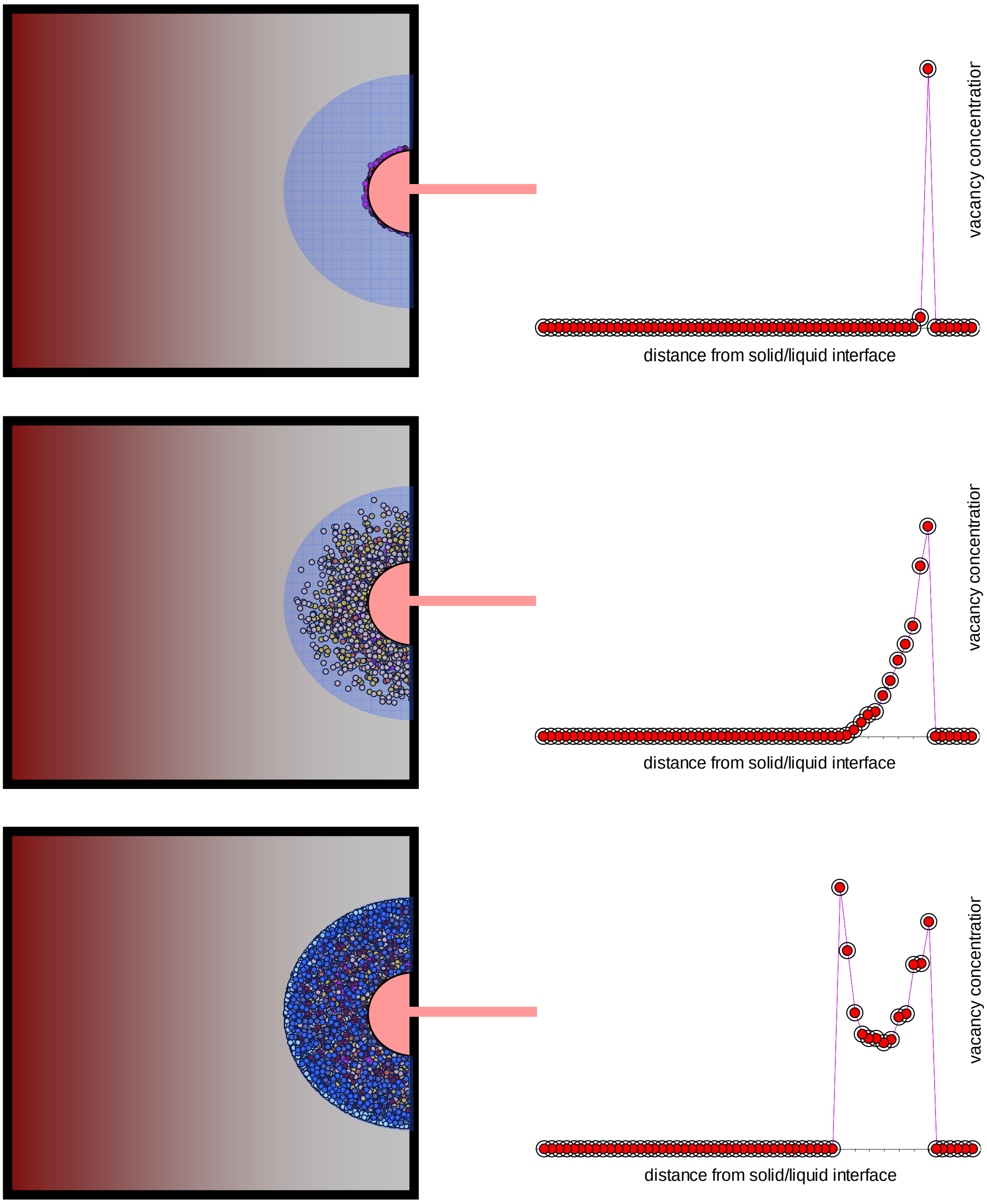

Figure 3.8: Simulation of the drift of vacancies in a uniform pressure gradient. At t = 0 the vacancies are generated at the solid/liquid interface. This situation corresponds to the behavior at t = 0 when the vacancies move under the influence of diffusion. The outer edge of the blue half-circle remarks the source pressure p_0. At this ring the vacancies start to accumulate because the pressure gradient vanishes.

the solid. The vacancy concentration decreases linearly from the top margin at the solid/liquid interface down to zero. The vacancies stop moving if they reach the region where the pressure is equal to the source pressure p_0. The outer edge of the blue half-circle marks the cross section S_0 that corresponds to the source pressure p_0. At a certain distance from the interface the vacancies start to accumulate because the pressure gradient vanishes and the force F is zero. At the solid cross section S_0 the vacancy concentration increases rapidly and the simulation indicates that x_v^c is even higher than at the solid/liquid interface. As to be seen in the following section, the rapidly increase of the vacancy concentration at S_0 is responsible for the periodic effect.

3.3.3 Theoretical Explanation for the Geyser Effect

In this section the influence of drift and diffusion will be combined to obtain a model that explains the oscillations in the beam flux intensity. To complete the model the remaining processes are the vacancy generation and annihilation caused by recombination with interstitial atoms. The vacancy generation and the effect of suppressed recombination are already introduced in section 3.1.

The vacancy current $j_v(t)$ consists of the two terms that combine the diffusional and the drift current:

$$j_v(t) = -D_v x_v'(r_{sl}, t) + u_v x_v(r_{sl}, t), \tag{3.7}$$

where $x_v(r_{sl,t})$ is the concentration of the excess vacancies injected at the solid/liquid interface. The excess vacancy concentration - including the recombination and generation term - can be found by solving the kinetic equation in one dimension:

$$\frac{\partial x_v}{\partial t} = D_v \frac{\partial^2 x_v}{\partial r} - u_v \frac{\partial x_v}{\partial r} - \frac{x_v}{\tau} + G(r,t) \tag{3.8}$$

The first and second term in equation 3.8 describe diffusion and drift of the vacancies. The third part reduces the concentration by thermal induced recombination with interstitial atoms with a recombination time τ_r. The external generation function G(r,t) includes terms describing the generation of excess vacancies by:

$$G(r,t) = -x_v^0 \delta(t-t_0)\theta(r-r_{sl})\theta(r-r_0) + x_v^0 u_s \delta(t-t_0)\theta(r-r_{sl}), \tag{3.9}$$

where θ is the Heaviside step function. $G(r,t)$ consists of two terms. The first term describes the sudden depletion of the vacancies with respect to the equilibrium value x_v^0 in the region between $r_{sl} \leq r \leq r_0$ starting at time $t = t_0$. The second term describes the subsequent vacancy injection at the solid/liquid interface with the vacancy generation velocity u_s.

Integrate equation 3.8 one obtains for the time dependent excess vacancy concentration:

$$x(r,t) = X_0[-\frac{1}{2}e^{-t/\tau_r}\ erfc\frac{u_v t - r}{\sqrt{4D_v\, t}} + u_s \int_0^t \frac{dt'}{\sqrt{4\pi D_v\, t'}} e^{-t'/\tau_r}\ e^{-(u_v t' - r)^2/4D_v\, t'}], \tag{3.10}$$

where erf is the "error function" and erfc its complementary. Both are defined in appendix A.2. As a solution the derivation of the time dependent vacancy concentration gives the vacancy current that corresponds to the oscillating beam flux:

$$\begin{aligned} j_v(t) &= -D_v x_v'(r_{sl}, t) + u_v x_v(r_{sl}, t) \\ &= X_0 u_v \left(\frac{1}{4}\sqrt{\frac{\tau_v}{\pi t}}\ e^{-t/\tau^*} + \frac{1}{2}\ e^{-t/\tau_v}\ erf\sqrt{\frac{t}{\tau_v}} + \frac{u_s}{2u_v}\sqrt{\frac{\tau^*}{\tau_v}}\ erf\sqrt{\frac{t}{\tau^*}} \right) \end{aligned} \tag{3.11}$$

In a reduced form the beam flux can be described by [9]:

$$j_{osc}(t) = \frac{1}{4}X_v^0 u_v[\frac{e^{-\beta y}}{\sqrt{\pi\beta}} + 2e^{-y} erf\sqrt{y} + \frac{\alpha}{\sqrt{\beta}} erf\sqrt{\beta y}], \tag{3.12}$$

with $y = t/\tau_v$, $\alpha = 2u_s/u_v$, $\beta = \tau_v/\tau^* \geq 1$, the reduced time $\tau^* = \tau_v\tau_r/(\tau_v + \tau_r)$, the vacancy generation velocity $u_s \cong 2u_v + \lambda/\tau_r$ and the thermalization time $\tau_v = 4D_v/u_v^2 = 4kT/Fu_v$. The thermalization time τ_v is the time required to dissipate an amount of energy of the order of the thermal energy $4kT$.

Thus, the periodic curve shape can be fitted with only two parameters α and β. Applying equation 3.12 the periodical curve shape can be perfectly reproduced in a wide range of pressure and temperature. In figure 3.9 the time dependent developing of $j_{osc}(t)$ is shown in comparrison with the experimental oscillating beam flux intensity. This measurement is done at source pressure p_0 = 32 bar and source temperature T$_0$ = 1.70 K. By fit the experimental beam flux with equation 3.11 one reproduces the experimental beam flux with the parameters α = 1.0 and β = 8.0 . Table 3.1 gives the values that are derived from the both fit parameters α and β. As a result the obtained value for the diffusion coefficient D_0 corresponds to experimental results of D_v in the literature [13, 131]. This result indicates that the present model is able to describe the shape of the periodic behavior at the expansion of solid Helium into a vaccum, but the periodic peak can‘t be reproduced. This is due to two aspects that is not included in the transport equation: The pressure gradient is assumed not vanish at distance l, where the pressure is equal to the source pressure p_0. The distance l is set to be infinite and therefore the vacancies do not accumulate. Furthermore, the periodic peak occurs due to a collapse of the lattice. This mechanism is presented in the next section.

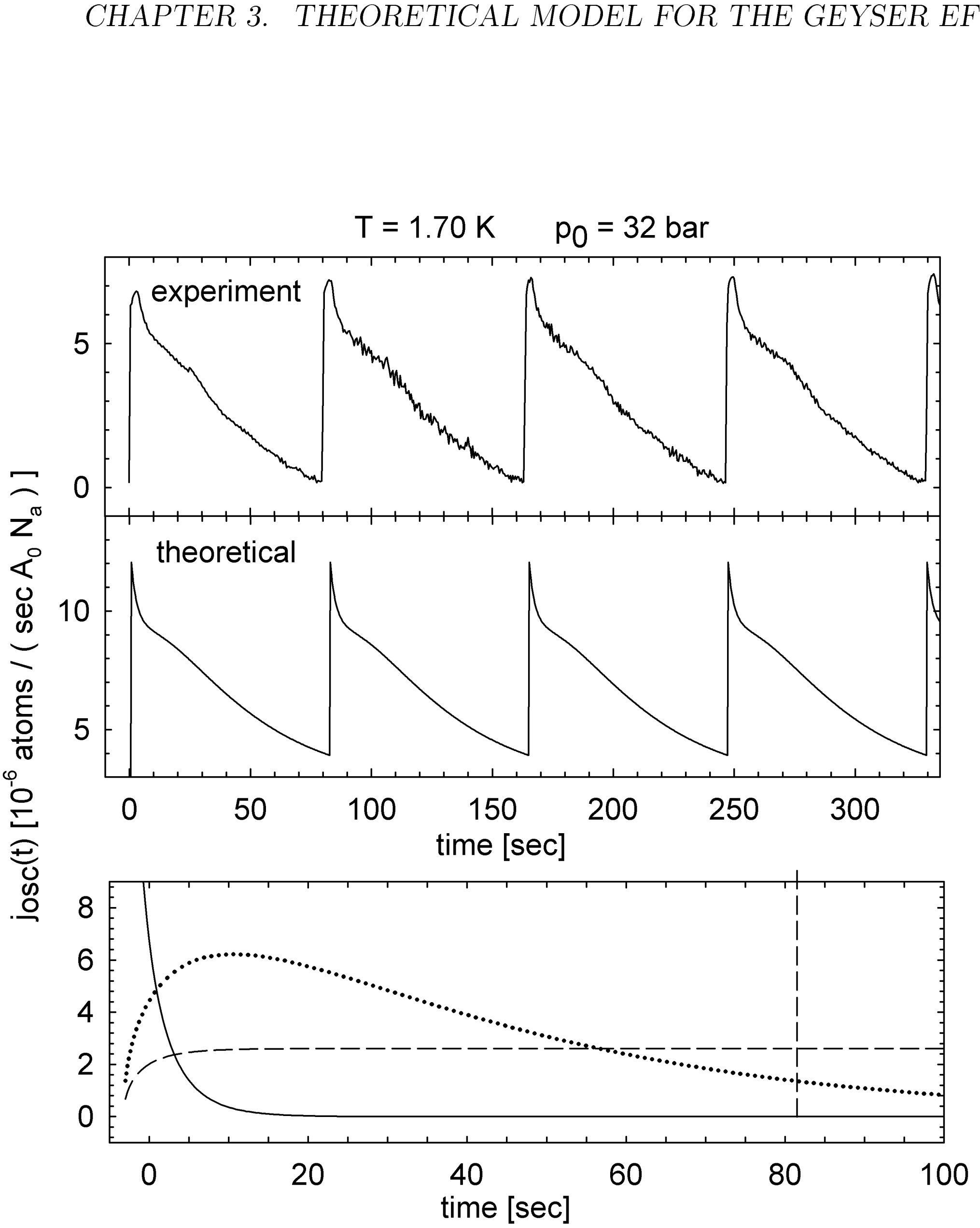

Figure 3.9: Theoretical fit of the experimental data obtained by applying equation 3.12. The experimental data were observed at source pressure $p_0 = 32$ bar and temperature $\mathrm{T}_0 = 1.70$ K. The best fit was obtained for $\alpha = 1.0$ and $\beta = 8.0$. The explanation of the unit j_{osc} follows in the next section. Below the single terms of equation 3.11 is shown: The straight line indicates the first term that describes the diffusion of vacancies. The dotted line represents the motion by drift and the dashed line describes the third term of 3.11 that determines the recombination. For this measurement the recombination time is obtained to be $\tau_r \approx 5$ seconds. After this time the recombination term becomes constant. (nozzle diameter: $d_0(\#17) = 2.28$ μm)

Source pressure	p_0	=	32 bar
Source temperature	T_0	=	1.70 K
Period	τ_0	=	82 sec
Diffusion coefficient	D_v	=	$3.6\ 10^{-5}$ cm^2/sec
Mobility of vacancies	μ_v	=	$1.5\ 10^{11}$ sec/g
Drift velocity of the bulk solid	u_v	=	$2\ 10^{-3}$ cm/sec
Vacancy generation velocity	u_s	=	$2\ u_v$
Recombination time	τ_r	=	5.14 sec
Thermalization time	τ_v	=	36 sec
Reduced time	τ^*	=	4.5 sec
Ratio of the critical concentration	$X_v^{c,\infty}/X_v^0$	=	1.82

Table 3.1: Overview of the obtained values derived from the parameters α and β of equation 3.12 by fit the periodic curve shape in figure 3.9.

3.3.4 The Mechanism of Periodicity

In the previous section the theoretical approach was introduced that describes the time dependent vacancy current. Now the approach is applicated to show the occurence of the periodicity in the beam flux. Corresponding to the two dimensional illustrations in section 3.3.1 and 3.3.2 the vacancy distribution is shown as an interaction of diffusion and drift. The illustrations are presented in figure 3.10 and 3.11. Again the vacancy concentration is shown as a function of the distance to the solid/liquid interface.

Similar to the previous considerations the illustration starts at t = 0, corresponding to the occurence of the the peak in the signal. As seen in figure 3.10 at t = 0 the vacancy concentration profile shows a step-wise character. The step behavior at short times is less pronounced because of the influence of both diffusion and drift. At a certain time between t = 0 and the collapse the vacancies move under the influence of diffusion and drift and accumulate at a distance l that corresponds to the cross section S_0.

As already seen in figure 3.3, this behavior corresponds to the location where the pressure gradient vanishes and the forced motion of drift stops (fig. 3.10, middle). After a certain time a new aspect arises. In the zone of accumulation the vacancy concentration increases more and more. Thus, an additional vacancy concentration gradient appears. This concentration gradient forces the vacancies to diffuse in both directions away from the accumulation zone. On the one hand the vacancies disperse into the bulk solid Helium. On the other hand they diffuse back into the direction of the solid/liquid interface. This process is called backward diffusion.

To clarify the difference: On the bottom of figure 3.10 the vacancy concentration separates into two different lines. Additionally the white circles illustrate the vacancy concentration without the influence of backward diffusion. The following considerations regard only the red line that includes the additional backward diffusion. Under the influence of backward diffusion the vacancy concentration inside the accumula-

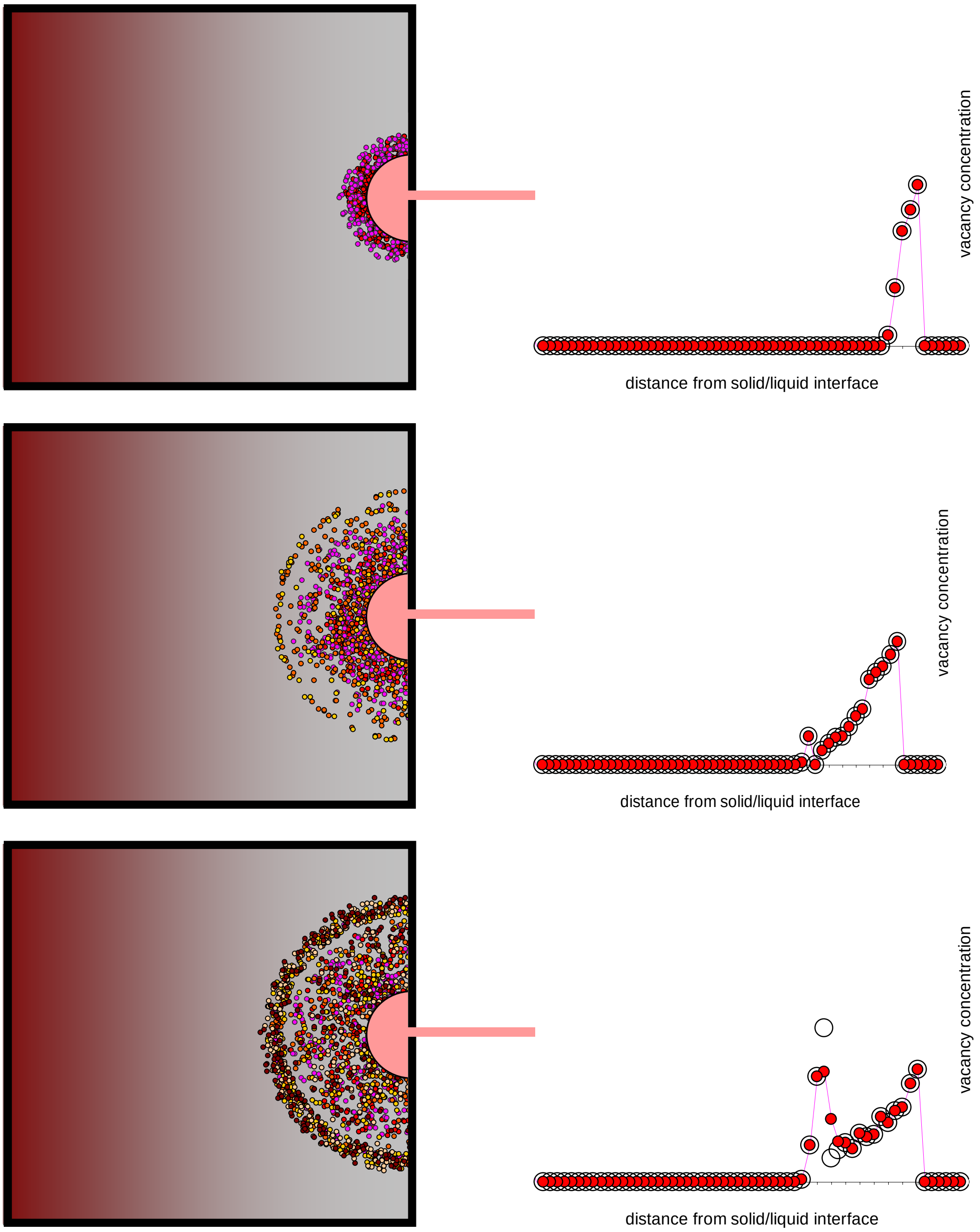

Figure 3.10: Drift and Diffusion of vacancies applied to the present model. Top: Vacancy generation at the solid/liquid interface. Beside the vacancy concentration as a function of distance from the solid/liquid interface. Middle: The vacancies are forced to move under the influence of drift and diffusion. At the zone where the pressure gradient vanishes the vacancies accumulate. Bottom: Starting from the accumulation zone the vacancies diffuse forward into the solid and backward in direction of the solid/liquid interface because of the high concentration of vacancies that causes a concentration gradient. The red line regards to the backward diffusion mechanism while the white circles correspond to the vacancy concentration without diffusing back to the solid/liquid interface.

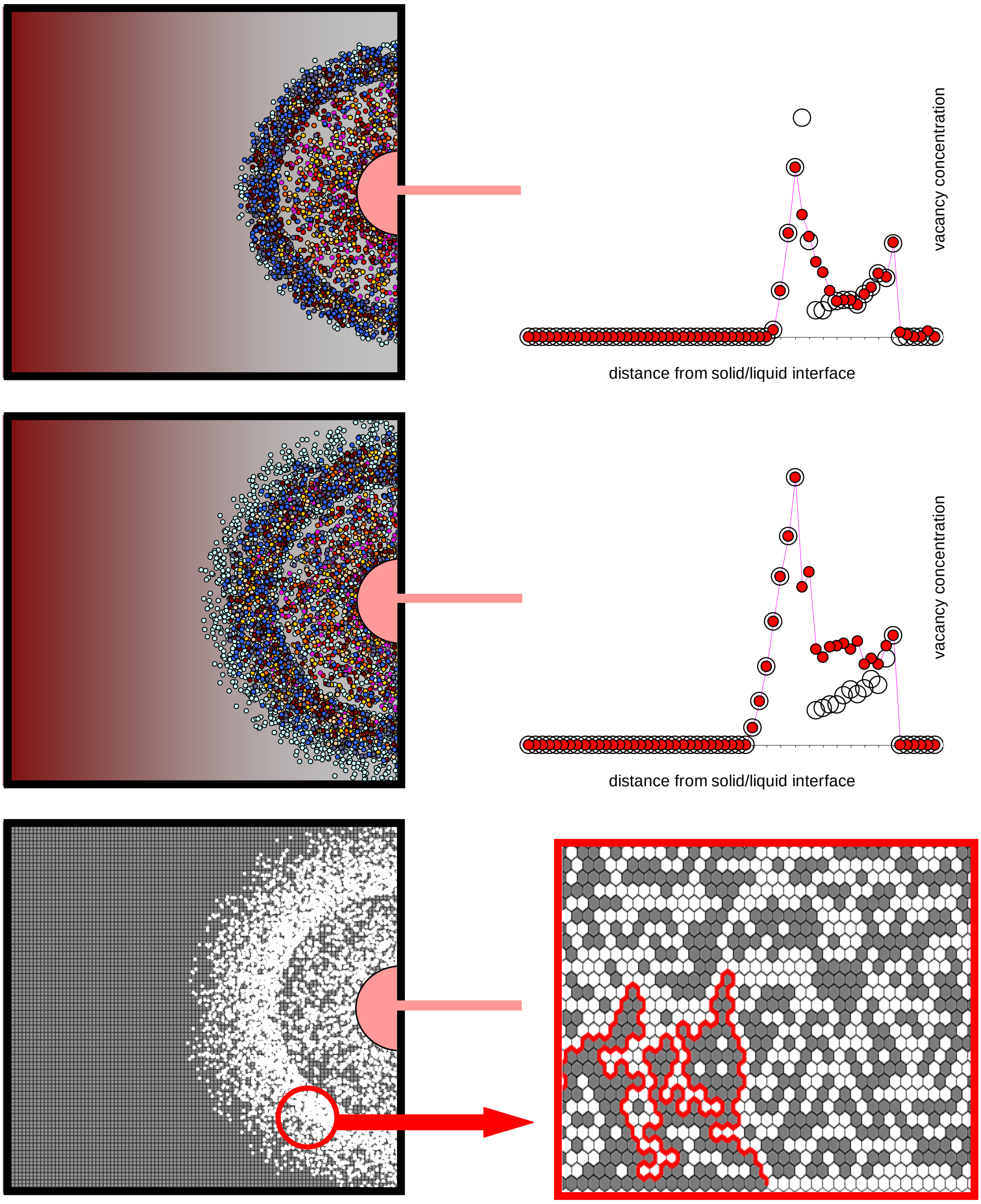

Figure 3.11: The continuation to the presented model of figure 3.10. Top: Increase of the vacancy concentration in the accumulation zone. Middle: After a while the concentration in the accumulation zone reaches a critical threshold of the vacancy concentration. At this time the lattice collapses. The mechanism of percolative collapse is demonstrated on the bottom: The red line indicates a continuous path of vacancies in the lattice. If the path is closed the lattice collapses.

tion zone decreases. Thus, the vacancy flow coming from the solid/liquid interface decreases because of the backward current in the opposite direction. As long as the net vacancy current into the direction away from the solid/liquid interface occurs the vacancy concentration in the accumulation zone increases, as seen in figure 3.11. In the middle of figure 3.11 the region where the vacancies accumulate is clearly pronounced.

The periodic peak is a statistical process of percolative[5] collapse of the crystal. This collapse occurs when the number of vacancies reaches a critical concentration X_v^c. An illustration of a percolative collapse is shown in the right picture at the bottom of figure 3.11: The grey fields mark a vacant lattice site. If a closed connection line of vacant lattice sites occurs the vacant sites build a perfect vaccum. As a result this region collapses under the influence of the outer pressure. As a consequence of the collapse all vacancies in the crystal are annihilated (vacancy bleaching). Thus, the collapse acts as a reset of the initial conditions at t = 0, and the concentration of vacancies is even below the equilibrium concentration. The lattice collapse is the reason for the periodic peak in the signal. After the collapse vacancies are generated again at the solid/liquid interface and the process occurs again.

The collapse of the lattice occurs if the critical concentration X_v^c is below or equal a definit maximal vacancy concentration $X_v^{c,\infty}$. This vacancy concentration $X_v^{c,\infty}$ gives the maximal possible vacancy concentration that can be reached, because with the increase of the vacancy concentration at the cross section S_0 the resulting concentration gradient forces the vacancies to diffuse away. Thus, the collapse occurs only if $X_v^c \leq X_v^{c,\infty}$. The condition for the collapse follows from the solution of the transport equation for finite l [9]:

$$\frac{\tau_0}{\tau^*} = \left[erf^{-1} \frac{X_v^c - X_v^0}{X_v^c + \frac{1}{2} X_v^0} \sqrt{\frac{\tau_v}{\tau^*}} \right]^2 . \tag{3.13}$$

From 3.13 it follows for ratio between the maximal vacancy concentration $X_v^{c,\infty}$ and the equilibrium concentration X_v^0:

$$\frac{X_v^{c,\infty}}{X_v^0} = \frac{1 + \frac{1}{2}\sqrt{\frac{\tau^*}{\tau_v}}}{1 - \sqrt{\frac{\tau^*}{\tau_v}}} \tag{3.14}$$

The ratio can be determined from fit the curve shape with equation 3.12. Table 3.1 gives the results for τ^* and τ_v. Thus, for the ratio of the excess vacancy concentration to the equilibrium concentration equation 3.14 gives $\frac{X_v^{c,\infty}}{X_c^0} \approx 2$.

The periodic peaks in the signal shows that the condition $X_v^c \leq X_v^{c,\infty}$ is fulfilled, whereas the occurrence of backward diffusion suggests that $X_v^c \simeq X_v^{c,\infty}$. Therefore, the concentration of vacancies is increased of a factor two above the thermal equilibrium concentration.

---

[5] Percolation describes a mathematical processes that searches for the probability to find a continuous path through a multidimensional network. In the theoretical model the network is represented by the crystal lattice and the closed connection line has to be filled with vacancies.

In the present model one process is neglected that was already mentioned which influences the periodic process. As mentioned in section 3.3.3 vacancies in equilibrium condition recombine with interstitial atoms. In separating the vacancies from interstitials by drift and diffusion the recombination time τ_r increases as well. If the period τ_0 is shorter than the recombination time τ_r the vacancies do not recombine with interstitial atoms. On the other hand the period τ_0 increases if the recombination time τ_r is shorter than the time till the collapse occurs, because the vacancy concentration decreases if vacancies begin to recombine. The enlarged recombination time itself increases the period but does not suppress the periodic effect itself.

To summarize the presented model: The periodic oscillations and the liquid beam flow is produced by the injection of excess vacancies at the solid/liquid interface. The high concentration of vacancies produces the melting of the solid and eventually a periodic collapse of the crystalline structure. The model shows that the periodic curve shape can be reproduced theoretically with the vacancy current in the solid that is mainly caused by drift and diffusion.

In this experimental work the temperature and pressure dependence of the Geyser effect is investigated. The main observable is the period that acts as an indicator for the vacancy mobility. Furthermore the influence of the isotope Helium-3 to the period τ is investigated as a function of pressure, temperature and concentration.

Chapter 4

Previous Experiments with Solid Helium

At low temperatures quantum effects in solids such as Helium play a major role. The characteristic features of quantum crystals make their experimental investigation very interesting. Helium as the best candidate to observe quantum effects has attracted a lot of experimental research.

In their measurements of longitudinal velocity of first sound Vignos and Fairbank observed in 1969 a new phase transition in solid Helium-4 [123]. In comparison with the phase diagram of ^{3}He they concluded that the new phase is body-centered-cubic ordered, as to be seen in fig.2.1. Experimental investigations are often separated in concerning the bcc or the hcp phase. Because of the lower density - and the resulting larger interatomic distance - quantum effects in the bcc phase are more pronounced than in the hcp crystal. The main interest in quantum crystal was in the investigation of diffusion of defects.

This chapter illustrates the most common experiments done with solid Helium to investigate the diffusion of defects, plastic flow and the existence of the supersolid state in solid Helium.

4.1 Vacancy Diffusion

The main topic in the research on solid Helium is the generation and motion of vacancies. The main interest concerns the determination of the energy of formation ϕ_f that is necessary to unhinge an atom out of its lattice site. At it‘s former position the atom leaves a vacant lattice site. Further interest concerns the activation energy ϕ_a to overcome the potential barrier of two neighboring lattice particles. Because of the existent tunneling probability the activation energy can be treated as a band gab of a specified width Δ. Thus, Δ is the third observable in experiments concerning the motion of vacancies.

The motion of vacancies is mainly determined by diffusion. The most common method to investigate the diffusivity is the nuclear magnetic resonance (NMR) method. This method observes the motion of Helium-3 which has a nuclear spin. As mentioned in section 2.2.4 vacancies in Helium-4 cause inward relaxation. A Helium-3 atom in solid Helium-4 causes outward relaxation because of the smaller mass. Therefore, a Helium-3 atom and a neighboring vacant lattice site remain together as a vacancy-Helium-3 pair because this compensates partly their inward and outward relaxation. Thus, the Helium-3 atoms act as a kind of marker for vacancies. In chapter 6.4 the experimental results of vacancies and Helium-3 is investigated and therefore the generation of vacancy-Helium-3 pairs is explained more detailed.

In NMR experiments Berent *et al.* [13] found for mixtures of Helium-3-Helium-4 in the bcc phase that the vacancy-Helium-3 pair even moves faster than Helium-3 atoms in superfluid Helium-4. The high mobility of vacancy-Helium-3 pairs indicates the extraordinary mobility of vacancies inside a quantum solid. In several experiments [62, 93] using NMR-spectroscopy the activation energy for a vacancy in hcp solid Helium was determined to be $\phi_a \sim 15$ K .

Another method to investigate vacancies in solid Helium is to explore the lattice parameter by X-ray Bragg scattering. If a vacancy occurs inside the lattice the lattice parameters will increase. X-ray scattering allows mainly to determine the energy of formation ϕ_f. The determination of ϕ_f gives information about the vacancy concentration by following $x_v = exp(-\phi_f/kT)$. The first direct measurement of the vacancy concentration in bcc solid Helium was done by Granfors *et al.* [59]. The energy of formation was obtained to be about $\phi_f = 9 \pm 1$ K and the thermal vacancy concentration received from calculations was about $7 \cdot 10^{-3}$. Experiments with hcp solid Helium [45] obtained at 1.6 K a vacancy concentration of $x_v \approx 5 \cdot 10^{-5}$ that depends exponentially on the temperature. In this experiment the formation energy of hcp solid Helium was determined to be the same as for the bcc phase.

A new method to investigate vacancy properties in solid Helium-4 more directly was proposed and applied by Zuev *et al.* [131]. Solid Helium-4 was forced through a porous membrane. The membrane‘s pore width was $\approx 2\mu m$. From the results the vacancy mobility in solid Helium was determined. The experiment was done to investigate the steady-state velocity in the membrane as a function of the applied pressure. The linear behavior of the stress-strain relation was verified to pressures up to $1.8 \cdot 10^4$ dyn/cm^2 for hcp Helium-4 and $0.5 \cdot 10^4$ dyn/cm^2 for bcc Helium-4. As to be seen in figure 4.1 the linear behavior between stress and strain indicates elastic strain in solid Helium. From these results the obtained dependence D_v (T) for Helium-4 can be interpreted as stimulated tunneling of vacancies associated with phonons [44]. The activation energy obtained from the experiment was found to be $\phi_a \sim$ 6-7 K.

In similar experiments concerning plastic flow the influence of vacancy diffusion was investigated by Berent and Polturak [12, 13]. In these experiment a superconducting wire of diameter 80 and 24 μm was forced to move through solid Helium driven by a magnetic field. The forced motion was controlled by the Lorentz force, induced by a dc current through the wire. To neglect melting effects by heat transfer the wire was chosen to be superconductive. A linear dependence of the wire velocity v to the

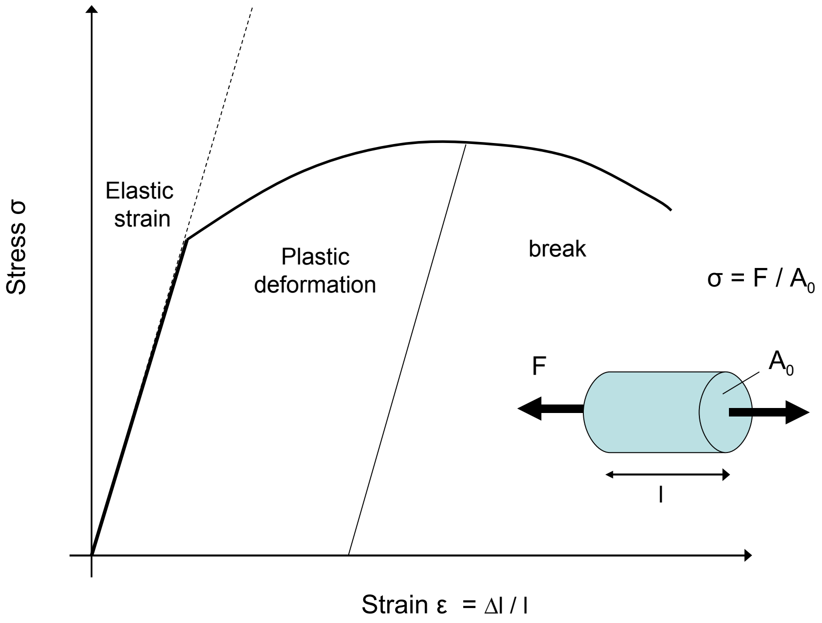

Figure 4.1: Stress strain relation of a solid

applied stress σ is characteristic for the Nabarro-Herring mechanism, where the mass flow takes place through counter-diffusion of vacancies and atoms due to a vacancy concentration gradient. In this mechanism the atomic diffusion takes place between the front of the wire where the stress is high and the back of the wire where the stress is low. It is interpreted as an exchange mechanism of atoms and vacancies. If an atom jumps from the front of the wire to the back it leaves a vacant lattice site. Atoms and vacancies change their position depending on the applied stress. The vacancy concentration in the front differs from the concentration behind the wire. One assumes that the motion of the wire takes place through diffusion of vacancies towards the wire while atoms diffuse in the opposite direction. Because of the unequal vacancy concentration before and behind the wire a concentration gradient appears. Following Fick‘s Law of diffusion one obtains a direct relation between the wire´s velocity v and the atomic diffusion coefficient D_s:

$$\frac{v}{\Omega} = D_s \frac{\sigma}{k_B T l}, \tag{4.1}$$

where Ω is the atomic volume, σ the applied stress and l the wire diameter. As a result the wire´s velocity increased of about two orders of magnitude in crossing the bcc-hcp transition. Corresponding to the increase of the velocity the activation energy ϕ_a decreased from 15 K down to $\sim$ 10 K. The decrease of the activation energy was interpreted as a result from the interaction of phonons. The self diffusion coefficients of Helium atoms is related to the vacancy diffusion coefficient by the vacancy concentration:

$$D_s = x_v D_v. \tag{4.2}$$

Therefore, the investigated atomic diffusion coefficient is always related to the diffusion coefficient of vacancies. Various experiments determined D_v in the order of 10^{-5} cm^2/sec which is in the same order of magnitude as for a liquid. Whereas even after almost forty years of investigating the behavior of vacancies in solid Helium-4 the exact determination of the parameters Δ and ϕ_a is still an unsolved problem.

4.2 Plastic Flow

One of the first experiment to investigate the plastic flow in hcp solid Helium-4 was to measure the force required to move a steel ball through the crystal at nearly constant velocity [117]. Andreev *et al.* already attempted a forced motion of a small ball driven by a magnetic field [2]. In these experiments at about 0.5 K there was no observable displacement of the ball. The velocity was estimated to be less than $2 \cdot 10^{-7}$ cm/sec. Suzuki‘s measurements were carried out at pressures between 29 and 51 atmospheres and temperatures between 1.38 and 2.13 K. Because of the exponential increase of the diffusion coefficient with increasing temperature the temperature range investigated by Suzuki is related with a higher mobility of defects. Velocity rates from 10^{-3} up to 1 mm/sec were observed while a force in the order of 10 Newton was applied to the ball. After the maximum force was applied to the ball the force could be reduced to obtain a steady motion. Because of the drop in the force-displacement dependence the migration of vacancies was assumed to explain the plastic flow in solid Helium. Instead of vacancy assisted motion the motion of crystal dislocations sufficiently explains the observed behavior.

Another way to investigate the plastic flow in solid Helium was applied by Sanders *et al.* [106]. The process of deformation was done by increasing the pressure linearly in time in order to push a piston down to an approximately constant rate. The investigation of the bcc ordered crystal showed that in the case of plastic deformation the crystal behaves more like a viscous liquid than an ordinary crystalline solid. This result was attributed to the higher concentration of vacancies in the bcc phase. In these experiments the process of crystal growth was of a special interest. This was done to investigate if the process of plastic deformation inside the crystal is supported by dislocations, which was not observed.

4.3 The Supersolid Phase

In section 2.4 the theoretical aspects of the supersolid state in Helium-4 are discussed. After long decades of discussions [25, 108] and experimental research the supersolid state is today assumed to be a Bose-Einstein condensate of vacancies.

The supersolid is assumed to occur right at the melting line, favored at the bcc phase between 1.45 K and 1.78 K. Due to the lower density[1] near the melting line the vacancy mobility is maximal. It is unclear however at which critical temperature T_c the supersolid phase should occur. On the other hand the assumed existence of zero-point-vacancies at $T = 0$ suggest that the supersolid could occur at very low temperatures down to $T = 0$. The second aspect that remains is that just a limited fraction of the solid becomes supersolid. The ratio of the supersolid to the normal solid fraction $(\rho_s/\rho) > 0$ is one of the most interesting aspects that has to be investigated. Another aspect is the critical velocity v_c of the particles that form the supersolid fraction. According to the superfluidity of liquid Helium the critical velocity v_c marks the upper limit for superfluid flow. Above v_c the particles loose the property of frictionless motion. The velocity of the supersolid fraction should also have such an upper limit. In superfluid Helium the occurrence of rotons restricts the flow velocity to ≈ 50 m/sec, a value that is not proven experimentally. One might expect that there is also an upper threshold for the velocity of supersolid flow.

During the last 35 years various experimental approaches were taken to search for the supersolid. Plastic flow in solid Helium-4 was investigated [117, 38, 12][2]. The motion of different kind of objects (wire, bullets) through solid Helium was investigated. The temperature range was chosen between 0.5 and 2.12 K. In the supersolid phase the particles motion should be frictionless or at least significantly higher than in normal solid Helium. The experiments showed no evidence of supersolid behavior. A lower limit for the critical velocity of 10^{-10} and 10^{-4} cm/sec depending on the size and geometric properties of the used object was obtained from the experiments.

Greywall‘s method [61] to verify the supersolid state was to measure the capillary flow of solid Helium-4 between two pressurized chambers of different pressure. The pressure gradient should produce a measurable flow between the two chambers. If the supersolid phase should occur the flow in the capillary would have been assumed to be superfluid. The temperature range was chosen between 30 mK and 1K. The behavior at pressures between 25 bar (corresponding to the melting pressure) and 50 bar was investigated. The capillary consists of 25 stainless steel capillaries and each capillary had a diameter of 20 μm. The pressure difference between both chambers was up to 5 bar. No superfluid flow in the capillary was found.

In 1970 Leggett [87] was the first who proposed an experimental possibility to observe the supersolid state. His approach was to rotate a cylindrical annulus (hollow cylinder) filled with solid Helium-4 with constant angular velocity ω. The free energy is given by:

---

[1] especially at the bcc phase

[2] as described in the former section

$$F(\omega) = F_0 + \frac{1}{2}I_0\omega^2 + \Delta F(\omega), \tag{4.3}$$

where $F_0 = F(0)$ is the free energy at $\omega = 0$ when the system is non rotating and $I_0 = NmR^2$ the classical moment of inertia in the superfluid liquid. The term $\Delta F(\omega)$ describes the supersolid behavior in the system. $\Delta F(\omega)$ is assumed to be even and periodic in ω with period ω_0:

$$\omega_0 = \frac{\hbar}{\chi m R^2}, \tag{4.4}$$

where χ is of the order 1. For $\omega < \omega_0/2$ the function $\Delta F(\omega)$ can be written as:

$$\Delta F(\omega) = -\frac{1}{2}(\rho_s/\rho)I_0\omega^2 \tag{4.5}$$

The expression (ρ_s/ρ) defines the supersolid fraction. In a classical system $\rho_s = 0$ and the expression $\Delta F(\omega)$ is identical zero. If $(\rho_s/\rho) \rightarrow 1$ even at T = 0 the system differs from classical rotational inertia. Thus, Non-classical-rotational-inertia (NCRI) would be evidence for a superfluid component.

Reppy *et al.* [16] investigated the possible phenomenon of NCRI. The assumed lost of inertia was investigated at 25 mK and pressures starting from the melting line at 25 bar up to 48 bar. Nevertheless, no anomalous behavior was found. The supersolid fraction was measured to be $\rho_s/\rho < 5 \cdot 10^{-6}$, two orders of magnitude smaller than estimated by Leggett. The critical velocity v_c was assumed to be less than $5 \cdot 10^{-4}$ cm/sec. Even after reducing the average cavity velocity from $5 \cdot 10^{-3}$ cm/sec down to $5 \cdot 10^{-4}$cm/sec the experiment did not show any observable effective change of the results. A small fraction of about 0.04 % of the isotope Helium-3 was added. Even after reducing the Helium-3 concentration down to $3 \cdot 10^{-4}$ % and variations in pressure as mentioned above a NCRI-behavior could not been observed. For some decades the observation of supersolid Helium failed.

In 2004 E. Kim and H.W. Chan did another search for NCRI using a torsional oscillator containing a porous vycor glass disc [75]. The oscillator was filled with Helium-4 at definite pressures and temperatures corresponding to the solid phase. The use of vycor as a porous media was used as a possibility to increase the vacancy concentration. The vycor was mounted in the hollow cylinder and had an average pore diameter of 7 nm and pore length 30 nm. In using vycor glass the melting pressure at temperatures below 1.3 K shifts up to 40 bar, as experimentally observed by several investigations, i.e. [7]. Otherwise Helium remains superfluid on the tube walls and the motion of the solid is just an effect of the slip motion on a superfluid Helium film.

The results of the investigations are presented in figure 4.2 showing that below 175 mK the drop in the period ΔP indicates some abnormal behavior, which might be an indication for NCRI. This result was interpreted as the evidence for the existence of the supersolid phase. Adding a small concentration of Helium-3 made the effect disappear. The observed phenomenon caused a flood of publications concerning the

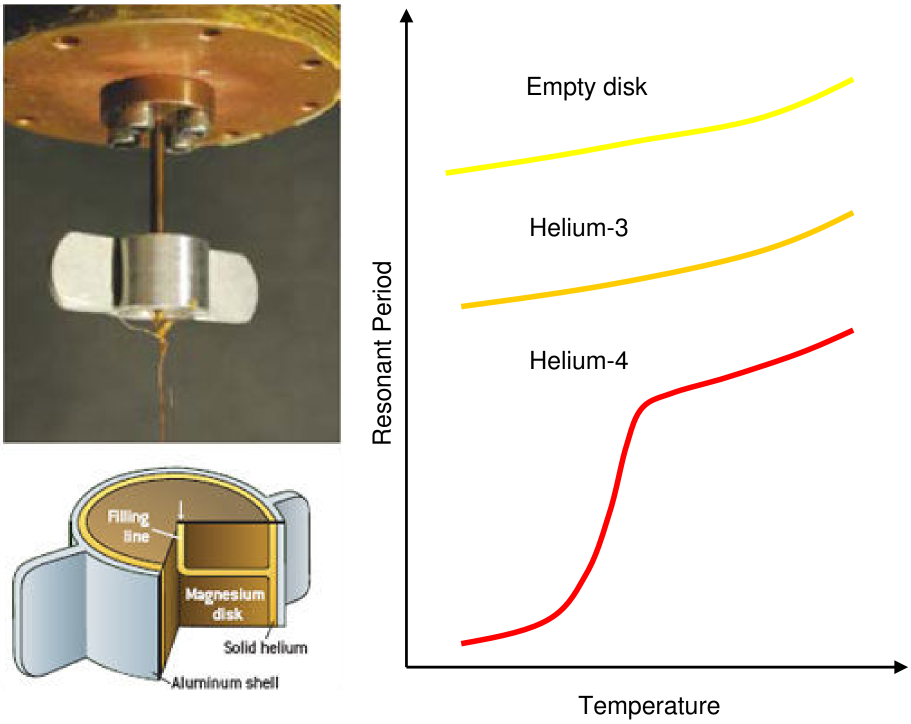

Figure 4.2: The left part shows the experimental setup used by Kim and Chan. The arrangement mainly consists of the rotating annulus mounted on the bottom of a cryostat. The picture is taken from [78]. On the right the results for the period at a function of temperature are shown. The dropdown of the period using Helium-4 occurs at temperatures T $<$ 175 mK. The effect does not occur using Helium-3 or an empty disk, respectively.

possible observation of the supersolid state in solid Helium-4 [5, 6, 14, 21, 22, 23, 26, 29, 30, 31, 35, 49, 50, 73, 82, 83, 84, 86, 100, 104, 107, 109, 115, 120, 124, 125, 128, 129]. The main critics that arose about the observation was the possible effect of slip motion on a liquid film [126]. The possible influence of the vycor glass was not satisfyingly sufficient to accept the evidence for the supersolid state. Therefore, Kim and Chan repeated the experiment with the same conditions except the use of vycor. The oscillatory tube was filled with bulk Helium-4.

They observed a decrease of the period at the same critical temperature as with vycor. From these results they proposed a phase line for the supersolid, as to be seen in figure 4.3. The supersolid fraction was calculated from the results. It depended on the maximum oscillation frequency and the temperature, respectively. Below 230 mK the Non-Classic-Rotational-Inertia-Fraction NCRI increased from zero up to between 1 and 2 %. In these experiments it was shown that the supersolid fraction increases with the applied pressure.

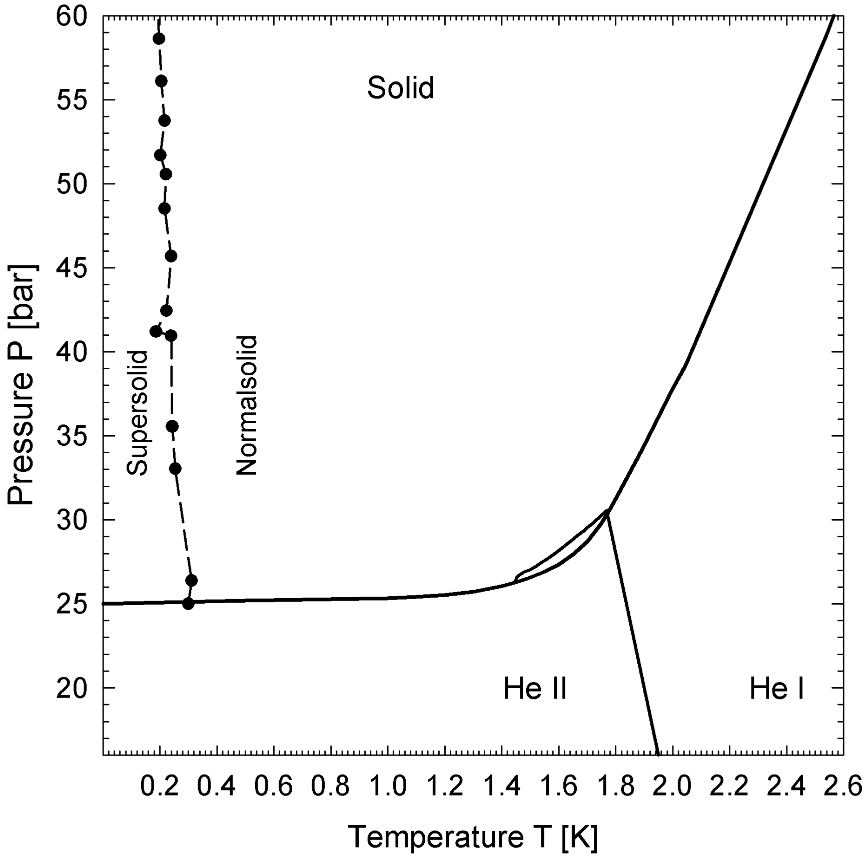

Figure 4.3: The experimental observed phase line of the supersolid state for solid Helium-4 at 230 mK obtained by Kim and Chan in 2004 [76]. Below $T_c \approx 230$ mK the resonant period of the rotating annulus decreases as seen in figure 4.2.

The results are controversial because the supersolid state was assumed to occur most probable close to the melting line. The occurrence of NCRI at such high pressures is still not solved. Osheroff[3] mentioned this lack in an article of Collins [27]. Solid Helium at high pressure turns into a classic solid. The critical velocity was found to be up to $20 - 25$ μm / sec. The effect could not be observed using pure Helium-3. Unfortunately, the experiments have not been done using mixtures of both isotopes.

It is still unclear why earlier experiments of Creppy *et al.* [16] did not observe NCRI. It is suggested that the concentration of Helium-3 might have been to be too high. Further experiments are necessary to prove the occurrence of the supersolid at temperatures and pressures obtained by Kim and Chan.

---

[3] D. Osheroff: "If they are correct, then I don't understand how supersolids become super. I hope the theorists are thinking about it seriously." [27]

Chapter 5

Experimental Setup

In this experiment ultra pure (99.9999 %) Helium-4 at temperatures between 1.3 and 2.3 K and pressures according to the solid phase up to 20 bar above the melting pressure p_m was expanded into vacuum through a small pinhole orifice of diameter between 1 and 5 μm. The Helium gas was cooled by means of a bath cryostat providing temperatures T_0 = 1.3 - 4.3 K. Originally, the apparatus was designed to investigate molecular beams of liquid Helium [64].

In figure 5.1 the scheme of the apparatus is shown. The apparatus mainly consists of a bath cryostat (3) and two separate vacuum chambers (1),(2). The nozzle assembly (4) is mounted at the bottom of the cryostat.

5.1 Vacuum System

The apparatus consists of two vacuum chambers, as shown in 5.1. The source vacuum chamber (1) contains the cryostat (3) and the nozzle assembly (4). The setup of the nozzle assembly is explained in section 5.3. The second vacuum chamber (2) is used as a pitot detector chamber. The pressure p_{det} measured in this chamber is used to investigate the oscillations in the beam flux intensity. Both chambers are connected by an aperture of 30 mm diameter at a variable distance of 10-50 mm from the jet source. The experimental setup is shown in figure 5.3 and figure 5.2.

Several fore-pumps were used to produce a fore-vacuum in the range of 10^{-2} mbar. Table 5.1 gives an overview of the different pumping units (5-8) used in both chambers. Additionally, figure 5.3 and 5.2 show the position of the pumps. The source chamber is pumped by two turbomolcular pumps, a Pfeiffer TPH 170 (fig. 5.3 (7)) and a Leybold Turbovac 1000 (fig. 5.2 (5)), and one diffusion pump (6) having a pumping speed of 6000 l/sec. An additional baffel is used to prevent oil diffusion into the vacuum chamber. Thus, the pumping speed of the diffusion pump is reduced to about 3000 l/sec. The detector chamber is pumped by two Pfeiffer TMH 1601 P (fig. 5.2 (8)) turbomolecular pumps.

While cooling with liquid Helium down to temperature T = 4.3 K the Helium gas jet

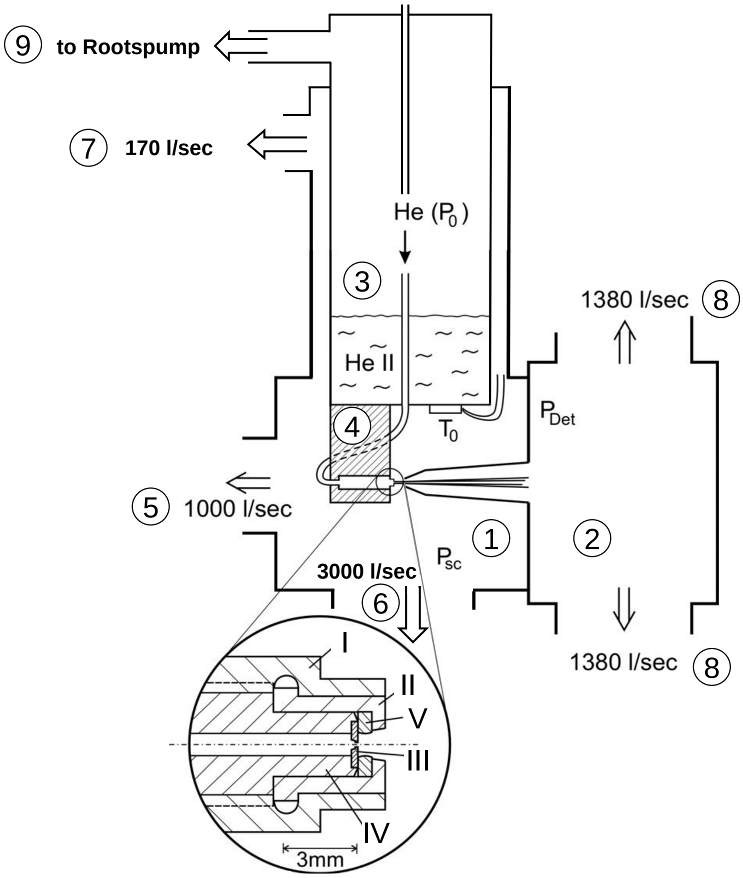

Figure 5.1: Scheme of the apparatus. The cryostat (3) is mounted in the source chamber. The supply tube for the Helium 6.0 gas leads through the Helium reservoir. Thus, the gas is pre-cooled in the inner reservoir before it enters the nozzle assembly (4) at the bottom of the cryostat. In this scheme the outer reservoir of the bath cryostat for LN2 is not shown. On the inset the nozzle head is shown. Point (I) marks the outer screw pressing on the steel-made socket (II). The nozzle (IV) has a diameter between 1 and 5 μm. The nozzle is placed in the nozzle head (V). A gold seal (III) keeps the assembly hermetically sealed.

Description	Pumping speed [l/sec]	Application
2 · Pfeiffer TMH 1601 P	2 · 1380	Detector chamber
Pfeiffer TPH 170	170	Source chamber
Leybold Turbovac 1000	1000	Source chamber
Diffusion pump	3000	Source chamber

Table 5.1: Overview of the different pumping units. The total pumping speed of both vacuum chambers is 6930 liters per second. In figure 5.2 the different pumping units (except the Pfeiffer THP 170) are shown: Leybold Turbovac 1000(5), Diffusion pump (6) , Pfeiffer TMH 1601 P (8)

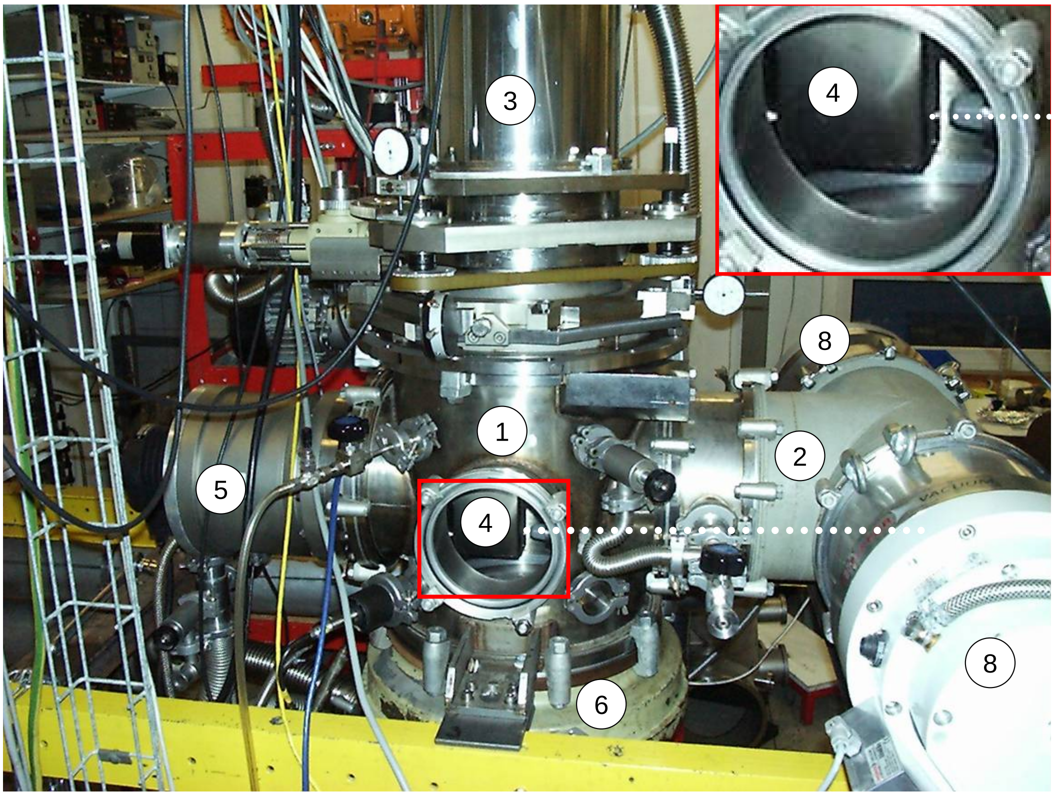

Figure 5.2: Experimental setup of the apparatus. The left vacuum chamber (1) contains the bath-cryostat (3). Through the window (enlarged at the inlet) the position of the nozzle assembly (4) is visible, which is covered by a radiation shield. The beam direction is indicated by the white points. The beam leaves the nozzle and enters the detector chamber (2) through an aperture with a diameter of 30 mm. Inside the detector chamber the single droplets hit the wall and vaporize (end of the white dotted line). The different pumping units are shown (5-8) according to table 5.1.

becomes liquid. This process is observable as an increase of the detector chamber´s pressure p_{det} and the source chamber´s pressure p_{source} of about one order of magnitude. The jet enters the detector chamber through the aperture and vaporizes by hitting the chambers wall. Thus, the amount of emerging gas in the detector chamber is in the range of 50 liters per second at a corresponding pressure $p_{det} \approx 10^{-5}$ mbar with a pumping speed of approximately 2760 l/sec[1].

5.2 Cooling Technique and Cryostat Application

The cooling is achieved by means of a bath cryostat. The bath cryostat (CryoVac 3 - 04 - 3957 A) consists of two separate cylindrical reservoirs for liquid Nitrogen

---

[1] Calibrated to N_2

(LN2)[2] (outer reservoir) and liquid Helium (inner reservoir). The capacity of the Helium reservoir is 7.5 l. To decrease and finally to control the temperature a roots pump and a fore-pump is connected to the Helium reservoir, as shown in figure 5.3 (9). The pumping speed is sufficient to decrease the vapor pressure down to $p_{vap} \geq$ 1.6 mbar. This pressure mainly determines the minimal temperature of the system (around 1.3 Kelvin) as explained in the next section. The minimal temperature is furthermore depending on the nozzle diameter and on the pressure p_{source} in the source chamber. The beam flux intensity is proportional to the square of the nozzle diameter. A high beam flux increases the vacuum pressure p_{source} and p_{det}. Especially a high vacuum pressure p_{source} in the source chamber increases the heat transfer between the chamber´s wall and the cryostat. This causes an increase of the temperature. Because of the high amount of vaporized Helium gas the pressure in the upper part of the vacuum chamber is up to one order of magnitude higher than in the lower part of the chamber. Therefore, a 170 l/sec Pfeiffer turbo pump (fig. 5.3 (7)) was used to achieve a vacuum in the order of 10^{-6} mbar and finally to reach low temperatures.

The cooling process occurs in the following steps. First the outer reservoir is filled up with liquid Nitrogen (LN2) by pumping the liquid with an overpressure of about 0.3 bar from a LN2 tank through a teflon connection line into the Nitrogen reservoir of the cryostat. The connection line is visible in figure 5.3 (10): It leads from the reservoir can to the top of the cryostat.

After the outer LN2 reservoir is filled up, the inner Helium reservoir is pre-cooled with LN2. To fill liquid LN2 into the inner reservoir a hopper is used. After approximately 4-5 liters[3] of LN2 are vaporized the final temperature in the inner reservoir is about 120 Kelvin. This LN2 pre-cooling saves approximately 20 liters of liquid Helium. When the temperature increases again the Nitrogen is completely vaporized and the liquid Helium can be filled in. A connection line from the Helium can is put into the orifice of the inner reservoir. By overpressure the liquid Helium flows from the Helium dewar into the inner reservoir. Helium gas that vaporizes inside the reservoir of the cryostat flows out of the cryostat, passes the roots pump and the fore-pump and is finally recycled in a Helium recovery system.

By filling the inner reservoir with liquid Helium the temperature decreases down to 4.3 Kelvin. This temperature corresponds to the vapor pressure of liquid Helium-4 at one atmosphere. Figure 5.4 shows the vapor pressure of Helium-4 in dependence of temperature. After filling the inner reservoir with about 7.5 liters of liquid Helium the connection line is taken out of the cryostat and the orifice of the inner Helium-reservoir is closed. By pumping the vaporized Helium gas by a fore-pump a final vapor pressure about 30-40 mbar is achievable. This pressure corresponds to a temperature of about $T_0 = 2.3$ K. An additional roots pump (fig. 5.3 (9)) reduces the vapor pressure down to 1.6 mbar. The pressure $p_{vap} = 1.6$ mbar corresponds to the temperature $T_0 = 1.3$ K (fig. 5.4 (3)). This is the lowest temperature that can be reached.

---

[2] Instead of "liquid Nitrogen" the shortcut "LN2" will be used

[3] The quantity of 4-5 liters of LN2 is an empirical value.

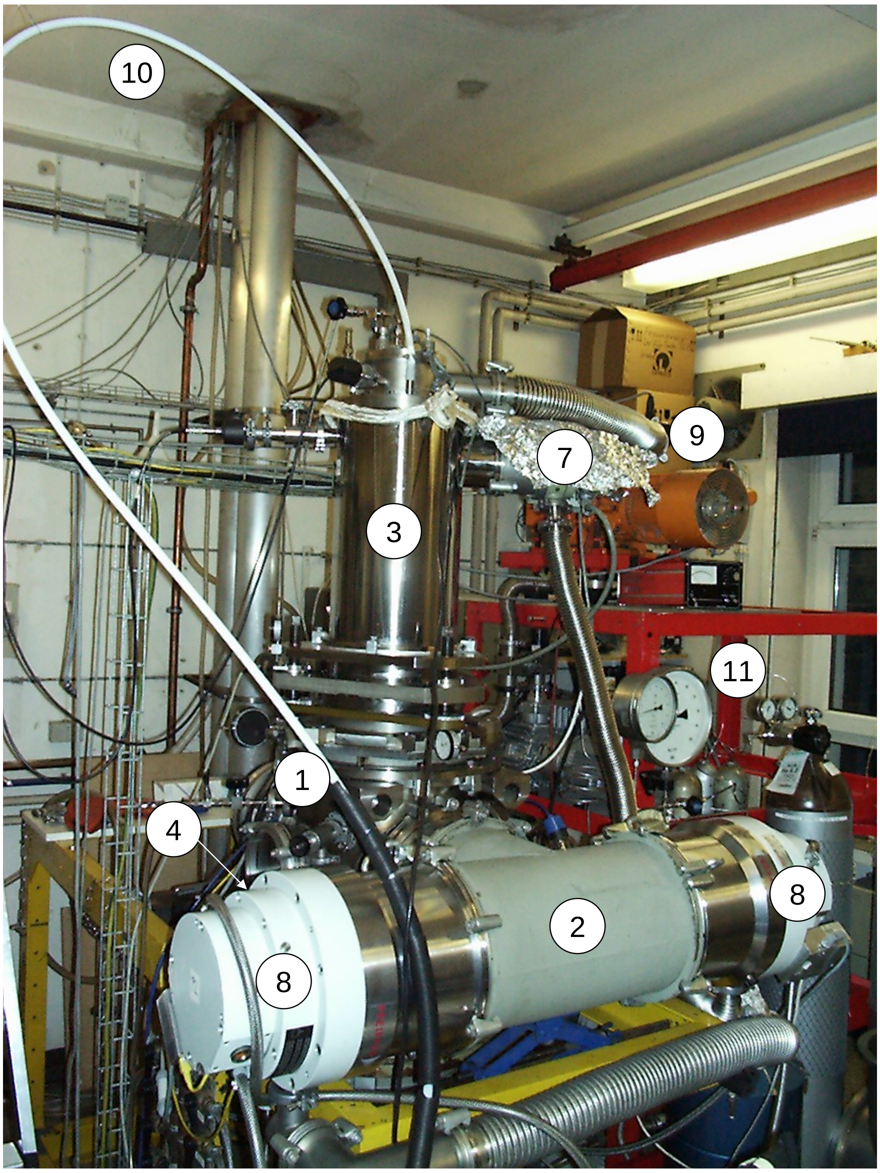

Figure 5.3: Experimental setup of the apparatus. The bath cryostat (3) is mounted on the top of the source chamber. Through the white connection line (10) liquid N_2 is transported into the cryostat. On the top of the vertical bath-cryostat the corrugated tube connects the roots pump (9) to the liquid Helium bath. By pumping the vapor above the liquid Helium the temperature is defined by the vapor pressure for Helium. The detector chamber (2) is used as a pitot detector chamber. The ultra pure Helium 6.0 gas is transferred from the bottle (11) to the cryostat. The nozzle pressure p_0 is indicated at the pressure gauge (11) Through the window the nozzle assembly (4) and the liquid jet is visible. An additionally turbo pump (7) is used to achieve a better vacuum in the source chamber, as described in section 5.2.

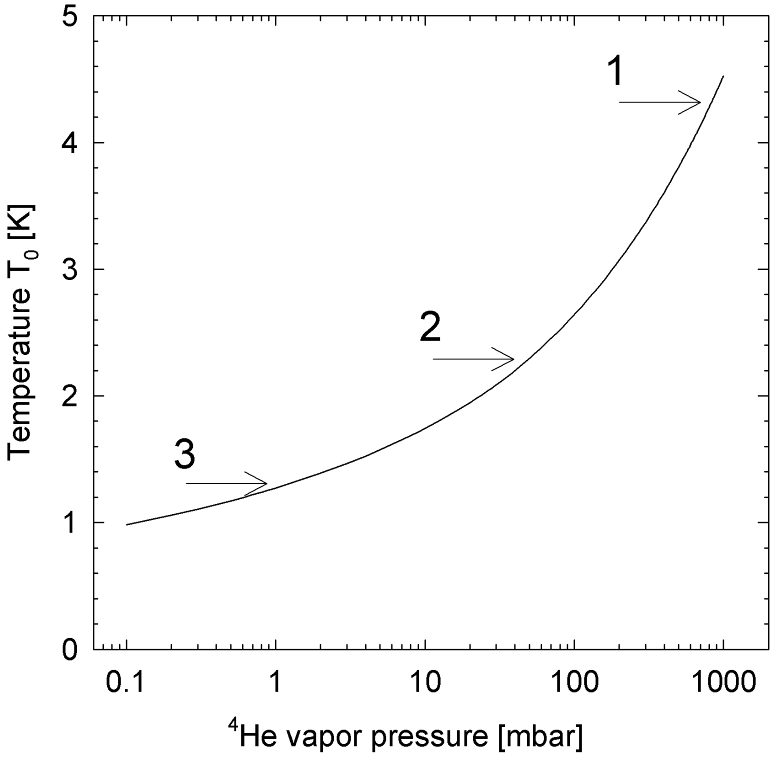

Figure 5.4: Vapor pressure of Helium-4 in dependence of temperature. Point (1) marks the temperature $\mathrm{T}_0 = 4.3$ K that corresponds to a vapor pressure of atmosphere pressure. Using the first pumping stage the vapor pressure can be reduced down to approximately 40 mbar, which corresponds to a temperature of about $\mathrm{T}_0 = 2.3$ K (Point 2). The second pumping stage allows the reduction of the vapor pressure down to 1.6 mbar. This pressure corresponds to the lowest temperature reachable in this experiment (Point 3) $\mathrm{T}_0 \simeq 1.3$ K.

5.3 Nozzle Assembly

The ultra pure Helium gas is injected through a steel tube. It leads through the bath cryostat into the copper made cooling head (figure 5.5) at the bottom of the cryostat.

Figure 5.5 shows the complete nozzle assembly mounted at the bottom of the cryostat. The upper block is made of copper and is hollow at the inside. The lower copper block consists the actual nozzle assembly. On the top of the upper block the supply tube of the ultra pure 6.0 Helium-4 leads directly into the block. The Helium gas is already pre-cooled on entering the nozzle assembly because the supply tube goes through the inner reservoir which is at the temperature of the liquid Helium $1.3 \text{ K} < \text{T} < 4.3$ K.

In the inset of figure 5.1 the construction scheme of the nozzle head (4) is shown. The nozzle (IV) is placed in front of the cooling head. Through this orifice Helium 6.0 is expanded into vacuum by a controllable source pressure p_0 in the supply line. Point (I)

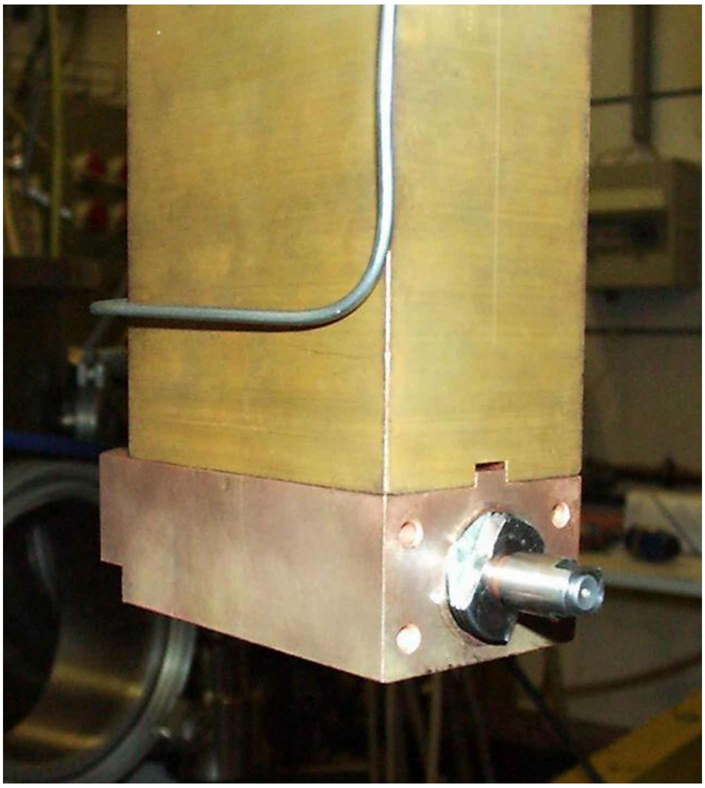

Figure 5.5: Nozzle assembly that is mounted at the bottom of the cryostat. The upper block is also filled with liquid Helium. The lower block is mounted by screws. In the front the supply line for the ultra pure 6.0 Helium-4 gas is shown. The supply line enters the lower copper block at the opposite site as the nozzle head. In the front the mounted nozzle holder is shown. The schematic drawing in figure 5.1 shows the build up of the nozzle holder.

marks the outer screw pressing on the steel-made socket (II). A gold seal (III) keeps the alignment hermetically sealed. The nozzles are produced by Rofin [103]. They consist of an outer ring and a thin foil of a thickness which is comparable to the orifice diameter. The orifice itself is cut by a laser beam. The producer gives a tolerance of the diameter of between 20 and 40 percent. As one can see in figure 5.6 the orifice is not perfectly round and the diameter varies depending on the deepness. Because of the distorted geometry unexpected effects during the experiments are always present. In this experiment mainly 2 μm were used, but nozzles with diameter 1, 3 and 5 μm were also used.

A problem that often occurred was the clogging of the nozzle. Because of the small nozzle diameters even smallest particles were able to clog the orifice. Thus, the purification of the system and mainly of the supply line of the He 6.0 gas was a very important aspect. Several filters were mounted into the supply line. One filter with an average pore diameter of 0.5 μm was also mounted into the nozzle head. The extremely carefully handling of those filter elements and the clean-up of the nozzle

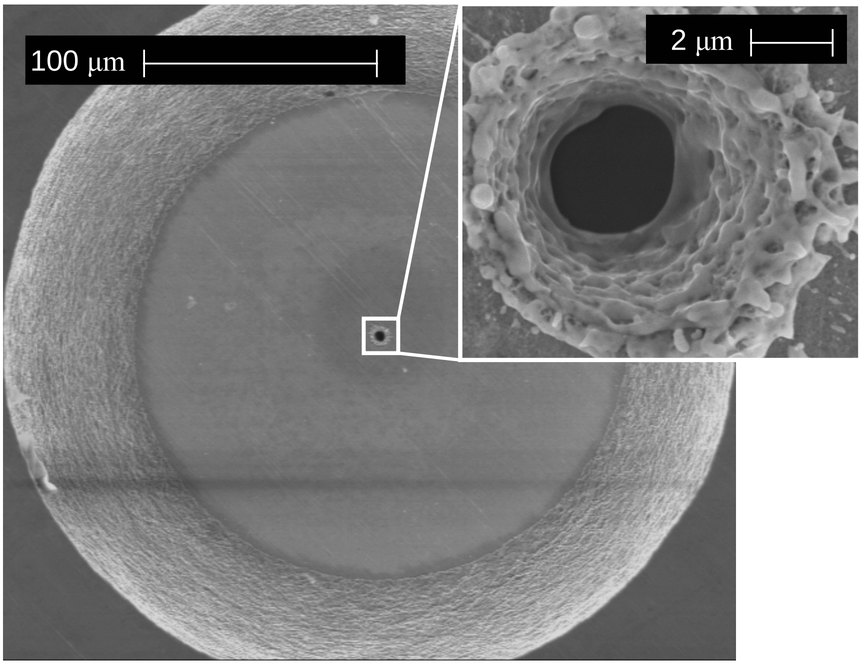

Figure 5.6: Electron microscope illumination of the conventional nozzles. The orifice is made by a laser beam. In the inlet the magnification of the orifice shows the distorted geometry caused by the laser. Thus, the nozzle diameter d_0 has a tolerance of between 20 and 40 percent. The nozzles are produced by Rofin [103]. Nozzles with diameter between 1 and 5 μ m were used, but mainly the experiments were done with $d_0 = 2$ μm nozzles. This microscope illumination shows a nozzle with $d_0 = 2$ μm. The tube channel‘s length is comparable to the nozzle diameter.

assembly prevents any contamination. If the suspicion arose that any pollution could have occurred the nozzle assembly and the supply line was cleaned several times.

5.4 Calibration of the Nozzle Diameter

Investigating the nozzle diameter´s influence to the present effect such as the period of the oscillations the exact nozzle diameter must be determined. Measuring the beam flux intensity through the orifice offers a practical method to determine the exact nozzle diameter [63]. Given by the continuity equation the mass flow rate for a steady, one-dimensional, isentropic flow in a channel is given by

$$\dot{m} = \rho u_{exit} A, \tag{5.1}$$

where ρ is the density, u_{exit} the flow velocity and A the cross section at a given point in a channel. In this approximation Helium is assumed to behave as an ideal gas, so that the flow properties at the nozzle outlet ($A = \pi d_0^2/4$) can be expressed analytically in terms of the source pressure p_0 and temperature T_0. Following the ideal gas equation one obtains

$$\dot{m} = \frac{\pi}{4} d_0^2 \frac{f(\gamma)}{\sqrt{R}} \frac{p_0}{\sqrt{T_0}}, \tag{5.2}$$

with

$$f(\gamma) = \frac{\gamma^{\frac{1}{2}}}{\left(\frac{\gamma+1}{2}\right)^{\frac{\gamma+1}{2(\gamma-1)}}}, \tag{5.3}$$

where R = R/M, with R the universal gas constant and M the molar mass. For Helium one obtains for the quotient $\gamma = c_p/c_v = 5/3$ and R = 2078 J/kg · K. For an ideal gas the mass m is given by $m = pV/RT_{gas}$, whereas the mass flow $\dot{m}$ must coincide with the pV-flow $\dot{Q}$ through the intake port of the source chamber‘s pump. The derivation of the pV-energy can be expressed by $\dot{Q} = p^*_{source} S_1$, where S_1 is the pumping speed at the intake partial pressure in the source chamber p^*_{source}. Assuming that T_{gas} is the temperature of the gas streaming through the pump it follows from the ideal gas equation:

$$pV = mRT_{gas} \Longrightarrow m = \frac{pV}{RT_{gas}} = \frac{Q}{RT_{gas}} \Longrightarrow \dot{m} = \frac{\dot{Q}}{RT_{gas}} \tag{5.4}$$

$$\frac{\Pi}{4} d_0^2 \frac{f(\gamma)}{\sqrt{R}} \frac{p_0}{\sqrt{T_0}} = \frac{\dot{Q}}{RT_{gas}} = \frac{p^*_{source} S_1}{RT_{gas}} \tag{5.5}$$

One obtains for the nozzle diameter d_0

$$d_0 = \sqrt{\frac{4}{\pi} \frac{S_1}{f(\gamma)\sqrt{RT_{source}}} \frac{p^*_{source}}{p_0} \sqrt{\frac{T_0}{T_{source}}}} = d_1 \sqrt{\frac{p^*_{source}}{p_0} \sqrt{\frac{T_0}{T_{source}}}}, \tag{5.6}$$

where $d_1 \simeq 8.16$ cm is a constant obtained with $S_1 = 3 \cdot 10^3$ l/sec and $T_{gas} \approx 300$ K. Equation 5.6 was derived for a single chamber vacuum system, whereas the present experiment consists of two chambers. Both vacuum chambers are equipped with different pumps. Thus, both vacuum systems have different pumping speeds. Therefore, the equation has to be expanded under the assumption that the beam partly evaporates in the source chamber and is finally annihilated in the detection chamber. The calibration was done at room temperature so that the squareroot relation between T_0 and T_{source} in equation 5.6 simplifies. The relation for the nozzle diameter is expressed in the following way:

$$d_0 = 81600 \sqrt{\left(\frac{3.2}{3} \frac{(p^1_{source} - p^2_{source})}{(p^1_0 - p^2_0)} + \frac{2.5}{3} \frac{(p^1_{det} - p^2_{det})}{(p^1_0 - p^2_0)}\right) \cdot \frac{5.9}{1000}} \cdot 10^3 \;\; [\mu m] \tag{5.7}$$

As a standard procedure the pressure in the source chamber pressure p_{source} and detector chamber p_{det} was measured at two different source pressures p_0, generally $p_0^1 =$ 10-20 bar and $p_0^2 = 0$ bar. Comparing the diameter obtained by calibration and the diameter given by the producer it varies in a range of approximately 5-30 percent. The deviation is significantly larger for the 1 μm nozzles. Appendix D gives an overview of the used nozzles.

5.5 Temperature and Pressure Controlling

In section 5.2 the cooling process was described, whereas in this section the procedure of temperature controlling is illustrated. The liquid Helium bath‘s vapor pressure p_{vap} is controlled by a valve[4] placed between the Helium reservoir of the bath-cryostat and the roots pump, as seen in figure 5.3(3). The valve opens or closes depending on p_{vap} with an accuracy of 0.2 mbar. In changing the vapor pressure the temperature is estimated according to:

$$T_0 = 0.432 + 0.00476 * P_{vap}^{0.838} + 0.78955 * P_{vap}^{0.1822} \tag{5.8}$$

According to the exponential dependence between temperature T_0 and vapor pressure p_{vap} the resolution of the vapor pressure p_{vap} ($\pm$ 0.2 mbar) affects the resolution of the temperature T_0, as shown in figure 5.7: For low temperatures $\mathrm{T} < 1.4$ K the temperature resolution approximately amounts to be between 15 and 20 mK, whereas at higher temperatures around 1.86 K the average resolution of the temperature is approximately 4 mK. Nevertheless, the temperature resolution is sufficient for this experiment, even in the low temperature limit.

The source pressure´s resolution is determined visually by a manometer. The pressure is regulated manually by increasing or decreasing the valve. The manometer‘s range is between 0 and 100 bar with a resolution of 0.5 bar. The source pressure p_0 was detected manually. Thus, an error for p_0 of +/- 0.1 bar is assumed.

5.6 Data Acquisition and Processing

The most interesting observable in this experiment is the detector pressure p_{det} . This pressure p_{det} is measured as a function of time. To determine p_{det} a conventional Bayard-Alpert ionization pressure gauge of type Huntington Typ TK-150 was used. The signal was amplified with a Granville Phillips Ionization Gauge Controller type 330 and finally digitalized with a Keithley 2000 voltmeter. Via a GPIB interface card (IEEE 488) the signal was recorded with a conventional Lab View Software [85] of National Instruments. The corresponding Lab View programm recorded the detector pressure as a function of time with a minimal resolution of one data value each 100

---

[4] Control Butterfly Valve by VAT with included step motor DN 63 Series 61.1, controlled by a VAT Adaptive Pressure Controller PL-3

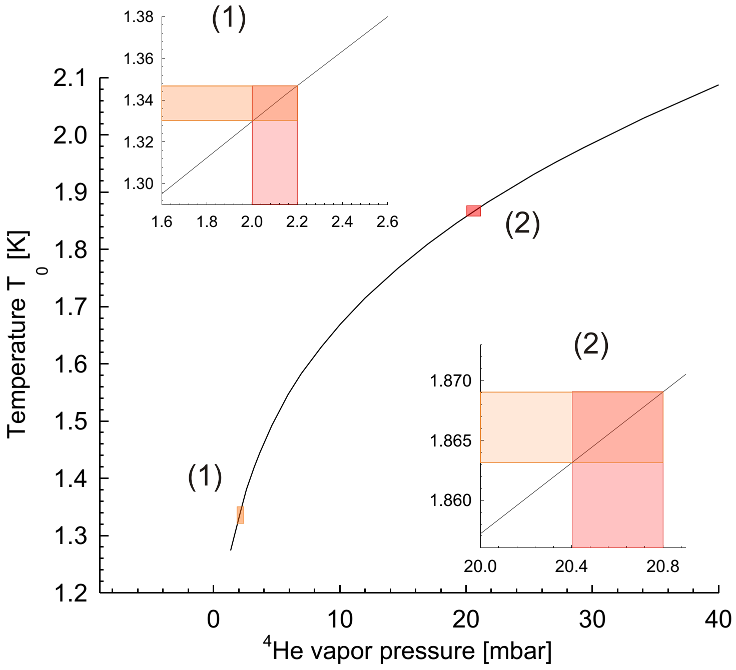

Figure 5.7: Temperature T_0 as a function of the vapor pressure p_{vap} in the low temperature regime. The exponential dependence affects the resolution in temperature: At temperatures above 1.8 K the resolution of $p_{vap} = 0.2$ mbar changes the temperature of about 4 mK. At lower temperatures $T_0 < 1.4$ K the resolution amounts between 15 and 20 mK. The data of $p_{vap}(T)$ are taken from [122].

msec. The average resolution in time was 250 msec up to 500 msec. Additionally the synchronous recording of the source temperature T_0 was also done with the same data acquisition via GPIB.

Chapter 6

Experimental Results

6.1 Investigations of the Liquid Beam

If the cryostat‘s temperature reaches 4.3 K the Helium gas streaming through the nozzle liquifies and generates a beam of liquid Helium. The liquid jet propagates as a smooth cylindrical filament until it spontaneously breaks up into a stream of monodisperse droplets [46]. Figure 6.1 shows a picture of the liquid Helium jet. Additionally, the mechanism of Rayleigh break up is illustrated, where L is the filament‘s length.

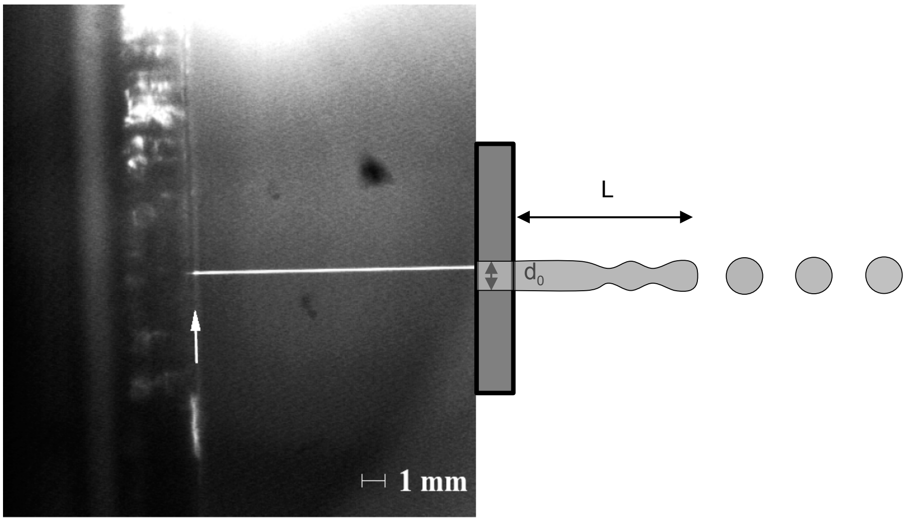

Figure 6.1: Left: Picture of the uniform Helium jet [64]. Right: According to the behavior of Rayleigh breakup the uniform filament breaks up into single droplets at a definite decay length L.

The condition for this type of jet decay is a laminar flow inside the orifice, defined by the Reynolds numbers $Re = \rho v d_0/\eta \approx 1200$, where ρ, v and η are the density, velocity and viscosity of the liquid, respectively. In this regime the decay length L is given by [64]

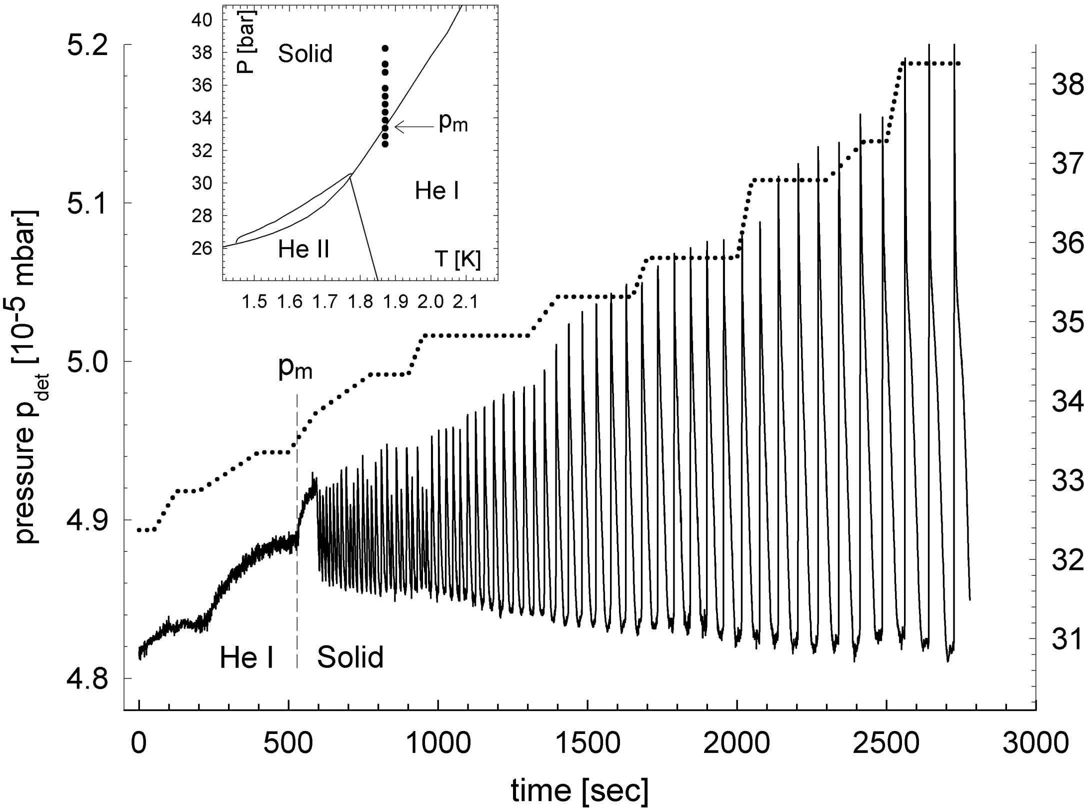

Figure 6.2: Detector chamber pressure p_{det} as a function of time. At a constant temperature T = 1.87 K the source pressure p_0 (dotted line) is increased stepwise from below to above the melting pressure p_m (right scale). At pressures p_0 above the melting pressure the detector pressure p_{det} starts to oscillate with a definite period τ in the range of seconds up to minutes. The amplitude and the period τ increases with the source pressure p_0. ($d_0(\#16) = 2.0\ \mu$m)

$$L \simeq 12v[\sqrt{\frac{\rho d_0^3}{\sigma} + \frac{3\eta d_0}{\sigma}}] \tag{6.1}$$

where σ is the surface tension of the liquid. For low viscosity fluids the droplet formation point primarily depends on the first term in equation 6.1. With $d_0 = 2\mu$m, $\rho(^4\text{He}) = 125$ kg/m^3, $\sigma(^4\text{He}) = 2.39 \cdot 10^{-4}$ N/m and the exit velocity $v \approx 200$ m/sec the filaments length can be determined to be L ≈ 5 mm. After leaving the nozzle the liquid Helium beam is cooled down by evaporative cooling to a final temperature of about $T = 0.42$ K. Approximately 20% of the liquid vaporizes and sees to it that the pressure p_{source} inside the source chamber increases, as well.

Liquid Helium jets have been copiously investigated by Grisenti [64] and Grams [56]. This work is devoted to investigate the oscillations of the beam flux intensity. The most interesting observable is the period τ and its dependence on temperature T and source pressure p_0. The investigation of the Geyser effect separates in two parts. As to be seen the behavior of the period τ changes at temperatures below $T_c = 1.58$ K. Section 6.2 shows the experimental results at $T_0 > 1.7$ K and the following section 6.3 presents the investigations obtained in the temperature range below 1.7 K. Section 6.4 illuminates the investigations of the influence of Helium-3, and finally the influence of the nozzle diameter is presented in section 6.5.

6.2 Experimental Results at $T_0 > 1.7$ Kelvin

This section shows the experimental results of the period‘s dependence on source pressure p_0 and temperature $T_0 > 1.7$ K. The section begins with the results of τ as a function of the source pressure p_0 at fixed temperature T_0. Then the dependence of the period τ is shown as a function of temperature T_0 at fixed source pressure p_0.

6.2.1 Dependence on Source Pressure with Fixed Temperature

The experimental results of the investigation of the Geyser effect in solid Helium-4 begins with the dependence on the source pressure p_0 at constant temperatures $T_0 > 1.7$ K. Figure 6.2 shows the time dependent pressure p_{det} in the detector chamber while the source pressure p_0 is increased from pressures below p_m corresponding to the liquid phase at a constant temperature T = 1.87 K. As long as the source pressure $p_0 < p_m$ (0 - 500 seconds) the detector pressure p_{det} is related to the source pressure p_0 by the bernoulli relation $p_{det} \propto \sqrt{p_0}$, as seen for $p_0 < 33.4$ bar. After 200 and 500 seconds the pressure p_0 is increased of 0.5 bar, respectively. By increasing p_0 above p_m the beam flux intensity starts to oscillate. The period τ and the amplitude increases with increasing the source pressure p_0. In figure 6.3 the time dependent detector pressure p_{det} of the measurement shown in figure 6.2 is shown for several source pressures p_0 in a stretched time scale. The oscillations occur not right at source pressure $p_0 = p_m = 33.4$ bar, but slightly above at a certain pressure p_τ that is between the melting pressure p_m and 34 bar. The oscillations are constant in period, period shape and in intensity, as well. The period τ at $p_0 = 34$ bar is in order of seconds ($\tau \approx 7$ seconds) and increases up to $\tau \approx 82$ seconds for $p_0 = 38.4$ bar.

The same kind of measurement is also done for several source temperatures to show that p_τ corresponds to p_m. Figure 6.4 shows the result obtained with four different temperatures between 1.78 and 1.98 K. The source pressure p_0 (dotted line) is increased of about 0.5 bar at time intervals of $\approx$ 100 seconds, respectively. The detector pressure p_{det} is observed to oscillate if the source pressures p_0 is right above the melting pressure p_m. Investigating the temperature range between 2.1 K and 1.78 K the periodic behavior always occurs at the melting line by increasing the source pressure p_0 at fixed temperature, as seen in figure 6.5. Deviations of p_τ(T) from the melting line are explained by the resolution of the source pressure: the increase of the source pressure occurred with a resolution of 0.5 bar according to the minimum scale range of the manometer. The pressure was recorded visually. Regarding figure 6.4 the change of

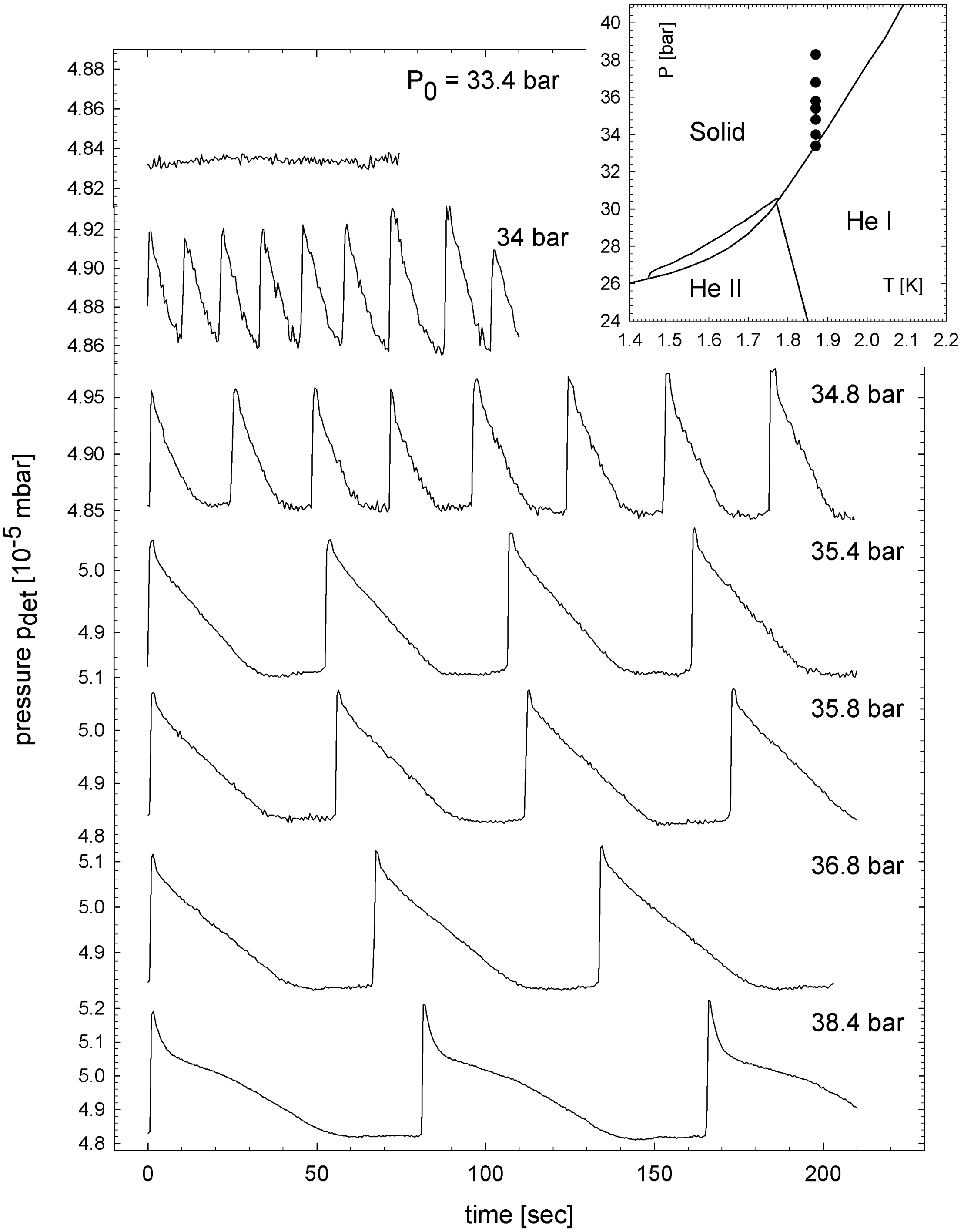

Figure 6.3: Increasing the source pressure p_0 at a source temperature T = 1.87 K. The measurement is also shown in figure 6.2. Following the corresponding points in the phase diagram the pressure p_{det} inside the detection chamber increases. If the source pressure overcome the melting line the detector pressure signal starts oscillating. The period τ increases with increasing the source pressure p_0. ($d_0(\#16) = 2.0\ \mu$m)

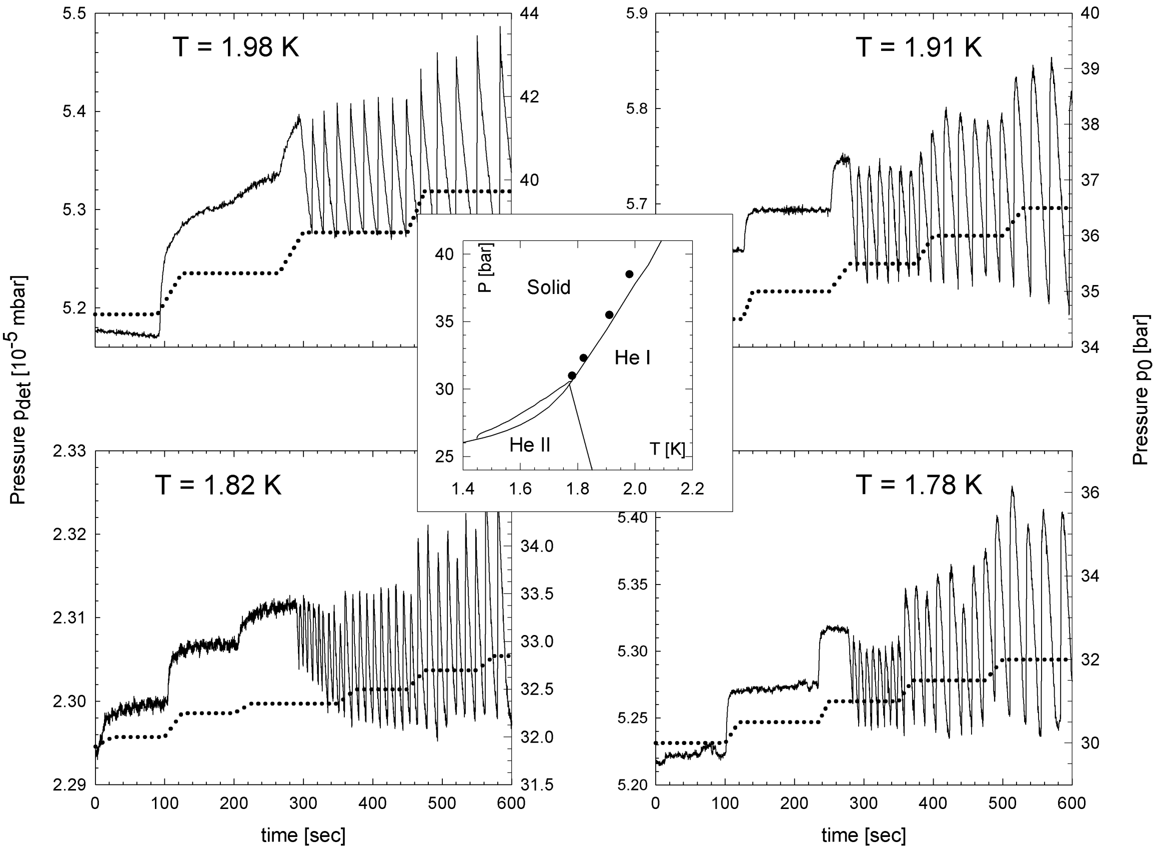

Figure 6.4: Time dependence of the detector pressure p_{det} at constant source temperatures T between 1.78 and 1.98 K by increasing the source pressure p_0. Starting from pressures below p_m the source pressure p_0 (dotted line) is increased of about 0.5 bar in time intervals of $\approx$ 100 seconds. At pressures $p_0 > p_m$ the detector pressure p_{det} oscillates in the range of seconds. The corresponding pressure p_τ(T) is found to be approximately the melting pressure p_m The points in the phase diagram indicate p_τ(T) at the temperatures T and source pressures p_0, at which the oscillations occur. (nozzle diameter: T = 1.98 K $d_0(\#16) = 2.0$ μm, T = 1.91 K and T = 1.78 $d_0(\#26)$ = 1.3 μm, T = 1.82 K ($d_0(\#27) = 1.81$ μm)

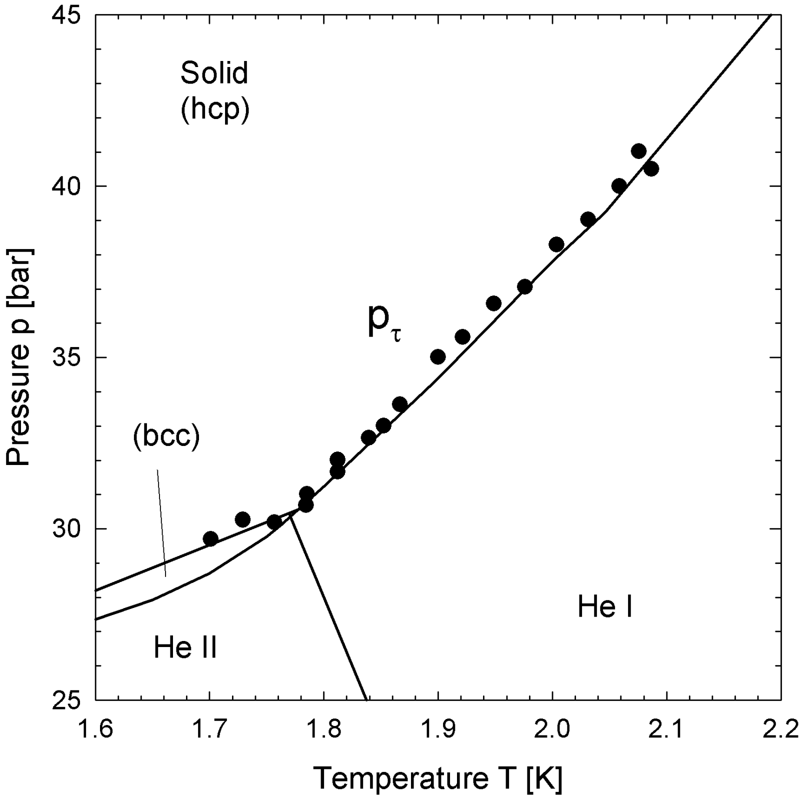

Figure 6.5: Pressure p_τ(T) at which the oscillations start to occur by increasing the source pressure p_0 starting in the liquid phase in a temperature range between 2.1 and 1.7 K: The pressure $p_\tau \approx p_m$ indicates that the effect is related to the solid phase of Helium-4. Small deviations of p_τ from the melting pressure are explained by the resolution of the source pressure: the increase of p_0 occurred with a resolution of 0.5 bar according to the minimum scale range of the manometer.

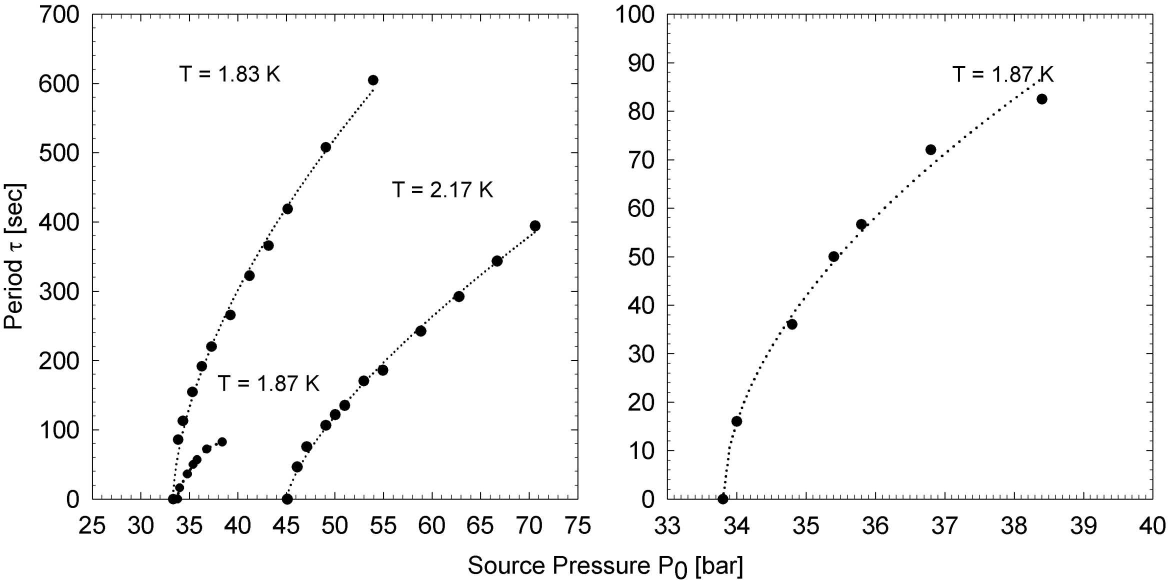

Figure 6.6: Period τ as a function of source pressure p_0 at fixed source temperature T = 1.83, 1.87 and 2.17 K, respectively. On the right side the dependence $\tau(p_0)$ is shown again at temperature T = 1.87 in a corresponding scale. The pressure range of p_0 up to 30 bar above the melting pressure offers a relation between p_0 and τ as derived in equation 7.1

the source pressure p_0 and the detection pressure p_{det} practically occurs without any delay.

The dependence $\tau(p_0)$ for three different temperatures T = 1.83, 1.87 and 2.17 K is shown in figure 6.6. The dependence of the period as a function of the source pressure is found to be non-linear. The period is investigated for source pressures up to 30 bar above the melting pressure p_m. As p_0 increases above the melting pressure p_m the period τ changes according to:

$$\tau = \varrho(p_0 - p_m)^\gamma, \tag{6.2}$$

with a critical exponent γ between ≈ 0.5 and 0.7 and ϱ as a pre-factor in the range about $10 - 10^2$. In section 7.10 the coefficients are presented separately for each temperature.

The period τ is obtained from the oscillating detector pressure p_{det}. Figure 6.7 shows the time dependent detector pressure p_{det} monitored at temperature T = 1.83 K for source pressures p_0 between 32 and 54 bar. At pressures $p_0 > p_m$ the detector pressure shows the expected oscillations. The period τ increases with increasing source pressures p_0. The noisy signal of the vacuum detector pressure p_{det} results from an early experimental setup where the noise of the used roots pump in the source chamber affected the detector signal. Typically, for pressures close to p_m the periodic curve shape shows a sawtooth like behavior. For higher source pressures $p_0 > 45$ bar the curve

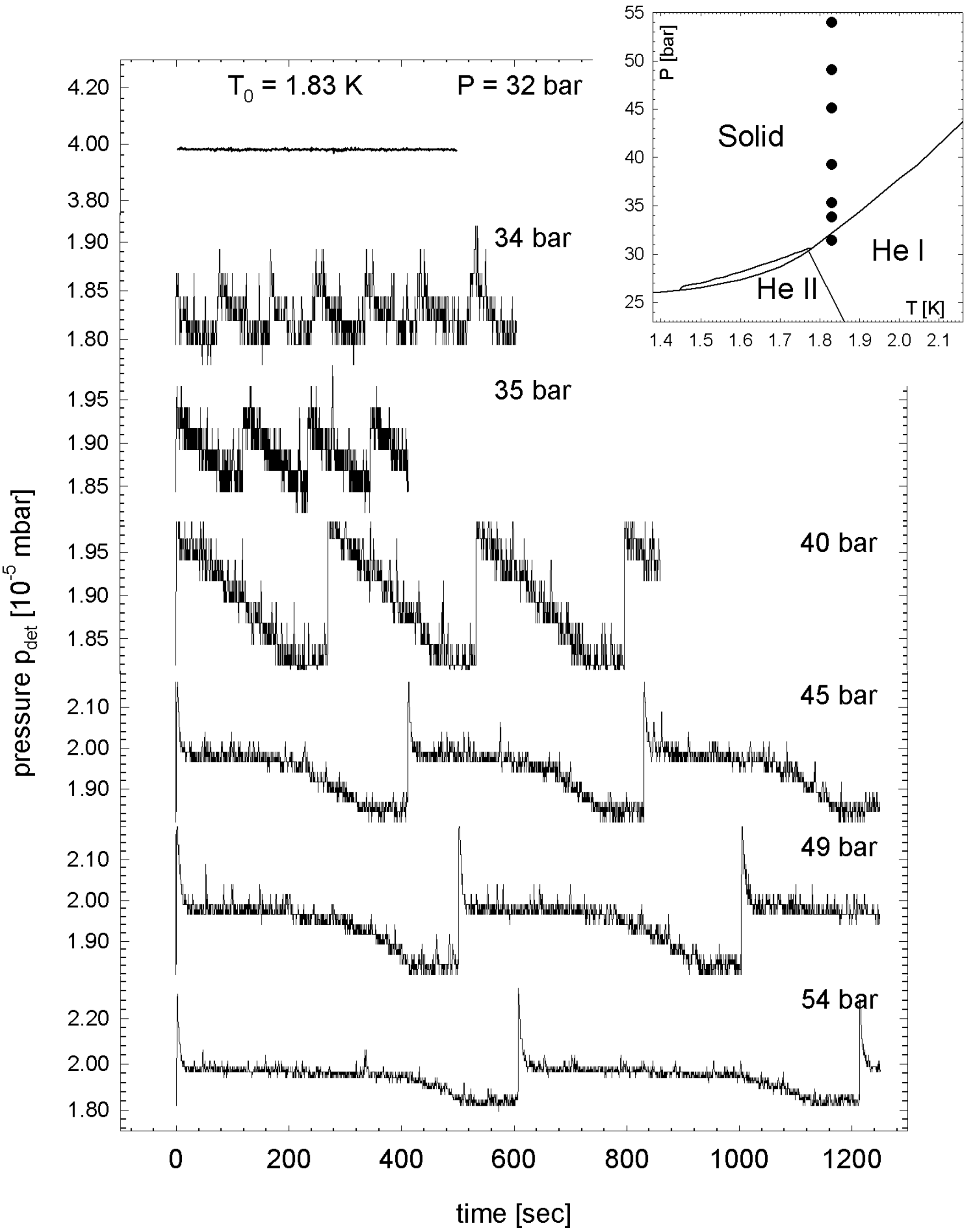

Figure 6.7: Time dependent detector pressure p_{det} monitored at temperature T = 1.83 K for source pressures p_0 between 32 and 54 bar. The phase diagram in the inlet shows the corresponding source pressures p_0. At pressures $p_0 > p_m$ the detector pressure shows the expected oscillations. The period τ increases with increasing source pressures p_0. ($d_0(\#05) = 2.0$ μm)

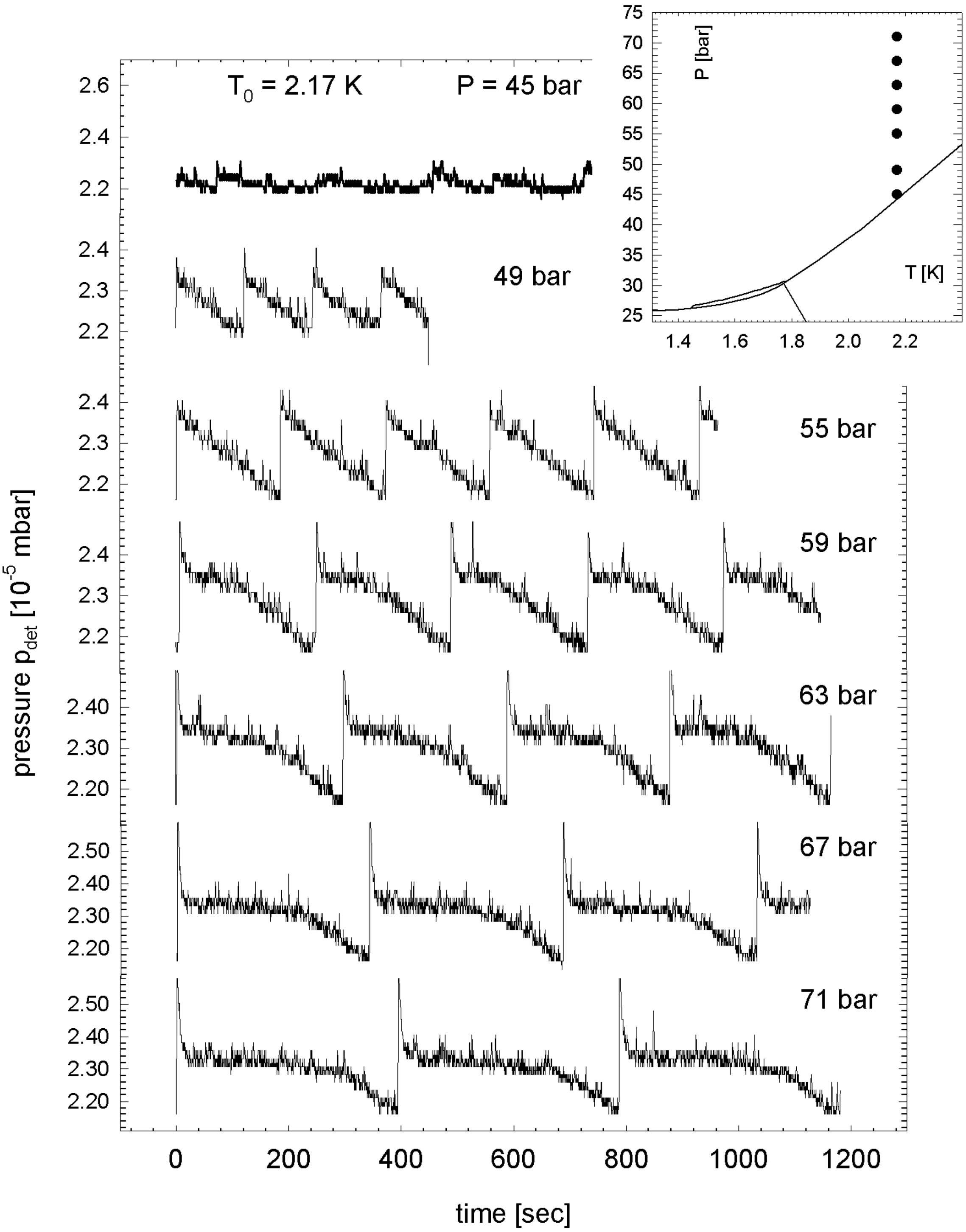

Figure 6.8: Time dependent detector pressure p_{det} monitored at temperature T = 2.17 K. The source pressures p_0 was increased between 45 and 71 bar. The phase diagram in the inlet shows the corresponding source pressures p_0. At pressures $p_0 > p_m \approx 45$ bar the detector pressure p_{det} shows the oscillating character. The period τ increases with increasing source pressures p_0. ($d_0(\#05) = 2.0$ μm)

shape shows a sharp peak. In figure 6.6 the period $\tau(p_0)$ is also shown for temperature T = 2.17 K. The corresponding oscillations of the detector pressure p_{det} are presented in figure 6.8 at source pressures between 45 and 71 bar. For both temperatures T = 1.83 and 2.17 the curve shape of the oscillating detector pressure p_{det} is found to be identical.

The results can be summarized as follows: The period $\tau(p_0)$ is found to be increasing with increased source pressure p_0. In the temperature range between 2.1 and 1.8 K the oscillation of the detector pressure p_{det} occurs at source pressures $p_0 \approx p_m$. One more detail can be observed in the experimental results: In figure 6.6: At a constant source pressure $p_0 = 50$ bar the period is found to be $\tau(\mathrm{T}_1) \approx 140$ sec at temperature $\mathrm{T}_1 = 2.17$ K. For the same source pressure p_0 and temperature $\mathrm{T}_2 = 1.83$ K is found to be $\tau(\mathrm{T}_1) \approx 530$ sec. Thus, the results show that with decreasing temperature T and constant source pressure p_0 the period τ increases. The investigation of this behavior is shown in the following section.

6.2.2 Dependence on Temperature with Fixed Source Pressure

In this section the beam flux intensity is investigated at fixed source pressure p_0 and decreasing source temperature T_0 starting from the liquid phase, respectively. In this work one of the main topics is the investigation of the period τ as a function of temperature T. The first experimental results are shown in figure 6.9. Beginning at temperature $\mathrm{T}_0 = 1.9$ K and fixed source pressure $p_0 = 35$ bar the detector pressure p_{det} is monitored as a function of time. In intervals of approximately 300 till 1500 seconds the temperature was stepwise decreased about $\Delta\mathrm{T} \approx 0.2$ K. In the inset of figure 6.9 the phase diagram indicates the process of the measurement. The detector pressure doesn't show any oscillating character as long as the conditions belong to the liquid phase, similar to the results obtained in the previous section. The maximum of the oscillating peaks is observed to be always constant at $p_{det} \approx 4.16 \cdot 10^{-5}$ mbar. The observation indicates that the beam flux intensity after the collapse is temperature independent. Besides the peak´s amplitude the period is the second parameter that increases with decreasing temperature.

The same data are presented in figure 6.10 where the obtained period τ is shown as a function of temperature. The oscillations of p_{det} occur at T = 1.9 K with a period $\tau \approx$ 10 sec. At temperatures T > 1.78 K the period increases almost linear with decreasing temperature. At T = 1.78 K the extraordinary increase of the period is recognizable. This temperature corresponds to the transition between the hcp and bcc phase, as to be seen in the phase diagram of figure 6.10 (dashed line). In figure 6.9 the temperature is T = 1.78 K is reached at time t = 3600 sec which is indicated with the dashed line. The time range is split into times according to temperatures above (1) and below (2) the hcp-bcc transition temperature T = 1.78 K. Whereas in this illustration of the time dependent detector pressure $p_{det}(t)$ the enormous increase of the period is not pronounced.

To show the effect more distinctive the oscillating detector pressure p_{det} is shown in

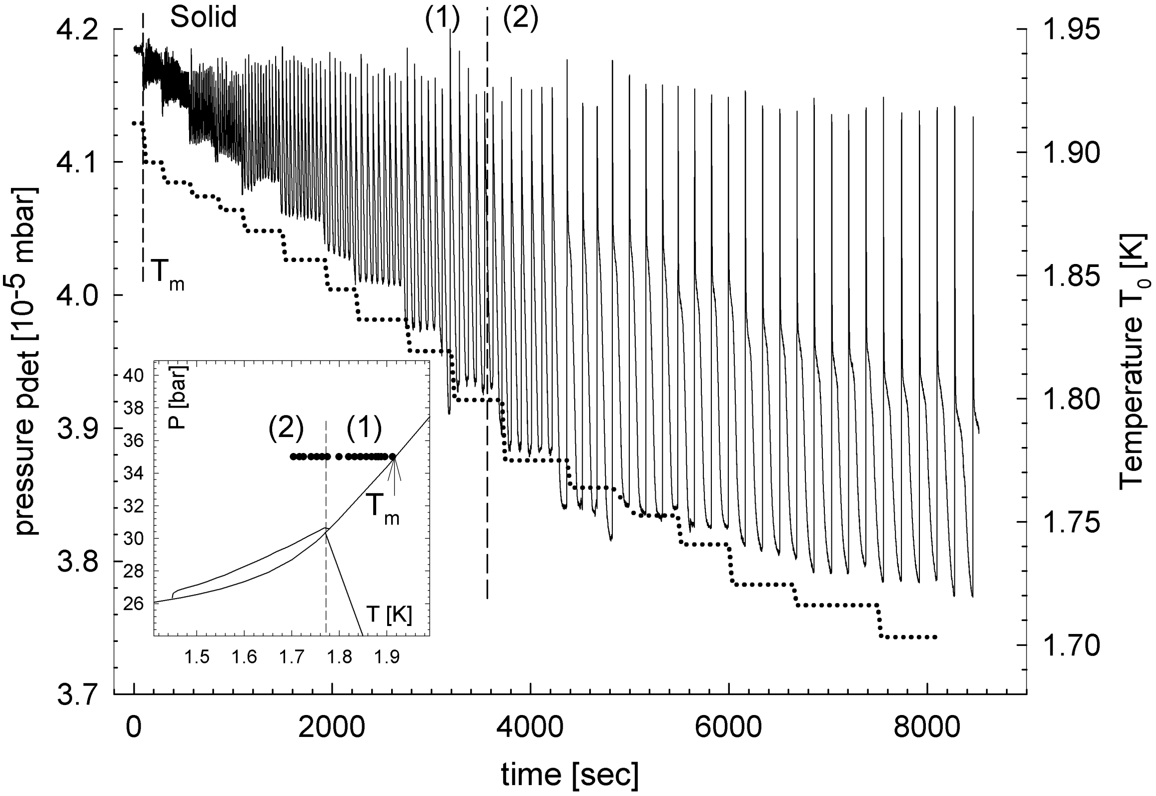

Figure 6.9: Time dependent measurement of the detector pressure p_{det} with decreasing source temperature from 1.9 K down to 1.7 K and fixed source pressure $p_0 = 35$ bar. The temperature is indicated with the dotted line (right scale). The left scale shows the detector pressure p_{det}. The temperature was decreased stepwise in intervals of 300 till 1500 seconds. The inset shows the region of the measurement in the phase diagram. At temperatures below the melting temperature T$_m$ the detector pressure p_{det} oscillates. With decreasing temperature the period τ and the period‘s amplitude increases. The top of the amplitude shows a fixed line at the maximum detector pressure $p_{det} \approx 4.16 \cdot 10^{-5}$ mbar. The temperature range is split (dashed line at t = 3600 sec): at temperatures T > 1.78 K (1) the solid is hcp ordered, whereas at T < 1.78 K (2) for low pressures the bcc phase occurs. (nozzle diameter: $d_0(\#17) = 2.28$ μm)

figure 6.11 with an increased time resolution for some selected temperatures above and below T = 1.78 K. For T > 1.78 K the oscillating curve shape is observed to be almost independent of temperature. The curve shape at temperatures close to the melting line (T = 1.90 K) is comparable with an asymmetric sawtooth signal. The shape shows a linear positive slope up to the maximum of p_{det} followed by a negative linear slope down to the minimum detector pressure $p_{det,bg}$. With the increased time resolution the enormous increase of the period τ is presented much more detailed at temperatures T < 1.78 K. Also the periodic curve shape changes explicitly. The sharp peak is identical, whereas the attenuating part shows a much more detailed shape.

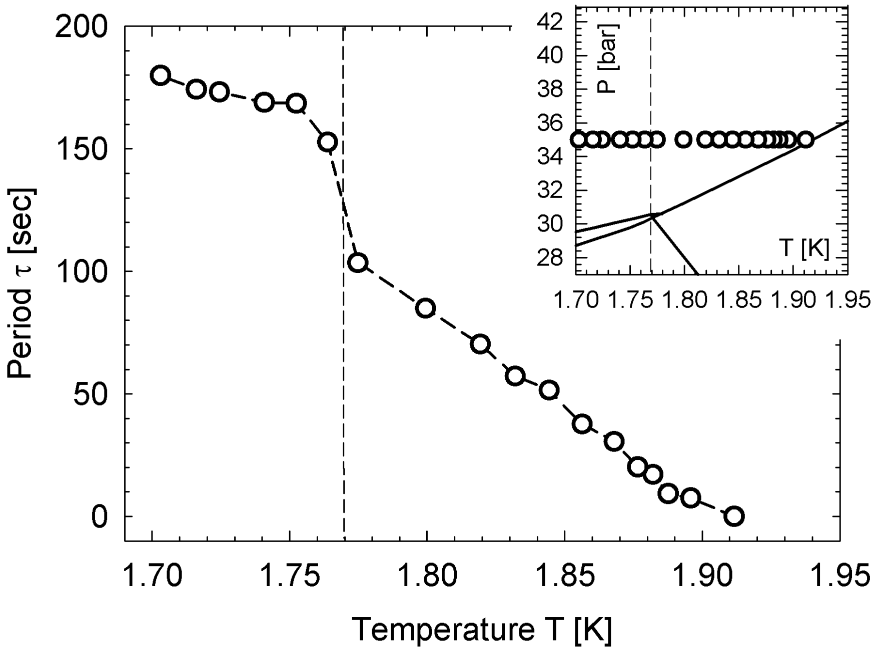

Figure 6.10: Period τ as a function of temperature at p_0 = 35 bar according to the measurement of figure 6.9. The temperature range is split for temperatures above and below 1.78 K (dashed line) For T > 1.78 K the period τ increases almost linear with decreasing temperature. At T < 1.78 K the period τ increases extraordinarily. The separation of the temperature range is also shown in the phase diagram. At T = 1.78 K the transition between the hcp and bcc phase of Helium-4 occurs.

The temperature dependence of the period τ is also investigated for several source pressures p_0. The results obtained for τ(T) for source pressure p_0 = 32, 35 and 41 bar, respectively, is presented in figure 6.12. Independent of the source pressure the period τ increases almost linearly with decreasing temperature. At temperatures T ≈ 1.78 K the period increases extraordinarily. The measurements show that the increase is independent of the source pressure p_0 and depends only on the temperature T. A possible explanation is given by considering the phase diagram: The temperature T = 1.78 K corresponds to the hcp-bcc phase transition.

The investigation of the temperature dependence of the period τ shows that the period

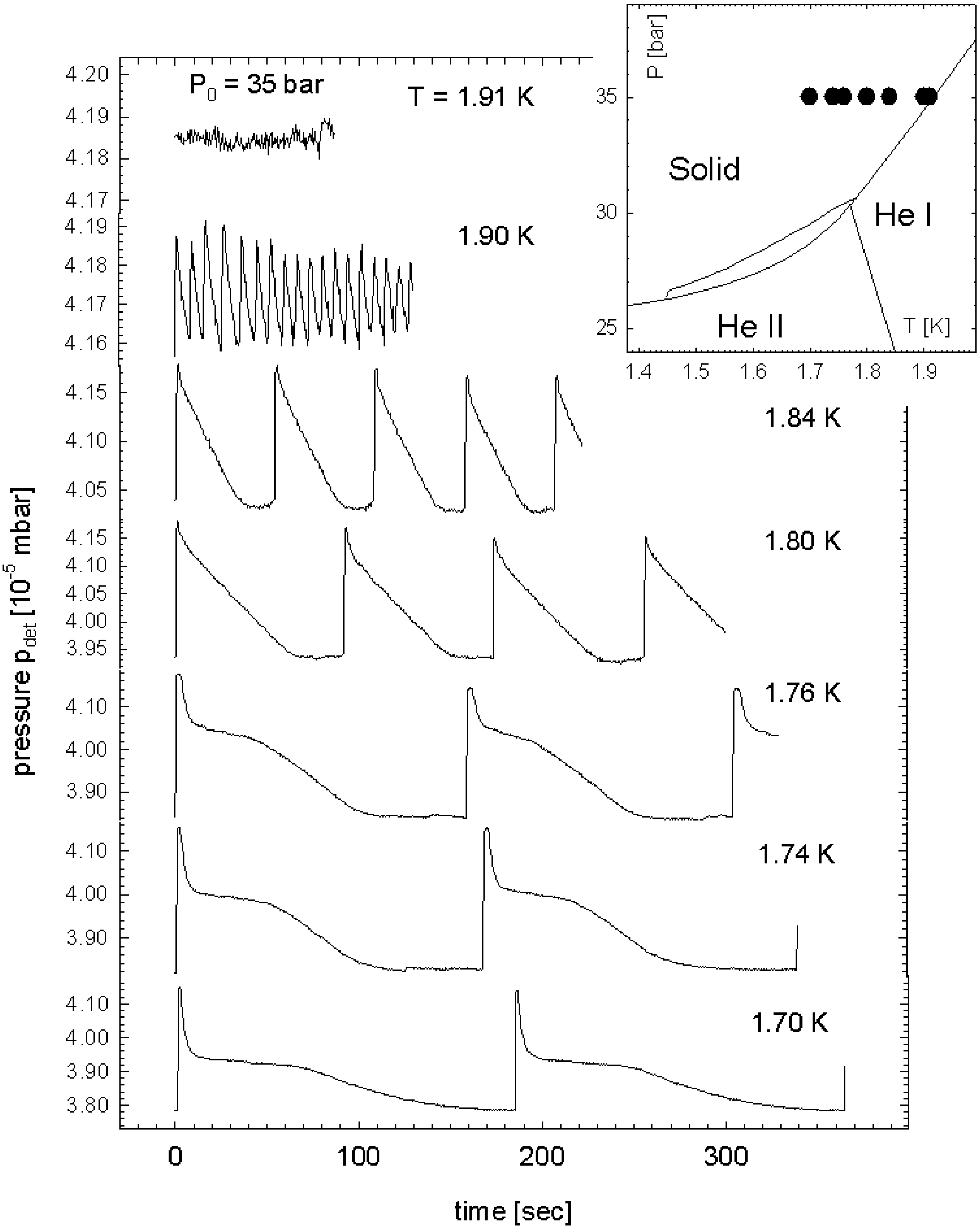

Figure 6.11: The oscillating detector pressure p_{det} as a function of temperature and constant source pressure $p_0 = 35$ bar. According to figure 6.9 the signal is shown with an increased time resolution for some selected temperatures above and below T = 1.78 K. At temperatures T = 1.78 K the period τ increases extraordinarily and the periodic curve shape alters for low temperatures. ($d_0(\#17) = 2.28$ μm)

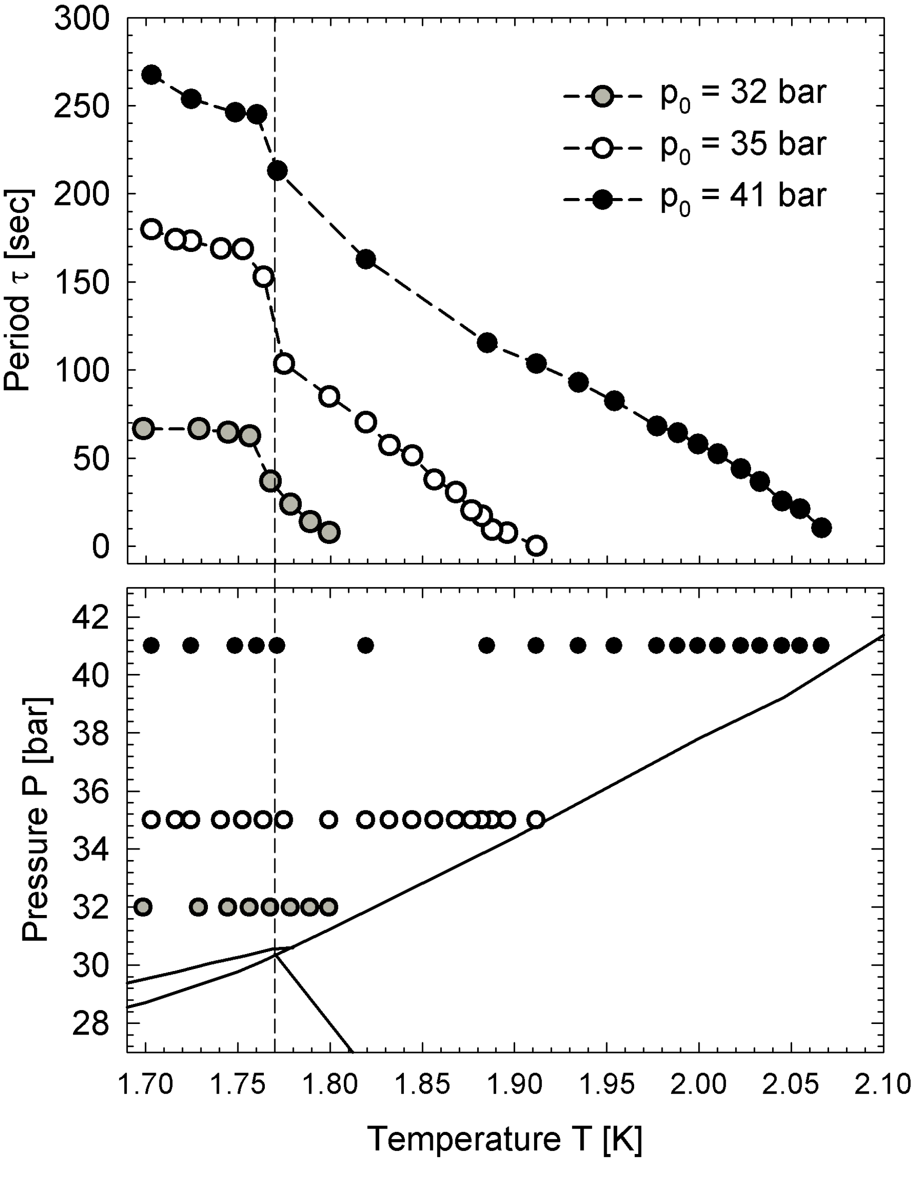

Figure 6.12: Period τ as a function of temperature at three different source pressures $p_0 = 32$, 35 and 41 bar, respectively. Independent of p_0 the period jumps up at $T_0 \approx 1.78$ K, indicated by the dashed line. The result is associated to be depending on the hcp-bcc phase transition. Similar to the investigations of increasing the source pressure the periodic effect appears right at the melting line at corresponding melting temperature. ($d_0(\#17) = 2.28\ \mu$m)

increases with decreasing temperature. The enormous increase of τ at T = 1.78 K will be explained by the change of the crystalline structure in section 7.9. The results show that the period acts very sensitive to changes in the structure of solid Helium. As to be seen in the next section the periodic behavior exhibits an unknown behavior of solid Helium-4 that can be investigated explicitly by the dependence of the period as a function of pressure and temperature.

6.3 Experimental Results at $T_0 < 1.7$ Kelvin

In this section the investigation of the period τ in the temperature regime below 1.7 K is presented. The experimental results are obtained in the same way as the results in the previous section. The period is investigated as a function of temperature at fixed source pressure, and vice versa. First, the periodic behavior is illustrated as a function of temperature at fixed source pressure. As a main result below $T_c = 1.58$ K the period decreases with decreasing temperature, showing the exact opposite behavior as for temperatures above 1.58 K. Therefore, a critical temperature $T_c = 1.58$ K is introduced. As to be seen in figure 6.13 the curve shape is independent of the source pressures and temperatures $T < T_c$. Finally the periodic behavior depending on source pressure p_0 is shown. The results exhibit the existence of two regimes in the phase diagram of solid Helium-4 in which oscillations are not observable in the signal of the detector pressure p_{det}.

6.3.1 Period as a Function of Temperature

In this section the period τ is investigated as a function of temperature below 1.7 K at constant source pressure p_0. In figure 6.14 the period τ is shown at fixed source pressure $p_0 = 33$ bar. For temperatures between $T_0 = 1.85$ K and 1.42 K. The corresponding temperatures and pressures are shown in the phase diagram below. Down to T = 1.78 K the period τ increases linearly with decreasing temperature. At 1.78 K (right dotted line) there is a step rise in the period as already discussed. Further decreasing of the temperature down to $T_c = 1.58$ K let the period increase to a maximum value of τ_{max} = 124 seconds (left dotted line). The temperature where the maximum of τ occurs is denoted as the critical temperature T_c. For temperatures between $T_c = 1.58$ K and 1.5 K the period decreases. Below T = 1.5 K the period is almost constant around $\tau_{min} \approx 50$ seconds. The critical temperature T_c seems to split the phase diagram in two temperature regimes.

The first hint is given by the corresponding detector pressure p_{det}. According to the measurement shown in figure 6.14 the oscillating detector pressure p_{det} is presented for several temperatures in figure 6.15. The observed oscillations at temperatures T > 1.64 K correspond to the results of the previous section: the curve shape of the oscillations changes significantly at temperatures below T = 1.78 K. After the peak occurs (t = 0) the detector pressure p_{det} decreases down to a plateau ($\approx 4.52 \cdot 10^{-5}$ mbar for T = 1.64 K). Again, the detector pressure p_{det} decreases for times t > 60 seconds till the next peak occurs. At temperature $T_c = 1.58$ K the period τ is maximal. Comparing the corresponding curve shape with the plateau at T = 1.65 K the detector pressure decreases to $p_{det,bg}$. Below T_c the shape canges to a single narrow spike followed by a plateau. Furthermore the period‘s amplitude decreases with decreasing temperature.

The temperature dependence of the period τ in the regime above and below 1.58 K is also investigated for several source pressures p_0. In figure 6.16 the period τ is shown as a function of temperature for six different source pressures p_0 between 29 and 40.3

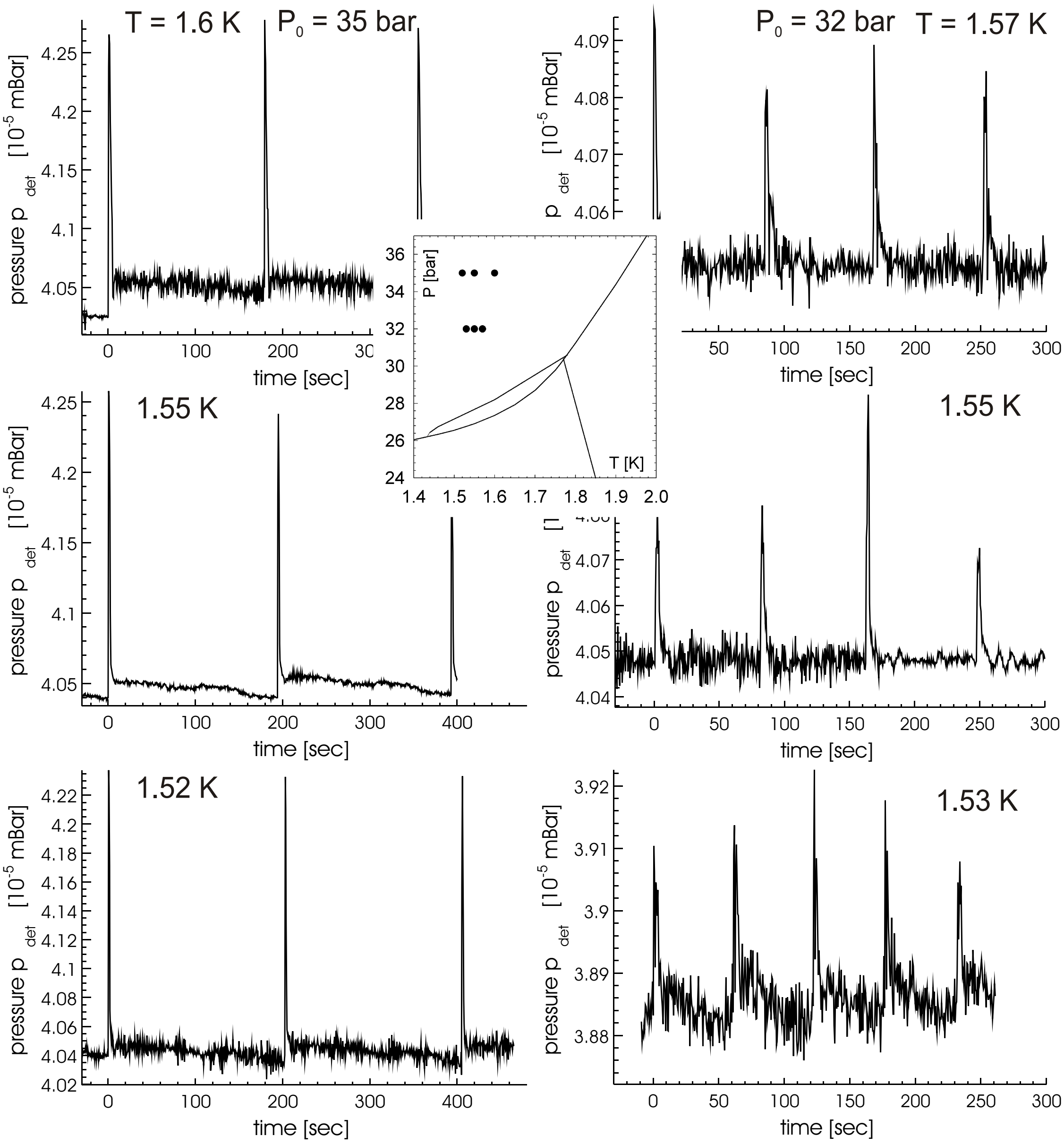

Figure 6.13: Periodic shape below 1.58 K at different source pressures and temperatures T < 1.58 K. The shape is always identical, whereas the peak´s amplitude depends on the source pressure. As a main result the period τ is shorter than for temperatures T $\approx$ 1.58 K. ($d_0(\#17) = 2.28\ \mu$m)

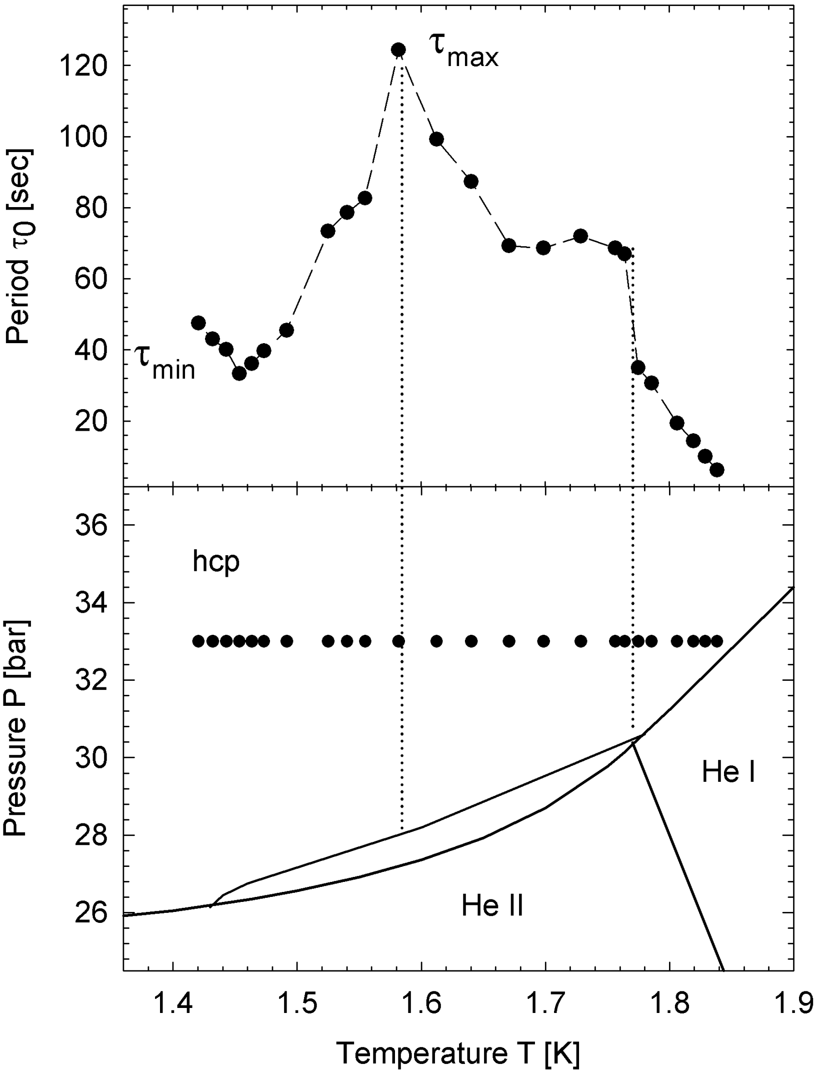

Figure 6.14: The period τ as a function of temperature at constant source pressure p_0 = 33 bar. Below the points of the measurements are indicated in the phase diagram of Helium-4. At temperatures T > 1.58 K the period τ increases with decreasing temperature. At T = 1.78 K (right dotted line) the period τ increases extraordinarily. At T_c = 1.58 (left dotted line) the period τ_{max} = 124 seconds is maximal. Whith decreasing the temperature below 1.58 K the period decreases down to $\tau_{min} \approx 50$ seconds. ($d_0(\#20) = 2.07\ \mu$m)

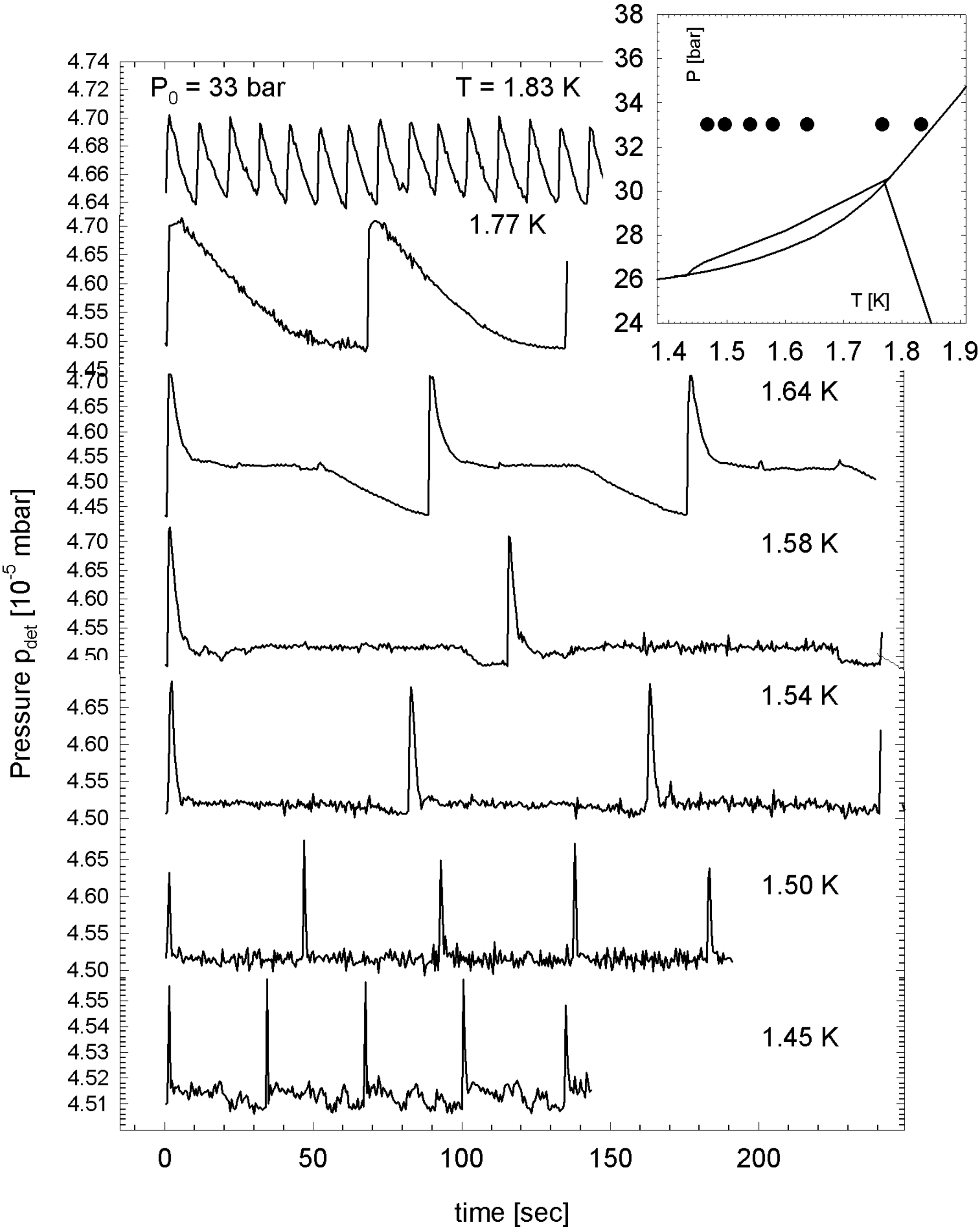

Figure 6.15: Time dependent detector pressure p_{det} for several temperatures at constant source pressure $p_0 = 33$ bar. The curve shape of the oscillations alters in crossing T = 1.78 K. As seen for T = 1.64 K the signal decreases down to a plateau ($\approx 4.52 \cdot 10^{-5}$ mbar) after the peak occurred. For times t > 60 seconds the detector pressure p_{det} decreases again till the next peak occurs. At temperature $T_c = 1.58$ K the period τ_{max} is maximal. Compared with the plateau at T = 1.64 K the detector pressure decreases more intensive. This behavior becomes more detailed at temperatures T < T_c. The period decreases and the periodic signal just consists of a peak and a flat plateau. As a further observation the period‘s amplitude decreases with decreasing temperature. ($d_0(\#20) = 2.07$ μm)

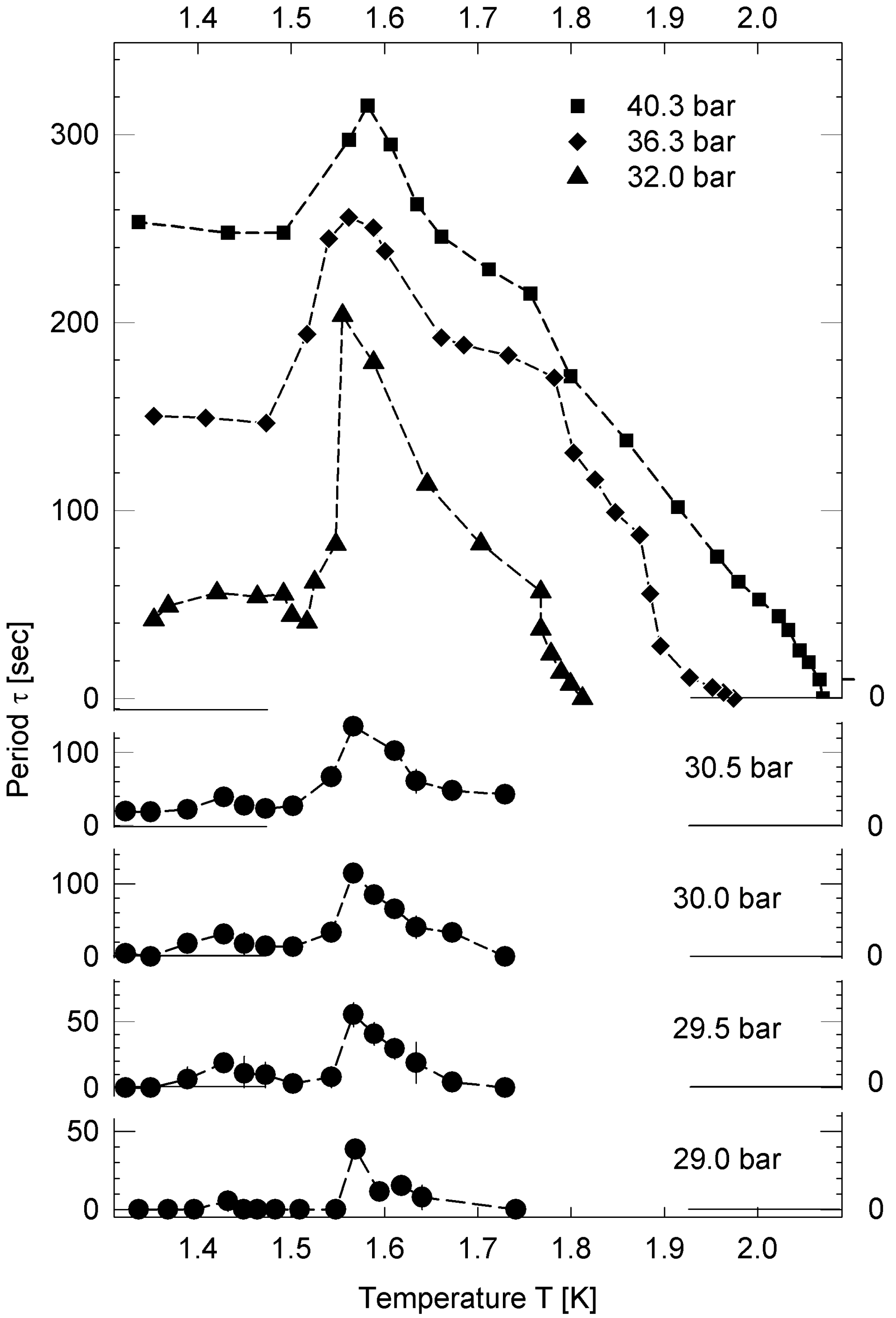

Figure 6.16: Period as a function of temperature for a wide range of source pressure between 29 and 40.3 bar. At 1.58 K the period peaks whereas it drops down with decreasing the temperature T. The phenomenon seems to be depending on the source pressure in that way that the percentage dropdown increases in decreasing the source pressure. For the regime of source pressures below $p_0 = 31$ bar the period drops down to zero, whereby the oscillating character of p_{det} vanishes. (nozzle diameters: $p_0 =$ 29.0-30.5 bar $d_0(\#22) = 2.2$ μm $p_0 = 32.0$ bar $d_0(\#17) = 2.28$ μm, $p_0 = 36.3$ and 40.3 bar $d_0(\#06) = 2.2$ μm)

bar. The measurements at source pressures p_0 = 32, 36.3 and 40.3 bar show in a distinctive way the decrease of the period τ at temperatures below $T_c = 1.58$ K. The critical temperature varies by only ± 0.02 K.

At 29 bar the periodic effect below 1.58 K vanishes completely, excluding at T = 1.42 K. At low source pressures a second maximum of the period appears. The temperature of 1.42 K marks the temperature at which the bcc-hcp transition occurs at the melting line. Comparing the increase of the period τ at T = 1.78 K and 1.42 K it seems that the phase transition bcc-hcp back and forth affects the period τ, as already seen in the previous section. For high pressures the effect at 1.42 K seems to vanish, which is probably related to the low resolution of the temperature.

The vanishing of the oscillating character of the detector pressure p_{det} below 1.58 K and 30 bar indicates a phase transition. For temperatures above 1.78 K the melting line is found to be the phase line for vanishing oscillations. Compared with this temperature regime the new phenomenon of vanishing oscillations in the solid phase indicates that solid Helium-4 below 1.58 K and source pressures of 3-5 bar above the melting line behaves like a liquid.

Investigations at pressures between the melting line and close above do not exhibit any oscillations of the detector pressure p_{det}. The method of varying temperature at fixed source pressures gives rise of a new phase line in solid Helium-4, but is not very useful to detect such a phase line. The method of increasing pressure at fixed temperature seems to be more promising. In section 6.2.1 the phase line for temperatures $T > 1.7$ K is determined in finding the pressure p_τ at which the detector pressure p_{det} starts to show the oscillatory behavior.

6.3.2 Period as a Function of Pressure

As a main result of section 6.2.1 the oscillating character occurs by increasing the source pressure p_0 above the melting pressure p_m at constant temperature $T > 1.78$ K. In this section the same measurements at temperatures below 1.78 K are presented. The source pressure p_0 is increased with time in intervals of about 0.5 bar to determine the pressure p_τ at which the detector pressure p_{det} begins to oscillate. The results show that at temperatures between T = 1.78 K and $T_c = 1.58$ K the periodic behavior of p_{det} appears not in crossing the melting line, but slightly above the bcc-hcp phase transition.

In figure 6.17 the increase of the source pressure p_0 as a function of time (right scale) is shown together with the simultaneous signal of the detector pressure p_{det} (left scale). The measurement is shown for two temperatures T = 1.68 K and 1.59 K. At T = 1.68 K the oscillatory effect occurs at t = 1100 sec. The corresponding source pressure p_0 = 30 bar is indicated with the dashed arrow. Because of the low resolution of the pressure gauge the actual pressure p_τ is between 29.5 and 30 bar.

Above temperatures T = 1.7 K the period τ and the amplitude is found to increase with increasing source pressure p_0. The investigation of the occurrence of the period τ as a function of p_0 is shown at T = 1.59 K that is close to the critical temperature T_c

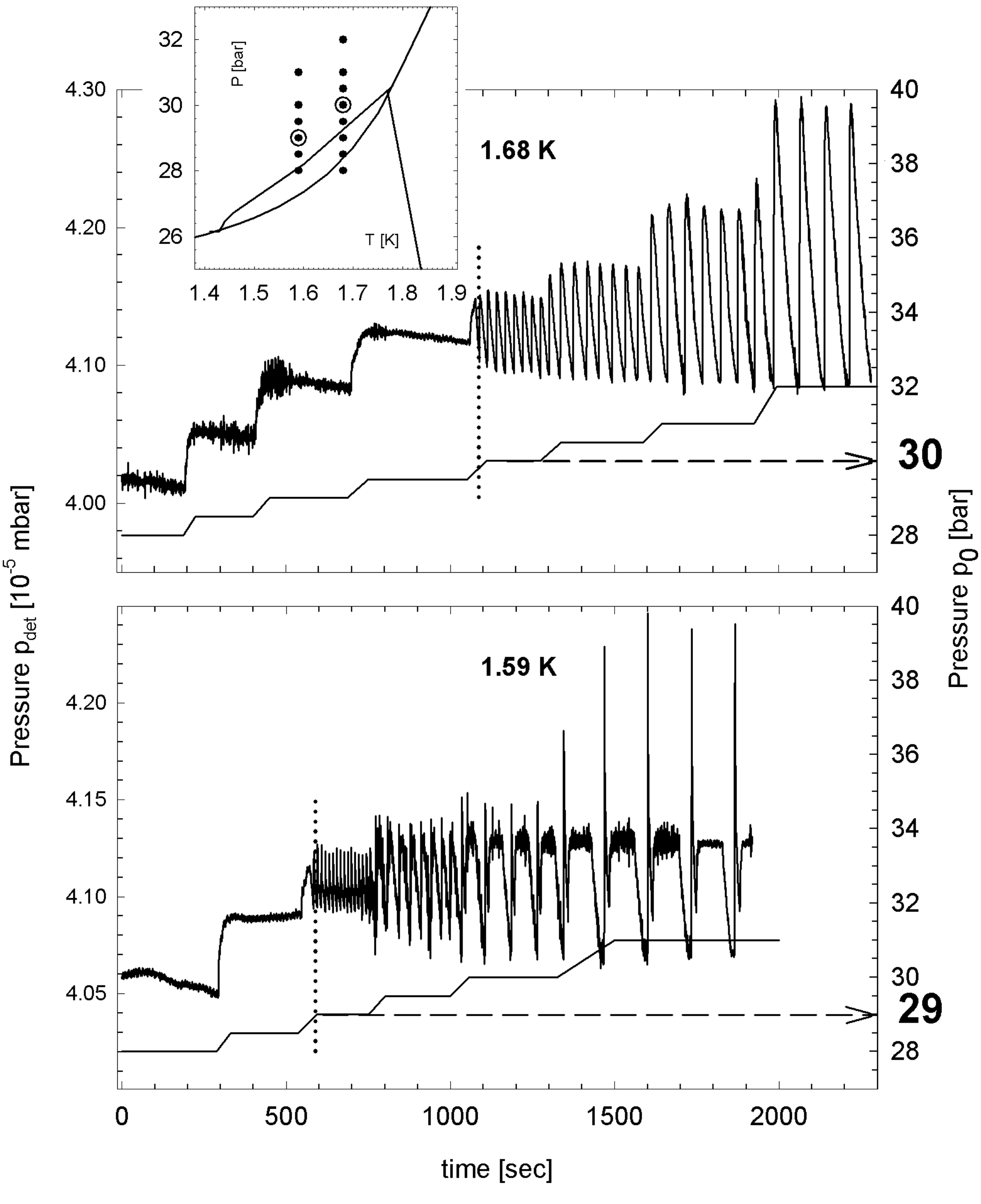

Figure 6.17: Increasing the source pressure p_0 (right scale) at fixed temperature T = 1.68 K and 1.59 K. Both measurements show the time dependent detector pressure p_{det} between 1.78 K and 1.58 K. In this temperature regime the period τ still increases with decreasing temperature. By increasing the source pressure in intervals of 0.5 bar the periodic behavior of p_{det} does not occur at the melting line but slightly above the bcc-hcp transition. The corresponding source pressure p_0 is indicated with the dashed arrow. In the phase diagram the source pressure $p_0 = p_\tau$ is indicated with a ring, whereas the actual value of p_τ is not the corresponding source pressure p_0, but is determined by the interval of the increased source pressure. Therefore, p_τ is determined to be 0.25 bar below the corresponding source pressure at which the oscillations occur. Obviously the investigations inside the bcc phase does not show any oscillatory effect. ($d_0(\#22) = 2.2$ μm)

where the period τ is found to be maximal. The oscillations of the detector pressure occurs at source pressure $p_0 = 29$ bar. Once again the actual pressure is assumed to be $p_\tau = 28.75$ bar. For both temperatures that are investigated in figure 6.17 the period increases with increasing the source pressure. As a first result the Geyser effect is not observable inside the bcc phase for pure solid Helium-4. In the temperature regime between 1.78 K and T_c = 1.58 K the periodic effect occurs right above the bcc-hcp phase line, as to be seen in the phase diagram of figure 6.17. The corresponding source pressure p_0 is indicated with a ring, whereas $p_\tau = p_0$ - 0.25 bar.

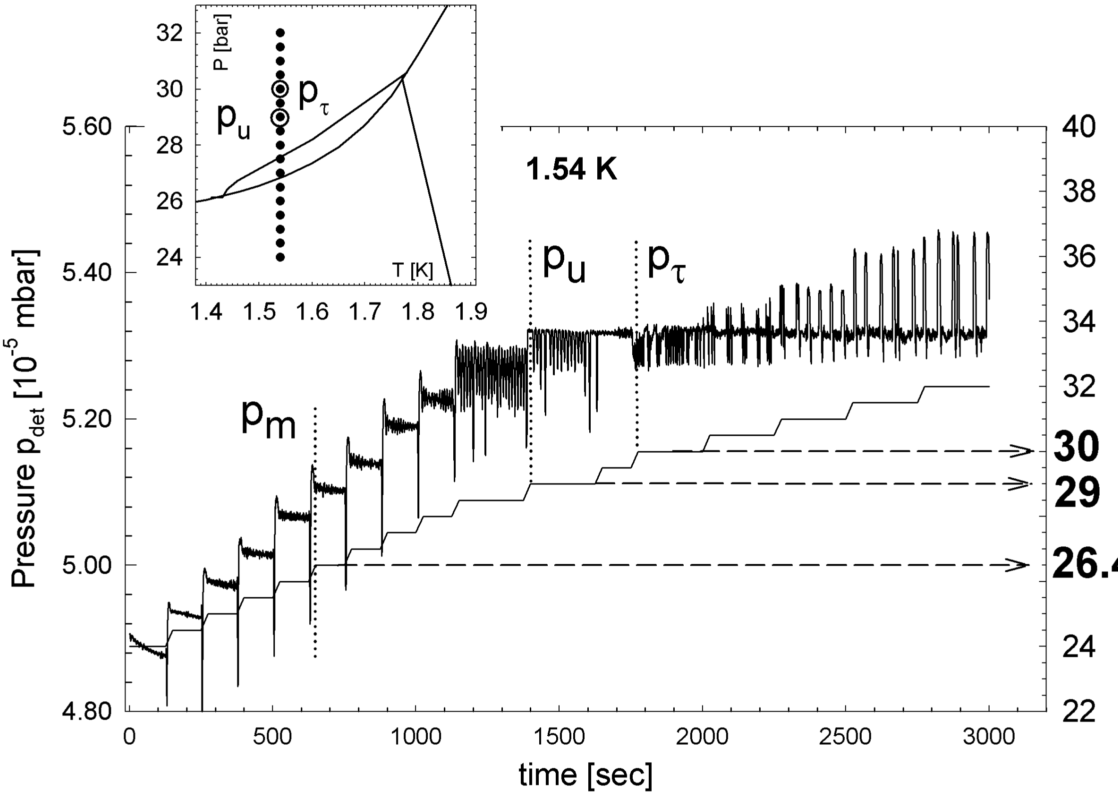

Figure 6.18: Vacuum detector pressure p_{det} at a function of time. At constant temperature T = 1.54 K the source pressure p_0 is increased. The pressure p_0 is monitored by the staircase-like line below (right scale). As seen in the phase diagram the pressure p_0 is increased starting from the liquid phase up to pressures of 32 bar. Comparing with figure 6.17 at t = 1800 seconds the oscillating character of p_{det} does not occur at the bcc-hcp transition but almost 3 bar above at $p_\tau = 30$ bar. Before the oscillations occurred the detector pressure p_{det} remains constant for times t > 1400 seconds. The corresponding pressure is defined as p_u. In the phase diagram both pressures p_τ and p_u are indicated with rings, respectively. ($d_0(\#26) = 2.92$ μm)

In figure 6.18 the vacuum detector pressure p_{det} is monitored as a function of time similar to the previous measurements, whereas the temperatures are chosen to be below T_c. At constant temperature T = 1.54 K the source pressure is again increased stepwise in steps of about 0.5 bar. The corresponding source pressure p_0 is indicated by the staircase-like line below (right scale). Comparing with figure 6.17 the detector pressure p_{det} increases with increasing source pressure p_0 up to $p_0 = 29$ bar that is almost 3 bar above the melting pressure p_m. For source pressures $p_0 > 29$ bar the detector pressure does not show the typical oscillations. Therefore, p_τ no longer coincides with the pressure p_m, as observed for T > 1.78 K. The corresponding pressure at which the detector pressure p_{det} is independent of p_0 is defined as p_u. As an intriguing result, although the nozzle head is filled with a solid it continues to flow as if a liquid up to source pressures p_u. Above p_u there is a region of pressures in which the flow is constant, but the typical Geyser oscillations are not observed. When measured at increasing or decreasing pressures and constant temperature T_0 the perfect reversibility of the relation between $p_u(\mathrm{T})$ and p_{det} indicates that some change in the properties of solid Helium-4 occurs at $p_u(\mathrm{T})$, presumably induced by the injected excess vacancies. The fluid like behavior below pressures $p_u(\mathrm{T})$ is assumed to be responsible for the dropdown of the period τ at temperatures $\mathrm{T} < \mathrm{T}_c$. Regarding figure 6.13 where the oscillating detector pressure p_{det} is shown for temperatures below $\mathrm{T}_c = 1.58$ K the periodic curve shape can be seen in figure 6.17 at times t > 1800 seconds.

For lower temperatures the results obtained at T = 1.54 K are confirmed even more explicitly. To avoid undesirable effects of phase transitions the measurement in figure 6.19 is done at T = 1.39 K, at which the liquid phase directly transits into the hcp phase. The measurement starts inside the liquid phase about 4 bar below the melting pressure. Once more the detector pressure p_{det} is monitored as a function of time by increasing the source pressure p_0. To obtain better results for p_u and p_τ the source pressure´s resolution is increased: The indicator´s position at the pressure gauge is determined by eye to estimate the pressure in smaller intervals than 0.5 bar. Even through this kind of procedure increases the inaccuracy of the source pressure p_0. Nevertheless, the smaller steps of increasing the source pressure are useful to analyze the behavior of the detector pressure p_{det} in figure 6.19. At source pressure $p_0 = 26$ bar (t = 1800 sec) the source pressure overcomes the melting pressure without any change in the relation between p_0 and the detector pressure. In figure 6.19 the vertical line indicates the source pressure p_0 that corresponds to the melting pressure p_m. Thus, for times t > 1800 seconds the Helium in the nozzle head seems to be solid. Surprisingly the detector pressure‘s intensity changes with the source pressure according to the bernoulli relation and therefore the solid behaves like the liquid phase while the source pressure is increased up to 27.2 bar. By increasing p_0 above 27.3 bar (t > 2500 seconds) the detector pressure p_{det} does not change with the source pressure. Corresponding to the results at T = 1.54 K the source pressure p_0 corresponds to the pressure p_u. This plateau in figure 6.19 persists up to $p_\tau = 30.2$ bar, at which the oscillating character occurs (t = 4000 seconds). The corresponding pressures p_u and p_τ are indicated in the phase diagram by rings.

For a better determination of p_τ the time interval between 3900 and 4800 seconds is magnified in figure 6.19. With the better time resolution the occurrence of the periodic signal of p_{det} can be determined to occur at t = 4140 seconds. At this time the source pressure $p_0 = 30.2$ bar. Additionally, the oscillating signal of p_{det} is shown in more details. It shows the same characteristic curve shape as observed in figure 6.13. In

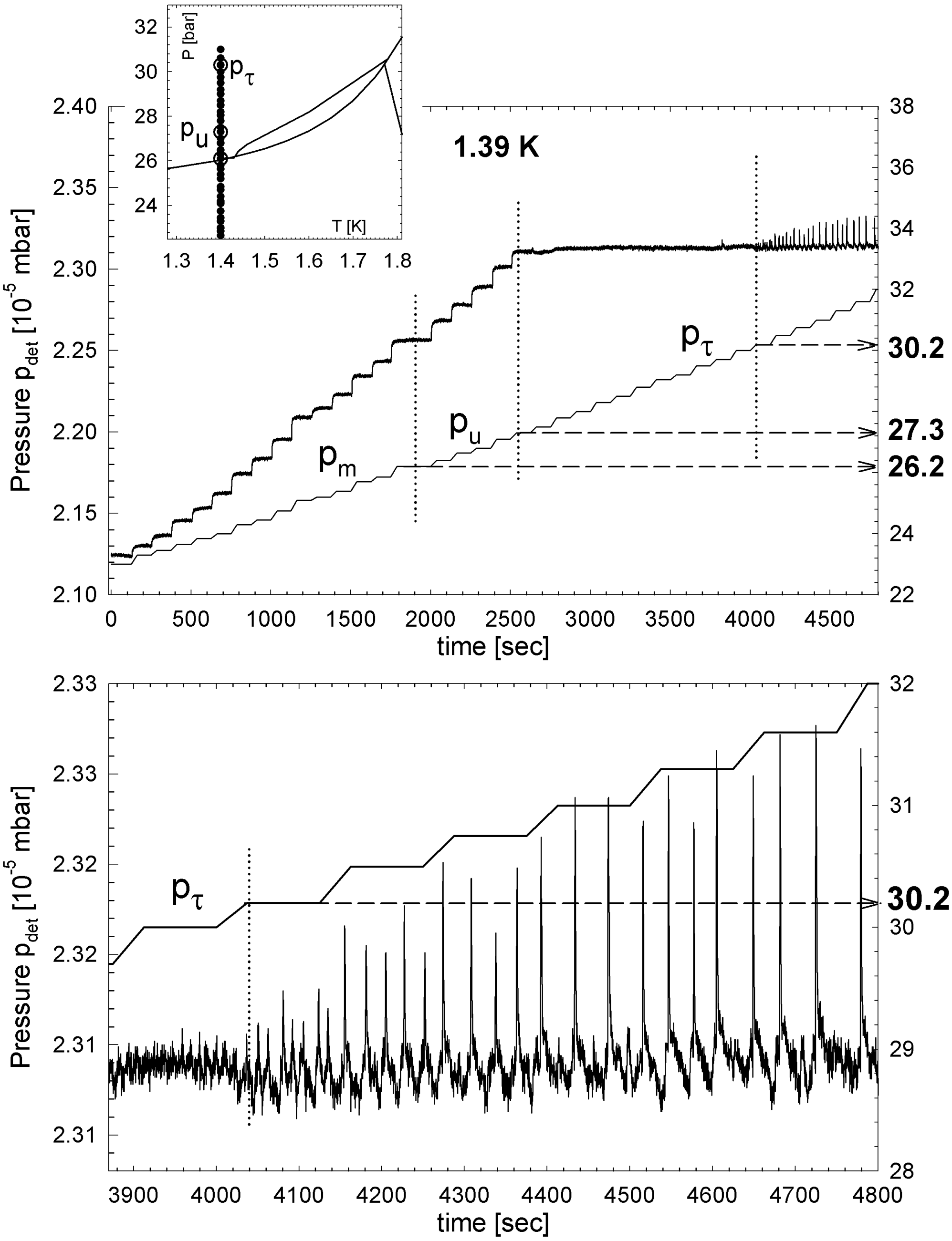

Figure 6.19: Time dependent detector pressure p_{det} as a function of source pressure p_0 at constant temperature T = 1.39 K. As seen in the phase diagram at this temperature the liquid phase directly transits into the hcp phase. Thus, undesirable effects of bcc-hcp phase transitions can be ruled out. The source pressure p_0 (right scale) is increased in intervals of ≈ 0.2 bar. At time t = 1800 seconds the phase transition between liquid and solid phase occurs. Surprisingly the behavior between p_{det} and p_0 does not change up to pressure $p_u = 27.3$ bar. Above source pressures $p_0 = 27.3$ bar the detector pressure p_{det} is constant and herewith independent of p_0. At pressures $p_\tau = 30.2$ bar the oscillations in the detector pressure signal occurs (t > 4000 seconds). Below the regime at which the oscillations occur is enlarged. The pressure p_τ can be determined very exactly. The transition from the non-oscillating to the oscillating regime is well defined. In the phase diagram the pressure p_u and p_τ is indicated with a ring. p_τ is observed to be 4 bar above the melting pressure p_m. ($d_0(\#27) = 1.81$ μm)

this regime the period τ and the amplitude increases with the source pressure p_0. The shape of the oscillations mainly consists of a sharp peak with a comparable simple structure and alters to look like the structure for temperatures T > T$_c$ as to be seen in figure 3.6 and 3.9. The sharp peak´s structure is also observed in the periodic structure shown in figure 6.15, where only the peak itself marks the periodical signal in the detector pressure. This interesting behavior show in figure 6.19 demands for a complete new explanation.

The results indicate that solid Helium-4 undergoes two phase transitions. The first phase transition occurs at pressures between p_m and p_u, where the solid exhibits a fluid like behavior. The second phase line is determined by the pressure p_τ. To investigate the fluid-like component between p_m and p_u the average detector pressure $\overline{p_{det}}$ as a function of the source pressure p_0 is plotted in figure 6.20. The dependence between $\overline{p_{det}}$ and p_0 seems to be linear, whereas the behavior follows the equation of bernoulli for a fluid flow: in the liquid phase for pressures below 26 bar the beam intensity changes with the increase of the source pressure by following the Bernoulli behavior for ideal fluids $p_{det} \propto p_0^{\frac{1}{2}}$. At source pressures $p_0 > p_m = 26$ bar the behavior between p_{det} and p_0 does not change significantly, whereas at pressures $p_0 > p_u = 27.3$ bar the detector pressure remains constant. Following the bernoulli relation the dependence between p_{det} and p_0, the exponent 1/2 can be treated as an indicator for fluid-like flow in the nozzle head. If the exponent is equal to zero the beam flux (which is proportional to the detector pressure p_{det}) does not change in varying the source pressure p_0. In figure 6.20 the exponent is plotted as a function of the source pressure p_0. Once more the dropdown of the exponent at $p_u = 27.3$ bar and not at the melting pressure p_m indicates that the solid shows a fluid like behavior.

The measurements shown in figure 6.17, 6.18 and 6.19 were extended to the entire temperature regime between 2.1 K and 1.3 K. In section 6.2.1 the pressure p_τ was found to be approximately the melting pressure p_m for temperatures T > 1.78 K. In the phase diagram seen in figure 6.21 the pressure p_τ(T) and p_u(T) is plotted as a function of temperature in the regime between 2.1 K and 1.3 K. At temperatures between T$_c$ = 1.58 K and 1.78 K the pressure p_τ was determined to occur slightly above the bcc-hcp phase line. Below T$_c$ the pressure p_τ(T) deviates from the phase transitions to be up to 4 bar above the melting pressure p_m. The phase line of p_u is indicated with the dashed line. Below p_u(T) the solid behaves as a liquid. The method of increasing the source pressure p_0 at constant temperature is able to monitor the new phase line in solid Helium-4.

6.3.3 Sub-Oscillatory Behavior

A further phenomenon is observed below T$_c$ = 1.58 K at higher source pressures p_0, approximately 2 bar above p_τ(T). The measurement in figure 6.22 shows small oscillations of p_{det} that occur right after the main peak. The source pressure p_0 is 41 bar and the effect is shown for several temperatures between 1.56 K and 1.36 K. The amplitude of this sub-oscillations decreases with time and after 10-12 oscillations the

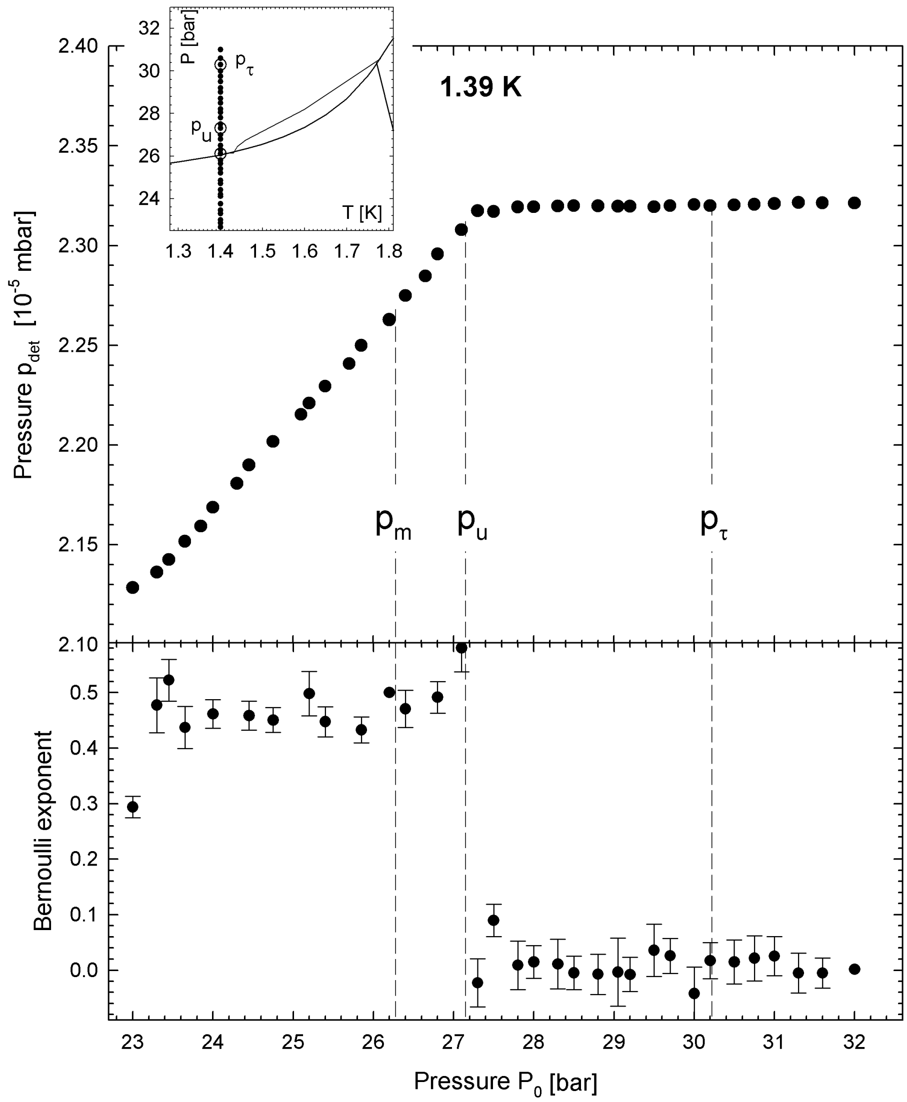

Figure 6.20: Average detector pressure $\overline{p_{det}}$ as a function of the source pressure p_0 obtained from the measurement at T = 1.39 K, as seen in figure 6.19. For source pressures p_0 according to the liquid phase the dependence is found to verify the Bernoulli relation $\overline{p_{det}} \propto p_0^{\frac{1}{2}}$, whereas for source pressures $p_0 \leq p_u$ the relation is still valid. This behavior indicates that the solid behaves as a liquid at pressures $p_m < p_0 \leq p_u$. For pressures $p_0 \geq p_u$ the detector pressure p_{det} is found to be constant, and herewith independent of p_0. In the figure below the exponent derived from the bernoulli relation $\overline{p_{det}} \propto p_0^{\frac{1}{2}}$ is shown as a function of p_0. The value of ≈ 0.5 indicates a fluid-like behavior that is still present at pressures between p_m and p_u. For pressures $p_0 > p_u$ the exponent drops down to zero and indicates a solid-like behavior.

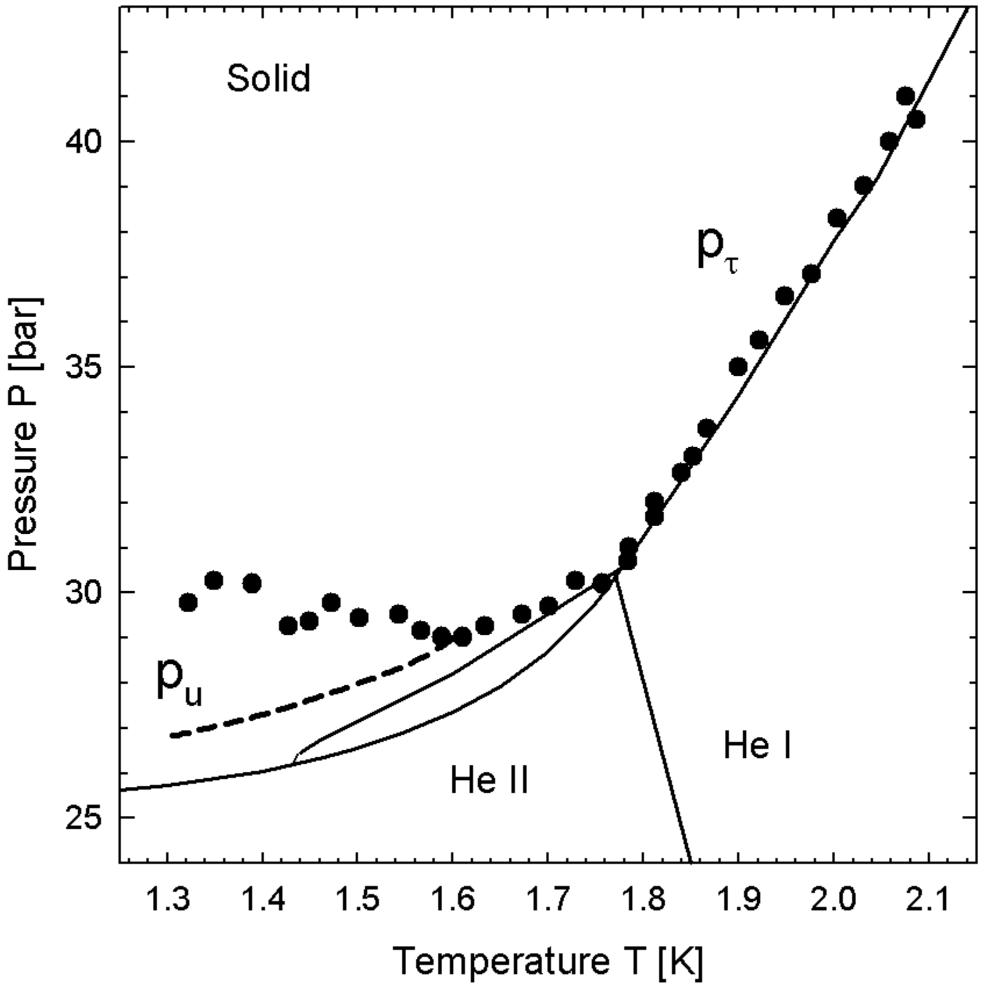

Figure 6.21: Investigating of the pressure p_τ in the temperature regime between 2.1 K and 1.3 K by increasing the source pressure p_0 at fixed temperature, as demonstrated in figure 6.18 and 6.19. At temperatures above 1.7 K the pressure p_τ was found to correspond to the melting pressure p_m. At temperatures below 1.7 K the pressure p_τ no longer coincides with the melting pressure p_m. At temperatures between $T_c = 1.58$ K and 1.7 K the pressure p_τ was determined to occur slightly above the bcc-hcp phase line. Below T_c the pressure p_τ deviates from the phase transitions to be up to 4 bar above the melting pressure p_m. The phase line of p_u is indicated with the dashes line. Below p_u(T) the solid behaves as a liquid.

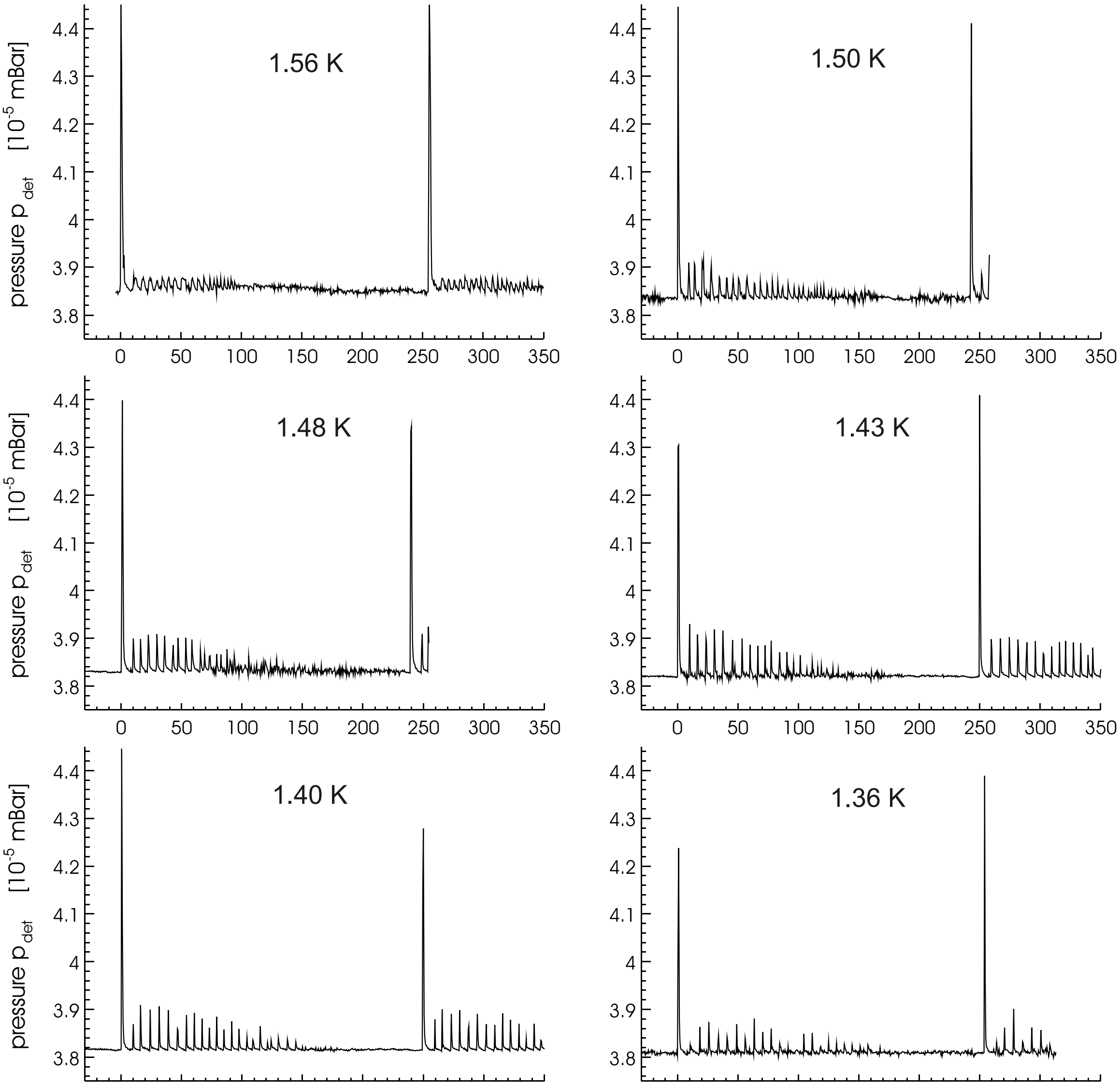

Figure 6.22: Oscillations of the detector pressure p_{det} observed at constant source pressure p_0 = 41 bar and varying temperature below T_c = 1.58 K. Beside the sharp regular peaks this measurement shows small oscillations that occur right after the main peak. The amplitude of this sub-oscillations decreases with time and after 10-12 oscillations the experimental noise overlays the effect. ($d_0(\#17) = 2.28\ \mu$m)

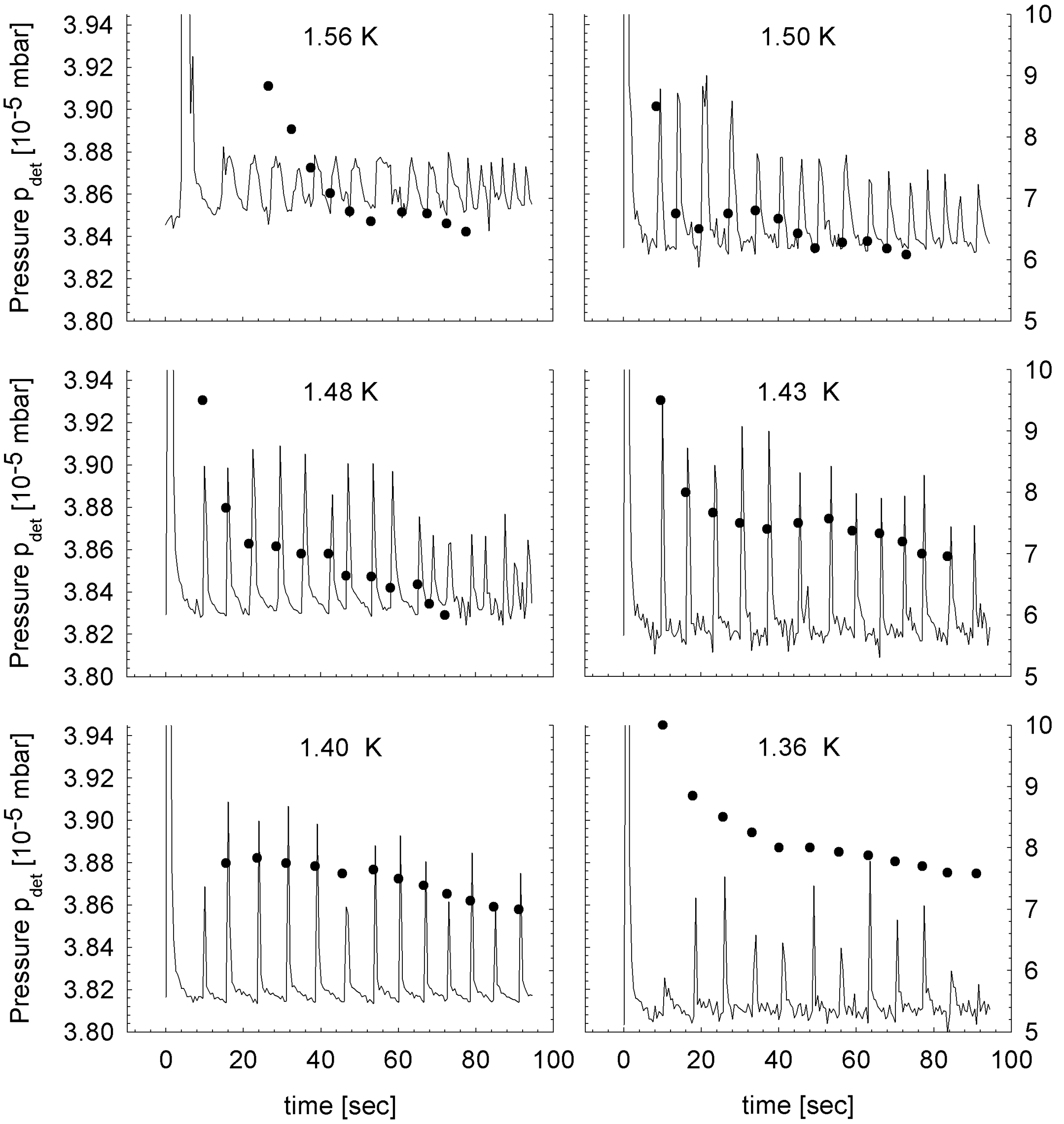

Figure 6.23: A section of the same measurements as presented in figure 6.22. The section enlarges the region where the sub-oscillations occur. The right scale shows the time between two peaks (black dots). As a surprising result the time interval between two sub-oscillations decreases together with the amplitude of the peak. After a certain time the sub-oscillations disappear. The sub-oscillations are more distinctive for lower temperatures, probably where the period τ_{min} is found to be independent of the temperature.

experimental noise overlays the effect. Comparing the main period in the range of $\tau \approx 250$ seconds the sub-oscillations have a period in the range of 6-10 seconds.

Additionally a section of the same measurements are presented in figure 6.23 that enlarges the region where the sub-oscillations occur. On the right scale of figure 6.23 the time distance of the corresponding peaks of the sub-oscillations is shown (black dots). Surprisingly, the time interval decreases with time. The observation is probably related to the disappearance of the sub-oscillations after a certain time.

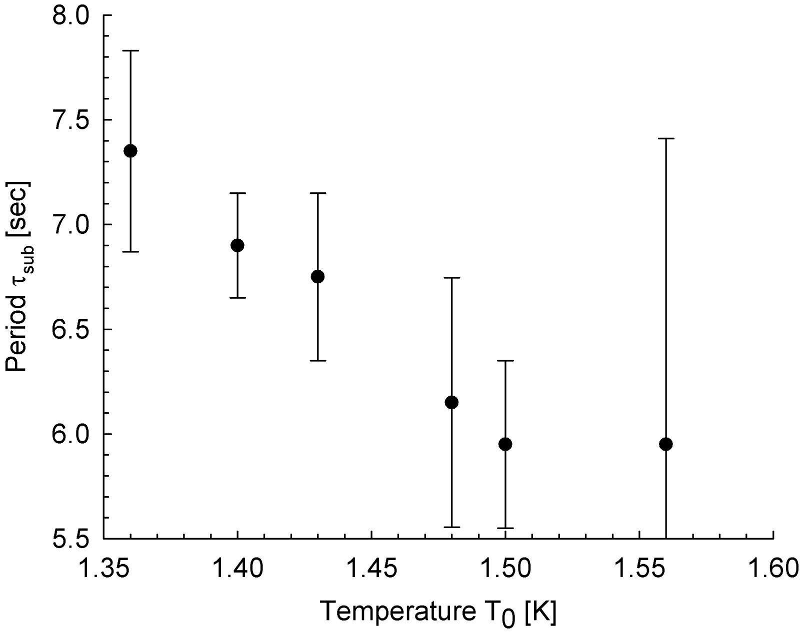

Figure 6.24: The average period τ_{sub}(T) of the sub-oscillations as a function of temperature. The average period increases with decreasing time. Therefore, τ_{sub} behaves controversy to the behavior of the main oscillations whose period τ decreases with decreasing temperature. Also controversy is that the sub-oscillations do not show the perfect periodicity of the main oscillations.

The average period τ_{sub}(T) of the small oscillations as a function of the temperature T is presented in figure 6.24. The period increases with decreasing temperature, contrary to the behavior of the main oscillations whose period τ decreases with decreasing temperature. Especially at higher temperature T = 1.56 K and 1.50 K, respectively, the period is non-uniform as seen by the large error bar.

In figure 6.25 the sub-oscillating behavior is shown as a function of source pressure at constant temperature T = 1.37 K. The effect occurs at source pressures $p_0 > 32$ bar, whereas for pressures below 32 bar the instrumental noise maybe overlays the sub-oscillatory effect. The data show that the effect becomes more significant for higher source pressures, whereas for low source pressures p_0 this effect is less distinctive.

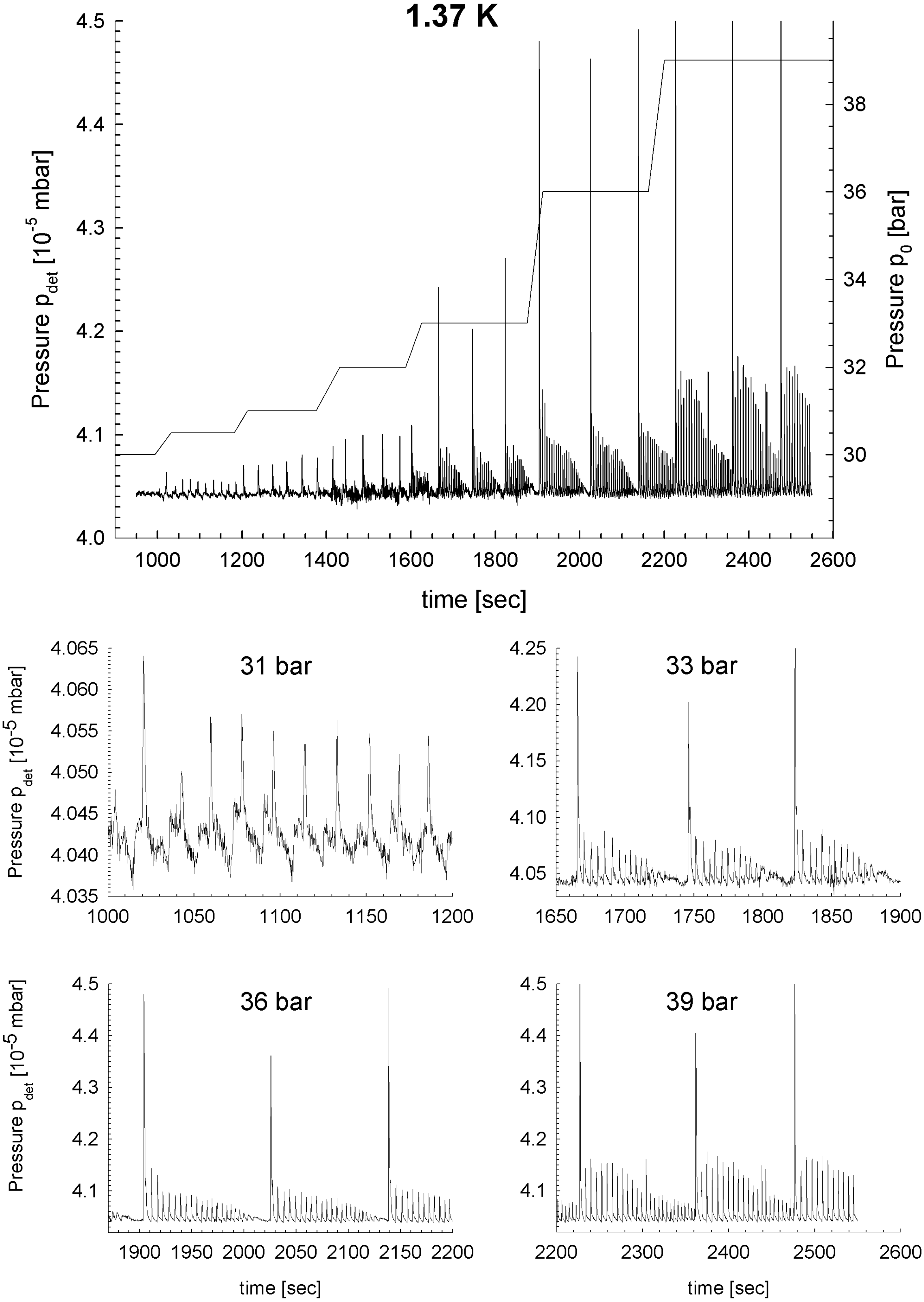

Figure 6.25: The source pressures dependence of the sub-oscillations at a constant temperature T = 1.37 K. For source pressures p_0 slightly above p_τ the sub-oscillations do not occur, as seen for $p_0 = 31$ bar. Only for source pressures $p_0 > 31$ bar the effect is observable. The dependence of p_0 shows that the sub-oscillations are more pronounced for higher source pressures, especially at $p_0 = 39$ bar, where the effect is present during the entire period. ($d_0(\#22) = 2.2\ \mu$m)

6.4 Experimental Results on the Influence of Helium-3

From the theoretical model presented in section 3 follows that the period τ acts as an indicator for the mobility of vacancies. If the period decreases the mobility of the vacancies increases. Therefore, as one of the most surprising results at $T < T_c$ the behavior of vacancies seems to alter. To investigate this effect Helium-3 is a suitable add-on to influence this behavior. The reason for the influence of Helium-3 will be explained in detail in chapter 7.13. The key point is that at corresponding temperatures vacancies and Helium-3 atoms form a vacancy-Helium-3-pair. Thus, the presence of Helium-3 in solid Helium-4 affects the mobility of vacancies.

In the investigated temperature regime between 1.3 K and 2.2 K the equilibrium vacancy concentration X_v^0 is estimated to be about 1 percent. Therefore, a mixture of 1 percent Helium-3 in Helium-4 is used. The investigations with Helium-3 occurred in three phases: Measuring the period τ while decreasing the source temperature T at constant source pressure p_0, increasing the source pressure at constant temperature and finally decreasing the concentration of Helium-3. This way a minimum concentration of Helium-3 could be estimated that still influences the vacancies in solid Helium.

The first measurement is shown in figure 6.26. The period τ is measured as a function of temperature at fixed source pressure $p_0 = 32$ bar. Using pure Helium-4 the period $\tau(T)$ is indicated with the grey circles. The temperature dependent period τ exhibits the maximum of τ at $T = 1.6$ K, already discussed above. The second measurement (white squares) is obtained in using a mixture of one percent of Helium-3 in Helium-4.

Decreasing the temperature down to 1.74 K no significant influence of Helium-3 is found. At temperatures below 1.74 K a slight deviation of the period obtained with Helium-3 is observable that increases at $T_c \approx 1.6$ K. For temperatures below 1.6 K the period obtained with the Helium-3 mixture increases with decreasing temperature and offers the complete opposite behavior to the one with pure Helium-4. The presence of the oscillating effect itself suggests that the vacancies concentration is not affected by the presence of Helium-3. On the other hand by using Helium-3 the increase of the period τ suggests that the mobility of vacancies decreases with decreasing temperature, as actually expected for pure Helium-4.

As to be seen in figure 6.27 the periodic curve shape is also influenced by the presence of Helium-3. The periodic oscillations are shown for pure Helium-4 and the mixture of 1 percent Helium-3/Helium-4 at four different source temperatures. For high temperatures above 1.56 K the period does not change notably between the investigations with pure Helium and the isotope mixture. The curve shape at 1.74 K is also identical. Below $T_c \approx 1.56$ K the behavior changes. The periods obtained with pure Helium-4 decreases whereas with 1 percent of Helium-3 the period and the oscillating structure expands.

In summary the observed increase of the vacancies mobility below T_c is to be suppressed under the influence of Helium-3. Regarding the results obtained with Helium-

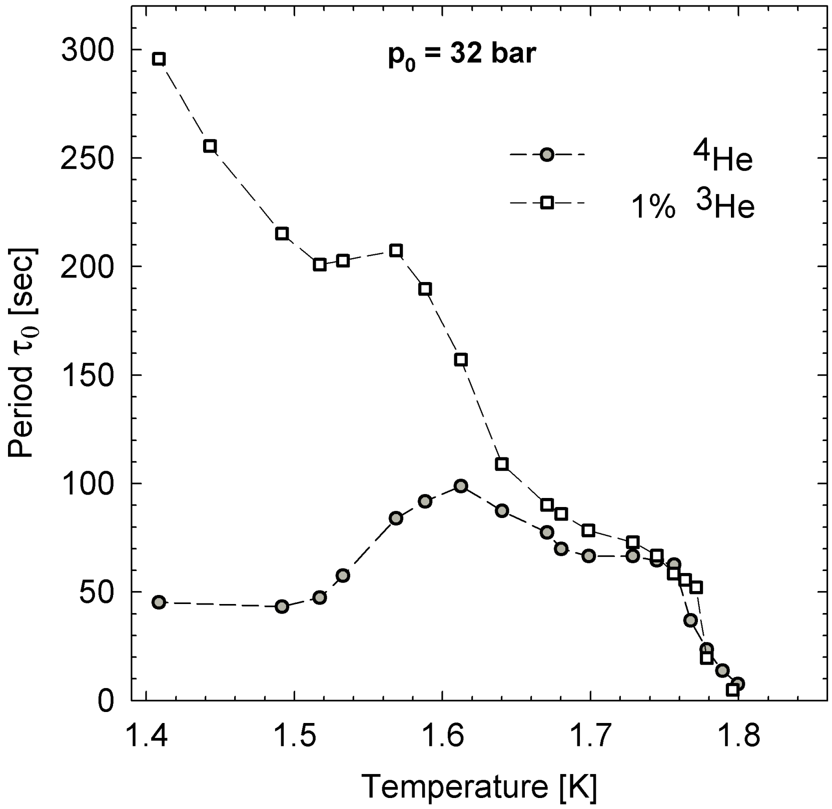

Figure 6.26: Period as a function of temperature. The grey circles show a measurement of the period at $p_0 = 32$ bar with pure Helium-4. The second measurement is obtained in using a mixture of one percent of Helium-3 in Helium-4, indicated with the white squares. Down to 1.74 K no significant deviation is recognizable. At temperatures below 1.74 K a slight deviation is observable that enlarges at $T_c \approx 1.6$ K. For temperatures below 1.6 K the period $\tau(T)$ obtained from the Helium-3 mixture increases with decreasing temperature and offer the complete opposite behavior than with pure Helium-4. (Mixture $d_0(\#27) = 1.81$ μm, pure Helium-4 $d_0(\#17) = 2.28$ μm)

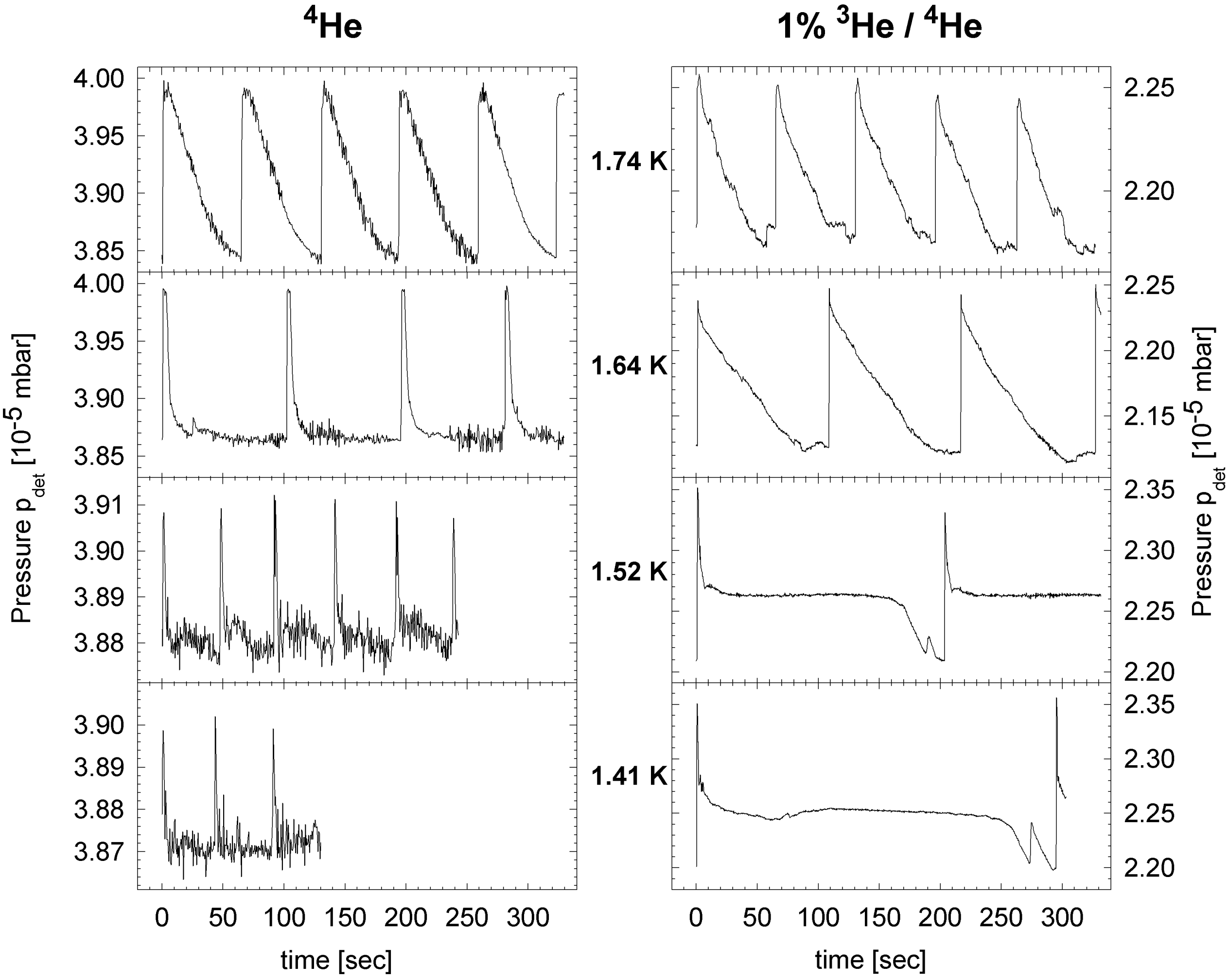

Figure 6.27: Periodic oscillations under the influence of 1 percent of Helium-3 at four different source temperatures. The curve shape shows that for a temperature T above 1.56 K the oscillations seems to be independent of the influence of Helium-3. Below $T_c \approx 1.56$ K the period and it's shape alters under the influence of Helium-3: The period $\tau(T)$ obtained with pure Helium-4 decreases whereas with 1 percent of Helium-3 the period and the oscillating structure expands.

4 the decrease of the period below 1.58 K finally lead to the discovery of a fluid-like phase at pressures below p_u(T). This suggests that the fluid-like behavior is associated with the probable increase of the vacancies mobility. Thus, the influence of Helium-3 at temperatures T $<$ 1.58 K and pressures close to the melting line is investigated to observe a possible change of the new phase lines p_u(T) and p_τ(T). The detector pressure p_{det} is investigated at constant temperatures above and below T$_c$ and increasing source pressure p_0 with a mixture of 1 percent Helium-3/Helium-4.

In figure 6.28 the detector pressure p_{det} as a function of the source pressure at temperatures T = 1.85 K and 1.61 K is presented. The temperatures are chosen to investigate the regime above the critical temperature T$_c$. At T = 1.85 K the oscillations occur right above the melting pressure p_m in agreement with the former results. Decreasing the temperature down to 1.61 K the periodic behavior occurs at the bcc-hcp transition. At first sight the result seems to be similar to the behavior in using pure Helium-4. But in using a mixture of 1 percent Helium-3/Helium-4 the phase diagram is shifted half a bar upwards [93]. Thus, the periodic oscillations appear right above the melting line at $p_\tau = 28$ bar [1], in contrast to the pressure $p_\tau = 29$ bar obtained with pure Helium-4. In figure 6.29 the same kind of measurements are presented at the constant temperatures T = 1.53 K and 1.40 K , both below the critical temperature T$_c$. Now the pressure p_τ corresponds to the melting pressure p_m. For T = 1.4 K the pressure p_τ is found to be slightly below p_m. The phase line p_u(T) is not observable. The investigations with Helium-4 below T = 1.78 K and especially below 1.56 K show the decrease of the period τ and the fluid-like behavior above the melting line. The influence of Helium-3 seems to suppress this strange behavior, as seen in figure 6.30, where the pressures p_τ(T) are shown for pure Helium-4 and the Helium-3 mixture, respectively.

In figure 6.31 the average detector pressure $\overline{p_{det}}$ is shown as a function of the source pressure p_0. The black circles show the results obtained with pure Helium-4, whereas the white circles represent the same measurement with a mixture of 1 percent Helium-3/Helium-4 at constant temperature T = 1.39 K. Both measurements show that for source pressures p_0 according to the liquid phase the dependence between $\overline{p_{det}}$ and p_0 verifies the Bernoulli relation $\overline{p_{det}} \propto p_0^{\frac{1}{2}}$. Increasing p_0 above 26.5 bar p_{det} remains constant and independent of p_0 in using the mixture of Helium-3. Comparing the result with the investigations using pure Helium-4 the difference is obvious: the admixture of Helium-3 eliminates the effect of fluid-like behavior. In summary: Helium-3 does not eliminate the oscillating effect in expanding Helium-4 into a vacuum under solid state condition.

The final investigation with Helium-3 concerns the influence of the concentration. The investigation searches for an upper marginal value of Helium-3 that does not affect the maximum of the period τ at T$_c$ = 1.58 K. Therefore, the period τ is measured as a function of temperature T at constant source pressure $p_0 = 32$ bar. Figure 6.32 shows the results for different concentrations of Helium-3 between 1 and 0.0015 percent and pure Helium-4. Down to T = 1.67 K the period is independent of the Helium-3

---

[1] Actually, p_τ is determined to be 28.5 bar, whereas the value is reduced because of the shifted phase diagram

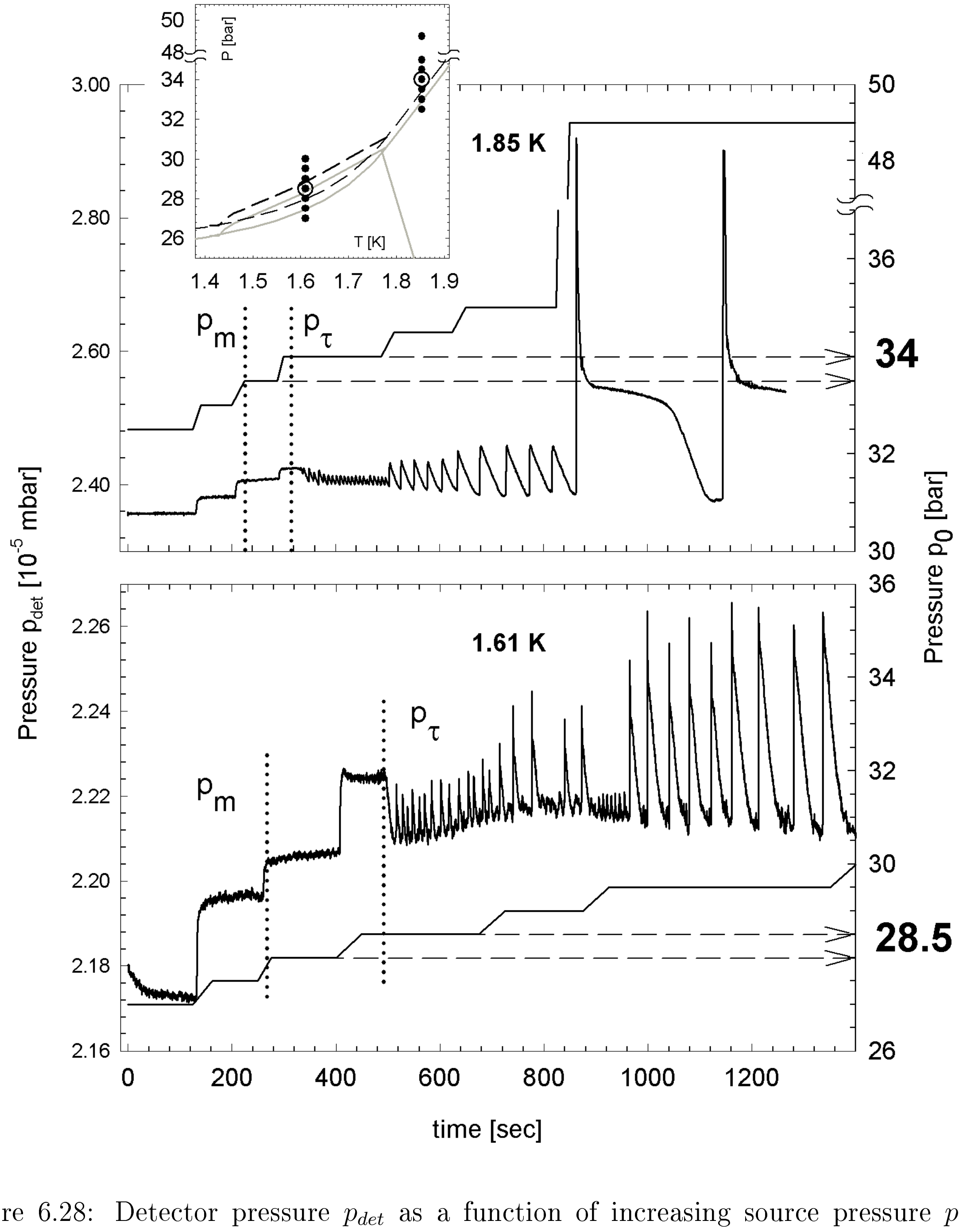

Figure 6.28: Detector pressure p_{det} as a function of increasing source pressure p_0. The source pressure is increased stepwise about 0.5 bar (right scale). The phase diagram indicates the corresponding temperatures and pressures. In using a mixture of 1 percent Helium-3 the phase diagram is shifted up of about 0.5 bar, which is indicated by the dashed line that represents the valid phase diagram for the mixture. The grey colored phase diagram corresponds to pure Helium-4. The measurements are done at T = 1.85 and 1.61 K. Both temperatures are above the critical temperature T_c. The results for both temperatures show that the detector pressure p_{det} oscillates at corresponding pressure p_τ that is slightly above the melting pressure p_m. (d_0(#27) = 1.81 μm)

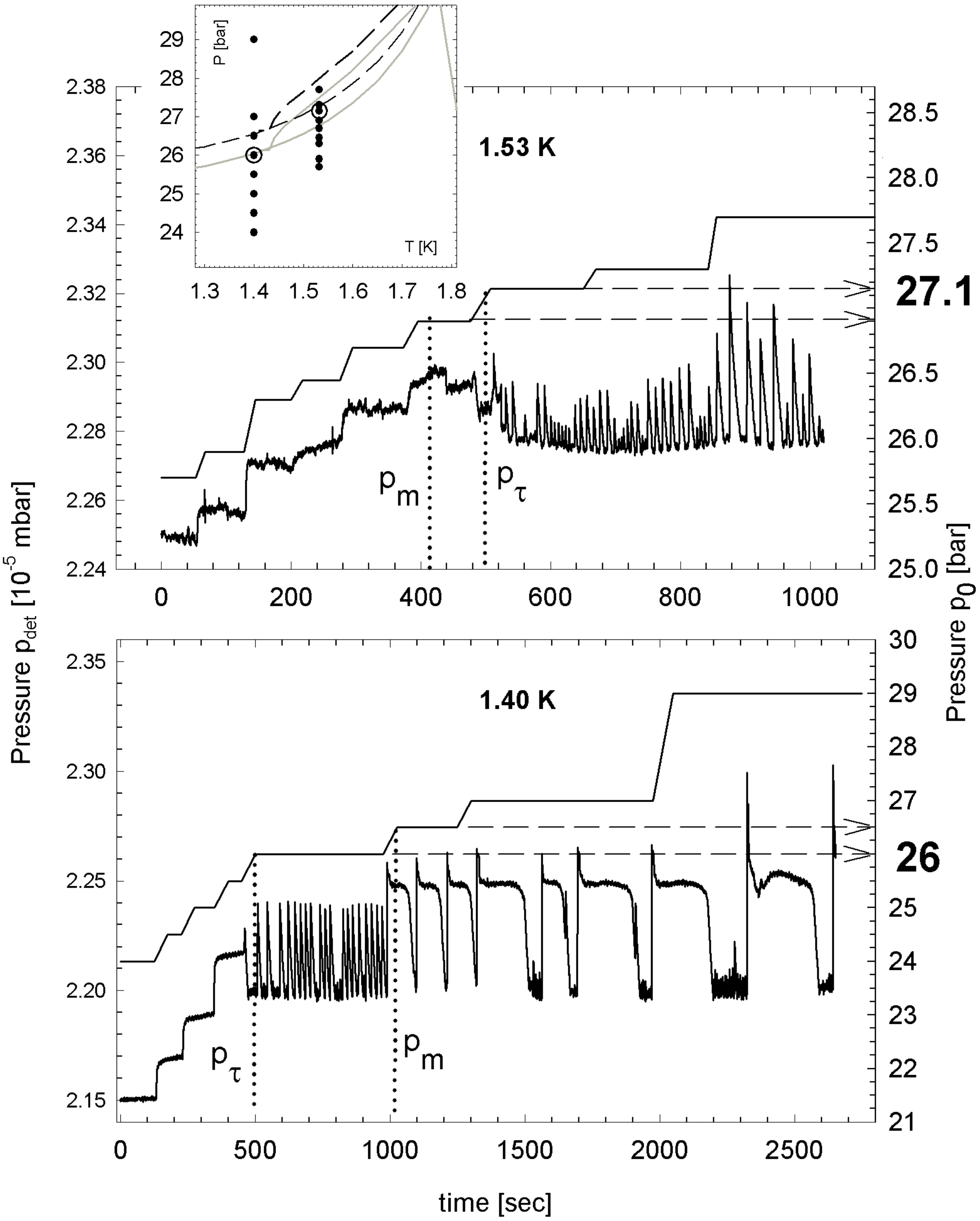

Figure 6.29: Detector pressure p_{det} as a function of source pressure p_0. The source pressure is increased stepwise about 0.5 bar (right scale). The phase diagram at the inset indicates the corresponding temperatures and pressures. The phase lines are shifted, as mentioned in figure 6.28. The measurements are done at T = 1.53 and 1.40 K. Both temperatures are below the critical temperature T_c. The results for both temperatures show that the detector pressure p_{det} oscillates at corresponding pressure p_τ that is even slightly below the melting pressure p_m. ($d_0(\#27) = 1.81$ μm)

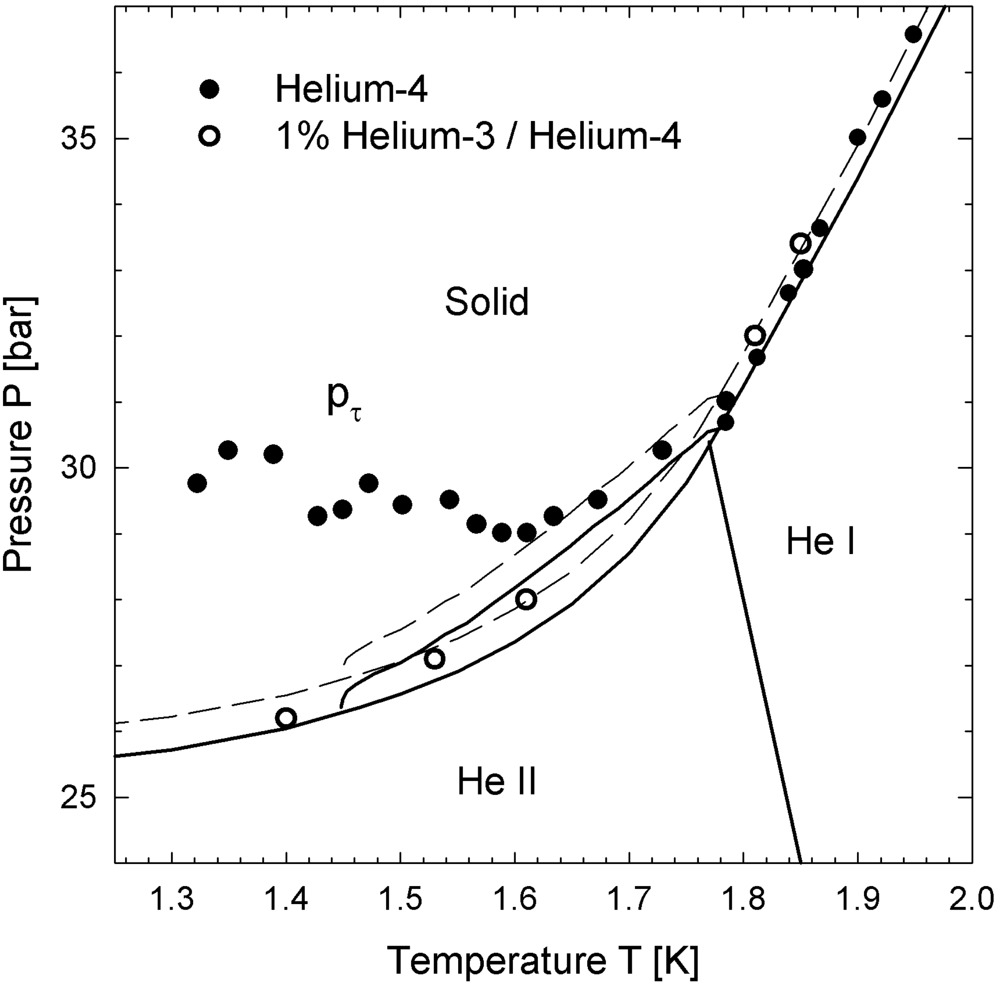

Figure 6.30: Pressures p_τ obtained with pure Helium-4 (black circles) and the mixture of 1 percent Helium-3/Helium-4 (white circles). At temperatures T > 1.78 K the pressure p_τ corresponds to the melting pressure for both, Helium-4 and the Helium-3 mixture. For temperatures below T < 1.78 K the pressure p_τ deviates from the melting pressure in using Helium-4. Whereas the results for p_τ obtained Helium-3 mixture shows that p_τ corresponds to the melting pressure p_m. The abnormal behavior of p_τ and p_u is completely suppressed in using a small Helium-3 concentration.

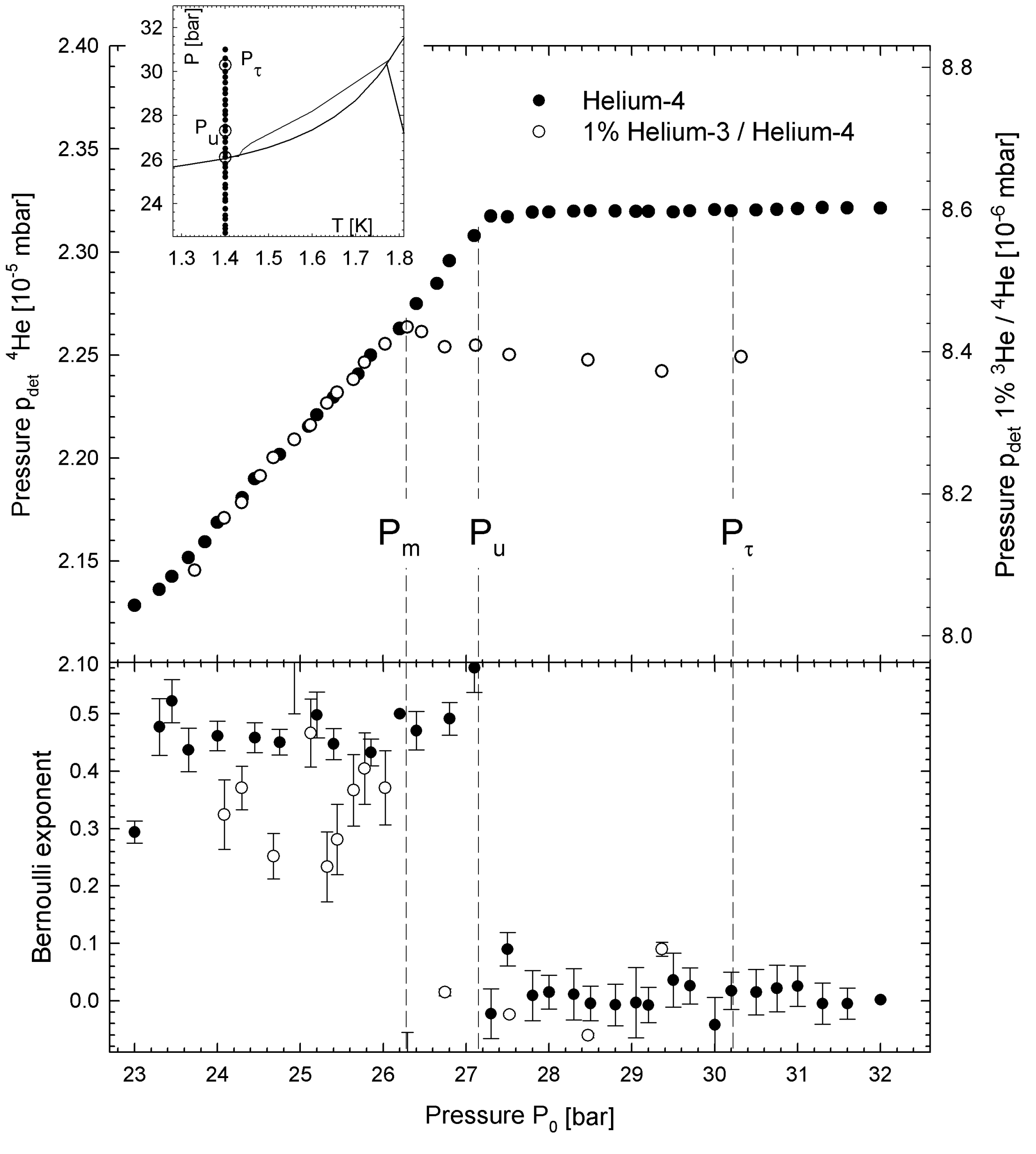

Figure 6.31: Average detector pressure $\overline{p_{det}}$ as a function of the source pressure p_0 at constant temperature T = 1.4 K. The black circles show the results obtained with pure Helium-4, whereas the white circles represent the same measurement with a mixture of 1 percent Helium-3/Helium-4. Both measurements show that for source pressures p_0 according to the liquid phase the dependence between $\overline{p_{det}}$ and p_0 verifies the Bernoulli relation $\overline{p_{det}} \propto p_0^{\frac{1}{2}}$. For source pressures p_0 above the melting pressure the bernoulli relation is still valid for pure Helium-4, whereas the mixture of Helium-3 shows that $\overline{p_{det}}$ is independent of p_0. In the figure below the exponent derived from the bernoulli relation $\overline{p_{det}} \propto p_0^{\frac{1}{2}}$ is shown as a function of p_0. The value of ≈ 0.5 indicates a fluid-like behavior, that is still present for Helium-4 at pressures between p_m and p_u. For pressures $p_0 > p_u$ the exponent drops down to zero and indicates a solid-like behavior. The results with Helium-3 show that the bernoulli exponent drops down to zero right above the melting pressure p_m. (Mixture d_0(#35) = 1.39 μm (partly clogged), pure Helium-4 d_0(#27) = 1.81 μm)

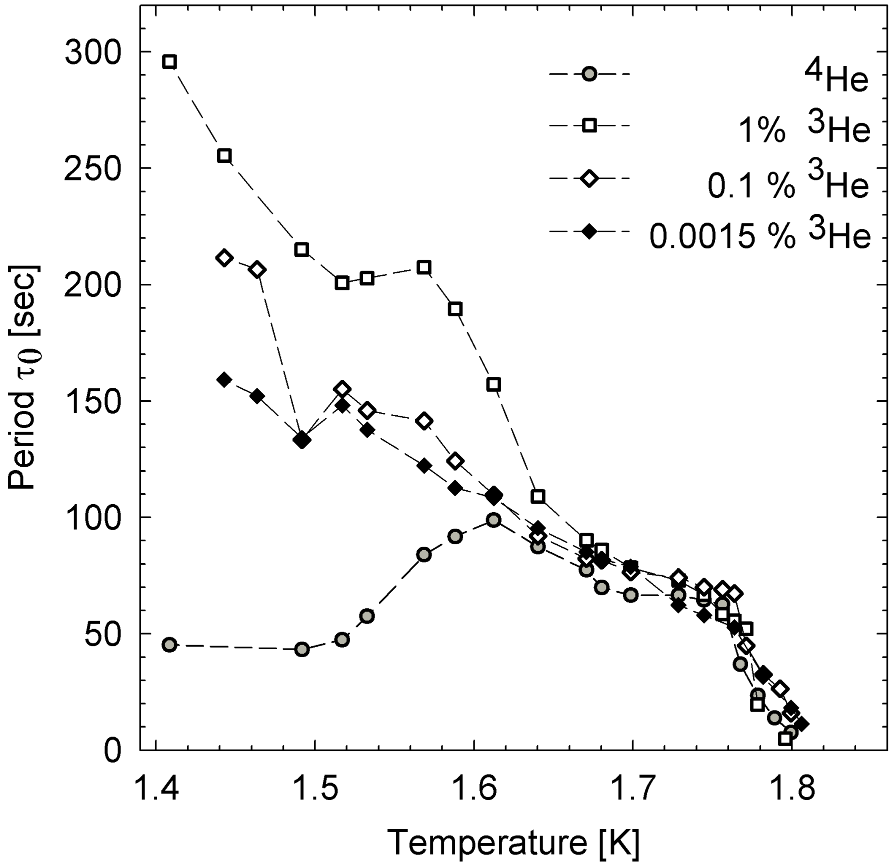

Figure 6.32: Period as a function of temperature at fixed source pressure for different concentrations of Helium-3 and pure Helium-4. Down to T = 1.67 K the period is independent of the Helium-3 fraction. Down to T = 1.54 K the period τ always increases, whereas the dependence of the Helium-3 concentration is obvious. (Mixtures 0.1 and 0.0015 percent Helium-3 $d_0(\#28) = 1.78$ μm, whereas the obtained period is multiplied by a factor of 2 to fit the period with the data for pure Helium-4 and 1 percent Helium-3.)

fraction. Down to T = 1.54 K the period τ always increases, whereas the dependence of the Helium-3 concentration is obvious. Reducing the Helium-3 fraction from 1 to 0.1 percent makes the biggest difference. But already a concentration of only $1.5 \cdot 10^{-3}$ percent of Helium-3 results in a decrease of the period τ below T_c.

Using one percent of Helium-3 the different behavior between the mixture and pure Helium-4 occurs at temperatures below 1.66 K. As shown in figure 6.27 the periodic character at 1.74 K is absolutely identic. For lower temperatures the period and the curve shape changes dramatically. This effect is presented in figure 6.33 for different concentrations of Helium-3. On the top of figure 6.33 the oscillating detector pressure p_{det} is shown at temperature T = 1.78 K and source pressure p_0 = 32 bar for four different concentrations (0, 0.1 , 0.015 and 0.0015 percent) of Helium-3. Besides the common period τ[2] the oscillating curve shape is found to be the same. The same behavior of the oscillating detector pressure p_{det} is also presented in figure 6.33 for the same concentrations of Helium-3 at temperature T = 1.49 K. The periodic behavior shows the sharp peak, whereas the amplitude flattens especially at the measurement done with 0.001 percent of Helium-3.

Obviously, the presence of Helium-3 has an intriguing influence on the period τ and the behavior of p_τ and p_u at temperatures below the critical temperature $T_c = 1.58$ K. Moreover the results indicate that the observed phenomenon of the oscillating beam flux intensity is related to the dynamics and presence of vacancies in solid Helium-4. The exact analyze and interpretation of the influence of Helium-3 follows in section 7.8.

6.5 Influence of the Nozzle Diameter

In this experiment the orifice acts as a source for the generation of excess vacancies. Thus, the orifice‘s diameter d_0 should have an enormous influence to the experimental results. Several nozzle diameters between 1 and 5 μm are used, but mainly nozzles with diameter 2 μm are mounted. This section shows the experimental results obtained with different nozzle diameters by measuring the detector pressure p_{det} at constant temperature T and constant source pressure p_0, respectively. In figure 6.34 the oscillating detector pressure p_{det} is shown for p_0 = 29 bar and T = 1.59 K for two different nozzle diameters (2.2 μm and 1.52 μm, respectively). Besides the different average beam flux the period τ is found to be shorter for larger nozzle diameter d_0.

The dotted line marks the average detector pressure that is proportional to the beam flux. The detector pressure p_{det} is reduced for a smaller nozzle diameter, as expected. The relation between the detector pressure p_{det} and the nozzle diameter d_0 is given by:

$$\frac{d_{0_1}^2}{d_{0_2}^2} = \frac{p_{det_1}}{p_{det_2}} \tag{6.3}$$

---

[2] The period is determined with different nozzle diameters that influences the period. The period can be calibrated to one reference nozzle diameter as seen in the next section.

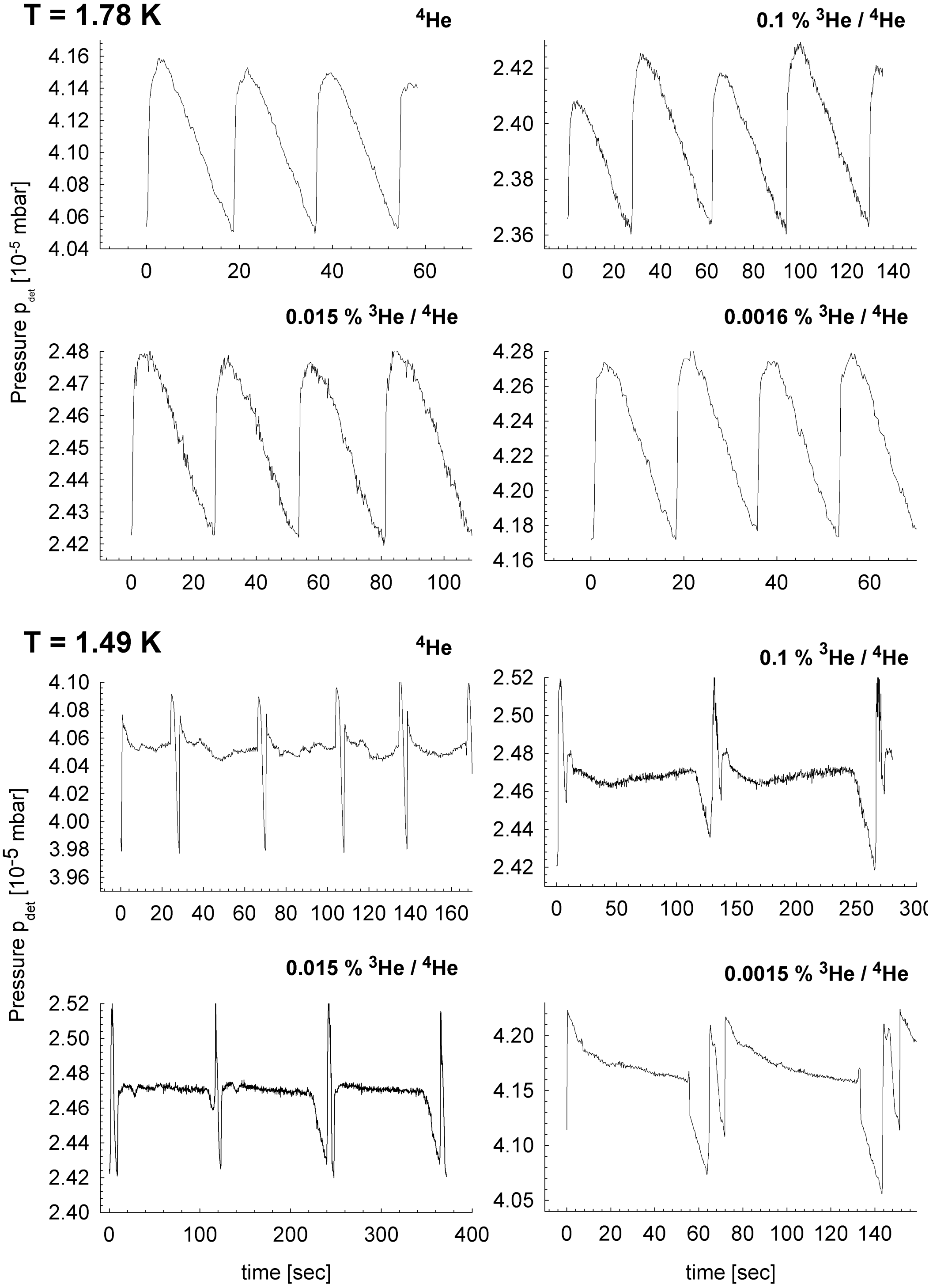

Figure 6.33: Oscillating detector pressure p_{det} obtained for four different concentrations (0.1, 0.015, 0.0015, 0 percent) of Helium-3 constant at temperature T = 1.78 K and T = 1.49 K and constant source pressure $p_0 = 32$ bar. At T = 1.78 K the periodic curve shape is found to be identical. The period is obtained with different nozzle diameters, whereas in calibrating the period to one nozzle diameter the period is found to be equal for all concentrations of Helium-3. At T = 1.49 K for high concentrations of Helium-3 the curve shape exhibits the typical shape that is also found for high pressures at temperatures T $>$ 1.78 K. (Pure Helium-4 $d_0(\#17) = 2.28$ μm, mixtures 0.1 and 0.015 percent $d_0(\#28) = 1.78$ μm, mixture 0.0015 percent $d_0(\#30) = 2.4$ μm)

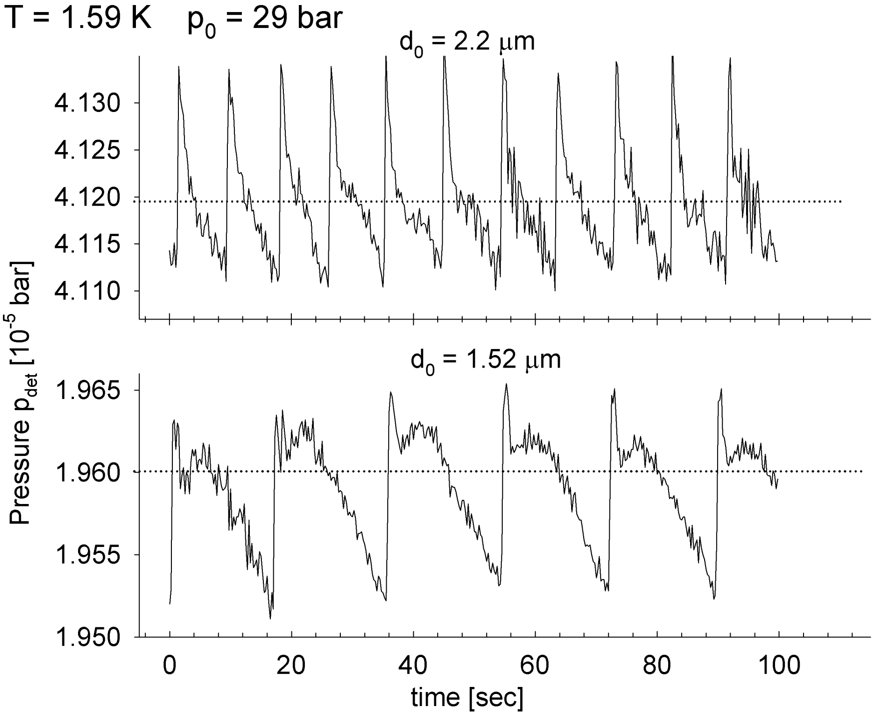

Figure 6.34: Measurements of the oscillating detector pressure p_{det} with two different nozzle diameters, 2.2 (#22) and 1.52 (#23) μm, respectively. The source pressure of p_0 = 29 bar and source temperature T_0 = 1.59 K is the same for both. The observed behavior shows that the period τ decreases for larger nozzle diameter whereas the mean beam flux intensity (indicated with the dotted line) increases.

Applied to the data in figure 6.34 one obtains:

$$\frac{d_{0_1}^2}{d_{0_2}^2} = \frac{(2.2\ \mu m)^2}{(1.52\ \mu m)^2} = 2.09 \qquad \frac{p_{det_1}}{p_{det_2}} = \frac{4.12 \cdot 10^{-5} mbar}{1.96 \cdot 10^{-5} mbar} = 2.10 \tag{6.4}$$

The influence of the nozzle diameter d_0 to the period τ in figure 6.34 is also obvious. The period is shorter for a larger nozzle diameter d_0. For the same source pressure p_0 = 29 bar and temperature T = 1.59 K one obtains a squareroot dependence between the period τ and the nozzle diameter d_0:

$$\frac{d_{0_1}}{d_{0_2}} = \sqrt{\frac{\tau_2}{\tau_1}} \tag{6.5}$$

that matches perfectly for the data in figure 6.34:

$$\frac{d_{0_1}}{d_{0_2}} = \frac{2.2\ \mu m}{1.52\ \mu m} = 1.44 \qquad \sqrt{\frac{\tau_2}{\tau_1}} = \sqrt{\frac{18 sec}{9 sec}} = 1.41 \tag{6.6}$$

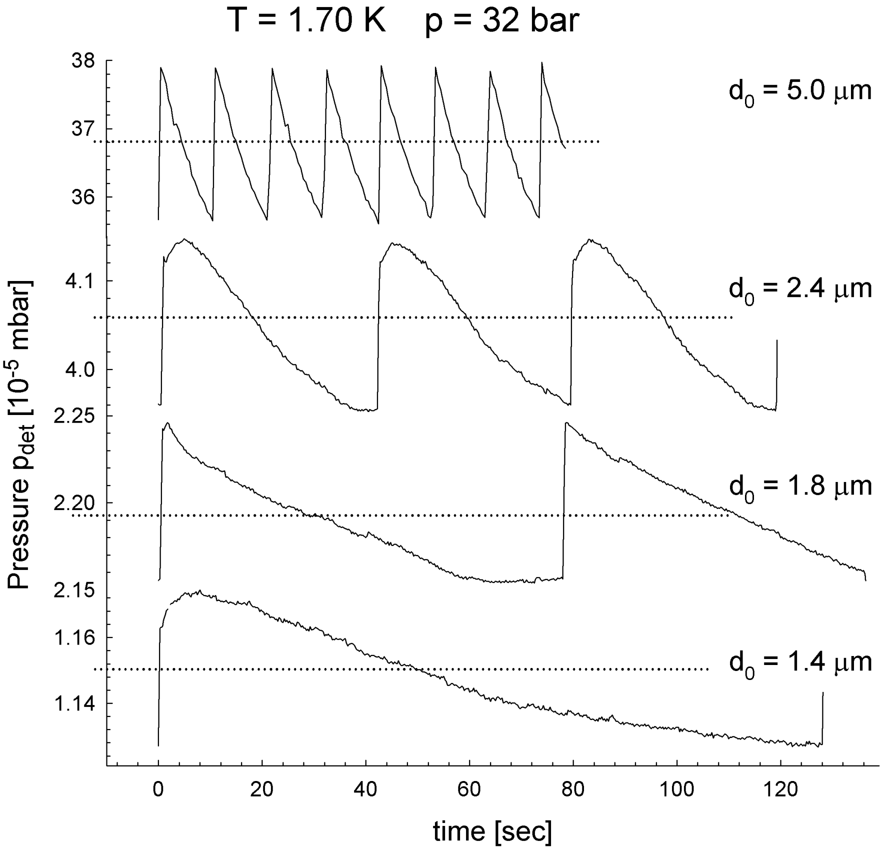

Figure 6.35: The oscillating detector pressure p_{det} of four different nozzle diameters ($d_0 = 1.39(\#35), 1.81(\#27), 2.4(\#30)$ and $5(\#19)$ μm, respectively) are investigated under the same conditions of source pressure $p_0 = 32$ bar and T = 1.7 K temperature. The increase of the period τ with decreasing nozzle diameters d_0 is obvious. The dotted line marks the average detector pressure p_{det} corresponding to the mean beam flux. The mean beam flux decreases with decreasing nozzle diameter d_0.

Because of the same dependence of the ratio $\frac{d_{0_1}}{d_{0_2}}$ between the period and the mean beam flux, both are related to each other for the same conditions of temperature and pressure:

$$\frac{\tau_2}{\tau_1} = \frac{p_{det_1}}{p_{det_2}} \tag{6.7}$$

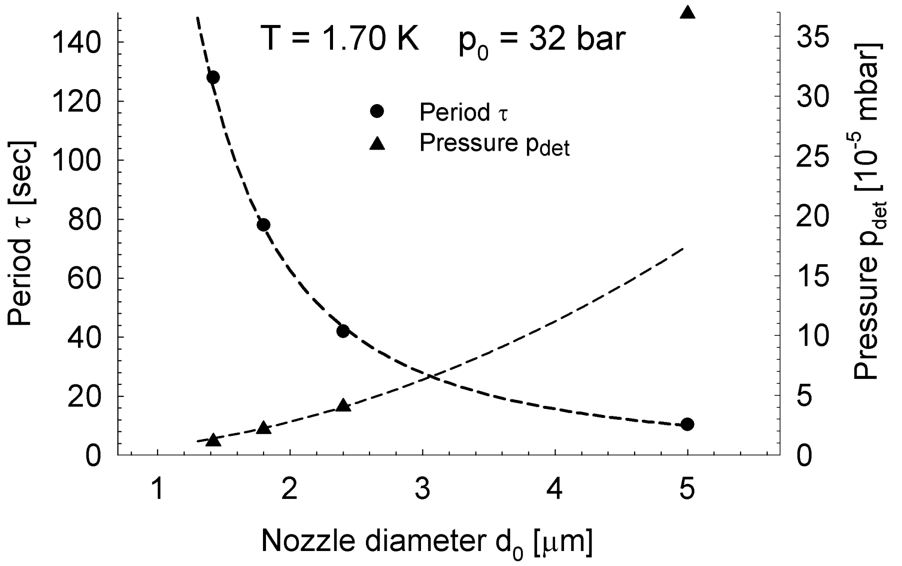

Figure 6.36: Period and mean vacuum pressure as a function of the nozzle diameter. The period and the mean vacuum pressure of four different nozzle diameters between 1.39 and 5 μm at the same conditions of temperature and pressure are summarized. Fit the period as a function of the nozzle diameter one obtains a squareroot dependence. The square dependence of the mean detector pressure is not varified

The dependence on the nozzle diameter is furthermore illustrated in figure 6.35 for four different nozzle diameters (1.39, 1.8, 2.4 and 5 μm, respectively) for the same conditions of source pressure $p_0 = 32$ bar and temperature T = 1.7 K. The dotted line marks the average detector pressure $\overline{p_{det}}$ (right axis scale) according to the mean beam flux. Obviously the periodic shape is not influenced by the nozzle diameter whereas the period τ increases with decreasing nozzle diameter d_0 (left axis scale). For this set of data the relation 6.3 can be verified. Figure 6.36 shows the period τ and the average detector pressure p_{det} as a function of the nozzle diameter d_0. Fit the data one obtains a perfect squareroot dependence between the period τ and the nozzle diameter d_0, in agreement with equation 6.3. These data are reliable whereas the average detector pressure p_{det} does not show the expected square-dependence for all four nozzle diameters d_0. The detector pressure p_{det} obtained for the 5 μm nozzle is probably increased because of a former experimental setup where the effective pumping speed is reduced. The explanation for the dependence between the period τ and the detector pressure p_{det} as a function of the nozzle diameter d_0 is presented in the next chapter.

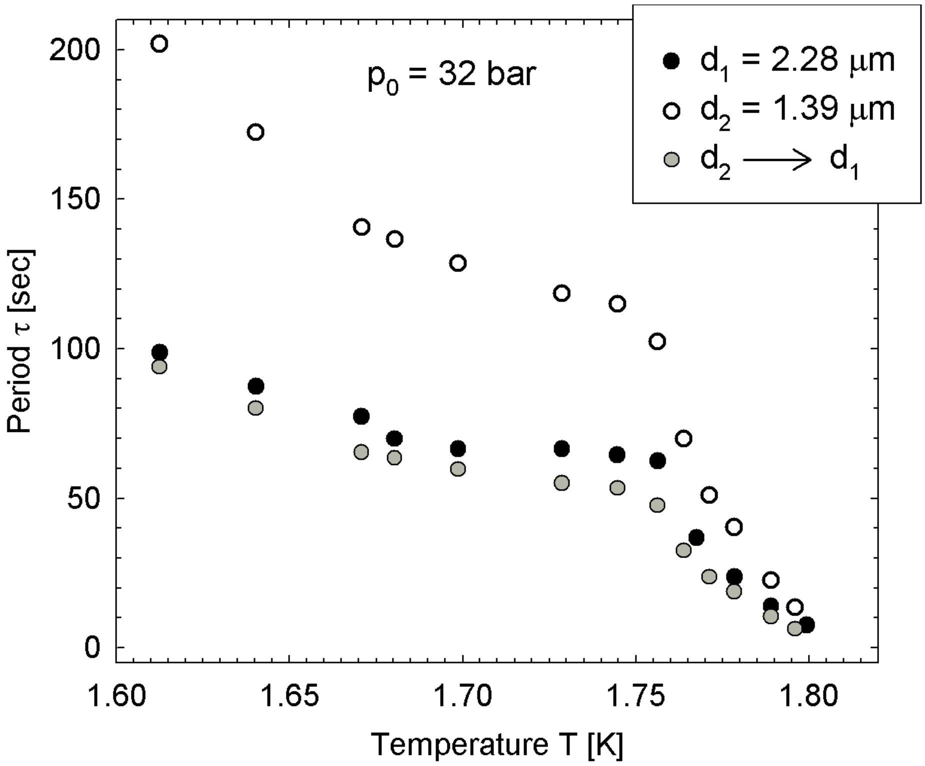

Figure 6.37: Temperature dependence of the period for two different nozzle diameters. The period enlarges for the small nozzle diameter of $d_0(\#35) = 1.39$ μm ± 0.1. Using relation 6.3 the data for the 1.39 μm nozzle have been transformed. The period corresponds almost perfectly to the data obtained with the larger nozzle $d_0(\#17) = 2.28 \pm 0.1$ μm.

Relation 6.3 can be applied to a full set of data measuring the period τ as a function of temperature T at a constant source pressure $p_0 = 32$ bar, as shown in figure 6.37. Two different nozzle diameters are used, $d_0 = 2.28$ and 1.39 μm, respectively. The period τ(T) obtained with the smaller nozzle diameter $d_0 = 1.39$ μm (white circles) is obtained to be larger. Following relation 6.3 the data for τ obtained with the 2.28 μm nozzle (black circles) are calibrated to a nozzle diameter of $d_0 = 1.38$ μm. Since an error for the calibrated nozzle diameter of ± 0.1 μm is assumed the period can be calibrated almost perfectly by multiplying with a factor of $2.2^2/1.5^2$ (grey circles).

As already seen in figure 6.21 the pressure p_τ, at which the oscillating character in the detector pressure signal appears, is measured in the entire temperature range between 2.1 and 1.3 K. The measurement is done with a nozzle of diameter $d_0 = 2$ μm. Two aspects of the nozzle diameter´s influence are interesting to investigate: First the behavior of p_τ above 1.78 K, where the periodic behavior appears right above the melting line, and second the strong deviation from that behavior at lower temperatures,

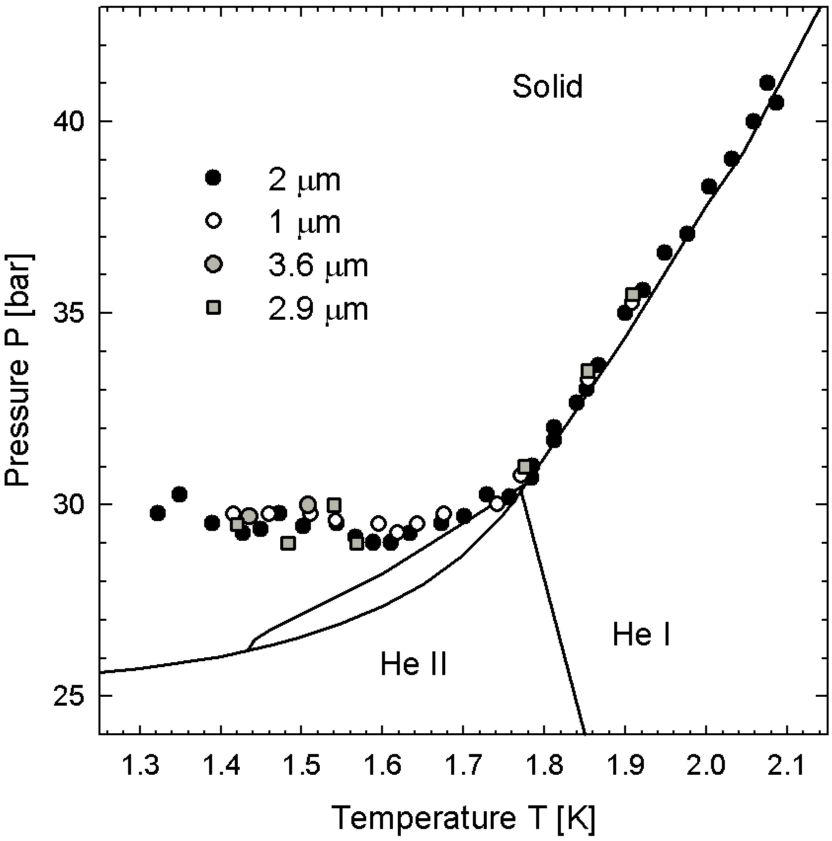

Figure 6.38: Pressure p_T measured in the entire temperature range between 2.1 and 1.3 K as a function of the nozzle diameter d_0 with nozzle diameters of 1, 2, 2.9(#25) and 3.6(#24) μm. The pressures p_T(T) obtained for the 1 and 2 μm nozzle are the most reliable because the measurements were done several times to obtain a better statistic. The pressure p_T observed with the larger nozzles were obtained in a single measurement. Above T = 1.78 K the pressure p_T is found to be independent of d_0.

where the periodic detector pressure p_{det} appears at pressures p_τ approximately 4 bar above the melting line. Figure 6.38 shows the phase line p_τ(T) of the 2 micron nozzle. Additionally the pressures p_τ(T) obtained with nozzle diameters of 1, 2.9 and 3.6 μm are presented. The pressures p_τ(T) obtained for the 1 and 2 μm nozzle are the most reliable because the measurements are done several times to check for reproducibility. Within the estimated experimental error the data for all diameters agree nicely. Maybe the pressures p_τ(T) obtained with the small 1 μm nozzle are slightly shifted above, but this result has to be confirmed.

Chapter 7

Discussion

The expansion of solid Helium into a vacuum offers a novel tool to investigate numerous properties of solid Helium, especially the behavior as a quantum solid. The oscillating intensity of the detector pressure p_{det} is explained by the interplay of diffusion and drift of vacancies. Thus, with the present experiment the dynamics of vacancies can be investigated. In the previous chapter the experimental data were presented. The interpretation and analysis of the data are given in this chapter. One of the key issues is the behavior below $T_c = 1.58$ K and the related occurrence of the supersolid state. Alternative explanations for the oscillating beam flux intensity and the behavior below $T_c = 1.58$ K are also discussed.

7.1 Slip Stick Mechanism as an Alternative Explanation for the Oscillatory Effect

The interpretation of the oscillating effect as a mechanism of slip-and-stick motion of solid Helium inside the source tube can be ruled out. Slip-and-stick motion is caused by the friction between the tube wall and the forced medium that moves through the tube. The motion changes continuously between slip and stick. The continues change causes an periodic effect with a definite slip-and-stick- frequency $f_{slip-stick}$, whereas the periodicity is similar to a sawtooth frequency. This kind of motion is well known and describes classical motion under the influence of friction. Figure 7.1 shows a measurement of the detector pressure p_{det} at constant temperature $T_0 = 1.775$ K and increasing source pressure p_0 above the melting pressure p_m. The detector pressure p_{det} starts oscillating right after increasing the source pressure p_0 above p_m. The shape of the oscillations close to the melting line corresponds to a sawtooth-like similar to a periodicity of slip-and-stick behavior.

Among other things the slip-stick frequency $f_{slip-stick}$ depends on the static and dynamic friction coefficient and the applied force. As shown by Rozman *et al.* [105], the slip-and-stick frequency increases with the velocity of the forced medium and therefore with the applied pressure. If the velocity increases the frequency increases as

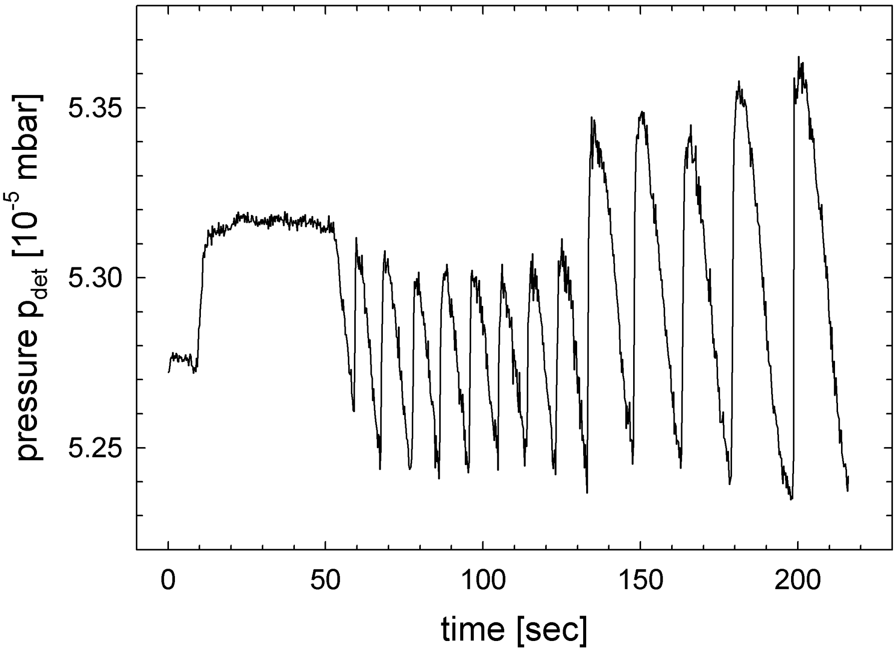

Figure 7.1: Measurement of the detector pressure p_{det} at constant temperature $T_0 = 1.775$ K and source pressures p_0 slightly above the melting pressure. The oscillations of the detector pressure p_{det} occur right after $p_0 > p_m$. The shape of the oscillations close to the melting line corresponds to a sawtooth-like shape as expected for slip-and-stick behavior. ($d_0(\sharp 25) = 2.92$ μm)

well.Figure 6.6 however shows that in our case for increased pressure the frequency decreases, ruling out the slip-and-stick mechanism.

Furthermore the flow of solid Helium inside a tube was investigated by Gordon *et al.* [54]. This experiment shows that inside a cylinder cell solid Helium flows with negligible friction at the cell´s wall even with a very small pressure gradient. This is explained with the Nabarro-Herring mechanism [68] that was introduced in section 3.3.2 of the theoretical model. At the region of a dent at the cell´s wall the stress increases. Following the Nabarro-Herring mechanism vacancies are forced to move to equilibrate the pressure gradient. Thus, the vacancies lubricate the region of the dent and the friction shrinks. As a result, inside the source tube the solid moves with negligible friction.

7.2 The Explanation for T > T$_c$

In the temperature regime $T > T_c = 1.58$ K the period τ was found to increase with increasing source pressure p_0 at constant source temperature T according to:

$$\tau = \varrho (p_0 - p_m)^{\gamma}, \tag{7.1}$$

with γ between ≈ 0.5 and 0.7 and ϱ in the range about $10 - 10^2$, as shown in section 6.2.1. In section 7.5 it is shown that at constant temperature T the period τ depends on the vacancy diffusion coefficient as $\tau \propto D_v^{-1}$. As found by Zuev *et al.* [131] in a temperature regime 1.25 K $<$ T $<$ 2 K the diffusion coefficient D_v decreases exponentially with increasing pressure. Thus, for temperatures T $>$ 1.58 K the dependence of $\tau(p_0)$ is related to the decrease of the vacancy diffusion coefficient for high pressures. The explanation of the temperature dependence of τ results from the same dependence of τ to the vacancy diffusion coefficient. The vacancy diffusion coefficient D_v depends on temperature as introduced in section 2.2.3:

$$D_v = D_0 \, e^{-\frac{\phi_a}{T}}. \tag{7.2}$$

Thus, the vacancy diffusion coefficient falls exponentially with decreasing temperature and the period τ increases, as experimentally observed in section 6.2.2. The increase of the period τ in the temperature regime around 1.78 K is discussed separately in section 7.9.

7.3 The Explanation for T $\leq$ T$_c$

The intriguing behavior at temperatures below 1.58 K and pressures p_0 close above the melting line leads to the observation of two new phase lines in solid Helium-4. These new phases have been neither experimentally observed nor predicted theoretically, previously. Generally, the occurrence of the phase lines p_u(T) and p_τ(T) is due to the increase of the vacancy concentration during the injection of excess vacancies at the solid/liquid interface.

For different source temperatures figure 7.2 marks the pressure p_τ(T) where the oscillations starts occurring. The points deviate from the melting line at 1.78 K and follows the bcc-hcp phase transition down to 1.58 K. Below 1.58 K the pressure p_u(T) increases slightly with decreasing temperature.

In this section the decrease of the period τ below T = 1.58 K is explained by the increase of the vacancies mobility. The period τ_0 is mainly determined by the travel time of the vacancies from the solid/liquid interface to the zone of accumulation and by the time to reach the critical concentration that triggers the percolative collapse. The faster the vacancies move the faster the critical concentration X_v^c is reached. Thus, an increase of the vacancies mobility causes a shorter period τ.

The pressure gradient $\nabla p = (p_1 - p_{s/l})/l$ does not change significantly for T $<$ T$_c$ by assuming that the distance l is constant. Since the pressure gradient ∇p is constant the drift force F_{Drift} is independent on the temperature. Thus, vacancies will be driven by the same net force F_{Drift} above and below T$_c$. Caused by interaction with neighboring atoms the vacancies move at a certain friction with a stationary velocity u_v. Thus,

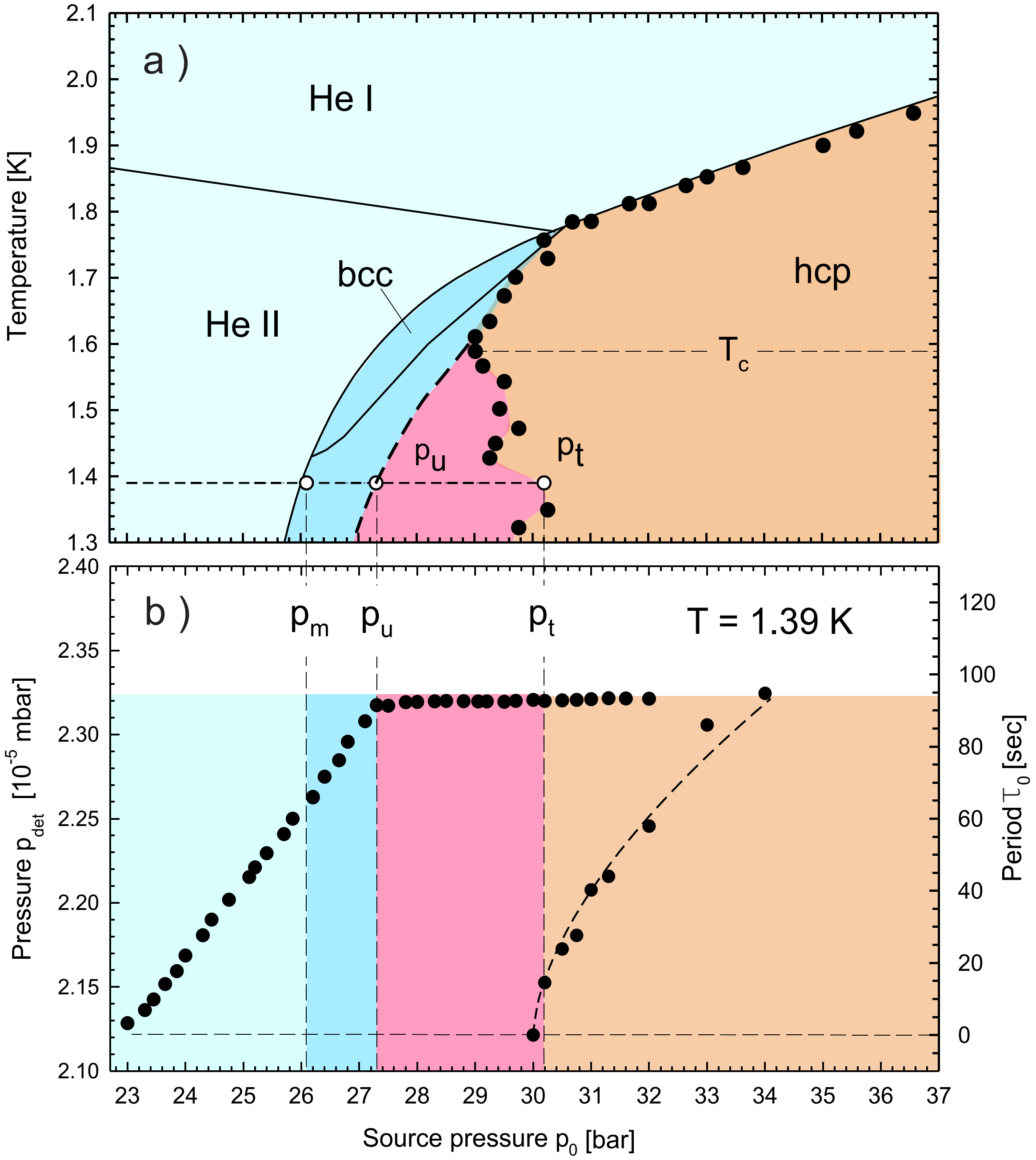

Figure 7.2: The new phase lines p_u(T) and p_τ(T) shown in the phase diagram of Helium-4, respectively: Beside the bcc (between 1.78 and 1.48 K) and hcp phase the first phase is located between the melting line and the phase line outlined by the pressure p_u(T). Below the average detector pressure $\overline{p_{det}}$ is shown as a function of the source pressure p_0 at constant temperature T = 1.4 K The pressures regimes of p_m, p_u and p_τ are indicated, respectively. In at pressures between p_m(T) and p_u(T) the solid is found to behave as a liquid. Between the phase line p_u(T) and p_τ(T) a second phase occur, that does not offer any oscillations in the beam flux intensity.

the change of the period τ above and below 1.58 K indicates a decrease of friction. As a main feature of these regimes below p_τ(T) in solid Helium below T = 1.58 K the vacancies partly move in a frictionless environment, or at least in an environment of reduced friction.

This scenario is indicated in figure 7.3 where the different phases are shown in the nozzle‘s source tube. The phase diagram shows the both phases (blue and red) at which the oscillating behavior is not observed. The line that separates the green and the yellow phase corresponds to the melting line that is shifted up to 10 bar above p_m. It is assumed that for source pressures p_0(T) the vacancies have to cross the same distance l from the solid liquid interface to the cross section S_0. For two temperatures T = 1.83 K (2) and T = 1.39 K (1) the scenarios inside the source tube are illustrated. The temperatures correspond to the temperature regime above and below T$_c$, respectively. For T = 1.83 K (1) the vacancies have to cross a region (yellow) of normal solid behavior. The corresponding period is $\tau \approx 320$ seconds. In the temperature regime below T$_c$ the vacancies cross two phases that are separated by p_u and p_τ. In both phases (blue and red) vacancies move with a higher mobility and therefore almost frictionless, because the period τ in this regions is found to be zero. Thus, the vacancies need less time to cover the distance l and the period τ decreases at temperatures T = 1.58 K. For the present temperature T = 1.39 K and source pressure $p_0 = 10$ bar + p_m the period is $\tau \approx 150$ seconds.

This model explains also the source pressure dependence of the ratio between the maximum period τ_{max} at T$_c$ = 1.58 K and the minimum period τ_{min} at temperatures T $\approx$ 1.48 K. Figure 6.6 indicates a dependence between the dropdown from the maximum period at T$_c$ to the shorter period at temperatures T $\leq$ 1.48 K. Below 1.48 K the period seems to be independent of the temperature. A little effect occurs at T = 1.42 K where the period shows a little maximum, but just for low source pressures up to 31 bar. In section 7.9 the meaning of this maximum at 1.42 K will be discussed.

From the model presented in figure 7.3 the phase line p_τ(T) can be derived from the dropdown of the period τ below 1.58 K, as shown by Benedek [8]. Below T$_c$ in a pressure range between $p_m < p < p_\tau$ the period τ_c is given by equation:

$$\tau_c = \frac{l}{u_v} = \frac{l}{\mu_v \Delta v_r \nabla p}, \tag{7.3}$$

but the critical pressure is now $p_c = p_\tau$ and $l = (p_0 - p_m)/\nabla p$ has to replaced by the shorter length $l' = (p_0 - p_\tau)/\nabla p$ that corresponds to the width of fraction of the normal solid behavior. It follows that

$$\frac{\tau_{min}}{\tau_{max}} = \frac{l'}{l} = \frac{p_0 - p_\tau(T)}{p_0 - p_m(T)} \tag{7.4}$$

In figure 7.4 the linear relation of equation 7.4 is demonstrated with the experimental data for τ_{min} and τ_{max} and the corresponding pressures. The ratio $\frac{\tau_{min}}{\tau_{max}}$ converges to 1 for higher source pressures $p_0 \simeq 43$ bar, because the vacancies have to cross a larger region under normal solid conditions, related to the distance l they have to

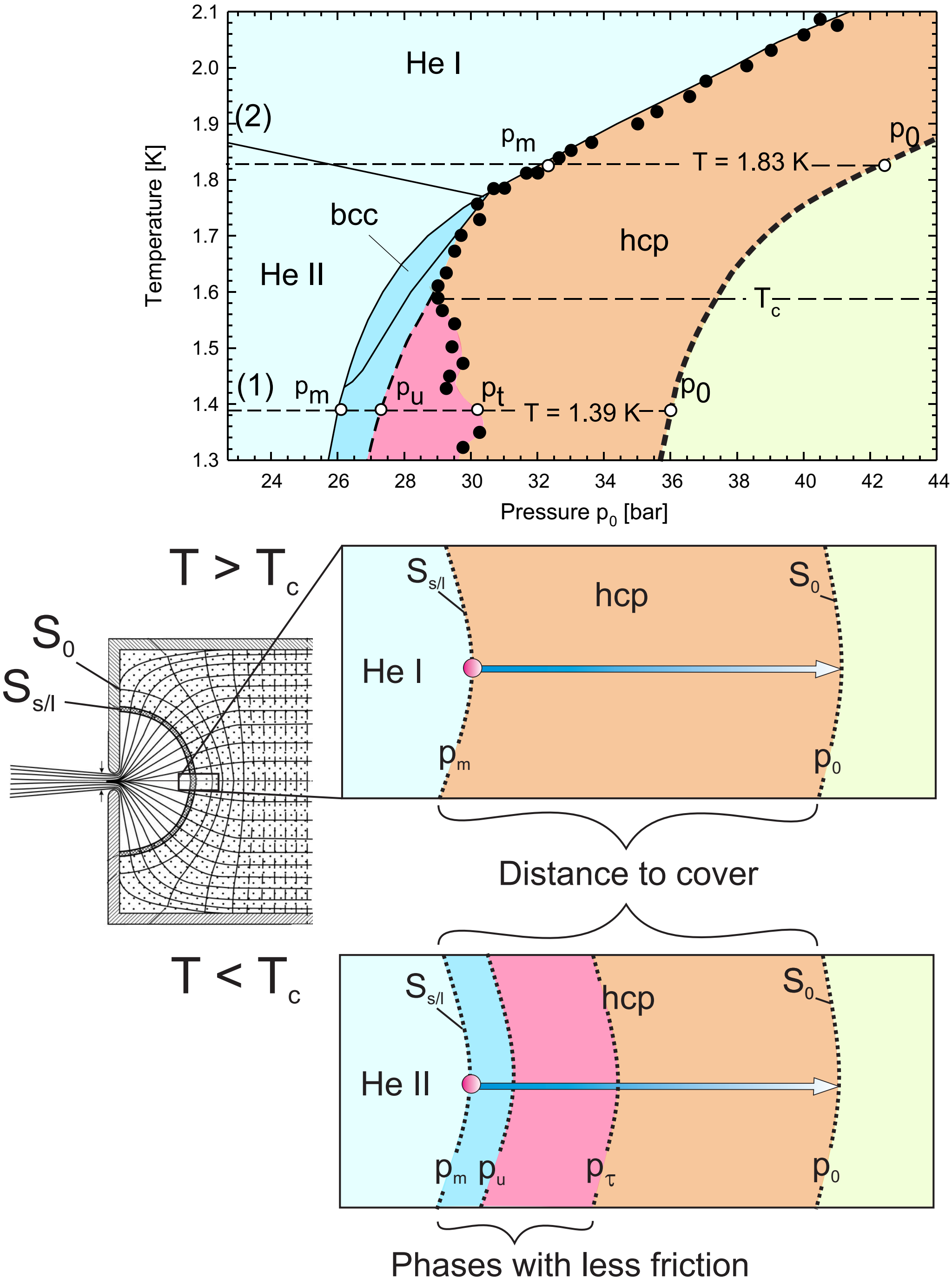

Figure 7.3: For temperatures above and below $T_c = 1.59$ K the scenario inside the nozzle tube changes. At temperatures $T > T_c$ (here indicated at (2) for $T = 1.83$ K) the vacancies move from the cross section $S_{s/l}$ up to the region S_0 were they meet the friction that corresponds to the normal solid behavior. In the phase diagram the yellow region indicates the regime of normal solid behavior. To compare the scenario above and below T_c the source pressure $p_0(T) = p_m(T) + 10$ bar is indicated by the transition between the yellow and green section. For temperatures $T < T_c$ (indicated at (1) for $T = 1.39$ K) the vacancies move almost frictionless up to pressures p_τ. Thus, the time they need to cover the distance l decreases below temperatures $T_c = 1.58$ K.

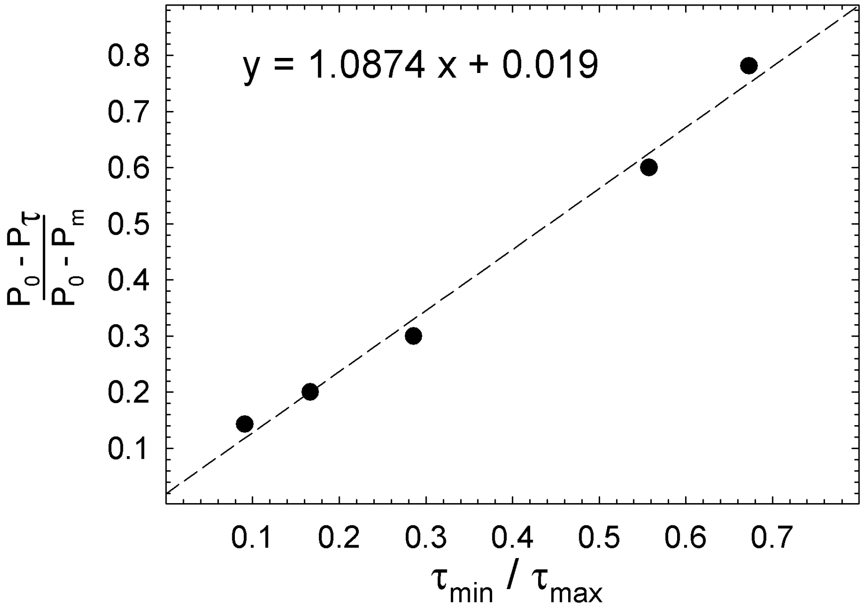

Figure 7.4: Applying equation 7.4 for measurements of the period τ_{max} and τ_{min} at source pressures p_0 = 30.5, 31, 32, 36.3 and 40.3 the linear dependence confirms the assumption that the phase line p_{tau} can be derived from the ratio between τ_{max} and τ_{min}. The exactness of this method is shown in the linear fit where y ≈ x verifies equation 7.4 and 7.6.

cover. Comparing the data for two measurements the phase line p_τ(T) can be derived because for p_τ it follows:

$$p_\tau = p_0 - \frac{\tau_{min}}{\tau_{max}}(p_0 - p_m), \tag{7.5}$$

and finally for the temperature dependent pressure p_τ(T):

$$p_\tau(T) = p_0 - \frac{\tau_{min}(T)}{\tau_{max}}(p_0 - p_m(T)). \tag{7.6}$$

In figure 7.5 the result for p_τ(T) derived with equation 7.6 are presented. For three different source pressures p_0 = 32, 36 and 41 bar, respectively, the results for p_τ(T) correspond in a good agreement with the experimental results.

Another effect presented in section 6.3.3 that occurred below temperatures T = 1.58 K is the sub-oscillations of the detector pressure p_{det}. From the Bernoulli relation between p_0 and p_{det} it follows that the lowest pressure $p_{det,bg}$ corresponds to the pressure p_u and the pressure observed at top of the small oscillations $p_{det,top}$ corresponds to the pressure p_τ for high source pressures. The sub-oscillations amplitude seems oscillates between p_u and p_τ, respectively. A possible explanation is given by comparing the phenomenon

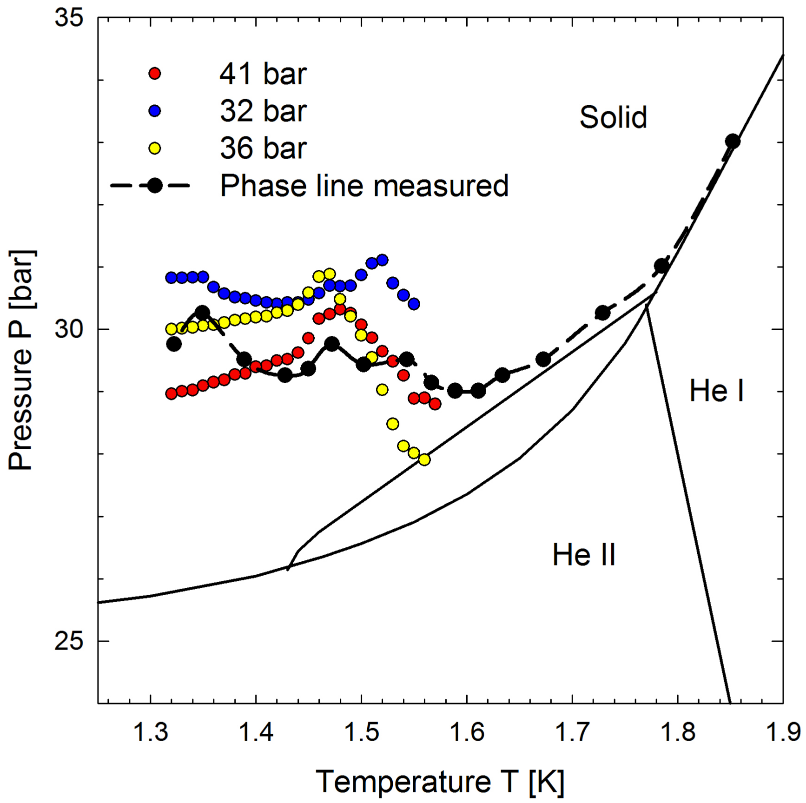

Figure 7.5: The theoretical phase line p_τ(T) obtained by applying equation 7.6 for measurements of the period τ for three different source pressures p_0 = 32, 36 and 41 bar, respectively. The good agreement between the theoretical approach and the experimental observation emphasizes that the decrease of the period τ is a direct consequence of the phase line p_τ(T).

with "gun-oscillations", that appear in semiconductors. Generally, oscillations occur between two unstable states.

The increase of the mobility below 1.58 K is caused by the increase of the vacancies concentration. Solid Helium-4 forms a new state of matter just if the concentration of vacancies overcome a threshold value X_c. The small oscillations can be explained in the following way: Vacancies are accelerated by the strong pressure and concentration gradient, respectively. The vacancies density in a defined space element V and time interval Δt can be described by $N_{vac}/(\Delta t * V)$, where N_{vac} is the number of vacancies. If the mobility is increased the vacancies density in the volume element V and time interval Δt decreases below X_c. In this case the solid behaves as normal solid Helium-4 and the vacancies mobility suddenly decreases. Afterwards the concentration increases again. Increasing the vacancies concentration causes again the formation of the new state of matter and the vacancies are accelerated again. If the velocity dependent concentration decreases below X_c again, the mechanism starts again.

In summary the sub-oscillations in the detector pressure signal can be explained by the oscillation between the new state of matter and the normal solid in Helium-4. The transition between both states is caused by the density of vacancies that depends on the mobility. In the case of normal solid the pressure inside the nozzle increases up to p_τ. If the vacancies mobility decreases and the concentration increases again the pressure drops down to p_u. The behavior itself occurs at high source pressures. The reason for this is still unclear. The increase of the vacancies mobility explains the decrease of the period below T$_c$, whereas the non oscillating region at constant detector pressure between p_u(T) and p_τ(T) is not understood at all. Possible explanations will be discussed in section 7.13.

7.4 Discussion of the bcc Phase Behavior

In figure 6.17 the stepwise increase of the source pressure p_0 and the detector pressure p_{det} is shown at temperatures T = 1.68 K and 1.59 K, respectively. The periodic oscillation occur at source pressures $p_0(1.68\text{ K}) = 30$ bar and $p_0(1.59\text{ K}) = 29$ bar, right at the bcc-hcp transition. As a general result the periodic Geyser-like oscillations are not observed for source conditions inside the bcc phase. In the temperature range between 1.78 K and 1.6 K figure 6.21 illustrates that the points of first periodic oscillating occurrence follow the bcc-hcp phase transition. Above 1.68 K the points follow the melting line. Below 1.6 K the points mark the phase line p_τ(T). The behavior inside the bcc phase corresponds to the fluid-like solid as observed below p_u(T). Investigating the increase of the beam flux no indication for a phase transition is observed. As mentioned in the previous section the period mainly depends on diffusion and drift. Diffusion itself is determined by the self diffusion coefficient for vacancies, D_v. The diffusion coefficient for hcp solid Helium was measured in many experiments and is of the order of 10^{-5} cm^2/sec [131, 98]. Inside the bcc phase the diffusion coefficient D_v was investigated by Zuev *et al.* and determined to be $\approx 10^{-4}$ cm^2/sec and herewith one order of magnitude larger that in hcp solid Helium. Thus, vacancies in the bcc phase of solid Helium move about one order of magnitude faster than in the hcp ordered phase. The diffusion constant is defined as the number of particles (in mole) that move through an area of 1 cm^2 in the time of 1 second. Responsible for the higher diffusion constant in the bcc phase is the difference in the activation energy ϕ_a for self diffusion. The diffusion constant is related to the activation energy ϕ_a as already shown in equation A.10,

$$D_v = D_0 \, e^{-\frac{\phi_a}{kT}} \tag{7.7}$$

.

Table 7.1 gives an overview of the experimental and theoretical results for ϕ_a.

As a result the activation energy for diffusively vacancy motion in the bcc ordered phase is in the range between 5-8 K, whereas in the hcp phase ϕ_a is quite higher between 6 and 20 K. Additionally, figure 7.6 [113] gives an overview of the experimental results for ϕ_a in hcp solid Helium-4. The data points have been obtained with different experimental techniques, which is surely one reason for the wide spread of the data. Even the wide range of results obtained for the hcp phase show that the activation

Phase	V_{mol} [cm^3/mole]	ϕ_a [K] theoretical	ϕ_a [K] experimental
bcc He4		8.08±2.76[a]	5.5±0.5[b]
		6.66±3.86[a]	6.5 ±0.2[c]
		7.66±4.73[a]	5.2 ±0.5[c]
	20.92-21.08		5.1[d]
hcp He4	20.3		6.3[d]
	20.49		6.1[d]
	20.67		6[d]
	20.82		5.8[d]
		15.63±3.85[a]	15±1[b]
		15.55±4.63[a]	14±3[c]
bcc He3	24.2		4.3[d]
	24.3		4.1[d]
	24.4		3.9[d]
	24.5		3.8[d]
	24.6		3.7[d]
	24.7		3.7[d]

Table 7.1: Overview of the activation energy, obtained by experimental and theoretical investigation. Especially the results for the activation energy in the hcp phase spread in a wide range. Regarding the results by Chaudhuri [24] , Schuster [110, 97] and Guyer [67] the difference between the bcc and hcp phase becomes clearly.

[a]Reference [24] [b]Reference [67] [c]Reference [110, 97] [d]Reference [131]

energy ϕ_a for solid Helium is a quantity that is difficult to access. Because of the quantum properties of vacancies in solid Helium the activation energy gives an upper limit for the energy that is necessary for vacancy motion. Moreover the real energy is determined by an energy band with band width Δ of the order of some degrees. That makes the investigation of ϕ_a difficult.

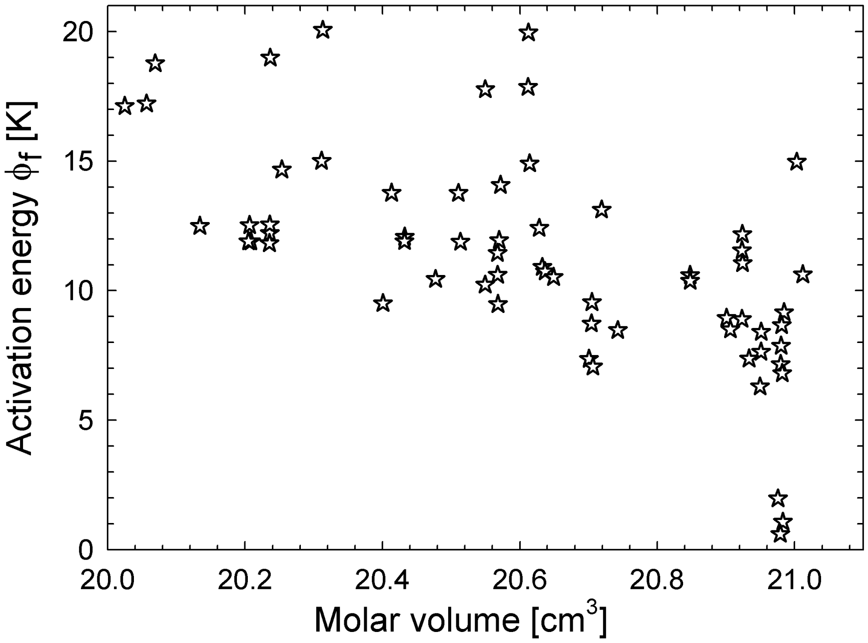

Figure 7.6: Activation energy ϕ_a as a function of the molar volume in hcp ^{4}He by Simmons [113]. Different experimental techniques have been used to obtain the data, like NMR Measurements, X-Ray scattering and acoustic excitations.

In the bcc-ordered solid the band with Δ is in the range of ϕ_a. Therefore, the vacancies tunnel through the crystal with a certain probability. Thus, the periodic effect at source pressures and temperatures corresponding to the bcc phase is expected to be shorter than in the hcp phase. Surprisingly, the period vanishes. Vacancies inside the bcc phase move under conditions sufficient to form the new state of matter even above $T_c = 1.58$ K. The fluid-like behavior observed in the bcc phase resembles the experimental results of Sanders [106], who obtained that in case the plastic deformation in the bcc phase the solid behaves more like a viscous fluid than a crystalline solid.

7.5 Results of the Diffusion Coefficient D_v

Many experiments [55, 12, 131, 101, 36] have been carried out during the last decades to determine the pressure and temperature dependence of the diffusion coefficient of vacancies D_v. In D_v the quantum nature of solid Helium becomes visible. D_v is in the range of $\sim 10^{-5}$ cm^2/sec, comparable to diffusion coefficients in a liquid [102].

In the present model the vacancies‘ dynamic is described by equation 3.11. The mobility, and therefore the diffusivity as well, changes during one period. Therefore, the obtained diffusion coefficient is averaged over the period τ_0. For short times $t \ll \tau_v, \tau_r$ in the range of some seconds the periodic mechanism is dominated by the diffusion of vacancies. Thus, equation 3.11 can be reduced for short times $t \ll \tau_v, \tau_r$ in the form:

$$u_{exit,osc}(t) = \sqrt{\frac{4D_v}{\pi t}} (\frac{\phi_s}{\phi_n})^2, \tag{7.8}$$

where $u_{exit,osc}(t)$ is the oscillating part of the jet velocity u_{exit}, and $\frac{\phi_s}{\phi_n}$ the ratio of the tube to the orifice‘s cross section. The jet velocity u_{exit} is given by

$$u_{exit} = \frac{4 \cdot 5.9\ S_{eff}}{R\ T_{gas}\ \pi d_0^2}\ p_{det}, \tag{7.9}$$

where the factor 5.9 comes from the conversion of the pressure gauge $p_{det}(He) = 5.9 \cdot\ p_{det}(N_2)$, S_{eff} is the corresponding pumping speed, R the gas constant, T_{gas} the room temperature and d_0 the nozzle diameter. For $d_0 = 2\mu m$ one obtains $u_{exit} = 5.52 \cdot 10^6 \frac{m}{sec\ mbar} \cdot p_{det}$.

One has to separate the beam flux into an oscillatory part and the underground flux because equation 7.8 just regards the oscillatory signal in the beam flux. Therefore, the velocity $u_{exit,osc}$ is given by the detector pressure $u_{exit,osc} = 5.52 \cdot 10^6 \frac{m}{sec\ mbar} \cdot p_{det}^{osc}$, with $p_{det}^{osc} = p_{det}(t) - p_{det,bg}$. One obtains for the diffusion coefficient D_v:

$$D_v = u_{exit,osc}^2 t \frac{\pi}{4} (\frac{\phi_n}{\phi_s})^4. \tag{7.10}$$

From equation 7.10 it follows that for short times t $\ll \tau_v, \tau_r D_v$ is proportional to $u_{exit,osc}^2 t$ that can generally be found in a certain time range Δt_{D_v}. Doing so the dashed line in figure 7.8 shows the result for D_v as a function of time t. Between 6 sec $< t <$ 15 sec the obtained value for $D_v \approx 1.4 \cdot 10^{-5}$ cm^2/sec. This value is in good agreement with the data of D_v from the literature [12, 131]. Another possibility is to fit the data of $u_{exit,osc}$ by equation 7.8 using D_v as one of the fit parameter:

$$u_{exit,osc}(t) = \sqrt{\frac{4D_v}{\pi(t - t_0)}} (\frac{\phi_s}{\phi_n})^2 + u_{exit,0} \tag{7.11}$$

where the two additional fit parameters t_0 and $u_{exit,0}$ are included to shift the data in time scale and the velocity scale. As defined in the theoretical model the detector pressure that separates the oscillatory part from the background signal is assumed to be $p_{det,bg}$, whereas the effective value is unknown. Therefore, $u_{exit,0}$ is introduced as a fit parameter in equation 7.11. For the same reason the time t_0 is introduced because the exact time t = 0 when the periodic peak occurs is only assumed to be equal to the begin of the oscillation. Fitting the data of the present experiment one obtains

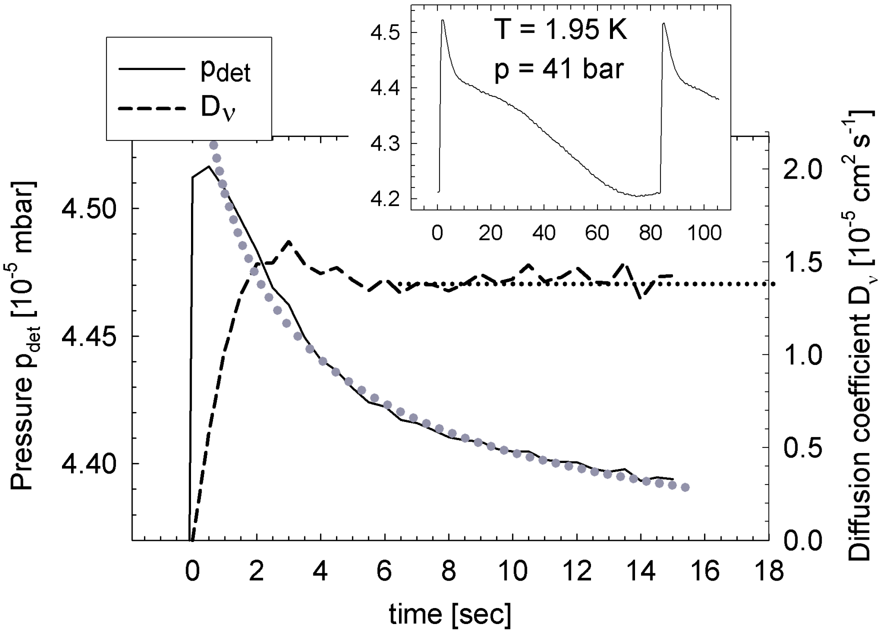

Figure 7.7: Diffusion coefficient D_v obtained from the oscillating detector pressure p_{det} at temperature T = 1.95 K and source pressure p_0 = 41 bar. The dotted line shows the obtained value for D_v by applying equation 7.10. Between 6 sec < t < 14 sec the value for $u^2_{exit,osc} \cdot t \propto D_v$ is constant, and the diffusion coefficient is derived to be $D_v \approx 1.4 \cdot 10^{-5}$ cm^2/sec. The grey dotted line at 1 sec < t < 15 sec shows the fit by applying equation 7.11. The corresponding diffusion coefficient is derived to be $D_v \approx 1.4 \cdot 10^{-5}$ cm^2/sec, as well. ($d_0(\sharp 17) = 2.28\ \mu$m)

the same result for $D_v \approx 1.4 \cdot 10^{-5}$ cm^2/sec in the entire range for t between 1 and 15 seconds.

This method works for temperatures above the critical temperature $T_c = 1.58$ K and $T \ll T(p_m)$. Close to the melting line the periodic shape (as seen, e.g., in figure 6.4) can not be fitted in a satisfactory way because the condition $t \ll \tau_v, \tau_r$ is not fulfilled. The corresponding results obtained for D_v decrease with increasing temperature and herewith it disagrees with the theory, because close to the melting line the diffusion coefficient has to increase. Below $T_c = 1.58$ K the diffusion coefficient can‘t be derived by equation 7.10 and 7.11, because the theoretical model just describes the normal solid behavior at temperatures T > 1.58 K. Another problem that makes the method inefficient is the time resolution of the data. The time resolution is set to be 250 and 500 msec, respectively. In some cases the time range Δt_{D_v} is less than 4-5 seconds. As the worst case less than 8-10 data points are available to obtain a value for D_v. As a result the temperature depending diffusion coefficient varies in a wide range so that the method can‘t be applied in a satisfactory way.

Whereas it is also possible to derive the diffusion coefficient D_v directly from the measured period. Since the period τ_0 is determined by the time the vacancies need to diffuse through the solid until they accumulate up to the critical concentration, the vacancy diffusivity D_v is found to be inversely proportional to the period τ, following:

$$D_v = 0.05 \frac{T^2}{\tau_0 (p_0 - p_\tau)}, \tag{7.12}$$

,

where the pre-factor 0.05 is a constant fitted to the pressure dependent data of D_v obtained by Zuev [131]. Applying equation 7.12 the diffusion coefficient is shown in figure 7.8 as a function of pressure $p_0 - p_\tau$ at constant temperature T = 2.17 and 1.83 K, respectively. The data are taken from figure 6.7 and 6.6. The slope in figure corresponds to the negative exponent γ in equation 7.1:

$$D_v \propto \tau_0^{-1} \propto (p_0 - p_\tau)^{-\gamma} \tag{7.13}$$

The temperature dependence of D_v is given in figure 7.9 by using the same method of the inverse proportionality of D_v to τ_0. The temperature dependence of the diffusion coefficient is shown for three different source pressures $p_0 = 32$, 36 and 41 bar, respectively. The data are taken from the measurement seen in figure 6.16. As expected, the diffusion coefficient decreases with decreasing temperature. As an intriguing result D_v has a minimum at $\mathrm{T}_c = 1.58$ K for source pressures $p_0 = 32$ and 36 bar. This minimum might be a direct consequence of the dropdown of the period τ_0 below T_c. The results of figure 7.9 are comparable with investigations of D_v done by e.g. Kishvarsanyi *et al.* [80] and Pushkarov [101]. In these experiments the diffusion coefficient of ^{3}He impuritons in solid Helium-4 are investigated. For low concentrations of ^{3}He the diffusion coefficient increases at decreasing temperatures similar to the results presented here. A detailed discussion is given in section 7.8.

7.6 Activation Energy ϕ_a Derived From D_v(T)

Beside the vacancy diffusion coefficient D_v the most interesting observable of vacancies in solid Helium is the activation energy ϕ_a, as introduced in section 2.2.3. Generally the activation energy ϕ_a can be derived from the temperature dependent diffusion coefficient D_v(T) according to the law of Arrhenius :

$$ln \frac{D_v}{T} = -\phi_a \, T^{-1} + const \tag{7.14}$$

As a result, in a linear regime between $ln(\frac{D_v}{T})$ and the inverse temperature one obtains the activation energy ϕ_a by:

$$-\frac{ln\left(\frac{D_{v1} T_2}{D_{v2} T_1}\right)}{T_2^{-1} - T_1^{-1}} = \phi_a \tag{7.15}$$

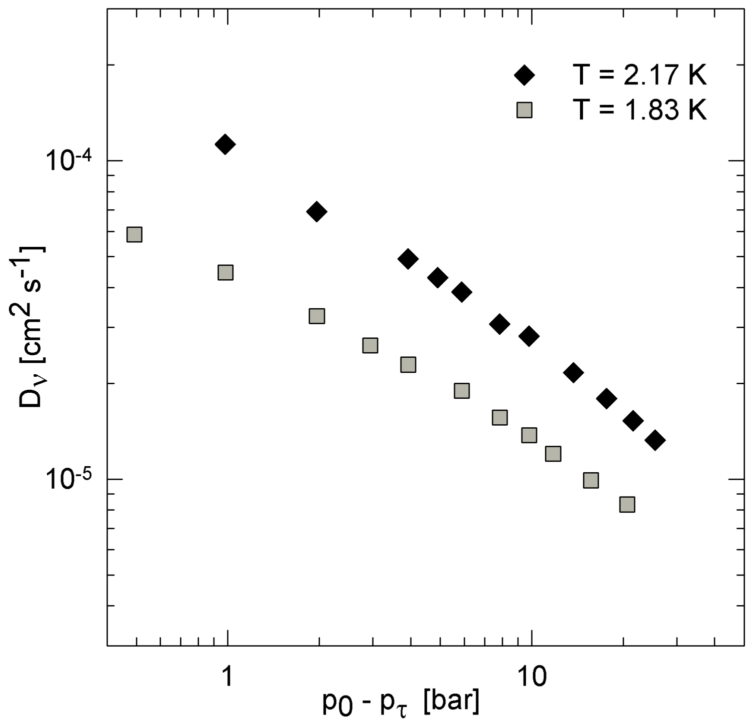

Figure 7.8: Diffusion coefficient D_v as a function of $p_0 - p_\tau$ derived from the source pressure dependent period $\tau(p_0)$ at two constant temperatures T = 2.17 K and 1.83 K, respectively. The data of τ are taken from the measurement seen in figure 6.6. The data confirm the temperature and pressure dependence of D_v measured by Zuev *et al.* [131] with an extension to higher pressures and temperatures.

Figure 7.9 shows D_v(T) as a function of temperature in a range between 2.1 and 1.3 K for three different source pressures $p_0 = 32.0$, 36.3 and 40.3 bar. Applying equation 7.14, figure 7.10 shows the logarithm of the Diffusion coefficient D_v divided by T as a function of inverse temperature. As a result one obtains a non exponential behavior of D_v so that the linear fits come out to be difficult. The increasing period at the region around 1.78 K (inverse temperature 0.56 K^{-1}) and the herewith related temperature dependent decrease of D_v is one of the handicaps that makes the fits difficult. But in some temperature range the Arrhenius dependence is found to be linear, as seen in figure 7.10 which is indicated by the larger circles. Especially at T$_c$ < 1.58 K, where the period τ decreases, the diffusion coefficient increases. Therefore, figure 7.10 is separated in two different regimes of inverse temperature, namely above and below 0.64 K^{-1} which corresponds to T$_c$ = 1.58 K. The activation energy ϕ_a is equal to the slope of the behavior in figure 7.10. Thus, one directly obtains that the activation energy ϕ_a decreases at temperatures below 1.58 K.

For $p_0 = 32$ bar and T > 1.58 K the activation energy is found to be $\phi_a(32bar) = 21.6$

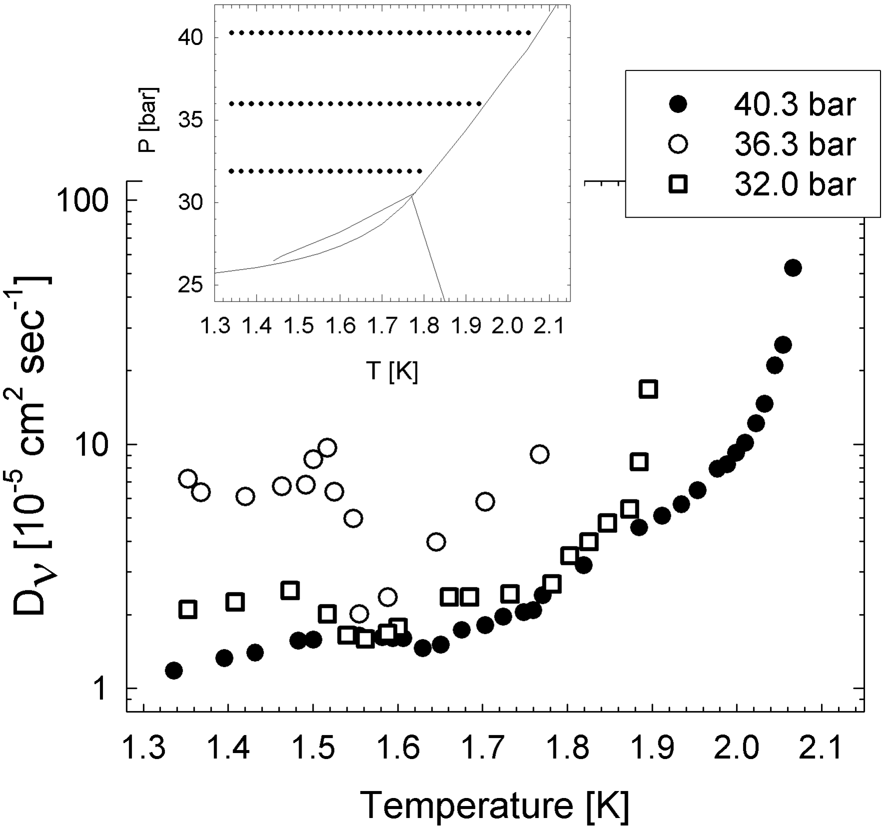

Figure 7.9: The temperature dependence of D_v by deriving D_v as a function of τ_0. The temperature dependent diffusion coefficient is shown for three different source pressures $p_0 = 32$, 36 and 41 bar, respectively. For source pressures $p_0 = 36.3$ and especially 32 bar the diffusion coefficient D_v(T) has a minimum at T$_c$ = 1.58 K, as a result out of the maximum period τ_{max}.

K. The obtained values for the activation energy ϕ_a for $p_0 = 36$ bar in the temperature range between T = 1.78 K and $T(p_m)$ are $\phi_a(36bar) = 27.0$ K and $\phi_a(41bar) = 25.5$ K. These values for the activation energy are in the right order of magnitude. Whereas the theoretical assumption is not verified that ϕ_a close to p_m is small because in figure 7.10 (36.3 and 40.3 bar) the slope increases for higher temperature. Applying the fits in a linear regime below T$_c$ = 1.58 K the activation energy ϕ_a decreases one order of magnitude. For the low pressure data $p_0 = 32$ bar the activation energy $\phi_a = 2.8$ K is minimal.

In a further application the activation energy is obtained from the diffusion coefficient derived in figure 7.9. At this measurement the diffusion coefficient is derived for constant temperatures 2.17 K and 1.83 K and pressures p_0 up to 80 bars. In figure 7.11 two values of D_v for both temperatures with the same source pressure $p_0 = 49$ bar, respectively, are summarized to obtain further values for ϕ_a. At source pressure $p_0 = 49$ bar the activation energy is derived to be $\phi_a = 16.7$ K between 2.17 K and 1.87 K. The activation energy is found to be in a good agreement with results shown

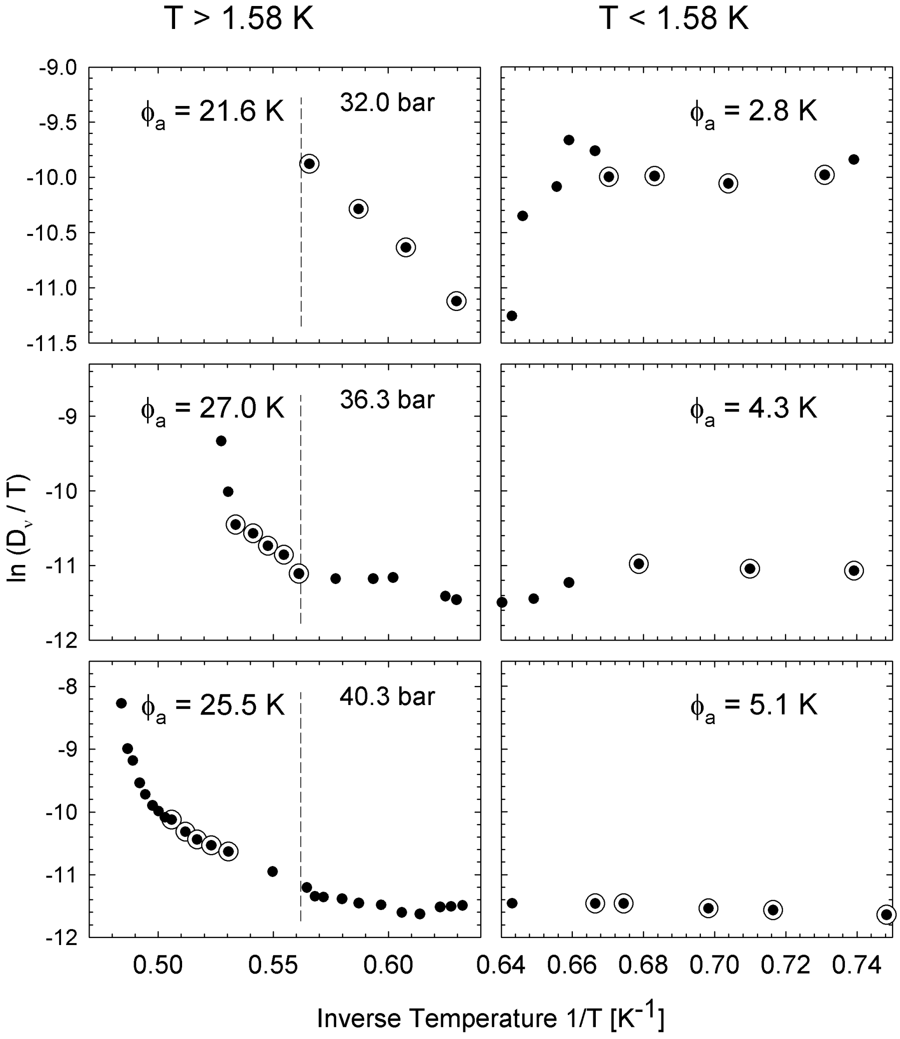

Figure 7.10: The Arrhenius plot is shown for three source pressures p_0 = 32, 36.3 and 40.3 bar, respectively. Following equation 7.14 the logarithm of the diffusion coefficient D_v(T) divided by temperature T as a function of the inverse temperature gives the Arrhenius plot to obtain the activation energy ϕ_a. The inverse temperature regime is separated into corresponding temperatures above and below $T_c = 1.58$ K. For temperatures above T = 1.58 K the activation energy ϕ_a is derived to be between 21.6 K (32 bar) and 25.5 K (40.3 bar) in a good agreement with data of ϕ_a as seen in figure 7.1. The vertical dashed line indicates the corresponding temperature T = 1.78 K, at which the hcp-bcc phase transition occurs. The increase of the period τ at T = 1.78 K affects the linear behavior between ln(D_v/T) and the inverse temperature, especially at source pressure p_0 = 36.6 bar. Thus, the activation energy has to be derived weather above or below T = 1.78 K. Below T = 1.58 K the constant diffusion coefficient D_v(T) causes a decrease of ϕ_a. The activation energy is derived to be between 2.8 K (32 bar) and 5.1 K (40.3 bar). Obviously the activation energy increases with increasing source pressure p_0, independent of the temperature regime.

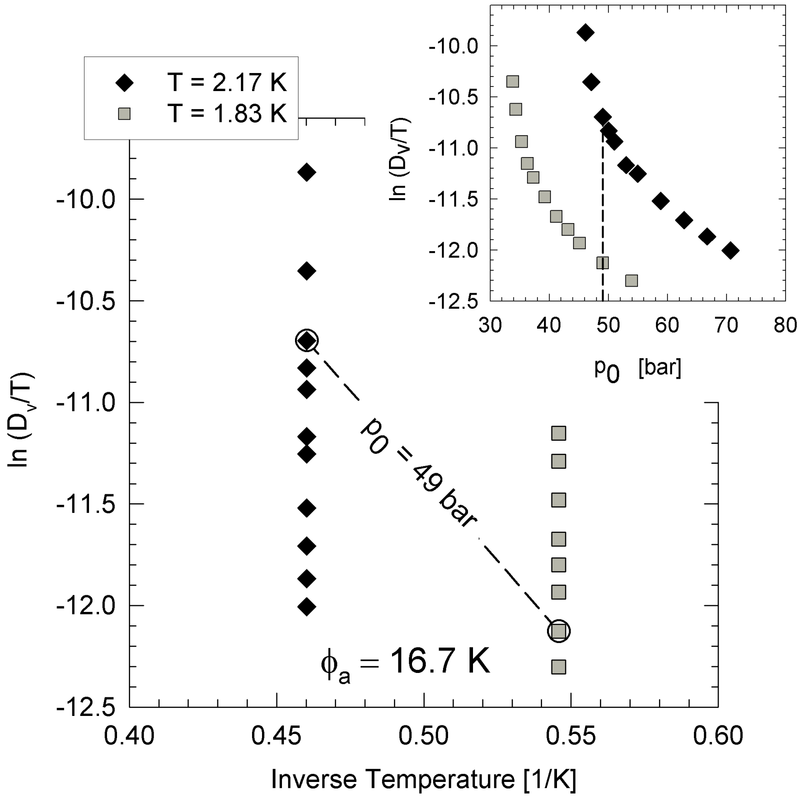

Figure 7.11: Arrhenius plot of the pressure dependent data of D_v, taken from figure 7.8. To obtain a value for the activation energy ϕ_a two values of $\ln(D_v/\mathrm{T})$ with the same source pressure $p_0 = 49$ bar are picked out, as seen in the inset The activation energy is derived to be $\phi_a = 16.7$ K.

in figure 7.6 for high pressures. As a general result the analysis of the activation energy indicates that the temperature and pressure dependence of the period τ of the Geyser oscillations offers a direct method to investigate the activation energy in solid Helium-4. In the future this method can be enlarged in a wide regime of temperature an pressure.

7.7 Analysis and Interpretation of the Integral A_{osc}

Each Helium atom that leaves the orifice creates a vacant lattice site inside the bulk solid. Thus, the signal of the detector pressure p_{det} corresponds directly to the vacancy generation rate. The background signal $p_{det,bg}$ consists of atoms whose vacancies are responsible for the melting process. The oscillatory part of the beam flux consists of atoms whose vacancies in the bulk solid are assumed to generate the periodic effect. Separating the mean beam flux and the oscillatory behavior as demonstrated in figure

7.12, the number of vacancies responsible for the periodic collapse of the solid is proportional to the area A_{osc} that indicates the oscillating beam flux.

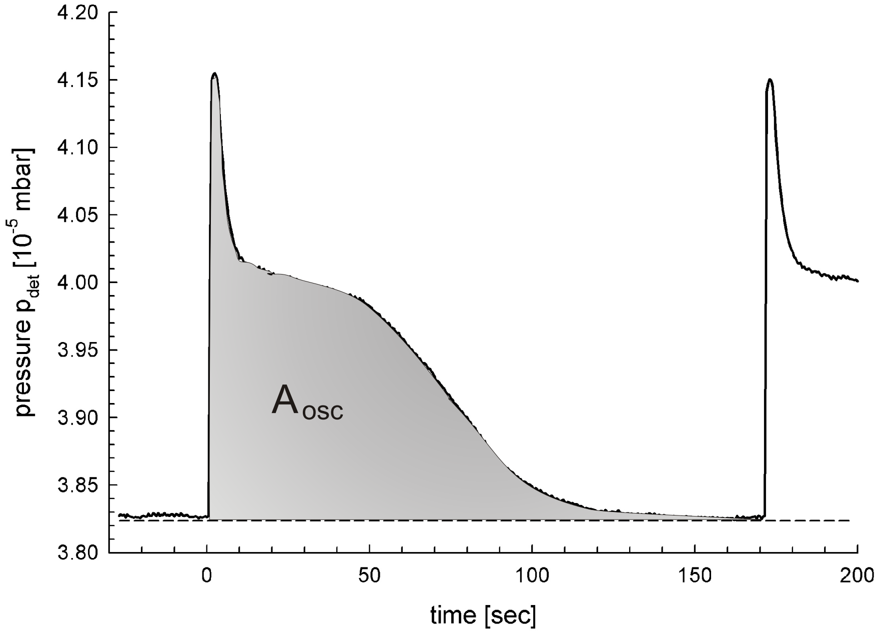

Figure 7.12: A single oscillation of the detector pressure inside the vacuum chamber p_{det} at 35 bar and T = 1.725 K. The dashed line at $3.83 \cdot 10^{-5}$ is a guide to the eye and remarks the separation between the oscillatory part and the background flow. According to the pressure at the top of the peak in relation to the background pressure the oscillatory part is about ≈ 8 percent of the entire flux. The grey area A_{osc} indicates the area of the oscillating beam flux. Because of each atom leaving the orifice generates a vacancy, the atoms that build the area A_{osc} corresponds to the number of vacancies that are responsible for the oscillatory effect. ($d_0(\sharp 17) = 2.28\ \mu$m)

In determine the area A_{osc} of the oscillatory part the number of vacancies necessary for the percolative collapse can be obtained as a function of temperature T and source pressure p_0, as well. In figure 7.13 the value of the area A_{osc} of the oscillating part in the signal is plotted as a function of temperature for two different source pressures $p_0 =$ 32 and 41 bar, respectively (upper figure). Additionally, the temperature dependence of the period τ is shown above. As an interesting result, for both measurements the maximum of A_{osc} is at temperature T = 1.78 K (right dashed line) and is not at the critical temperature T = 1.6 K (left dashed line), where the period τ has it's maximum. This result indicates that at T = 1.78 K the number of vacancies for the percolative collapse and the herewith related critical concentration X_c is maximal. As seen in figure 7.13 the period at T = 1.78 K increases, a result that is already shown in figure 6.12. As shown in the phase diagram at the inset of figure 6.12 the temperature T = 1.78 K corresponds to the bcc-hcp transition.

At temperatures below 1.78 K the value of the area A_{osc} decreases slightly for decreas-

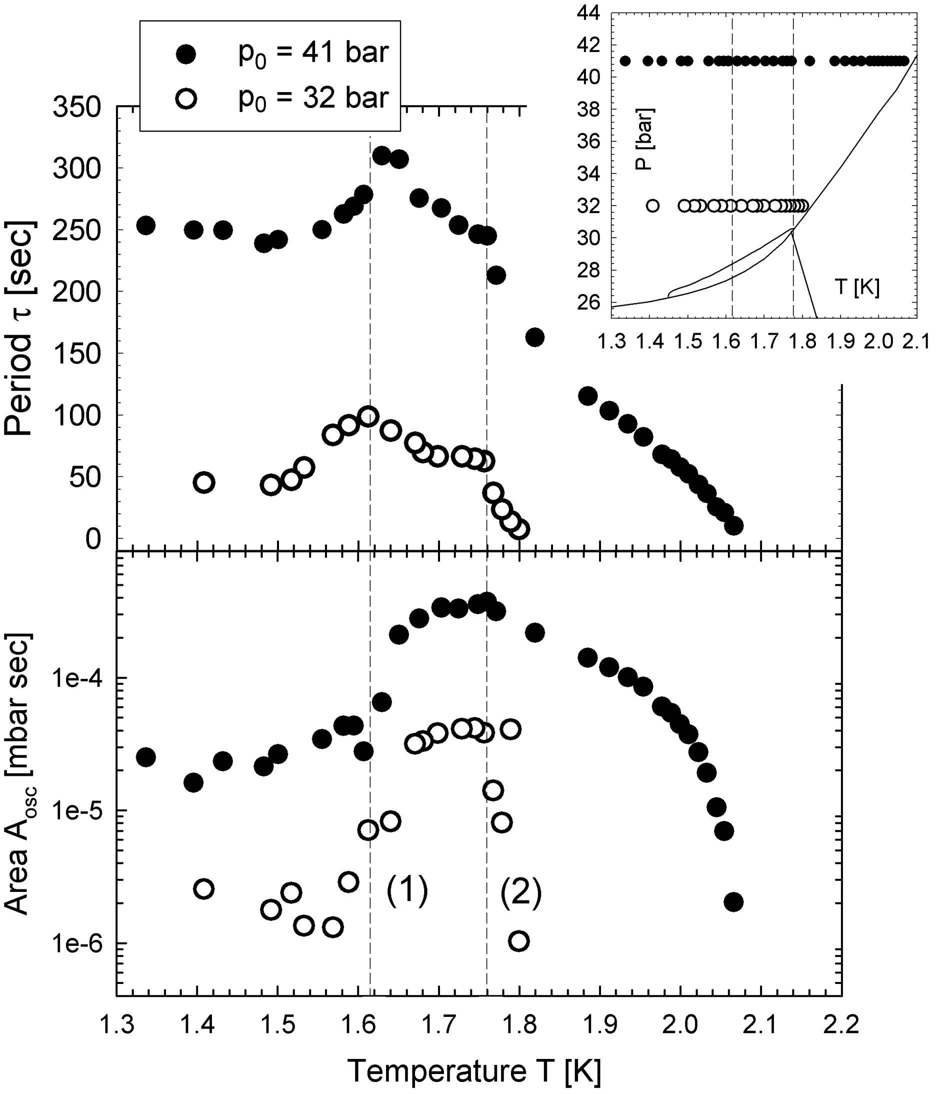

Figure 7.13: The area A_{osc} as a function of temperature for two measurements at source pressure $p_0 = 32$ bar and 41 bar, respectively. Additionally the temperature dependent period τ is shown above. The dashed lines correspond to the temperature T = 1.78 K (2) and the critical temperature $T_c = 1.58$ K (2), as seen in the phase diagram. As a result the area A_{osc} shows a maximum at T = 1.78 K. Below $T_c = 1.58$ K the area A_{osc} drops down about one order of magnitude. The maximum of A_{osc} can be interpreted by the proportionality of A_{osc} to the number of generated vacancies: More vacancies have to be generated to produce the collapse because a fraction of vacancies are responsible for the hcp-bcc phase transition. The dropdown of A_{osc} below T = 1.58 K is a consequence of the periodic curve shape that only consists of the sharp peak.

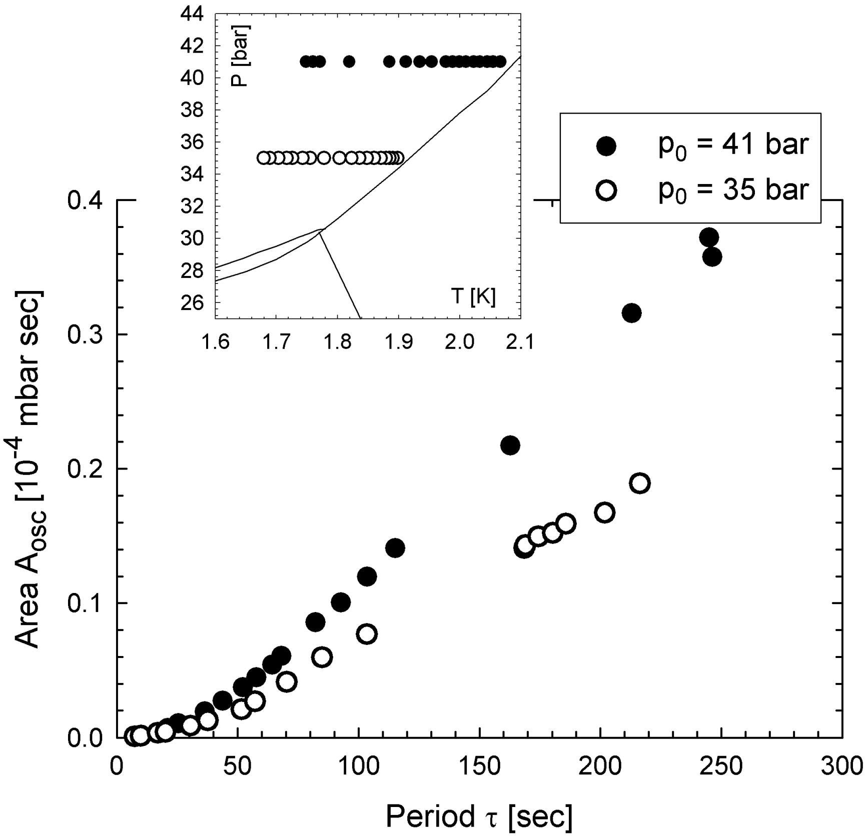

Figure 7.14: The area A_{osc} as a function of the period τ for two different measurements at decreasing temperature T and constant source pressure $p_0 = 35$ and 41 bar, respectively. For period $\tau > 50$ seconds the dependence between A_{osc} and τ is found to be almost linear. The linear behavior is found to be only for temperatures above T = 1.66 K (35 bar) and 1.74 K (41 bar). ($d_0(\sharp 17) = 2.28\ \mu$m)

ing temperatures. At T$_c$ = 1.6 K the period τ has its maximum and decreases with decreasing temperatures. The origin of this behavior can be seen in figure 6.15, where the oscillating detector pressure p_{det} is shown for several temperatures and constant source pressure $p_0 = 33$ bar: At temperatures above 1.64 K the area A_{osc} increases. The curve shape shows a peak and a huge "shoulder". In this picture the period increases down to 1.58 K, whereas the curve shape at 1.58 K already shows the typical behavior of the curve shape at low temperatures: the periodic signal just shows a sharp peak and a constant beam flux. The increase of the vacancies mobility affects that the vacancies spend less time in the volume between S_{sl} and S_0. Thus, the area A_{osc} decreases because less vacancies are needed to produce the collapse. The curve shape in figure 6.15 indicates, why the area A_{osc} decreases below temperatures T = 1.78 K. This result below 1.78 K shows that even though below 1.78 K the period τ increases the periodic behavior is influenced by the abnormal periodic behavior at low temperatures: In figure 6.21 the phase line p_{τ} already deviates from the melting line at temperatures below 1.78 K.

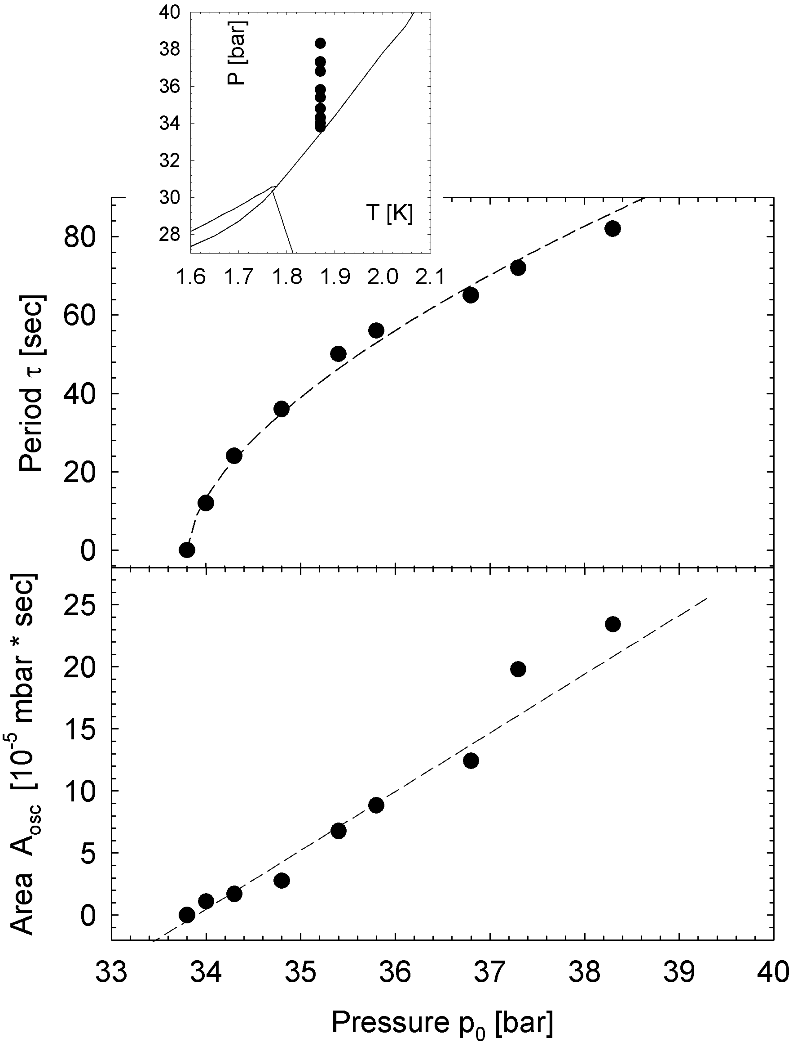

Figure 7.15: Area A_{osc} as a function of the source pressure at constant temperature T = 1.87 K. Instead of exponential increase of A_{osc} with increasing source pressure p_0 the area A_{osc} increases almost linear with increasing source pressure p_0.

For temperatures below $T_c = 1.6$ K the area A_{osc} decreases on order of magnitude, as seen in figure 7.13. As mentioned above the periodic signal just shows a sharp peak and a constant flux. According to this below 1.6 K the critical concentration of vacancies necessary for the percolative effect seems to be very small. Figure 7.14 captures this relation between the period τ and A_{osc}. For two source pressures $p_0 = 35$ and 41 bar the area A_{osc} is shown as a function of the period. The data are restricted to a temperature range T > 1.66 K, because for lower temperatures the dependence is not that distinctive. Whereas for T > 1.66 K the dependence is found to be almost

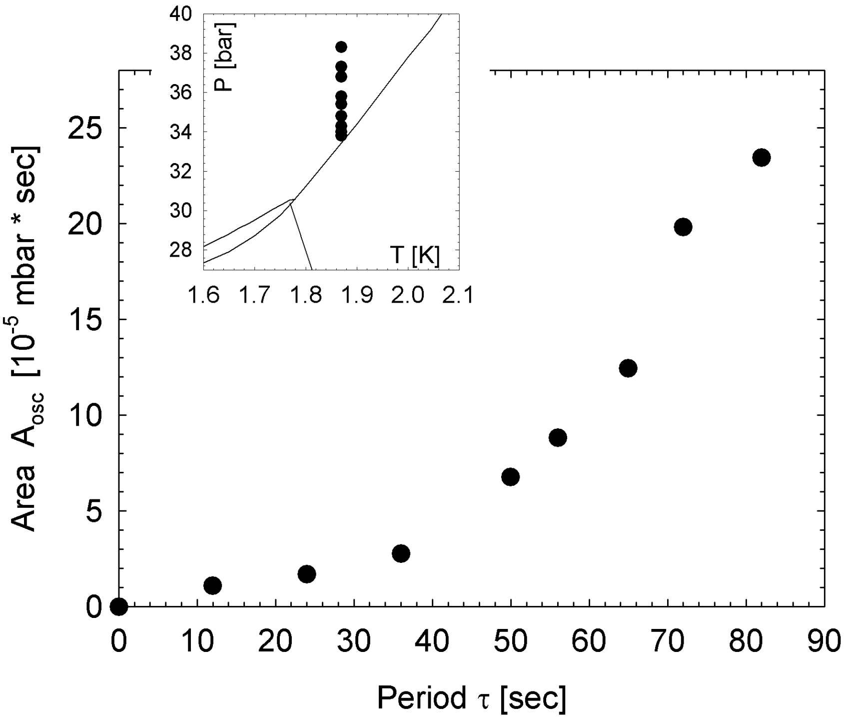

Figure 7.16: Area A_{osc} as a function of the period τ. The non-linearity between A_{osc} and τ is already indicated in figure 7.15. This result maybe gives an indication for the transition between the quantum and classical regime of solid Helium-4.

linear. This result shows that obviously the critical concentration of vacancies for the percolative collapse and the time till the collapse occurs (period τ) goes hand in hand. This temperature regime is mainly dominated by the hcp phase, so that the influence of the hcp/bcc transition and the deviation of the periodic behavior is negligible.

Another way to investigate the area A_{osc} is to look for the dependence of the source pressure p_0. The analysis is related to the measurement that is shown in figure 6.3: The source pressure p_0 is increased stepwise from 33.4 bar up to 38.4 at constant source pressure T = 1.87 K. In figure 7.15 the period τ and the area A_{osc} is shown as a function of the source pressure p_0. In contrast to the period τ, A_{osc} shows a linear dependence on the source pressure p_0, as seen in figure 7.15. As a result, the dependence between A_{osc} and period τ is not linear, as to be seen in figure 7.16. In the theoretical model the period τ can be interpreted as the time until the critical concentration for the collapse of the solid is reached. As obtained from the temperature dependent analyze, the linear dependence between A_{osc} and τ supported the argumentation of the model. Whereas now the data can be interpreted that for higher source pressures p_0 the number of vacancies for the periodic collapse is enlarged. It seems that an additional effect reduces the concentration of vacancies that strongly depends on the source pressure p_0.

In summary, the area A_{osc} gives direct information about the critical concentration of vacancies that provokes the collapse of the solid, producing the oscillatory effect. The temperature dependence of A_{osc} reflects the dependence of the period τ. At constant source pressure p_0 and varying temperature the dependence between the area A_{osc} and the period τ shows a linear behavior. This can be easily explained with the theoretical model that was introduced in chapter 3.3.4. The dependence of the source pressure shows a different behavior. With the present model an conclusive interpretation of the data is not possible.

7.8 The Influence of Helium-3

As shown in section 6.4 Helium-3 atoms influence the behavior of vacancies in solid Helium-4. To remind the essential features: A vacancy in Helium-4 causes inward relaxation: Surrounding Helium atoms at neighboring lattice sites are able to oscillate in a wider empty space because of the weak interatomic binding energy. Figure 7.17 shows the schematic distribution of lattice atoms under the presence of a vacant lattice site. Helium-3 atoms in solid Helium-4 act in the opposite way: Because of the smaller mass Helium-3 atoms oscillate in a wider range so that the neighboring atoms inside the lattice are restricted in their free space, as to be seen in figure 7.17. Thus, Helium-3 causes outward relaxation. Both behaviors, the inward relaxation of vacancies and the outward relaxation of Helium-3 are compensated by occupying neighboring lattice sites. Figure 7.17 illustrates the formation of such a vacancy-Helium-3-pair: A vacant lattice site and a Helium-3 atom diffuse through the crystal (1-3). If they occupy neighboring lattice sites (4) they form a vacancy-Helium-3-pair that moves through the crystal.

With this in mind the influence of Helium-3 to the present phenomenon is very interesting to investigate. Nevertheless the presence of Helium-3 does not decrease the vacancy concentration but hinders the free motion of vacancies inside the crystal. The investigations are presented in section 6.4. As a main result the presence of Helium-3 seems to reestablish the normal solid behavior at temperatures below $T_c \approx 1.6$ K. This result strongly indicates that indeed in solid Helium-4 at low pressures and temperatures below 1.6 K a fully new effect occurs. Under the influence of Helium-3 this unexpected behavior is completely suppressed, as to be seen in figure 7.18. This indicates that the formation of vacancy-Helium-3-pairs occurs at temperatures below 1.64 K. This seems reliable since the the binding energy of a vacancy and a Helium-3 atom is approximated to be around 1 Kelvin, which is approximated by the difference of the formation energy of vacancies in pure Helium-4 and mixtures of Helium-3 in Helium-4 [13]. Thus, the interaction of vacancies and Helium-3 occurs only at lower temperatures $T < 1.64$ K. This interpretation offers an exciting new possibility for the exact determination of the binding energy [11].

A further aspect is also shown in figure 7.18 (bottom). From the period τ one can easily determine the diffusion coefficient D_v, as already demonstrated in section 7.5. Thus, the diffusion coefficient D_v is shown as a function of temperature for the dif-

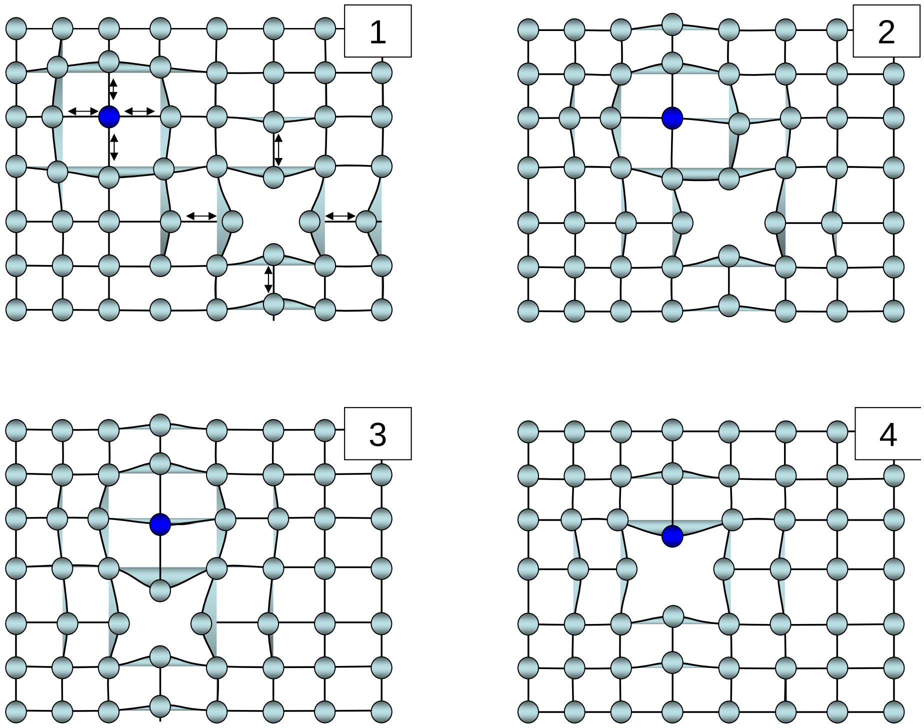

Figure 7.17: The model describes the generation of a vacancy-Helium-3-pair. In (1) the outward relaxation of Helium-3 atoms in solid Helium-4 is visible. The surrounding atoms are restricted in their free space because the zero point oscillation of Helium-3 is larger than for Helium-4. A vacancy causes the opposite behavior. The inward relaxation allows the neighboring Helium-4 atoms to stay in a wider regime. In (2) and (3) both, the vacancy and the Helium-3 atom move through the solid. If they occupy neighboring lattice sites (4) the inward and outward relaxation is partly compensated. Therefore, Helium-3 atoms and vacancies form a vacancy-Helium-3-pair that moves through the solid.

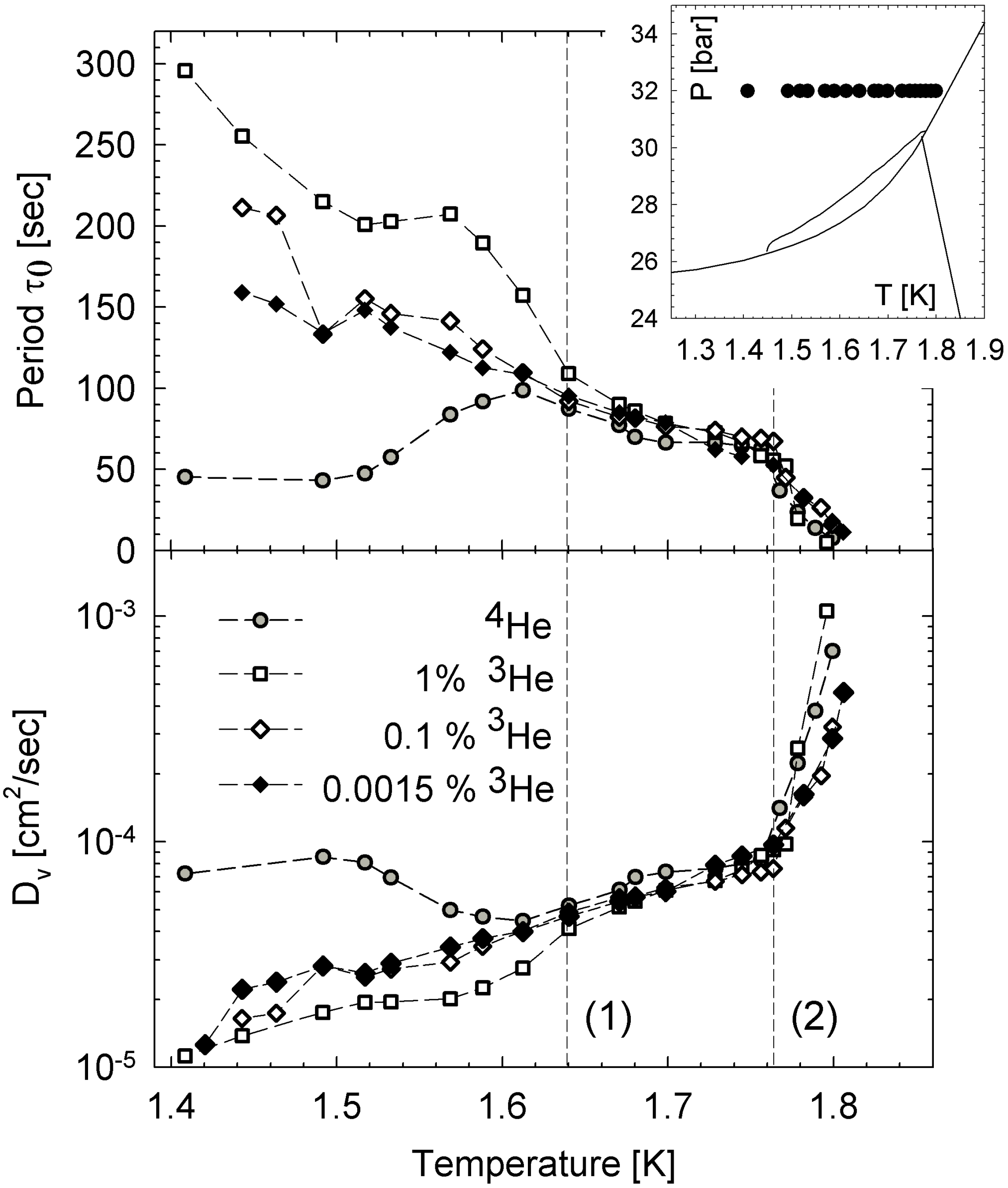

Figure 7.18: The diffusion coefficient D_v derived from the period τ for measurements at fixed source pressures $p_0 = 32$ bar and decreasing temperature T for pure Helium-4 and three mixtures of Helium-3 and Helium-4 with concentrations of between 1 and 0.0015 percent. The corresponding period τ is shown above as a function of temperature. Above T = 1.64 (1) the diffusion coefficient D_v is independent of the Helium-3 concentration. At T = 1.78 K (2) the temperature dependence of D_v - derived from the inverse period τ - changes also independent of the Helium-3 concentration according to the increase of the period at the hcp-bcc transition. According to the results for D_v with pure Helium-4 the diffusion coefficient shows a minimum at T = 1.6 K that corresponds to the maximum period τ_{max} at T_c. This maximum of the period τ is not found for the mixtures of Helium-3/Helium-4. The diffusion coefficient D_v decreases with decreasing temperature below T = 1.64 K. This behavior shows a dependence of the Helium-3 concentration.

ferent concentrations of Helium-3 between 1 and 0.0015 percent. For pure Helium-4 the behavior of D_v shows the typical minimum at $\mathrm{T}_c = 1.6$ K, as already seen for several source pressures in section 7.5. Under the influence of Helium-3 the diffusion coefficient D_v decreases smoothly with decreasing temperature, even below 1.6 K. On the first view this result corresponds to experimental results from several investigations concerning the diffusion coefficient D_v of Helium-3 in solid Helium-4, done by e.g. Allen and Richards [1], Mikheev *et al.* [92] and Kishvarsanyi and Sullivan [80]. These investigations were looking for quantum diffusion processes of Helium-3 impurities in solid Helium-4. Since Helium-3 and vacancies form pairs these investigations are also related to diffusion processes of vacancies. Indeed, for very low concentrations of Helium-3[1] they found a minimum of D_v at a corresponding temperature $\mathrm{T} = 1.43$ K. This minimum of D_v is found to be the transition of the quantum diffusion behavior of vacancies, that was introduced by Andreev and Lifshitz [3]. Quantum diffusion occurs at temperatures $\mathrm{T} \ll \Theta$, and D_v changes with temperature by:

$$D_v \approx \frac{a^2}{t} \frac{\hbar}{\Theta t} \left(\frac{\Theta}{T} \right)^9 , \tag{7.16}$$

where Θ is the Deybe temperature, t the time spent by a defecton on a specific lattice site, and a the interatomic distance. In this regime the vacancies turn into quasi particles (defectons) and the process of quantum tunneling occurs by the interaction with phonons [70]. But there are some reasons showing that the minimum of D_v measured in the present experiment has nothing to do with quantum diffusion. First, the diffusion coefficient of Helium-3 measured by Mikheev, Allen and Kisvarsanyi is about four orders of magnitude below the results obtained here. This indicates that in the present experiment the diffusion coefficient D_v is measured for vacancies and not for Helium-3 atoms. Next, the transition temperature from classical diffusion to quantum diffusion for Helium-3, where D_v is minimal, was determined to be about 1.42 K [80]. In the present experiment the temperature of minimal D_v is 1.6 K. Finally, the most important argument that contradicts the occurrence of quantum diffusion is that the minimum of D_v, presented here, is a consequence of the maximum of the period τ. The decrease of τ at temperatures below $\mathrm{T}_c = 1.6$ K results from the unexpected behavior at pressure p_τ, where the oscillating character completely disappears. Figure 7.5 clarifies the dependence between the decreasing period below 1.6 K and the resulting phase line p_τ, which was derived from the ratio between the maximum period at $\mathrm{T}_c = 1.6$ K and the decreased period at temperatures below. Thus, the dependence of D_v to the influence of Helium-3 can not be interpreted with the mechanism of phonon controlled quantum diffusion.

The reestablishment of the normal solid behavior below $\mathrm{T}_c = 1.6$ K under the influence of Helium-3 calls for a more detailed analysis. Thus, the next step is the analyze of the vacancy activation energy ϕ_a. With pure solid Helium-4 the analyze of ϕ_a shows an intriguing decrease at temperatures below $\mathrm{T}_c \approx 1.6$ K, as seen in figure 7.10. Below 1.6

---

[1] around 0.02 percent (Kisvarsanyi), 6 $\cdot 10^{-3}$ percent (Mikheev) and 0.005 percent (Allen and Richards)

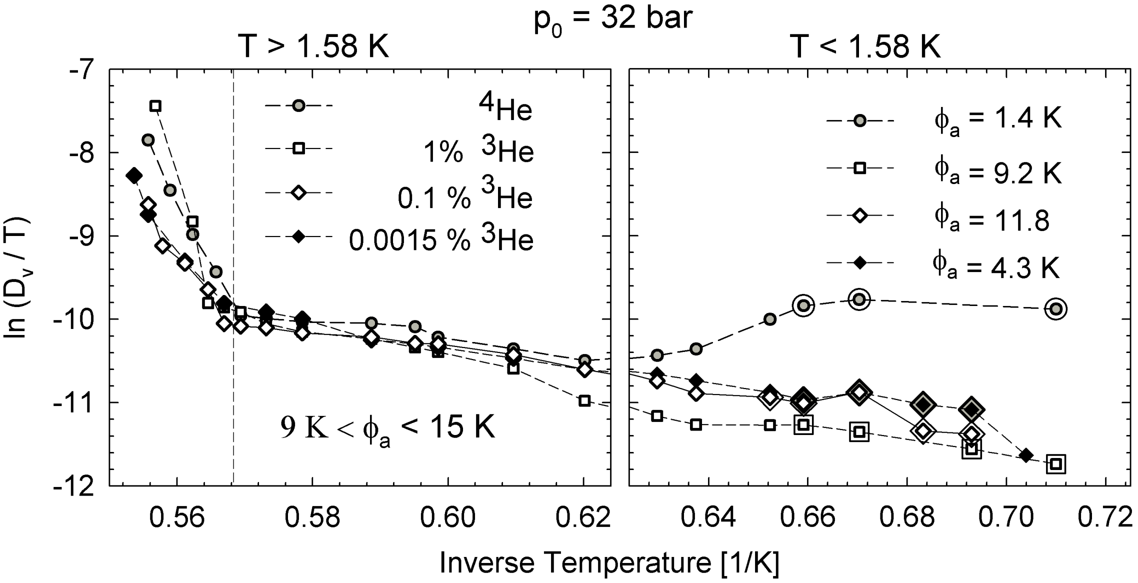

Figure 7.19: Activation energy ϕ_a derived from the slope of the dependence of $\ln(D_v/\mathrm{T})$ to the inverse temperature for different mixtures of Helium-3/Helium-4 and pure Helium-4. The Arrhenius plot is divided into two temperature regimes above and below T = 1.58 K. In the temperature regime above T = 1.58 K the activation energy is derived to be $9\ \mathrm{K} < \phi_a < 15\ \mathrm{K}$, which weakly depends on the Helium-3 concentration. The activation energy is derived from the slope in the regime below T = 1.78 K (dashed line) to avoid the influence of the hcp-bcc phase transition. Below T = 1.58 K the dependence of the Helium-3 concentration is obvious. The data points that are used to derive ϕ_a are indicated with enlarged symbols. The activation energy ϕ_a is found to increase with increasing Helium-3 concentration. This result indicates the reestablishment of the normal solid behavior under the influence of Helium-3.

K the activation energy was determined to be between $\phi_a = 2.8$ K at source pressure $p_0 = 32$ bar up to 5.1 K at 30.3 bar. In figure 7.19 the same analysis is presented at source pressure $p_0 = 32$ bar and different concentrations of Helium-3. The range of inverse temperature is separated in two regions, below and above 0.624 K^{-1}, that corresponds to the critical temperature $\mathrm{T}_c \approx 1.6$ K. At corresponding temperatures above T_c ($1/\mathrm{T} < 0.624\ \mathrm{K}^{-1}$) the activation energy ϕ_a is determined to be $9\ \mathrm{K} < \phi_a < 15$ K, depending on the concentration of Helium-3. For the low temperature regime below 1.6 K ($1/\mathrm{T} > 0.624\ \mathrm{K}^{-1}$) the activation energy is smaller, whereas ϕ_a clearly depends on the Helium-3 concentration. For $X_{^3He} = 1$ percent the value of ϕ_a amounts 9.2 K. For $X_{^3He} = 0.1$ percent the activation energy is even slightly above. For the lowest concentration of Helium-3 $X_{^3He} = 0.0015$ percent the activation energy decreases down to 4.3 K. Finally for pure Helium-4 the value of ϕ_a becomes very small, corresponding to the obtained values as in section 7.6. Especially the obtained values of ϕ_a for the high concentrations of Helium-3 are in good agreement with the activation energy that comes from the literature, as to be seen in figure 7.6. Once more, this result shows the influence of Helium-3, namely the reestablishment of a normal solid behavior below temperatures T = 1.6 K.

Another difficulty appeared with pure solid Helium-4. The investigation of the area A_{osc} in the previous section offered a linear behavior between A_{osc} and the period τ, but just in a region of temperatures above $\approx$ 1.7 K. As shown above, below temperatures of 1.6 K the presence of Helium-3 turns solid Helium-4 into normal solid conditions. Therefore, the analyze of A_{osc} under the influence of 1 percent Helium-3 is shown in figure 7.20. In the figure on the top of 7.20 the period τ is shown as a function of temperature at constant source pressure $p_0 = 32$ bar for pure Helium-4 and a mixture of 1 percent Helium-3. As already shown before, the period τ increases under the influence of Helium-3 even below $T_c \approx 1.6$ K. At the bottom of figure 7.20 the area A_{osc} is shown as a function of temperature, once more for pure Helium-4 and the 1 percent Helium-3 mixture. As expected, while A_{osc} decreases at temperatures below 1.7 K using pure Helium-4, the area A_{osc} increases with decreasing temperature under the influence of Helium-3. This result can also be found in figure 6.27, where the oscillating detector pressure p_{det} is shown as a function of time for several temperatures above and below $T_c \approx 1.6$ K, for pure Helium-4 and the mixture of 1 percent Helium-3, respectively. At low temperatures the periodic behavior of pure Helium-4 is just the sharp peak and constant flux, whereas for the Helium-3 mixture the curve shape shows the typical behavior with a sharp peak and an attenuating part, as generally observed at high pressures and temperatures between melting and the critical temperature $T_c \approx$ 1.6 K (e.g. figure 6.8, for $p_0 > 63$ bar).

Finally, in figure 7.21 the area A_{osc} is shown as a function of the period τ. The linear behavior between A_{osc} and τ, which was already denoted in figure 7.13, enlarges even at temperatures below 1.7 K under the influence of Helium-3. This results indicates once more, that the influence of Helium-3 reestablishes the normal solid behavior below 1.6 K. The different analyzes done in this section always leaded to the same result: In the present experiment the behavior of vacancies at temperatures below 1.6 K changes dramatically. The decreasing period indicates that the mobility increases extraordinarily. Even small concentrations of Helium-3 are sufficient to destroy this new and exciting behavior of vacancies in solid Helium-4. The presence of Helium-3 suppresses this behavior in any way: The period τ increases with decreasing temperature, the oscillating character occurs right at the melting line, the activation energy is in the range of values obtained by several investigations of ϕ_a and nevertheless the linear behavior between A_{osc} and τ stands for the reestablishment of the normal solid behavior. The investigations with Helium-3 gives the final evidence that the oscillatory behavior is a phenomenon related to vacancies.

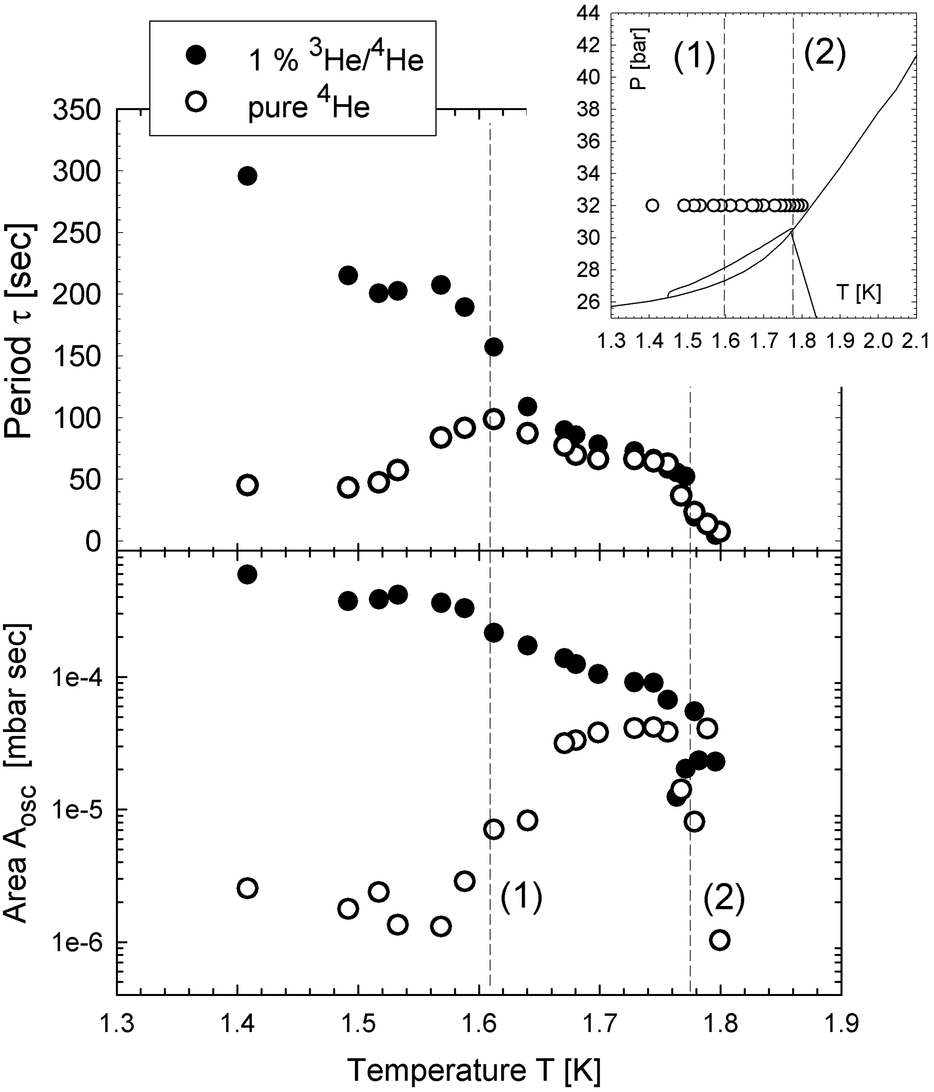

Figure 7.20: Area A_{osc} as a function of temperature T obtained for pure Helium-4 and a mixture of 1 percent Helium-3/Helium-4 at constant source pressure $p_0 = 32$ bar. At temperature T = 1.78 K (2) the area A_{osc} increases with decreasing temperature, accordingly to the results obtained in figure 7.13. In the temperature regime between 1.6 K (1) and 1.78 K (2) for the Helium-3 mixture the area A_{osc} increases with decreasing temperature even below T = 1.6 K. Compared to the data obtained for pure Helium-4 the difference appears already at T = 1.78 K. Once more this result indicates the reestablishment of the normal solid behavior of Helium-4 below T = 1.6 K by adding a small fraction of Helium-3.

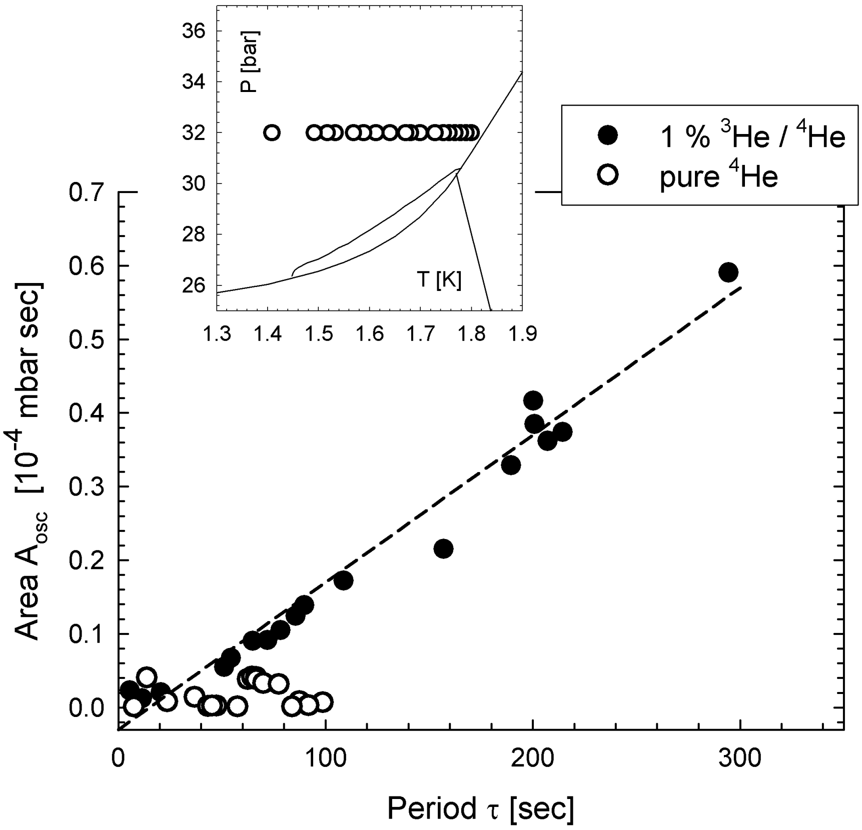

Figure 7.21: Area A_{osc} as a function of the period τ shown for the mixture of 1 percent Helium-3/Helium-4 and pure Helium-4, respectively. Using pure Helium-4 the linear dependence $A_{osc}(\tau)$ is found only for temperatures above 1.64 K, whereas for the Helium-3 mixture the linear dependence $A_{osc}(\tau)$ is observed in the total temperature regime down to T ≈ 1.4 K.

7.9 Discussion of the Behavior at T = 1.78 K (and 1.42 K)

In the very early experiments concerning the oscillations of the beam flux intensity, there is one phenomenon that has not been discussed so far. By decreasing the source temperature from melting down to temperatures below 1.7 K at constant source pressure p_0 the period τ increases almost linear with decreasing temperature. Whereas in the region of temperature T = 1.78 K the period deviates from the linear dependence of the temperature and increases of about a factor 1.6, as to be seen in figure 6.10 on page 64. The behavior is found to be independent of the source pressure p_0: The effect occurs always at temperatures right below 1.78 K. In figure 7.22 (top) the period τ is shown as a function of temperature in the regime 1.65 K < T < 1.85 K for three different source pressures p_0 = 32, 35 and 41 bar, respectively. The vertical dashed

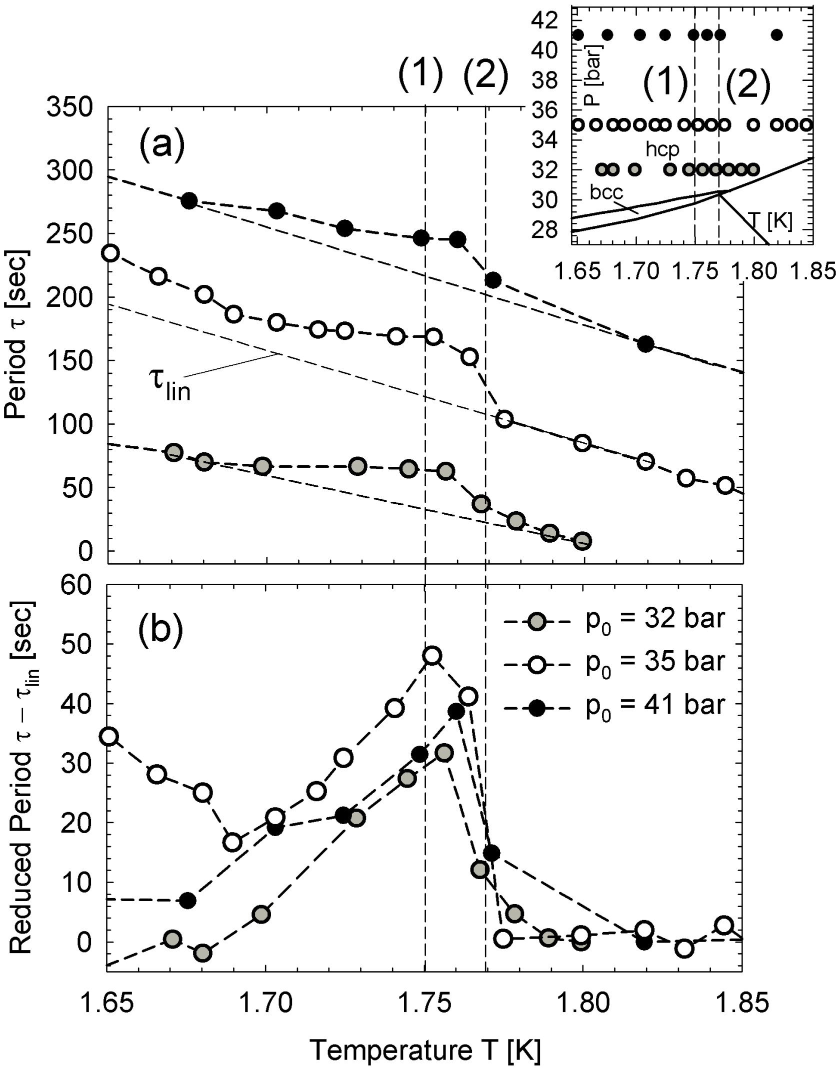

Figure 7.22: Period τ as a function of temperature in the regime above and below T = 1.78 K for three different source pressures p_0 = 32, 35 and 41 bar, respectively. In this regime the period τ shows an abnormal increase with decreasing temperature. To magnify the effect the period is shown as in (b) as a reduced period $\tau - \tau_{lin}$, where τ_{lin} is the assumed linear behavior τ(T), indicated with the dashed lines in (a). The reduced period shows a maximum at T = 1.75 K (1) whereas the increase of the period appears at T = 1.78 K (2). As a result the maximum of the reduced period $\tau - \tau_{lin}$ is almost independent of the source pressure p_0. As seen in the phase diagram line (2) corresponds to the temperature of the hcp-bcc phase transition, whereas the line (1) is slightly below (2).

line on the right marks the temperature T = 1.77 K, where the period deviates from the linear behavior. To clarify the effect figure 7.22 (bottom) shows the deviation of τ from the linear behavior. The reduced period $\tau - \tau_{lin}$ shows a very distinctive maximum at T = 1.75 K (left vertical dashed line). With decreasing temperature the reduced period $\tau - \tau_{lin}$ decreases, indicating that the effect is just related to the small temperature range around 1.75 K. As to be seen in the phase diagram in the inset of figure 7.22 the observed temperature range is strictly related to the hcp-bcc transition. The results point out that the change of the crystalline structure causes the increase of the period τ.

There is another indication for the evidence that the phase transition between the hcp and the bcc phase is responsible for the increase of τ. In decreasing the temperature the transition from hcp to bcc occurs at T = 1.45 K. At this temperature the period also increases, as to be seen in figure 7.23[2]. The temperature of maximum period T_{max} is about 0.02 K below the actual bcc-hcp transition temperature. This small shift was also observed at T = 1.78 K, where the maximum period was also about 20 mK below the hcp-bcc transition temperature.

Nevertheless, the increase of the period τ at T = 1.42 and 1.78 K seems to be related with the corresponding transition between the hcp and the bcc crystalline structure. Generally, the increase of the period τ is related whether with a decrease of the vacancies mobility or a decrease of the vacancy concentration. A possible explanation is given by Berent and Polturak [12]. In their experiments the self diffusion coefficient D_s of atoms in solid Helium was investigated near the bcc-hcp transition. The experiment was done in pulling a wire of diameter $d_0 \approx 100$ μm through the solid and measuring the wire‘s velocity. As a main result the diffusion coefficient D_s increases about 1.5 orders of magnitude in crossing the hcp-bcc transition at T = 1.78. Because of the direct proportionality between D_s and the diffusion coefficient of vacancies D_v the result does not explain the present effect of increasing period. Following equation 7.12 the diffusion coefficient is inverse proportional to τ, and herewith the behavior shoes the exact opposite of the results obtained by Berent and Polturak. Nevertheless, they mention that the critical behavior of the solid near the transition is controlled by vacancy diffusion. The presence of vacancies supports the phase transition, because the solid changes it‘s crystalline order. This process causes the motion of atoms, and the mobility of atoms is enlarged by the presence of vacancies. Thus, the possible explanation for the increase of the period at T = 1.78 K and 1.42 K is a reduction of the vacancy concentration that is responsible for the oscillatory effect. A decrease of the concentration affects an increase of the period, as observed. Furthermore, the reorganization of the crystalline structure is related to an increase of dislocations, which act as recombination centers of vacancies.

---

[2] The data are taken from figure 6.16

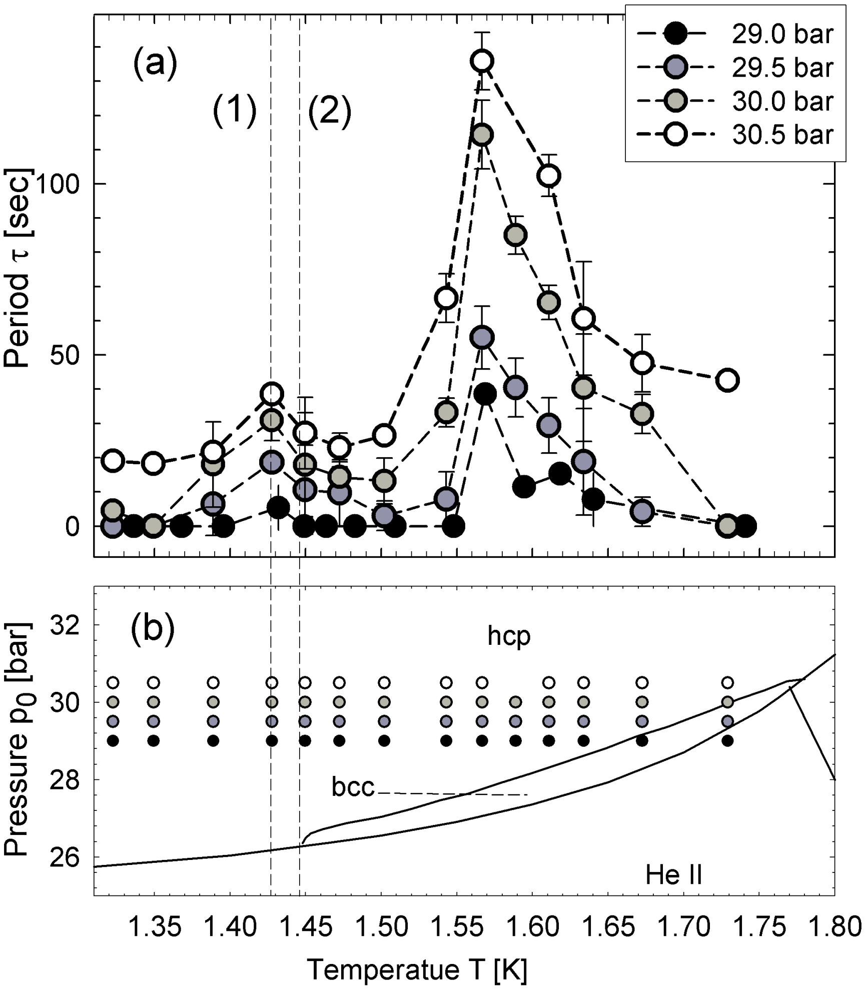

Figure 7.23: Temperature dependence of the period τ at constant source pressures p_0 = 29, 29.5, 30 and 30.5 bar, respectively (a). Beside the maximum of the period τ at T_c = 1.58 K there is a second maximum at T = 1.43 K (1). The increase of the period τ occurs slightly above at T = 1.45 K (2). The temperature corresponds to the bcc-hcp phase transition. The maximum of the period τ at (1) is also slightly below the actual phase transition temperature, as already observed at T = 1.78 K.

7.10 Discussion of the Deviating Period for High Pressure

Another feature that has been investigated is the source pressure´s dependence on the period τ. As the main result, the period increases with source pressure p_0 following equation 7.1 $\tau = \varrho(p_0 - p_\tau)^\gamma$, where p_τ is the pressure at which the oscillating beam flux occurs and ϱ and γ two fit parameters, respectively. This relation is applicable for temperatures T above temperatures T = 1.78 K, where the solid shows a normal solid behavior. In section 6.2 equation 7.1 is applied for two sets of measurements at temperatures T = 1.87 K and 2.17 K, respectively, and source pressures up to almost 30 bars above the melting pressure p_m. Fit the pressure dependence of τ one obtains:

$$\mathrm{T} = 1.83\ \mathrm{K} \rightarrow \tau = 97.50\ (\ p_0\ \text{-}\ 33.33\ \mathrm{bar}\ )^{\ 0.59}$$

$$\mathrm{T} = 2.17\ \mathrm{K} \rightarrow \tau = 38.45\ (\ p_0\ \text{-}\ 45.04\ \mathrm{bar}\ )^{\ 0.71}$$

The obtained values for ϱ and γ are in good agreement with the actual dependence between p_0 and τ. The exponent γ is also reflected in the slope of the logarithm of the diffusivity D_v as a function of the logarithm of the reduced pressure $(p_0 - p_\tau)$, as seen in figure 7.8. In figure 7.24 (a) the same plot is shown for the both measurements at constant temperatures T = 1.87 K and 2.17 K, respectively. At a pressure $p_0 - p_\tau \approx$ 10 bar the linear behavior of the double logarithmic plot of D_v as a function of $p_0 - p_\tau$ deviates. The corresponding pressure is indicated by p_{div}. For T = 1.83 K the dashed line (1) indicates the enlargement of the slope for higher pressures. The actual behavior is represented by line (2). The slope of (2) is constant for reduced pressures $p_0 - p_\tau >$ 4 bar. The same behavior of deviating slope is observable for T = 2.17 K. Once again, the dashed line indicates the original slope for reduced pressures $p_0 - p_\tau < p_{div} \approx$ 10 bar, and the actual behavior is shown in the straight line, whose slope is again constant.

Thus, the result indicates that the critical exponent γ changes at pressures of about 4-10 bar above the melting pressure p_m, which corresponds to p_τ in the investigated temperature region. This result is also reflected in figure 7.24 (b). The period τ is shown as a function of the source pressure. In this illustration the dependence is fitted with equation 7.1, whereas the fit is done for two different pressure ranges, namely between p_m and the corresponding transition pressure p_{div}, where the behavior between p_0 and τ changes, and a second pressure range for pressures above p_{div}. In table 7.2 the obtained parameters for ϱ and γ are summarized. Generally, the critical exponent γ increases for pressures above p_{div}, which corresponds to the increase of the slope of the dependence between $ln(D_v)$ and the reduced pressure $p_0 - p_\tau$

The different parameters of γ affect the theoretical dependence of the period τ as a function of the source pressure, as seen in figure 7.24 (b). Corresponding to the dashed (1) and straight (2) line in 7.24 (a) the behavior of τ is shown for the critical parameters ϱ and γ at source pressures above and below $p_{div} + p_\tau$: For the measurement done at T = 1.83 K (grey lines) the dashed line (1) gives the progression of the parameters ϱ and

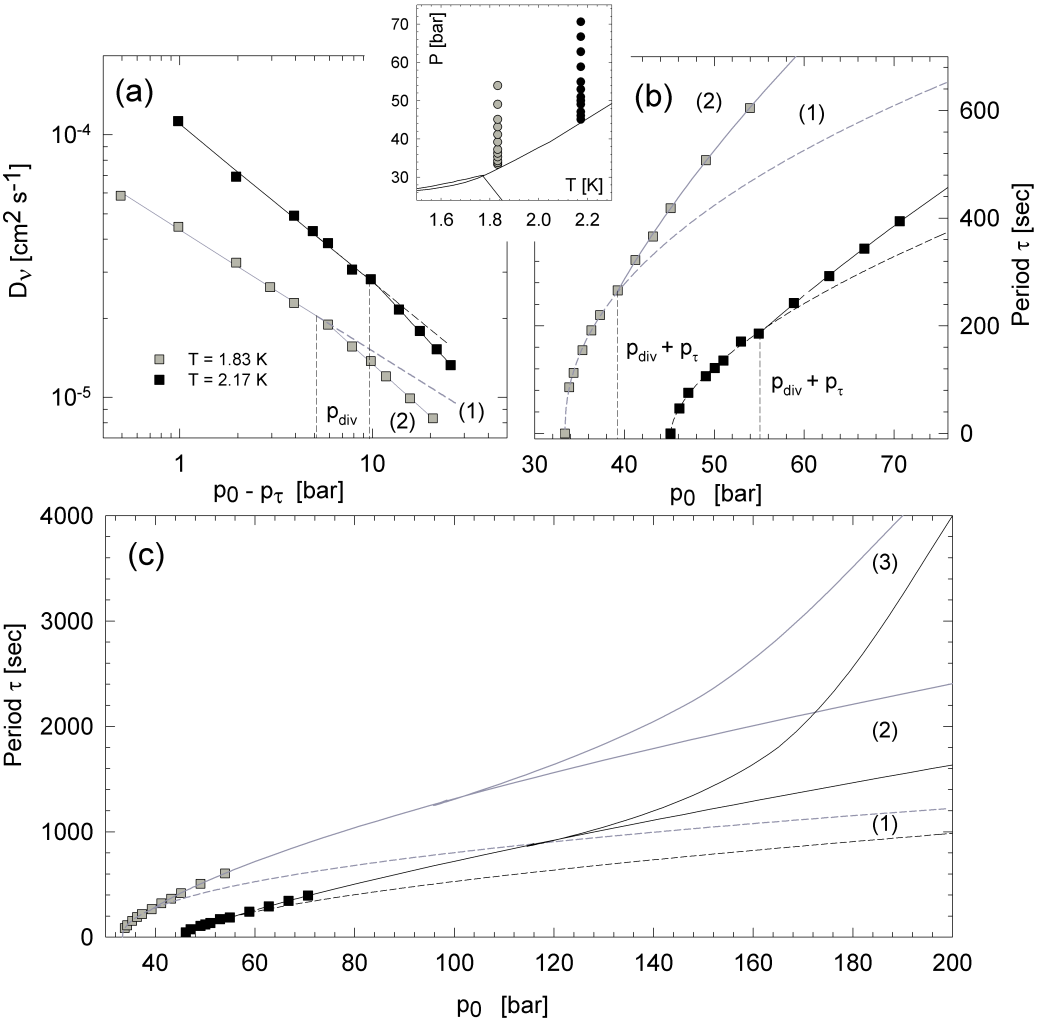

Figure 7.24: In (a) the diffusion coefficient at constant temperature T = 1.83 and 2.17 K is shown as a function of $p_0 - p_\tau$. At p_{div} the diffusion coefficient $D_v$do not follow a straight line in the double logarithmic plot. For T = 1.83 K the deviation is indicated by the dashed line (1). The actual behavior follows line (2). The pressure p_{div} is about 4 - 10 bar above the melting pressure p_m. In (b) the period τ is shown as a function of the source pressure p_0. The dependence between the period τ and the source pressure p_0 can be described by a critical exponent γ. At $p_0 = p_{div} + p_\tau$ the dependence changes, according to figure (a). The actual dependence between τ and p_0 is separated in two regimes. For T = 1.83 K line (1) shows the period $\tau(p_0)$ as if it would follow the critical exponent derived for pressures $p_0 < p_{div} + p_\tau$. Line (2) is fitted by regarding only the dependence of $\tau(p_0)$ for pressures $p_0 > p_{div} + p_\tau$. As a result the period τ and the diffusion coefficient deviates for high source pressures. In figure (c) three possible scenarios are indicated how the period τ develops for high source pressures up to 200 bar. For both temperatures the dashed line (1) shows the period $\tau(p_0)$ for critical exponent derived for pressures $p_0 < p_{div} + p_\tau$, according to (b). The same behavior is shown by the straight line (2). The third possibility in which way the period develops for high source pressures is indicated by the straight line (3). This behavior of τ is assumed to appear because for high pressures quantum solid become a classical system. Thus, the period τ becomes infinite for high source pressures, as assumed by Grisenti [65].

T [K]	p_0	ϱ	γ	equation
1.83	$p_0 < p_{div}$	116.19	0.46	$116.19\ (p_0 - 33.33\ \text{bar})^{0.46}$
	$p_0 > p_{div}$	82.17	0.66	$82.17\ (p_0 - 33.33\ \text{bar})^{0.66}$
2.17	$p_0 < p_{div}$	47.78	0.6	$47.78\ (p_0 - 45.04\ \text{bar})^{0.6}$
	$p_0 > p_{div}$	30.42	0.79	$30.42\ (p_0 - 45.04\ \text{bar})^{0.79}$

Table 7.2:

γ obtained for pressures below $p_{div} + p_\tau$. According to this the straight line (2) shows the behavior of τ for ϱ and γ corresponding to pressures above $p_{div} + p_\tau$. The same notification is done for the data obtained at T = 2.17 K (black lines). Generally, the dashed line (1) proceeds below the line (2), indicating that at corresponding source pressure the period $\tau(1)$ is below $\tau(2)$.

These different approaches are also reflected in figure 7.24 (c), which indicates possible scenarios, how the period τ develops for high pressures up to about 200 bars. The most probable way is given by the straight lines (2), because (2) describes the period τ fitted for pressures $p_0 > p_{div} + p_\tau$. Another way, how the period develops for high pressures is that τ follows a value between the two lines (1) and (2), whereas τ would be assumed to be closer to (2) than to (1). The third possibility is given by Grisenti [65] in arguing that for high pressures the system becomes more and more classical. In a classical crystal the periodic effect of the beam flux is non-existing, because of several reasons like e.g. the much smaller concentrations of vacancies and the very low diffusion coefficients D_v. The deviation of the period for high pressures is also given by the pressure dependence of the de Boer parameter. For high pressures the interatomic distance decreases and this affects the decrease of Λ, as mentioned by Andreev [4]. As a matter of fact, for high pressures quantum crystals, such as solid Helium-4, turn into classical crystals. Thus, for high pressures the period could increase, and could finally become infinite. This procedure is indicated with the straight lines (3) in figure 7.24 (c).

7.11 The Influence of the Nozzle Diameter

In section 6.5 the experimental results of the nozzle diameter‘s dependence to the period τ and the mean beam flux are presented. As the most important result the period τ depends on the nozzle diameter d_0 by the relation 6.5. This indicates that the generation rate of vacancies is proportional to the area of the cross section $S_{s/l}$. The area of this cross section corresponds to the area of a half sphere and is given by $A_{s/l} = 2\ \pi\ r^2$. With an increase of $A_{s/l}$ proportionally more vacancies are generated and herewith the excess vacancy concentration increases. As a result the critical vacancy concentration X_v^c is reached much faster and the period τ becomes shorter.

The second result of the investigation with nozzles of different diameter d_0 is the proportionality of d_0^2 and the detector pressure p_{det}. The proportionality is experimentally observed by the empirical ratio 6.3. The proportionality of p_{det} and the square of the nozzle diameter d_0 is confirmed experimentally: The orifice‘s area $A_0 = \frac{\pi d_0^2}{4}$ is proportional to the mass flow and herewith to the mean beam flux.

Generally, the occurrence of the oscillations in the detector pressure signal is found to be almost independent of the nozzle diameter d_0. The results are summarized in figure 6.38 where the phase line p_τ is shown that is obtained with nozzles of diameter between 1 and 3.6 μm, whereas the whole temperature range is just acquired for 1 and 2 μm nozzles. Down to 1.8 K there is no significant dependence on the phase line p_τ to the nozzle diameter d_0. For temperatures below 1.8 K the pressure p_τ(T) obtained with nozzles of 1 μm diameter seems to be slightly above the phase line of p_τ(T) for $d_0 = 2$ μm. If indeed the phase line p_τ(T) is shifted up to higher pressures by using nozzles with smaller diameter d_0 is a point that can not be verified in this experiment in a satisfactory way. This is because of the insufficient statistics especially for the data obtained with the 1 μm diameter nozzles. Assumed that the phase line p_τ(T) is indeed shifted upwards for nozzles with smaller diameter d_0 there should be a theoretical phase line p_τ(T) for $d_0 \rightarrow 0$. But if $d_0 = 0$ the system is in equilibrium because if there is no beam flux no excess vacancies would be injected into the system. Another point that has not yet been investigated at all is the nozzle diameter‘s dependence of the phase line p_u(T). The exact trend of p_u(T) can just be found exactly by increasing (or decreasing as well) the source pressure p_0 in small intervals, as demonstrated in figure 7.2 for nozzles with diameter $d_0 = 2$ μm. This kind of measurements has not been done for nozzles with smaller or larger diameter d_0. The dependence of p_τ(T) and especially p_u(T) on the nozzle diameter d_0 is of special interest because it could be a possible explanation for the occurrence of the both phase lines. This alternative explanation will be discussed in section 7.13.

7.12 Application of the Theoretical Model

During one period the different stages of the process (diffusion, drift, recombination) are also reflected in the period‘s curve shape. An example for the possible influence of drift, diffusion and recombination is illustrated in figure 7.25. At the bottom of the figure the possible interaction of diffusion and drift is shown by the dark blue (Drift) and bright blue (diffusion) arrows. The arrows indicate the direction in which the vacancies move: If the arrow shows upwards the vacancies move from the solid/liquid interface into the bulk solid, and vice versa. The amplitude of the arrows indicates the influence, whereas the amplitude is chosen only for demonstration. As to be seen, the dark blue arrow is chosen to be constant with time, because the pressure gradient that causes drift is always present. The bright blue arrow that indicates the motion of diffusion decreases with time and backward diffusion occurs when the arrow shows downward.

The oscillating curve shape can be explained as follows: The sharp peak at t = 0 seconds is caused by the percolative collapse of the lattice. Released by the collapse all excess vacancies and even the thermally activated vacancies are bleached as well.

Thus, the system is in a non-equilibrium condition because the vacancy concentration is below the equilibrium value. The first sharp decrease of the pressure p_{det} for t $\leq$ 11 seconds can be interpreted by the intensive generation of vacancies to restore the equilibrium condition. After the equilibrium vacancy concentration is reached the accumulation of vacancies at the cross section S_0 begins where the pressure gradient disappears (t $>$ 10 seconds).

The generation of excess vacancies causes an increase of the recombination time τ_r. As to be seen in the illustration in figure 7.25 the recombination of vacancies with interstitials is held to be responsible for the decrease of the signal intensity at t $\approx$ 50 seconds (yellow section). By the influence of backward diffusion the net vacancy current decreases (as shown in the blue section) until an equilibrium occurs in which drift, diffusion and recombination cancels out each other. The assumption that these three mechanisms equilibrate each other would lead to a zero vacancy current. As a consequence no more vacancies would be transported to the accumulation region at S_0. The occurrence of backward diffusion shows that indeed the maximum vacancy concentration $X_v^{c,\infty}$ is reached. Thus, the maximum vacancy concentration $X_v^{c,\infty}$ corresponds to the critical concentration maximum vacancy concentration X_v^c that causes the collapse.

On the other hand the increase of the vacancy concentration up to $X_v^{c,\infty}$ at S_0 causes that the collapse would not be released and the period would become infinite. A possible explanation is that the separation between background pressure and oscillatory signal is lower than indicated with the horizontal dashed grey line at $p_{det} \approx 3.83 \cdot 10^{-5}$ mbar in figure 7.25.

Since the oscillating detector pressure p_{det}^{osc} is proportional to the net vacancy current j_{osc} the integral over p_{det}^{osc} for times $0 <$ t $< \tau_0$ gives the number of excess vacancies necessary for the periodic effect: Each atom that leaves the nozzle gives rise to a vacant lattice site (as supposed for the model). In the following the number of vacancies is calculated considering as example of the measurement shown in figure 7.25. The atoms that produce the background flow $p_{det,bg}$ leave vacancies which are annihilated to melt the solid, as described in section 3.2. The vacancies that do not recombine produce the periodic effect and these vacancies are generated by atoms that build the corresponding oscillating beam flux that is proportional to p_{det}^{osc}. The number of these atoms can be derived from the integral of the oscillatory part p_{det}^{osc}. And this number of atoms is equal to the number of vacancies that are responsible for j_{osc}. The number of atoms that leave the nozzle can be derived in the following way: The volume of the liquid Helium-jet that leaves the nozzle per second can be determined by:

$$\begin{aligned} V_{He} &= u_{exit}\, \phi_n \\ &= 5.52 \cdot 10^6 \frac{m}{sec \cdot mbar}\; p_{det} \frac{\pi d_0^2}{4}\; [m^3], \end{aligned} \qquad (7.17)$$

where u_{exit} is the jet velocity in [m/sec] and ϕ_n the nozzle cross section [m^2]. The

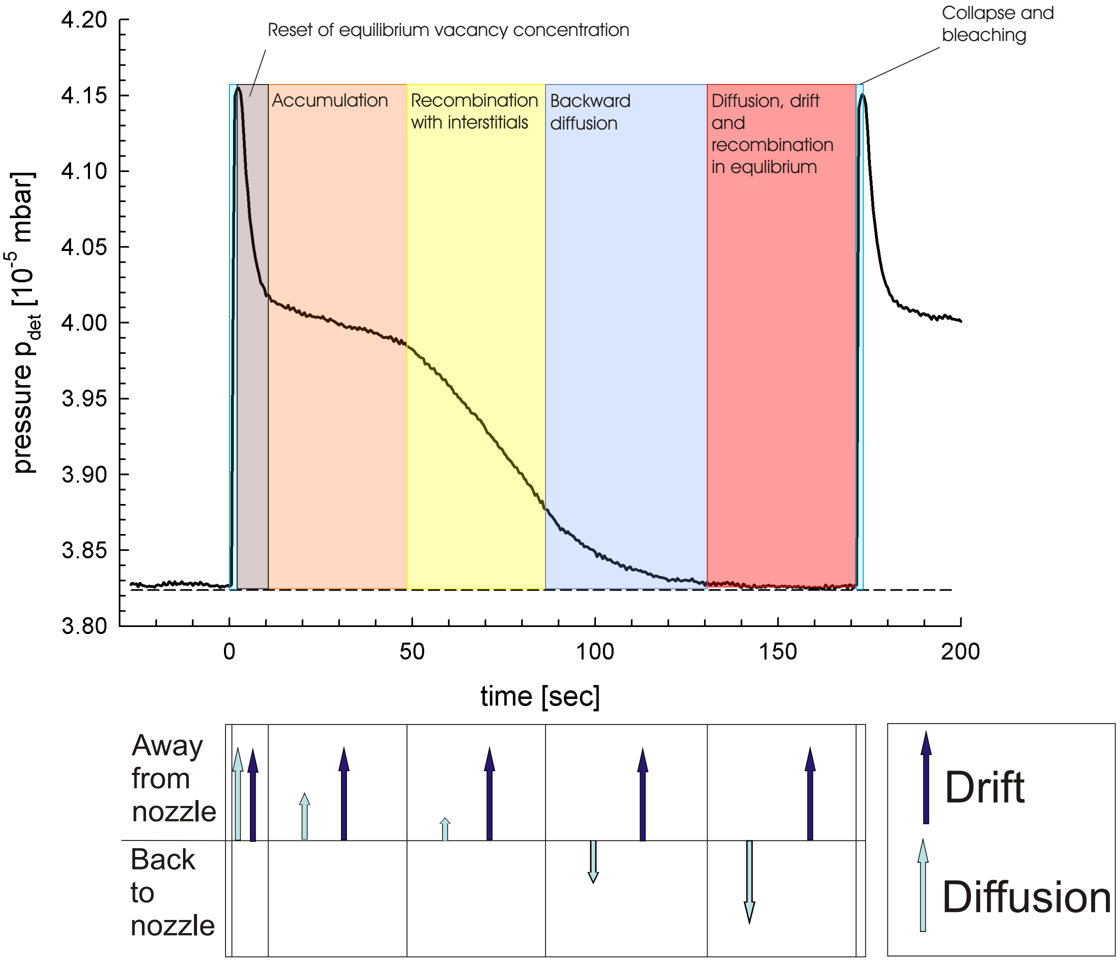

Figure 7.25: Application of the model to explain the curve shape of the oscillatory behavior in the beam flux. The sharp peak at $t = 0$ is assumed to be caused by the collapse of the region in which the vacancies accumulate. Because of the bleaching of all vacancies the system undergoes the equilibrium vacancy concentration. The system resets the equilibrium conditions at times $t \leq 11$ seconds with a high generation of excess vacancies. The high concentration of vacancies at the solid/liquid interface causes a high diffusivity, as indicated with the large amplitude of the arrow below. For times t larger than 11 seconds the vacancies start to accumulate and the diffusion of vacancies reduces. At a certain time $t \approx 50$ sec the recombination of vacancies with interstitials occurs as seen in the yellow section, whereas the actual recombination time τ_r is probably shorter. With increasing vacancy concentration at the cross section S_{sl} the corresponding concentration gradient causes backward diffusion which plays a major role at the flat region for times $t < 130$ seconds. This scenario is indicated with the negative amplitude of the dark blue arrow below. This effect holds on and causes an equilibrium between drift, diffusion and recombination for times $t > 130$ seconds. The arrows that indicate the direction of diffusion and drift have the same amplitude but it is negative for diffusion.

factor $5.52 \cdot 10^6 \frac{m}{sec \cdot mbar}$ comes from the inversion of pressure to jet velocity, which is derived in section 7.5. Thus, for the measurement shown in figure 3.6 the background pressure $p_{det,bg}/sec = 2 \cdot 3.83 \cdot 10^{-5}\ mbar/sec$ gives the number of Helium atoms per second at a corresponding time resolution of 500 msec. This gives:

$$\begin{aligned}
N_{He} &= \frac{N_a\, m_{He}}{m_{mol}} \\
&= \frac{N_a}{m_{mol}}\, \rho_{He}\ 5.52 \cdot 10^6 \frac{m}{sec \cdot mbar}\ \frac{p_{det,bg}}{sec} \frac{\pi d_0^2}{4} \\
&\approx 2.5 \cdot 10^{19}\ \frac{atoms}{sec},
\end{aligned} \tag{7.18}$$

where N_a is the Avogadro constant, m_{mol} the molar mass of Helium and ρ_{He} the density of liquid Helium. As a result each second $2.5 \cdot 10^{19}$ atoms cross the solid-to-liquid interface and generate the same number of vacant lattice sites. Thus, the same number of vacancies causes the constriction of the solid from the cross section S_0 to S_{sl}.

To derive the number of vacancies that produce the oscillatory effect the oscillatory part of the jet velocity $u_{exit,osc}$ during a whole period gives the corresponding volume $V_{He,osc}$ of liquid Helium-4:

$$\begin{aligned}
V_{He,osc} &= u_{exit,osc}\ \phi_n \\
&= 5.52 \cdot 10^6 \frac{m}{sec \cdot mbar}\ \int_{t=0}^{\tau} p_{det}^{osc}(t) \frac{\pi d_0^2}{4}\ [m^3],
\end{aligned} \tag{7.19}$$

where $p_{det}^{osc}(t)$ is the oscillating detector pressure at given time t. The integral $\int_{t=0}^{\tau} p_{det}^{osc}(t) = \int_{t=0}^{\tau} p_{det}(t) - p_{det,bg}$ describes the area A_0 between pressure $p_{det}(t)$ and $p_{det,bg}$ in the time interval $0 < \mathrm{t} < \tau$, as seen in figure 7.12. For the number of atoms that correspond to A_0 it follows from for the period $\tau = 173$ seconds in figure 3.6:

$$\begin{aligned}
N_{He,osc} &= \frac{N_a\, m_{He}}{m_{mol}} \\
&= \frac{N_a}{m_{mol}}\, \rho_{He}\ 5.52 \cdot 10^6 \frac{m}{sec \cdot mbar}\ \int_{t=0}^{\tau} p_{det}^{osc}(t) \frac{\pi d_0^2}{4} \\
&\approx 1.409 \cdot 10^{20}\ \frac{atoms}{period}.
\end{aligned} \tag{7.20}$$

This number of atoms gives the number of vacancies during the period $\tau = 173$ sec that are assumed to produce the oscillating effect. From equation 7.20 the experimental vacancy current $j_{osc}^{exp}(t)$ is given by:

$$j_{osc}^{exp}(t) = p_{det}^{osc} \cdot \frac{5.52 \cdot 10^6 \frac{m}{sec \cdot mbar}\, \rho_{He}\, A_0}{m_{mol}}, \tag{7.21}$$

where $A_0 = \frac{\pi d_0^2}{4}$ is the orifice‘s area. From the pre-factor $\frac{1}{4}X_v^0 u_v$ of j_{osc}^{theo} the experimental and the theoretical current are fitted to be in the same range.

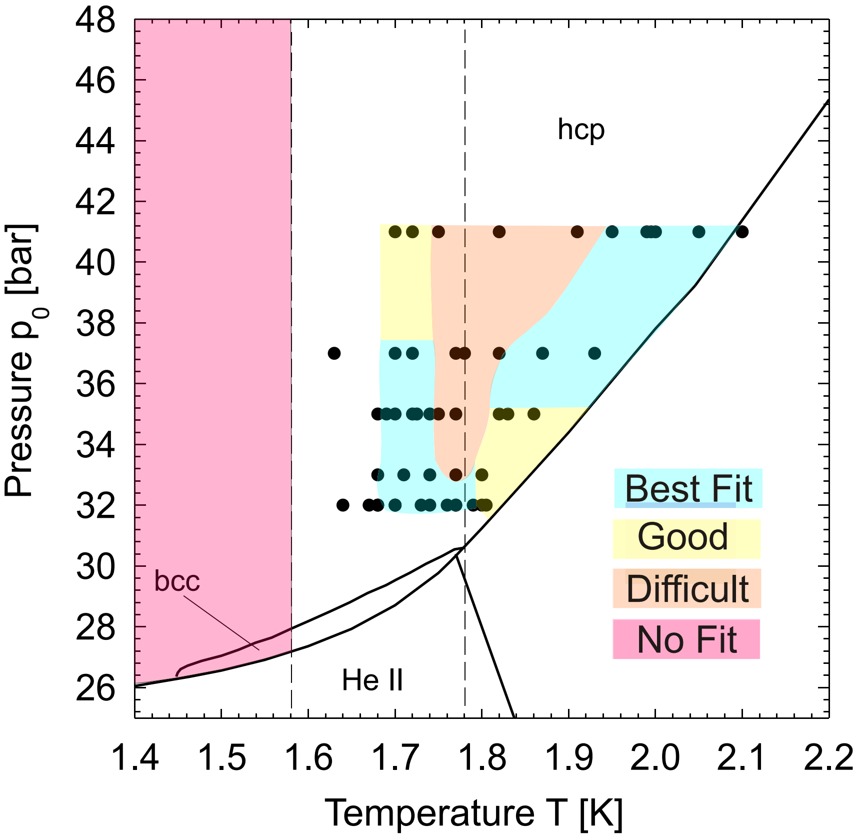

Figure 7.26: In the phase diagram the points show the corresponding pressures and temperatures at which the curve shape of p_{det}^{osc} is fitted. The different colored regimes indicate at which regimes the theoretical fits can reproduce the actual experimental curve shape. In the regime below temperatures T$_c$ = 1.58 K (red) the fits are not possible. At temperatures above 1.58 K the oscillations of p_{det} close to the melting line are reproducible in a good agreement with the theory (blue and yellow regimes). At temperatures around T = 1.78 K (orange regime) the fits are found to be difficult because of the phase transition between the hcp and bcc phase, where the period τ increases.

As demonstrated in chapter 3 the periodic curve shape of $p_{det}^{osc}(t)$ can be reproduced by deriving the vacancy current $j_{osc}(t)$ of the excess vacancies that are responsible for the periodic effect, as expressed by equation 3.11. In figure 3.9 the validity of the theoretical vacancy current $j_{osc}(t)$ is demonstrated, whereas $j_{osc}(t)$ is applied in a reduced form 3.12.

In appendix B the fits of the experimental beam flux to the theoretical expression of j_{osc} is shown for measurements of the oscillating detector pressure p_{det}^{osc} at temperatures 1.6 K $<$ T $<$ 2.2 K and source pressures 30 bar $< p_0 <$ 41 bar. For a given equilibrium vacancy concentration $X_v^0 \approx 1-2$ percent the theoretical beam flux intensity $j_{osc}^{theo}(t)$ and the experimental $j_{osc}^{exp}(t)$ is found to be in the same order of magnitude. From the fits several constants can be derived as a function of temperature and pressure, like the thermalization time τ_r, the recombination time τ_r, the ratio $X_v^{c,\infty}/X_v^0$ and the vacancy generation velocity u_v.

In figure 7.26 the measurements at corresponding temperature and source pressure are indicated in the phase diagram. Basically the fits are not applicable at temperatures below T$_c$ = 1.58 K because of the deviating curve shape as to be seen in figure 6.13 on page 69. Generally at temperatures T $>$ 1.58 K the fit of $j_{osc}(t)$ is possible whereas the reproducibility of the experimental data by the fit depends on temperature and source pressure as indicated in figure 7.26. Close to the melting line the theoretical flow $j_{osc}(t)$ is found to match perfectly together with the experimental curve shape of p_{det}^{osc}, especially at higher source pressures. At the temperature T = 1.78 K an optimal fit is difficult. The influence of the hcp-bcc phase transition is expected to play a role in the curve shape. As explained in section 7.9 the occurrence of dislocations at the hcp-bcc phase transition is assumed to reduce the vacancy concentration. Furthermore the theoretical expression for $j_{osc}(t)$ is derived with the assumption that the length l is infinite. Thus, the described processes of backward diffusion is not regarded in the time dependent behavior of $j_{osc}(t)$. This explains e.g. the insufficient length of the shoulder that is mainly depending on effects like backward diffusion are not reproducible by the theoretical beam flux intensity j_{osc}^{theo}.

If vacancies would not recombine the recombination time would be $\tau_r = \infty$. In this case the time scale of the periodicity would be determined by the thermalization time $\tau_v = 4D_v/u_v^2 = 4kT/Fu_v$. The expression Fu_v is the power that is dissipated by the vacancy drift. Thus, the thermalization time τ_v is the time required to dissipate an amount of energy of the order of the thermal energy kT. But because of recombination the thermalization time is in the range of the period τ_0, whereas $\tau_r < \tau_0$. In figure 7.27 the thermalization time τ_v is shown as obtained from the fits. Generally the thermalization time increases with decreasing temperature T and increasing source pressure p_0. This result shows the relation of the τ_v to the period τ_0.

In figure 7.28 the ratio of the period to the thermalization time τ_0/τ_v is shown as a function of temperature T at fixed source pressures p_0 = 32, 33, 35 and 41 bar, respectively. For $\tau_0/\tau_v = 1$ the thermalization time τ_v would determine the periodic time scale since $\tau_r = \infty$. This ratio is not observed. Furthermore for temperatures around T = 1.78 K the ratio τ_0/τ_v shows a maximum that is indicated with the dashed line which is a guide to the eye. The maximum is nearly independent on the source pressure and indicates a high rate of recombination at T = 1.78 K. This result confirms the assumption that the vacancies concentration in the system is reduced by crossing the hcp-bcc phase transition that causes an increase of the period τ_0.

The high rate of recombination is also shown in the temperature dependence of the re-

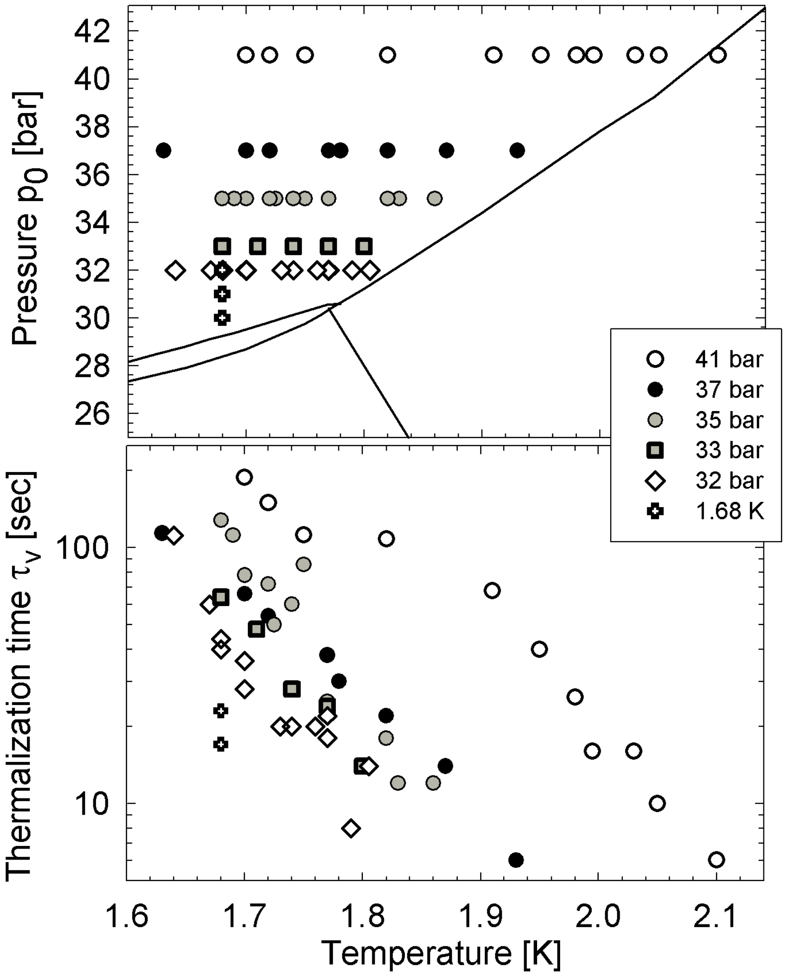

Figure 7.27: Thermalization time τ_v as a function of temperature T at constant source pressure p_0 in the range between 32 and 41 bar. The thermalization time τ_v increases with decreasing pressure and increases with increasing source pressure p_0 at fixed temperature T.

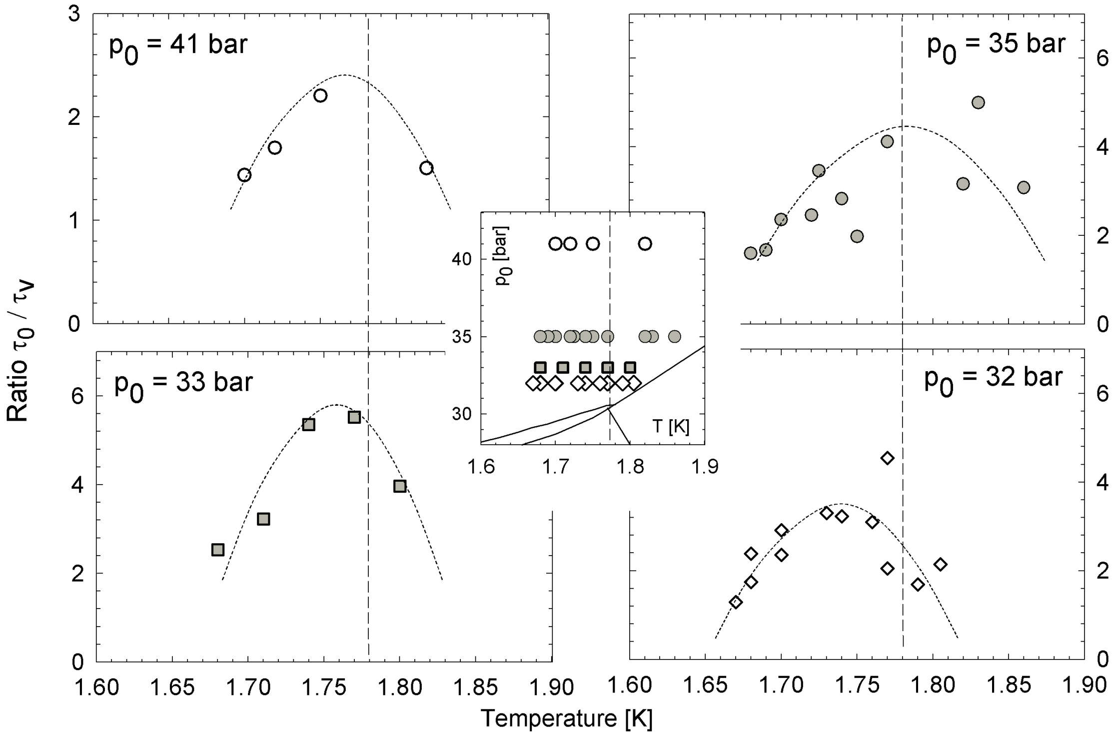

Figure 7.28: The temperature dependence of the ratio τ_0/τ_v shown for different source pressures p_0 = 32, 33, 35 and 41 bar, respectively. At temperatures T ≈ 1.78 K where the hcp-bcc phase transition occurs the ratio τ_0/τ_v has a maximum that is independent of the source pressure p_0. The dashed line is a guide to the eye that indicates the actual maximum of τ_0/τ_v. Because of the difficulty by fit the periodic curve shape in the region around T = 1.78 K the statistics in this regime is restricted.

combination time τ_r. The recombination time τ_r is obtained from the both parameters τ^* and τ_v:

$$\tau_r = \frac{\tau_v * \tau^*}{\tau_v - \tau^*}, \tag{7.22}$$

where $\tau^* = \tau_v/\beta$. This indicates a small recombination time τ_r if the parameter β is large. In figure 7.29 the temperature dependent recombination time τ_r is shown at constant source pressure p_0 = 32, 33, 35 and 41 bar, according to the data in figure 7.28. As expected from the behavior of τ_0/τ_v the recombination time τ_r in the range of ≈ 1-30 seconds shows a minimum at T = 1.78 K that is indicated by dashed line which is a guide to the eye. This result shows that the concentration of vacancies is indeed reduced because of the hcp-bcc phase transition. The reduction of the vacancy concentration x_v supports the reorientation of the crystalline structure, as already discussed in section 7.9.

An additional indicator of this behavior is also given by the ratio of the maximum vacancy concentration to the equilibrium vacancy concentration $X_v^{c,\infty}/X_v^0$. In figure

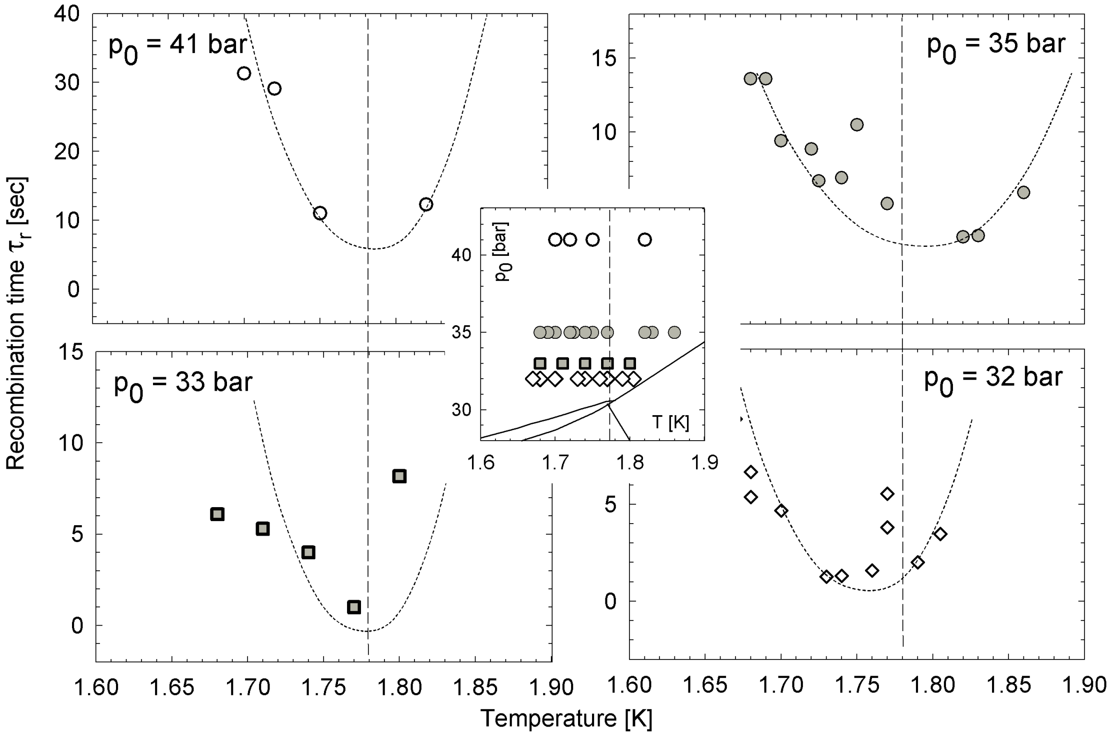

Figure 7.29: Recombination time τ_r as a function of temperature shown for different source pressures p_0 = 32, 33, 35 and 41 bar, respectively. The results indicate a minimum of τ_r in the region of T = 1.78 K, where the hcp-bcc phase transition occurs. The actual minimum at T = 1.78 K is not observable because in this region close to 1.78 K fit is difficult. The dashed line is a guide to the eye and shows the possible temperature dependency of τ_r(T). The results indicate that many vacancies recombine at T = 1.78 K because vacancies support the reorientation of the crystalline structure at the hcp-bcc phase transition.

7.30 the ratio is shown as a function of temperature T and source pressure p_0. The vertical dashed line indicates the hcp-bcc phase transition temperature T = 1.78 K, where the ratio probably decreases. Because of the insufficient statistics this effect has to be investigated more detailed. A decrease of the ratio would indicate a lower concentration of vacancies.

The critical ratio is always found to be $X_v^{c,\infty}/X_v^0 > 1$, as indicated with the equilibrium value for $X_v^{c,\infty}/X_v^0 = 1$. This result is important because it shows that the periodicity of the signal p_{det}^{osc} is associated with a percolative collapse of the crystal because of the increase of the vacancy concentration x_v. The increase of the vacancy concentration is one of the most important arguments for the interpretation of the behavior below T$_c$ = 1.58 K.

To determine the drift velocity u_v the diffusion coefficient has be derived from the period τ, as demonstrated in section 7.5. In figure 7.31 the diffusion coefficient D_v is

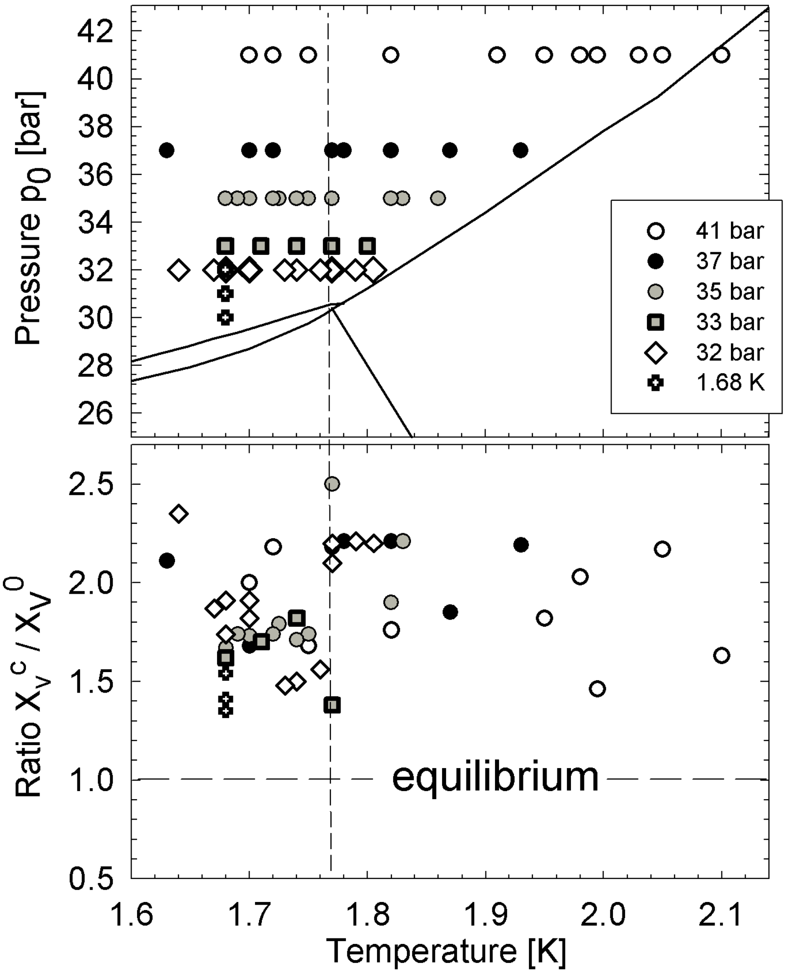

Figure 7.30: The critical ratio $X_v^{c,\infty}/X_v^0$ between the excess vacancy concentration necessary for the collapse X_v^c and the equilibrium vacancy concentration X_v^0 as a function of temperature T for different source pressures p_0 between 32 and 41 bar. The ratio is found to be $c, \infty/X_v^0 > 1$ for all fits. This result indicates that the vacancy concentration in the system is increased above the thermal equilibrium concentration. Thus, the system is not in equilibrium. The obtained values for $X_v^{c,\infty}/X_v^0$ do not show any dependence whether on temperature nor on pressure. Whereas at T = 1.78 K (dashed vertical line) the ratio probably decreases. This indicates that the vacancy concentration at T = 1.78 K decreases because of the hcp-bcc phase transition.

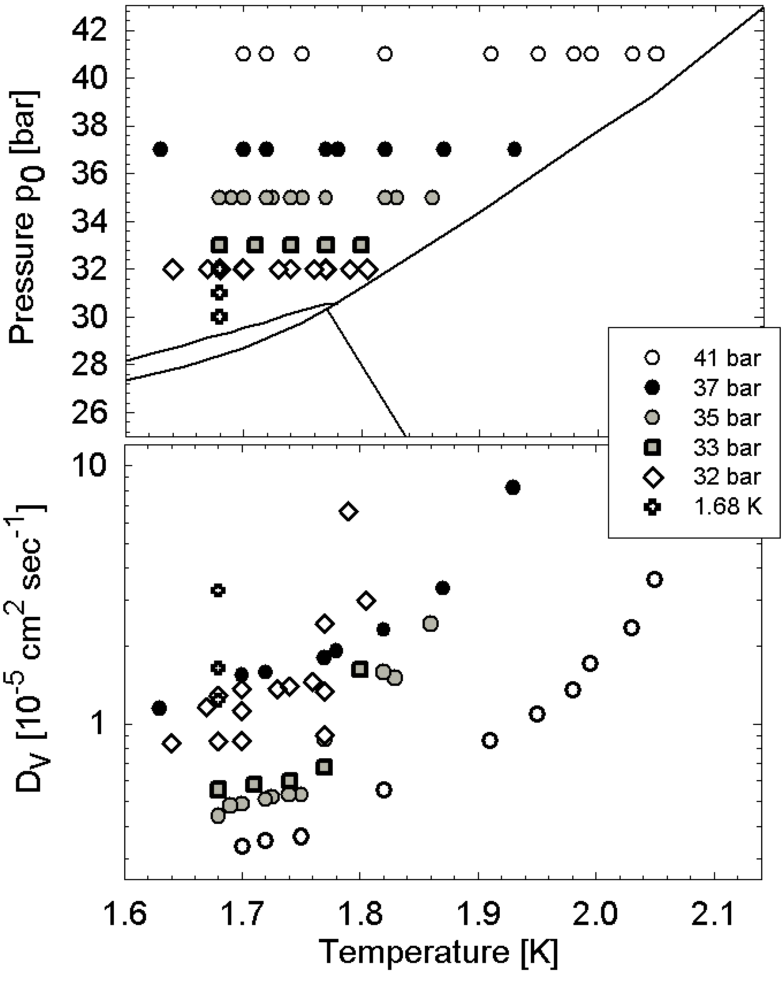

Figure 7.31: Temperature dependent diffusion coefficient D_v(T) at different source pressures p_0 in the range between 32 and 41 bar. The diffusion coefficient D_v(T) is derived from the period τ, as introduced in section 7.5 to determine the drift velocity u_v.

shown for the fitted data. With the diffusion coefficient D_v the drift velocity is given by:

$$u_v = 2 \cdot \sqrt{\frac{D_v}{\tau_v}}. \tag{7.23}$$

The corresponding values for u_v are shown in figure 7.32. Because of the Einstein-Nernst relation $D_v = kT\mu_v$ the drift velocity u_v depends on temperature and pressure as the diffusion coefficient D_v. From the drift velocity in the range of $\approx 10^{-3}$ cm/sec and a thermalization time τ_v in the order of $\approx 10 - 10^2$ seconds the vacancies cover a distance in the order of 0.1 - 1 mm, which gives the order of magnitude for the distance l.

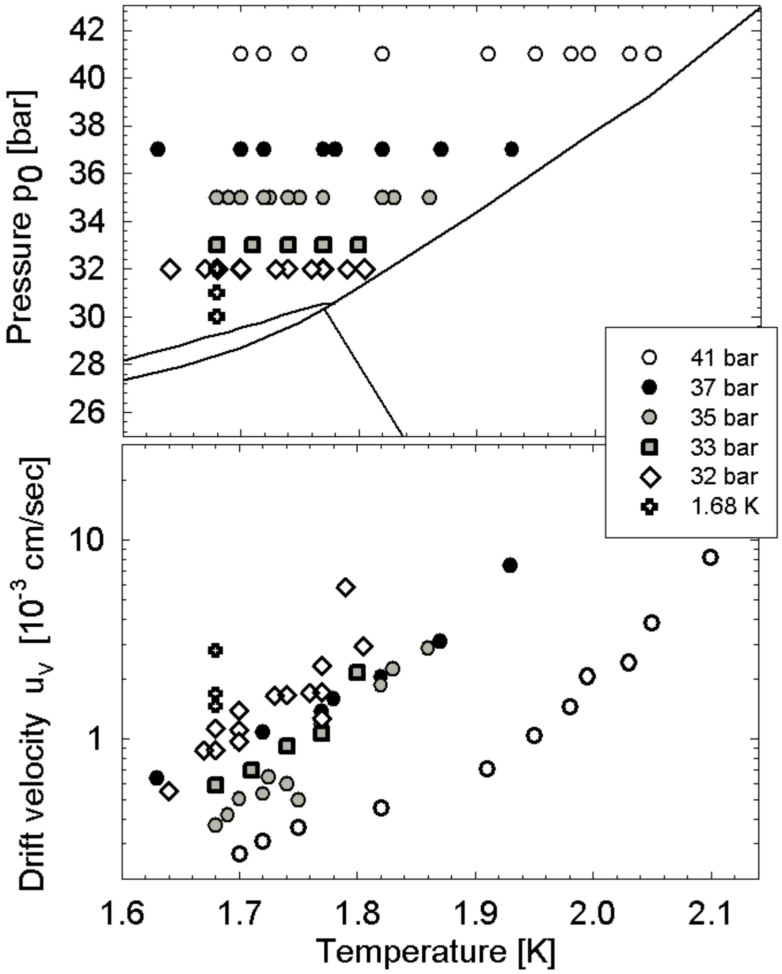

Figure 7.32: Drift velocity u_v obtained from the diffusion coefficient D_v and the thermalization time τ_r. Related to the motion of diffusion by the Einstein-Nernst relation the drift velocity gives the average velocity of vacancies.

Generally the application of the theoretical beam flux j_{osc} indicates that indeed the curve shape of periodicity can be explained by the model of vacancy injection into solid Helium-4.

7.13 Supersolid State

The interpretation of the regimes distinguished by p_τ(T) and moreover p_u(T) as regions in the phase diagram where solid Helium-4 behaves as a liquid with negligible friction leads to the suggestion that the expansion of solid Helium-4 into vacuum is the first experimental evidence of the supersolid state. So far, the final experimental confirmation about the existence of the supersolid state is missing, since the interpretation of the experimental results obtained by Kim and Chan [75, 76] is controversial. In this section p_τ(T) and moreover p_u(T) will be interpreted as the phase lines of the supersolid state.

The most obvious argument for the supersolid state is the fluid-like flow of the solid below pressures p_u(T). Because of the high mobility of particles the supersolid state is assumed to behave as a liquid. According to Bernoulli the dependence of the source pressure p_0 and detector pressure p_{det} can be expressed by:

$$log \Delta p_{det} = \frac{1}{2} log \Delta p_0 \tag{7.24}$$

The factor $\frac{1}{2}$ can be treated as a criterion for an ideal fluid behavior. The analysis in figure 6.20 shows the exponent in dependence of the source pressure p_0. Right up to 28 bar the exponent indicates a fluid-like behavior of the solid. At 28 bar the exponent drops down to zero because p_{det} and remains constant for higher source pressures.

An alternative explanation for the fluid flow below 1.58 K is given by Burovski [20] by assuming that inside the phase between p_m and p_u Helium is not solid, but superfluid that contains small crystalline clusters. As interpreted by Benedek [10] the fluid-like flow below p_u(T) would occur as long as the cluster size is below the nozzle diameter. In the region between p_u(T) and p_τ(T) the cluster‘s size exceeds the nozzle diameter and clogs the orifice. This scenario would explain the constant beam flux that is independent of p_0 and the missing oscillating character. At pressures above p_τ(T) Helium finally solidifies and the beam flux intensity corresponds to the behavior above T$_c$ = 1.58 K, as observed in the experiment. However, two strong arguments contradict to this interpretation.

If the fluid-like flow occurs as long as the crystallite´s size does not exceed the nozzle diameter then p_u(T) would indicate the pressure at which the size of the clusters correspond to d_0. According to this the phase line p_u(T) would be strongly determined by the nozzle‘s diameter: p_u(T) would be closer to the melting line by using nozzles with smaller diameter, and vice versa. However the phase line p_τ(T) shows a weak dependence of d_0. Moreover the weak dependence shows that p_τ(T) is shifted towards higher pressures by decreasing the nozzle diameter, completely opposite to the explanation of the cluster model.

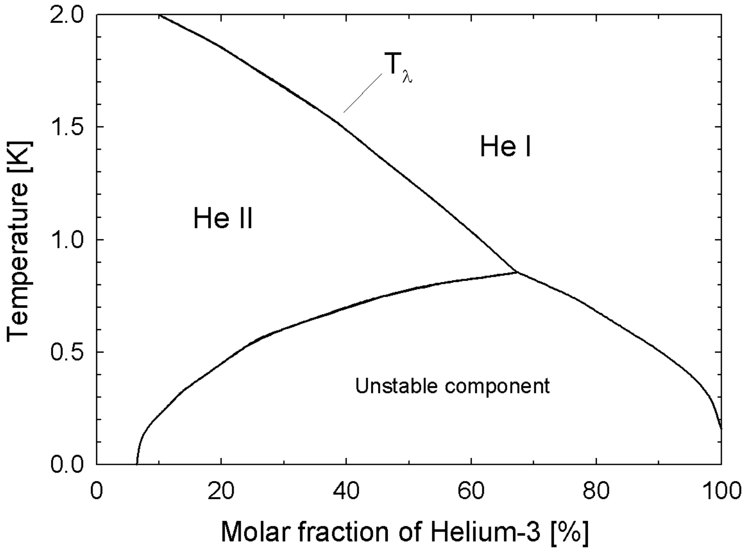

Figure 7.33: The phase separation in Helium-3-Helium-4 mixtures as a function of the molar fraction of Helium-3 [72]. With increasing the fraction of Helium-3 in Helium-4 the superfluidity is quenched and the lambda temperature T_λ decreases. At temperatures below 1 Kelvin and a molar fraction of 6 percent Helium-3 a unstable component of Helium-3-Helium-4 appears in which a superfluid coexists with and a normal fluid. For molar fractions of one percent - as used in the present experiment - the mixture is always superfluid at temperatures below 2.17 K.

The second argument is that already a small concentration of Helium-3 in Helium-4 is sufficient to quench the behavior of the solid below 1.58 K and p_T(T) corresponds to the melting pressure p_m. Since the fraction of one percent of Helium-3 does not affect the creation of the nanoclusters and the superfluid flow, as shown in figure 7.33, the experimental results should have shown no influence on Helium-3. This result indicates that the interpretation of the fluid-like flow by the creation of crystallites in superfluid Helium-4 can be ruled out. Another interpretation can be given by phonon-impuriton interaction as experimentally investigated e.g. by Kisvarsanyi *et al.* [80], whereas this interpretation is already ruled out as already mentioned in section 7.8.

In the introduction to his review on the supersolid state Lubchenko [89] discusses the existence of the supersolid phase in amorphous solids. He suggests that the normal component of He II could form a glassy network before it crystalizes at higher pressures. The result would be a coexistence of a solid and a superfluid in one system.

The high concentration of vacancies causes that the solid is highly incommensurate, especially in the shrinking region. In this region the crystal‘s structure changes permanently under the influence of dislocation climbing and therefore the solid is far away from crystalline order. The formation of a supersolid state by the superfluid motion of vacancies can surely be compared with the disorder of an amorphous solid. Furthermore the solid behavior can be interpreted as the formation of a superglass, as introduced by [116]. A possible interpretation for the non-existence of Geyser oscillations at pressures between p_τ(T) and p_u(T) could be given by the formation of a (super)-glass. In a highly disordered solid the pressure gradient could be stretched in a wide region of the solid so that the vacancies would not accumulate and therefore the collapse of the solid would not occur.

From the conclusions obtained for the properties of vacancies, like the derivation of the vacancy diffusion coefficient, the Geyser effect is doubtless confirmed to be vacancy assisted. As introduced in section 2.4 Andreev and Lifshitz [3] argued that the supersolid occurs only by the presence of vacancies. Owing to the large amplitude of the zero-point motion tunneling of a vacancy into a neighbor lattice sites occurs at significant rates. As a consequence vacancies become delocalized entities treated as elementary quasi-particle excitations. Thus, vacancies form an ideal ideal bose gas in the limit of small a small concentration X_v. Since the Bose-Einstein-condensation has not been confirmed experimentally the vacancy concentration at equilibrium is assumed to be to small for BEC. This assumption gives the most distinctive argument for the observation of the supersolid in this experiment since it is demonstrated that the vacancy concentration is increased of a factor of about 2 above the equilibrium concentration. Thus, the only possible and most favorable explanation for the behavior below $\mathrm{T}_c = 1.58$ K is given by the formation of the supersolid state.

Furthermore the observed phase line p_τ(T) corresponds to the general assumptions of the supersolid phase line, as shown in figure 7.34. Several theoretical attempt proposed the occurrence of the supersolid close to the melting line at pressures below ≈ 35 bar. Galli and Reatto [47] simulated the vacancy distribution with shadow wave functions in a Monte-Carlo simulation. They found that BEC occurred at T = 0 K at low density. By extending the results up to finite temperatures they found several scenarios for the supersolid phase line depending on quantities like the formation energy ϕ_f, the effective vacancy mass $m_v^\star$ and the ground state vacancy concentration X_v^* that are assumed to occur even at T = 0 K [96]. The different scenarios are sketched in figure 7.34: In the absence of ground state vacancies ($X_v^* = 0$) the supersolid phase is given by section III. They claim that this transition corresponds to a phase line that has been considered by Burns and Goodkind [19]. If the ground state vacancy concentration is non-zero then BEC should occur even at lowest temperatures. The possible scenarios would be that BEC would persist along the melting line (I, II, III) or that at a certain temperature T_{BEC}^1 the BEC state is destroyed by thermal fluctuations due to ground state vacancies but at a certain temperature T_{BEC}^2 the supersolid re-occurs due to thermal vacancies at sufficient concentration (I, III). The supersolid could also occur only at (I) if the formation energy ϕ_f is too high and therefore the thermal vacancy concentration too small. Another attempt is given by Bjisma and Stoof [15] who derived a phase line for the supersolid from experiments of investigating ultrasound attenuation in solid Helium-4 by Lengua and Goodkind [88]. Both proposals for the supersolid phase line correspond nearly in a perfect agreement with the phase line p_τ(T) that is indicated by the white circles in figure 7.34. Whereas the possible experimental confirmation of the

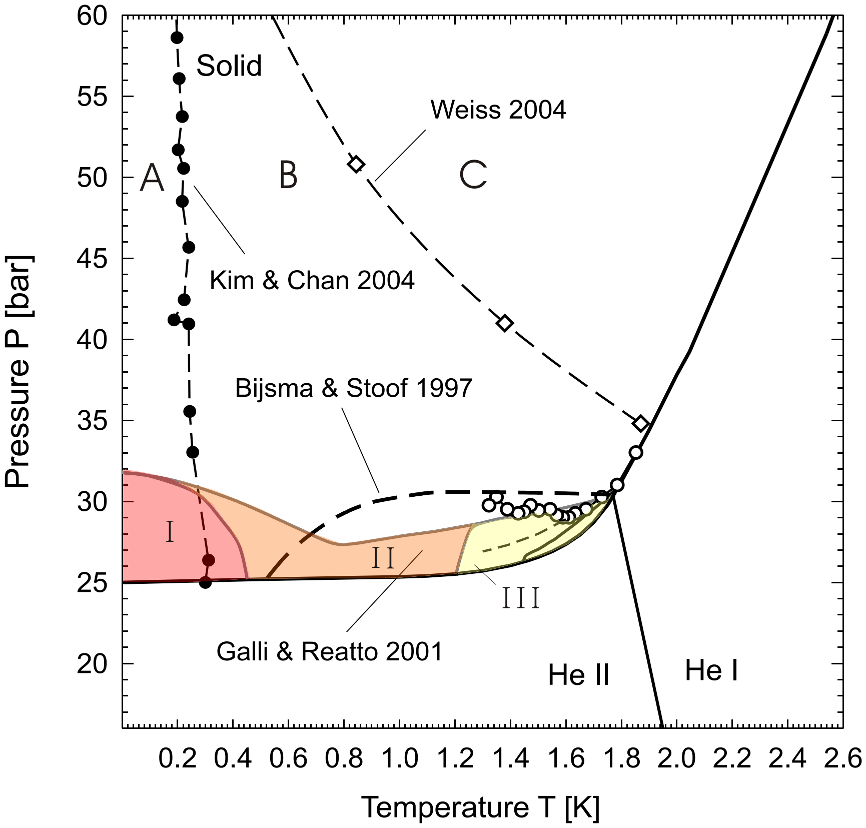

Figure 7.34: Possible phase lines for the supersolid state for solid Helium-4 obtained from theoretical and experimental investigations. The direct measurement of the supersolid phase line was done by Kim and Chan [75, 75] by observing NCRI at temperatures below 230 mK. From the detected phase line Weiss [124] separated the solid phase of Helium-4 into three regions: The equilibrium supersolid (A), the non-equilibrium supersolid (B) and the normal solid (C). Furthermore the phase line of the supersolid was proposed by Bijsma and Stoof [15], who derived the phase line from experiments of ultrasound attenuations in Helium-4 done by Lengua and Goodkind [88]. A theoretical scenario for the possible phase lines of the supersolid was proposed by Galli and Reatto [47]. The phase lines p_u(T) and p_τ(T) observed in this experiment are also shown (dashed line and white circles) and offer a good agreement with the theoretical supersolid by Galli and Reatto and also the one derived by Bijsma and Stoof. Surprisingly, the critical temperature - even by Weiss - is found to be $T_c \approx 1.8$ K.

supersolid phase by Kim and Chan [75, 76] at T $\approx$ 230 mK does not match with any of these theoretical assumptions. A possible explanation is given by Weiss [124]. He argued that Kim and Chan measured the supersolid for temperatures below T $\approx$ 230 mK at equilibrium conditions. Since the supersolid is assumed to occur only at higher vacancy concentration Weiss proposed three phases in solid Helium-4: An equilibrium supersolid state (A) below T $\approx$ 230 mK and furthermore an non-equilibrium supersolid state (B) and the normal solid (C). Out of the supersolid transition at T $\approx$ 230 mK Weiss derived a phase line that separates the non-equilibrium supersolid from the normal solid behavior. This line is indicated by the dashed line between (B) and (C), whereas the diamonds indicate temperatures and pressures derived by Weiss. The separation of the solid phase into an equilibrium supersolid, non-equilibrium supersolid and normal solid phase can interpreted as phases in which the supersolid occurs in dependence on the vacancy concentration. The probable supersolid seen by Kim and Chan was obtained at equilibrium whereas in this experiment the system is in non-equilibrium conditions, caused by the increase of the vacancy concentration. For the non-equilibrium supersolid the critical temperature is found to be T$_c$ $\approx$ 1.8 K by Weiss, Galli and Reatto and also Bijsma and Stoof. Assuming that the supersolid is a Bose-Einstein condensation of vacancies the critical temperature for BEC is given by:

$$T_{BEC} = \frac{2\pi\hbar^2}{mk_B}\left(\frac{N}{2.612\cdot V}\right)^{2/3}. \tag{7.25}$$

With the increase of the vacancy concentration of a factor of ≈ 3 above the equilibrium concentration the critical temperature is found to be $T_{BEC} \approx 1.2$ K. If the vacancies form a Bose-Einstein condensate it follows that the supersolid fraction is given by the critical vacancy concentration X_v^c that corresponds to the maximum vacancy concentration $X_v^{c,\infty} \approx 3 \cdot X_v^0$.

The results show that the pressures p_τ(T) and p_u(T) can be interpreted as the phase lines that mark the supersolid phase in solid Helium-4. The behavior of the solid below p_u(T) fulfills the requirement of the supersolid state: The solid shows a fluid-like behavior. Furthermore the effect is eliminated under the influence of small fractions of Helium-3. Finally the effect is assumed to occur because of an increase of the vacancy concentration above the thermal concentration X_v^0. A possible interpretation for the occurrence of the Geyser oscillation at p_τ(T) and not at p_u(T) can be given by the assumption that the vacancies overcome a certain critical velocity at p_u(T) that eliminates the supersolid.

Chapter 8

Summary and Outlook

The last three decades have seen a steady grow of interest in solid Helium as the most "quantum" quantum crystal and much experimental effort has been invested to elucidate the structure and behavior of this solid. The main focus was on the study of quantum properties manifested in quantum diffusion of vacancies at low enough temperatures. Final goal was the possible observation of the supersolid state, as the counterpart to Helium-II, the only real superfluid. Many different experimental approaches have been developed and investigated but the final evidence for this state is still missing.

This work gives a detailed introduction into a completely new experimental method to investigate the quantum crystal behavior of solid Helium-4. It has been discovered by Grisenti that in the expansion of solid Helium-4 into a vacuum through small micron-sized orifices a fascinating new effect occurs. The jet velocity in the range of 200 m/sec indicates that surprisingly the beam is a liquid jet, whereas the conditions in the source correspond to the solid state. Moreover, for source conditions corresponding to the solid phase the beam flux intensity shows periodic peaks and a distinct time dependent behavior. The periodic flux oscillates within seconds up to minutes and shows a strong dependence on temperature and source pressure. This new phenomenon has been studied for temperatures between 2.1 K and 1.3 K and pressures up to 30 bar above the melting pressure. The beam flux intensity has been recorded by the vacuum pressure in a pitot vacuum chamber.

In this work mainly the behavior of the period has been studied as a function of pressure and temperature and the influence of the isotope Helium-3. Furthermore geometrical aspects such as the influence of the nozzle diameter d_0 have been investigated.

In order to explain this fascinating phenomenon a kinetic model based on the injection of excess vacancies into the solid has been proposed. The so-called "Geyser oscillations" in solid Helium-4 are assumed to occur as a periodic collapse of the solid. This collapse is caused by the accumulation of excess vacancies that are generated at a solid/liquid interface close to the orifice. With the subsequent re-injection of vacancies the effect repeats periodically. The accumulation of vacancies is explained by the occurrence of a pressure gradient in the solid. Forced by drift and diffusion the vacancies accumulate at a fixed distance from the orifice where the pressure gradient disappears. With the injection of excess vacancies the vacancy concentration can be increased of a factor of 2 above the equilibrium vacancy concentration.

The theoretical description of the vacancy current reproduces the time dependent beam flux intensity, which is demonstrated for a wide range of temperatures and pressures. The kinetic model gives direct access to values such as the temperature and pressure dependence of the vacancy diffusion coefficient D_v which has been found to be in the range of 10^{-5} cm^2/sec. From the temperature dependent diffusion coefficient the vacancy activation energy was derived to be $\phi_f \approx 20$ K. Also the recombination time τ_r of vacancies with interstitial atoms in the lattice is observable. Typically τ_r was found in the range of $\approx 1-20$ sec. The good agreement of D_v with former experimental results by Zuev *et al.* [131] confirms the applicability of the theoretical model.

From the periodic behavior two temperature regimes can be distinguished:

(1) For temperatures above 1.78 K the oscillations in the beam flux intensity appear at a certain pressures p_τ(T) that corresponds to the melting pressure p_m. The period increases with increasing source pressure at constant temperature or increases with decreasing temperature at constant source pressure. The period is obtained to be inverse proportional to the vacancy diffusion coefficient D_v, and since the period increases with decreasing temperature the temperature dependence of D_v corresponds to experimental investigation of vacancy diffusion in solid Helium-4 [131].

(2) At temperatures below 1.78 K it is observed that the vacancies mobility is increased in a regime close to the melting line. This novel effect can be observed by decreasing - or increasing - the temperature at constant source pressure p_0, whereby the period suddenly drops down for temperatures below T = 1.58 K. With the method of increasing source pressures at constant temperature below T = 1.58 K it is surprisingly observed that up to almost 1.5 bar above the melting pressure the solid behaves as an ideal liquid by following the Bernoulli equation. As a result this liquid-like phase was detected by investigating the pressure p_u(T) at which the Bernoulli behavior vanishes. It is generally found that the periodic effect does not occur in the bcc ordered solid phase. Above pressures p_u(T) the beam flux intensity is found to be independent of the source pressure, but no oscillations are observed. The corresponding pressure p_τ(T) below T = 1.58 K appears up to 2 bar above p_u(T).

As the most important result the fluid-like flow of the solid below T = 1.58 K provides direct evidence for the existence of the supersolid state of matter, that was proposed by Andreev and Lifshitz more than 35 years ago [2] to occur as a Bose-Einstein-condensation of defects. The phase line p_τ(T) predicted for the supersolid by Galli and Reatto [47] is in good agreement with the findings of this experiment. The experimental investigation of mixtures of Helium-3 and Helium-4 with a fraction of Helium-3 of 1 percent and below shows that the presence of Helium-3 traps the vacancies, as suggested by Berent *et al.* [13] and suppresses liquid flow of the solid below 1.58 K. This results also supports the observation of the supersolid phase in solid Helium-4.

Outlook

Geyser Effect: Proposed Further Investigations

The most interesting question is the origin of the unexpected anomaly below T = 1.58 K. This clearly calls for extensions of experimental and theoretical work.

One goal will be the investigation of the Geyser effect down to temperatures well below 1.3 K to find the trend of the both phase lines p_u and p_T. Possible scenarios are given by Galli and Reatto [47], as shown in figure 7.34 with the interpretation as the supersolid state. With the bath-cryostat used here temperatures below 1.3 K can not be reached. Thus, the investigation of the Geyser oscillations below 1.3 K requires a completely new experimental setup. By using liquid Helium-3 instead of Helium-4 the pumping method is sufficient to cool down to ≈ 0.3 K, whereas the required amount of Helium-3 is far away from financial possibilities. The use of a Helium-3/Helium-4 mixture cryostat is a possible approach. Such cryostats use the effect of demixturing a dilute phase of Helium-3/Helium-4 below the equilibrium concentration. Therefore, Helium-3 atoms transit from a pure Helium-3 phase into the dilute phase. There they cool down because of the higher heat capacity of the Helium-3 atoms in Helium-4. With this method it is possible to to cool down below 100 mK. The cooling power is well below the cooling power of a Helium-4 bath cryostat. Whereas the expansion of Helium into a vacuum causes immense cooling power because of the steady cool down of Helium from 300 K down to 1.5 K.

The first hint for the supersolid state was found by Kim and Chan in observing Non-classical rotational inertia at temperatures below 230 mK in vycor and bulk solid Helium [75, 76]. Since the fluid-like behavior found in this experiment below 1.58 K indicates also supersolid flow the final evidence would be given in combine both experimental methods, namely NCRI measurements of the expansion of solid Helium into a vacuum. Whereas the technical setup forbids an experiment using a rotational cylinder because it builds a closed system. With the expansion of matter through the orifice the steady inaccuracy of mass makes the sensitive change of the rotating frequency difficult. Vibrational excitation of the nozzle head would be an alternative approach for an experiment comparable to the investigations of NCRI. Vertical oscillation of the nozzle head should also probably indicate the presence of a supersolid fraction by increasing the amplitude of the vibration.

Further insights could also be gained by studying the flow behavior through a porous membrane. The use of vycor or gelsil shifts the melting pressure up to 15 bars [95]. Thus, the investigation of the vacuum expansion of Helium through a vycor network that is placed right at the nozzle - or even used instead of the nozzle - could be an interesting experiment to investigate the oscillating phenomenon at pressures far above p_m in relation to the supersolid experiments done by Kim and Chan. On the other hand the presence of vycor directly at the nozzle could suppress the oscillating effect. The result would prove that vacancies accumulate near the orifice. The use of filter elements with a pore diameter of approximately 0.5 μm mounted close at the nozzle did not show any influence on the observed oscillating phenomenon.

The interpretation of the solid behavior as a formation of micro-sized clusters below 1.58 K and pressures close above the melting pressure could finally be ruled out by measuring the dependence of the pressure p_u of the nozzle diameter d_0. It has been shown that the pressure p_τ is almost independent of d_0, whereas the systematics is insufficient to give a final result.

Instead of pinhole orifices the use of pipettes would allow to investigate the oscillating behavior visually inside the source by measuring the difference in refraction of solid and liquid or to investigate the lattice structure by X-ray scattering. The use of micro-sized pipettes has been demonstrated for the liquid Helium jet by Grisenti [64] and Grams [58]. It is theoretically been assumed that the Geyser oscillations indeed should also occur by using micro-sized pipettes. The results would prove the existence of a solid/liquid interface close to the orifice. Furthermore it would also give a hint for the origin of the periodicity. Measuring a change in refraction is difficult since for Helium the refraction index for solid and liquid is almost the same and furthermore close to unity.

Also measurements of the period along isobars chosen to be a fixed pressure above the melting pressure would be a suitable method to investigate the Geyser phenomenon at constant pressure gradient by assuming that the distance l is constant. Probably the period shows a perfect exponential dependence on temperature or is even independent of T. The temperature independence of the minimum period τ_{min} at temperatures below T = 1.58 K could be related to the weak temperature dependence of the melting pressure below T = 1.6 K. With this measurement the dropdown of the period at T = 1.58 K and the increase at T = 1.4 and 1.78 K should be seen much more detailed.

Geyser Effect: Theoretical Model

Recent experiments of Toennies *et al.* [121] show that the pressure inside the source tube exhibits the same oscillating character. It matches in period and curve shape exactly with the beam flux intensity. The results demands for an refinement of the theoretical model since presumably the collapse is assumed to be placed at a much larger distance from the nozzle. The theoretical approach that explains the oscillations in the source tube assumes that with the injection of vacancies the pressure drops down below the melting pressure and therefore the collapse occurs [121]. A continually decrease of the pressure inside the source tube decreases the pressure gradient with time. In the present kinetic model the pressure gradient is assumed to constant, whereas the distance l at which the collapse occurs is set to be infinite.

Thus, the expansion of the theoretical expression j_{osc} for finite l will provide a better interpretation of the behavior inside the nozzle. Since the region of accumulation is assumed to be at an infinite distance l, processes like backward diffusion can not be reproduced by the kinetic model. Therefore, for temperatures in the range of T = 1.78 K the periodic curve shape can only be reproduced qualitatively. Generally, the periodic collapse has to be studies theoretically to fulfill the kinetic model and to simulate the periodicity. For this purpose the determination of the critical concentration

X_v^c is useful to achieve the complete description of the Geyser effect in solid Helium by determine the period τ. Below the critical temperature T = 1.58 K the periodic curve shape can not be interpreted by the kinetic model.

Investigating Other Quantum Crystals

The most interesting candidate to observe the oscillating effect is Helium-3. It is predicted that the Geyser oscillations also appear but with a shorter period τ. The vacancy diffusion coefficient of pure Helium-3 is about one order of magnitude smaller than for Helium-4. Whereas as already demonstrated an abnormal behavior below 1.58 K is ruled out since already smallest fractions of Helium-3 in solid Helium-4 suppress the interaction of the boson Helium-4.

The next best candidate is solid Hydrogen, as the element with the next highest de Boer parameter after Helium. Many experimentalists like e.g. Kishvarsanyi [81] investigated the quantum behavior of solid Hydrogen. The recent work of Kim and Chan finds the same supersolid behavior in solid Hydrogen [77] as in Helium, but at much lower temperature and smaller fraction. The results are very interesting since the existence of the supersolid state of Hydrogen would have been proven before the long-sought superfluid state. On the other hand if the anomaly in the rotating frequency observed by Kim and Chan turns out to be an effect of solid slip on a superfluid layer than the results obtained with Hydrogen would be the first evidence for superfluidity in Hydrogen, as proposed by [51]. It seems that Hydrogen is indeed really "super", at the latest since the first indication for superfluid Hydrogen in liquid Helium droplets has been observed by Grebenev *et al.* [60].

The unique technique of cryogenic micro-jets also allows the investigation of the superfluidity of para-Hydrogen, as proposed by [66]. And also the investigation of solid Hydrogen seems to be interesting. Whereas with the available cryostats the temperature range is also restricted and since NCRI in solid Hydrogen is observed at much lower temperatures than in solid Helium the confirmation of an abnormal behavior could not be investigated. Nevertheless the investigation of the beam flux intensity with solid Hydrogen would be an interesting study that probably shows the same oscillating behavior as solid Helium.

Whereas there are some reasons that the oscillations of the beam flux intensity do not occur by using Hydrogen: The much smaller concentration of vacancies in solid Hydrogen probably inhibit a melting of the solid. Therefore, no solid/liquid interface would occur and no excess vacancies would be generated. Furthermore, there would be no pressure gradient which is finally responsible for the periodicity of the beam flux. Instead of a liquid jet probably a solid filament would appear, as seen by Grams for solid Argon [57].

An alternative study of the Geyser effect could be done with mixtures of Helium-4 and Hydrogen. As investigated by Lee [74, 79] the mixtures of Helium and Hydrogen are highly porous van der Waals solids in which solid Hydrogen clusters are surrounded by a thin layer of solid Helium. In this context these impurity-Helium solids are treated as so-called quantum gels. In this context the study of the concentration of Hydrogen could exhibit a transition from the "Geyser"-like phenomenon to expansion of solid filaments.

Investigations with solid Neon would probably show no real quantum behavior. It is assumed that the exit beam would appear as a solid filament, as demonstrated by Grams [56, 57] by expanding solid Argon through a capillary of diameter $d_0 \approx 50\mu$m.

Search for the Supersolid

After the observation of NCRI in solid Helium the immense number of publications reflects the general confusion in the scientific community. Many different interpretations were given and it is still unclear if the observed phenomenon is due to a (super)-solid that behaves as a liquid or a solid motion on a superfluid layer. Beside this interpretations for the observed phenomenon a possible explanation for the obscure solid behavior could be that the centrifugal force causes an increase of the pressure at the cell‘s wall. Following the Nabarro-Herring mechanism the vacancies are forced to populate at higher pressures and herewith at the cell‘s wall. Thus, the vacancy concentration is increased which causes weather the formation of the supersolid state or just a lubrication of the solid that decreases the friction at the cell‘s wall.

Bishop *et al.* made the first experiment searching for the evidence of NCRI [16]. The question that remains is still not solved, why these earlier experiments done under the same conditions did not observe indications for the supersolid state. It is generally assumed that the remaining concentration of Helium-3 suppressed the NCRI. Recently, the confirmation of Kim and Chan‘s result in bulk solid Helium has been reported by Shirahama [112]. These experiments have been run with a higher frequency and crystals of higher quality. It was found indication for NCRI, whereas the fraction of NCRI was found to be one order of magnitude smaller than observed by Kim and Chan.

Vacancies are generally be agreed to be the key to the supersolid state. Thus, the appearance of the supersolid state has to be investigated as a function of the vacancy concentration and this will be one of the main result of the forty year search for this state. Beside the occurrence of the supersolid state at thermal equilibrium a possible result could also be the existence of a non-equilibrium supersolid state, which is probably found and investigated in this work. If and how both are related is a still open question. This final step to answer it can be done by two approaches: On the one hand the investigation of the Geyser phenomenon at temperatures well below the transition temperature of NCRI at T = 230 mK. On the other hand one has to find ways to increase the concentration of vacancies for to confirm the results obtained in this work. The present experiment paves the road to achieve such concentration.

Concluding Remarks

The expansion of solid Helium-4 into vacuum is a fascinating method that allows study of the intriguing quantum nature of solid Helium-4. The most important discovery is the possibility of generating a non-equilibrium quantum solid which exhibits unexpected behavior and a strong indication for the supersolid state.

Hopefully the uniqueness of the Geyser effect in solid Helium-4 and the simplicity of this method will motivate further investigation and inspire experimentalists to find other ways to generate non-equilibrium quantum solids.

Chapter 9

Zusammenfassung und Ausblick

Im Jahr 2001 wurde im Zusammenhang mit der Untersuchung der Vakuumexpansion flüssigen Helium-4 durch eine Düse mit Durchmessern im Bereich von 1-5 μm ein neuartiger Effekt beobachtet. Dieser Effekt bietet einen völlig neuen experimentellen Zugang zum Verständnis von sogenannten Quanten-Festkörpern. In diesen Experimenten zeigten sich periodische Fluktuationen des Vakuums, nachdem der Düsendruck soweit erhöht wurde, dass sich in der Düse Bedingungen für den Helium-Festkörper ergaben. Die Fluktuationen zeigten Periodendauern in der Größenordnung von Sekunden und Minuten und variierten sowohl mit der Düsentemperatur als auch mit dem Düsendruck. Der Ursprung dieser Oszillationen lässt sich auf Intensitätsschwankungen des interessanterweise flüssigen Helium-Strahls zurückführen.

Diese Arbeit bildet die erste systematische und detaillierte Untersuchung dieses Phänomens. Die oszillierende Fluktuation der Strahl-Intensität wurde im Bezug auf die Periodendauer und den Intensitätsverlauf innerhalb einer Periode im Bereich zwischen 2.1 und 1.3 Kelvin und Düsendrücken bis zu 30 bar oberhalb des Schmelzdruckes untersucht. Der oszillatorische Effekt wurde ebenfalls durch die Zugabe des Isotopes Helium-3 in Konzentrationen im Bereich von 0.0015 und 1 Prozent untersucht.

Ein theoretisches Modell erklärt den Effekt durch die Injektion von Gitterfehlstellen (Vacancies) in den Festkörper an einem flüssig-fest Phasenübergang, der unmittelbar an der Düse vermutet wird. Die Erzeugung von zusätzlichen Fehlstellen führt zu einem induzierten Kollaps des Festkörpers, welcher sich periodisch wiederholt. Das theoretische Modell zeigt, dass ein Quanten-Festkörper erzeugt wurde, welcher - aufgrund der erhöhten Fehlstellen-Konzentration - nicht im thermischen Gleichgewicht steht. Bei den Untersuchungen dieses Nicht-Gleichgewicht-Festkörpers zeigte sich ein Bereich im Phasendiagram des Festkörpers, in dem sich dieser wie eine ideale Flüssigkeit verhält. Dies ist ein eindeutiges Anzeichen für die Entdeckung des Supersolids, der im Jahre 1969 durch Andreev und Lifshitz [3] theoretisch als eine Bose-Einstein-Kondensation von Gitterfehlstellen progostiziert wurde. Dieser Zustand bildet das Pendant zu dem Effekt der Superfluidität in der flüssigen Phase von Helium-4 bei Temperaturen unterhalb der Lambda-Linie.

Theoretischer Hintergrund

Spätestens seit der Entdeckung der Superfluidität von Helium-4 durch Kapitza [71] im Jahre 1937 gilt Helium als eines der faszinierendsten Elemente. Die schwache Van-der-Waals-Bindung ermöglicht es, dass bei tiefen Temperaturen der Wellencharacter dieses leichten Elements in den Vordergrund tritt. Helium ist das einzige Element, das bei Atmosphärendruck bis zum absoluten Temperaturnullpunkt flüssig bleibt. Erst bei Drücken ab 25 bar und entsprechenden Temperaturen unterhalb 2 Kelvin bildet sich die feste Phase. Der Quanten-Charakter offenbart sich ebenfalls besonders im Helium-Festkörper. Bei entsprechend tiefen Temperaturen ist die deBroglie-Wellenlänge in der Größenordnung des interatomaren Abstandes. Dies gilt gleichermaßen als die Definition von Quanten-Festkörpern.

Durch die schwache Wechselwirkung sind die Helium-Atome im Festkörper äußerst mobil. Die Mobilität der Teilchen wird weiterhin in hohem Maße durch die Präsenz von Gitterfehlstellen unterstützt. Da die Energie zur Erzeugung einer Gitterfehlstelle mit etwa 6 Kelvin im Bereich der thermischen Energie liegt, beträgt deren Konzentration im Gleichgewicht etwa 1 bis 2 Prozent. Die Präsenz von Gitterfehlstellen erhöht die Amplitude der Nullpunkt-Oszillationen, so dass bei genügend tiefen Temperaturen die Teilchen sich vorwiegend durch Tunneln bewegen können. Die Gitterfehlstellen (Vacancies) werden zu delokalisierten Teilchen (Vacanions), und Quanten-Diffusion dominiert über den thermisch angeregten Diffusionsprozess. Quanten-Diffusion wird durch Phononen angeregt [3, 70]. Die Mobilität der Gitterfehlstellen in festem Helium-4 spiegelt sich in dem entsprechenden Diffusions Koeffizienten D_v wider. In Experimenten von Zuev *et al.* [131] wurde dieser in der Größenordnung von 10^{-5} cm^2/s gefunden, vergleichbar mit Diffusions Koeffizienten von Teilchen in Flüssigkeiten [102].

Die bei der Expansion von festem Helium-4 ins Vakuum auftretenden Oszillationen in der Jet-Intensität sind aufgrund eines theoretischen Modells ebenfalls auf die hohe Mobilität der Gitterfehlstellen zurückzuführen. Die beobachtete Jet-Geschwindigkeit im Bereich von etwa 200 m/s weisst auf einen flüssigen Strahl hin, obwohl der Druck und die Temperatur in der Düse dem festen Zustand entsprechen. Da die Oszillationen des Vakuumdrucks - der zur Jet-Intensität proportional ist - bei Temperaturen über 1.78 K genau oberhalb des Schmelzdruckes erscheinen, lässt sich ein Zusammenhang des periodischen Effektes mit der festen Phase belegen. Aufgrund dessen wird ein flüssig-fest Phasenübergang innerhalb des Düsenkopfes vermutet, an dem der Druck dem Schmelzdruck entspricht. Diese flüssig-fest Grenzschicht ist eine Quelle von Gitterfehlstellen: Tritt ein Atom von der festen in die flüssige Phase, so hinterlässt es eine Gitterfehlstelle unmittelbar an der Phasengrenze. Aufgrund der Separation von Zwischengitteratomen (Interstitials) ist die Konzentration der Gitterfehlstellen an der Phasengrenze außergewöhnlich erhöht. Zwei Prozesse sind für die Bewegung der künstlich erzeugten Gitterfehlstellen von der Phasengrenzfläche in den Festkörper verantwortlich:

(1) Diffusion: Aufgrund der erhöhten Konzentration der Gitterfehlstellen an der Phasengrenze tritt ein Konzentrationsgradient auf. Da die künstlichen Gitterfehlstellen kon-

tinulierlich erzeugt werden, erfolgt nach dem 2. Diffusionsgesetz von Fick [43] der Prozess von nicht-gleichförmiger Diffusion.

(2) Drift: Da unmittelbar am Phasenübergang der Druck dem Schmelzdruck entspricht, bildet sich wegen des höheren Düsendruckes im Festkörper ein Druckgradient. Nach dem Nabarro-Herring-Mechanismus [68] werden Gitterfehlstellen in festem Helium durch einen auftretenden Druckgradienten hin zu höheren Drücken bewegt. Dieser Effekt tritt auf, da Gitterfehlstellen in festem Helium so genannte "Inward Relaxation" verursachen. Hierbei vergößert sich aufgrund der schwachen Van-der-Waals-Wechselwirkung die Nullpunkt-Bewegung der benachbarten Gitteratome um die Fehlstelle. Aufgrund von "Inward Relaxation" und des Druckgradienten entsteht eine Kraft, welche Gitterfehlstellen zu höheren Drücken bewegt.

Die Erzeugung zusätzlicher Fehlstellen im Festkörper im Bereich des flüssig-fest Übergangs ist für den Schmelzprozess verantwortlich: Etwa 90 Prozent aller künstlich erzeugten Fehlstellen rekombinieren mit Atomen des sich zur Düse hin bewegenden Festkörpers. Durch die Rekombination reduziert sich die Anzahl der Gitterebenen (Dislocation climbing) und der Querschnitt des Festkörpers wird verringert. Weiterhin sinkt durch die Präsenz der Fehlstellen der Druck im Bereich der Düse bis hin zum Schmelzdruck ab, so dass ein flüssig-fest Übergang entsteht.

Fehlstellen, die nicht mit Gitteratomen rekombinieren, bewegen sich durch Drift und Diffusion in den Festkörper hinein. Bei einer gewissen Distanz zum flüssig-fest Übergang entspricht der Druck dem angelegten Düsendruck, was zum Verschwinden des Druckgradienten und der die damit verbundene Bewegung der Fehlstellen durch Drift führt. In dieser Region steigt die Konzentration der Gitterfehlstellen, bis die Kristallstruktur dem äußeren Druck nicht mehr entgegenwirken kann. Es erfolgt ein perkolativer Kollaps des gesamten Festkörpers, der als Ursache für den Peak in der Jet-Intensität vermutet wird. Durch die nachfolgende Erzeugung von Gitterfehlstellen sammeln sich diese erneut. Dieser sich wiederholende Prozess erzeugt die oszillierende Intensitäts-Schwankung des Jets. Durch die Bewegungsgleichungen von Diffusion und Drift wurde die Verteilung der Fehlstellen im Festkörper simuliert. Dabei trat tatsächlich eine Erhöhung der Konzentration in einem Bereich mit verschwindendem Drift auf.

Mit der Formulierung einer zeitabhängigen Transportgleichung der Fehlstellen konnte der zeitliche Verlauf der Jet-Intensität bei zahlreichen Temperaturen und Drücken reproduziert werden. Diese Gleichung berücksichtigt im Wesentlichen den zeitabhängigen Verlauf der Fehlstellen-Konzentration, welcher durch Drift, Diffusion und Erzeugung bzw. Rekombination der Fehlstellen bestimmt wird. Die Reproduktion der Fehlstellen-Konzentration ließ sich im Wesentlichen durch zwei Parameter erzeugen, wobei sich beispielsweise der Diffusions Koeffizient der Fehlstellen in einer Größenordnung von 10^{-5} cm^2/s ergab. Die Übereinstimmung dieser Observablen mit Ergebnissen aus früheren Untersuchungen unterstreicht die Validität des vorgestellten Modells.

Experimentelle Umsetzung

In diesem Experiment wurde ultra-reines Helium-4 (99.9999 %) bei Temperaturen unterhalb 2 Kelvin und Drücken gemäß der festen Phase durch eine punktförmige Öffnung mit Durchmessern im Mikrometerbereich ins Vakuum expandiert. Zu diesem Zweck wurde Helium-4 mit einem Badkryostaten auf die erforderlichen Temperaturen gekühlt. Die gesamte Apparatur besteht im Wesentlichen aus zwei separaten Vakuumkammern: Eine Quellenkammer, die den Badkryostaten samt entsprechender Düsenhalterung enthält, und eine Detektorkammer, in welcher die Intensität des Helium-Jets durch den entsprechenden Vakuum-Druck gemessen wird. Beide Vakuumkammern sind durch eine Öffnung mit einem Durchmesser von 30 mm und variabler Distanz zwischen 10-50 mm zur Düsenöffnung miteinander verbunden.

Zur Erzeugung des fluiden Strahls wird ultra-reines Helium 6.0 durch eine Stahlleitung zuerst zur Vorkühlung durch das Helium-Reservoir des Kryostaten und dann in einen Kühlkopf geleitet, in welchem sich die Düsenhalterung befindet. Die Untersuchungen wurden mit Düsendurchmessern im Bereich von 1 bis 5 μm durchgeführt. Die Länge des Düsenkanals entsprach in etwa der des Düsendurchmessers. Durch eine entsprechende Eichmessung konnte der tatsächliche Düsendurchmesser mit einer Genauigkeit von ± 0.2 μm bestimmt werden.

Die Jet-Intensität wurde durch eine zeitabhängige Messung des Vakuums in der Detektorkammer bestimmt. Hierzu wurde eine konventionelle Ionisationsmessröhre verwendet. Mit einem Voltmeter wurde das Signal ausgelesen und digitalisiert. Die Datenaufnahme erfolgte schließlich mit einer Zeitauflösung zwischen 250 und 500 Millisekunden.

Ergebnisse und Interpretation

Die periodischen Oszillationen der Jet-Intensität wurden in diesem Experiment in einem Bereich zwischen 1.3 und 2.1 K und Drücken bis zu 30 bar über dem entsprechenden Schmelzdruck untersucht. Das Hauptaugenmerk richtete sich auf das Verhalten der Periodendauer und dem zeitlichen Verlauf der Intensität innerhalb der Periode. Es zeigte sich, dass oberhalb von 1.78 K der oszillatorische Effekt bei einem Druck p_τ unmittelbar oberhalb des Schmelzdruckes mit Periodendauern im Bereich von unter 10 Sekunden auftrat. Bei konstanter Düsentemperatur und ansteigendem Düsendruck oberhalb von p_τ wurde ein Anstieg der Periodendauer beobachtet. Entsprechend umgekehrt stieg die Periodendauer mit sinkender Temperatur bei konstantem Düsendruck.

Diese Ergebnisse lassen sich mit Hilfe des theoretischen Modells dahingehend interpretieren, dass die Periodendauer von der Mobilität der Gitterfehlstellen abhängt: Eine Erhöhung der Periodendauer weisst auf eine Verminderung der Mobilität hin. Diese Ergebnisse stimmen mit den experimentellen Daten von Zuev *et al.* [131] überein, die auf einen exponentiellen Abfall des Diffusions Koeffizienten der Fehlstellen mit abnehmender Temperatur als auch ansteigendem Druck hinweisen.

Im Temperaturbereich zwischen 1.78 K und 1.58 K wurde der Druck p_τ(T) oberhalb der bcc-hcp Phasengrenze - und damit bis zu 2 bar oberhalb der Schmelzkuve - gefunden. Demzufolge tritt der oszillatorische Effekt nicht in der bcc Phase des Helium-Festkörpers auf. Unterhalb von 1.58 K wurde bei Messungen mit konstantem Düsendruck über 30 bar eine erstaunliche Abhängigkeit der Periodendauer von der Temperatur gefunden. Die Periodendauer steigt mit fallender Temperatur bis zu T = 1.58 K. Bei dieser Temperatur erreicht die Periodendauer ein Maximum. Bei tieferen Temperaturen fällt sie auf etwa ein Drittel ab. Dieser Effekt ist unabhängig vom Düsendruck, wobei der Abfall der Periodendauer im Verhältnis zur maximalen Periodendauer bei 1.58 K mit steigendem Düsendruck abnimmt.

Untersuchungen bei konstanter Temperatur unter 1.58 K und ansteigendem Düsendruck geben Aufschluss über die Beobachtung der maximalen Periodendauer. Im Vergleich des Vakuumdrucks zum Düsendruck findet sich für Drücke p_u(T) bis zu 2 bar oberhalb der Schmelzkurve kein Unterschied zur flüssigen Phase, gemäß dem Verhalten einer idealen Flüssigkeit (Bernoulli-Beziehung). Oberhalb dieses Bereiches p_u(T) ist der Vakuumdruck unabhängig vom Düsendruck, wobei kein periodisches Verhalten der Jet-Intensität gefunden wurde. Periodische Oszillationen zeigten sich im Vakuumdruck erst für Drücke p_τ(T) bis zu 4 bar über der Schmelzkurve. Damit liegt dieser Übergang weit in der festen Phase. Ein interessantes Ergebnis ist die Veränderung der periodischen Struktur unterhalb von 1.58 K. Diese war nur durch scharfe Peaks im Signal zu finden.

Diese Anomalie des Festkörpers kann durch das Verhalten der Periodendauer erklärt werden. Da die Periodendauer als Indikator für die Mobilität der Gitterfehlstellen angenommen wird, weisst die Verkürzung der Periodendauer auf eine Erhöhung der Mobilität hin. Wie die Ergebnisse zeigen, bildet sich demnach eine Phase unter p_u(T) mit erhöhter Fehlstellenmobilität, in der sich der Festkörper wie eine ideale Flüssigkeit verhält. Dies ist möglicherweise ein erster experimenteller Beweis des supersoliden Zustands in Helium-4, der vor mehr als 35 Jahren durch Andreev und Lifshitz [3] vorhergesagt wurde. In dieser theoretischen Arbeit wurde über die Möglichkeit einer Bose-Einstein-Kondensation von Gitterfehlstellen in festem Helium-4 diskutiert. Gitterfehlstellen in Helium-4 bilden ein schwach wechselwirkendes Bose-Gas, das bei genügend tiefer Temperatur als ein Bose-Einstein-Kondensat erscheinen kann.

Mehrere Argumente sprechen für die Beobachtung des supersoliden Zustands. Es zeigte sich, dass durch die Zugabe kleinster Mengen des Isotopes Helium-3 im Bereich zwischen 0.0015 und 1 Prozent die Zunahme der Mobilität der Gitterfehlstellen unterdrückt werden konnte. Der Einfluss von Helium-3 konnte durch das Auftreten des periodischen Effekts bei Temperaturen unterhalb 1.58 K direkt oberhalb der Schmelzkurve beobachtet werden. Ebenso stieg - im Gegensatz zum Verhalten reines Helium-4 - die Periodendauer durch die Zugabe von Helium-3 mit sinkender Temperatur auch unter 1.58 K weiter an.

Ein weiterer Hinweis für die Beobachtung des Supersolid ist die Übereinstimmung der Phasenlinie $p_{\mathcal{T}}(\mathrm{T})$ mit theoretischen Vorhersagen von Galli und Reatto [47] für Bose-Einstein-Kondensation von Fehlstellen.

Die Möglichkeit der Einbringung künstlicher Fehlstellen in den Helium-Festkörper ist das wichtigste Argument für die Bildung des Supersolids. Generell wurde angenommen, dass der Supersolid wegen zu kleiner Konzentration der Gitterfehlstellen nicht zu beobachten wäre. Mit dieser experimentellen Technik - der Vakuumexpansion von festem Helium-4 ins Vakuum - scheint diese Hürde jedoch überwunden zu sein.

Zusammenfassung und Ausblick

In diesem Experiment wurde die Expansion eines Quantum Festkörpers ins Vakuum untersucht. Es zeigte sich ein periodisches Verhalten der Jet-Intensität bei Konditionen entsprechend dem festen Zustand. Ein theoretisches Modell erklärt diesen Effekt als eine künstliche Einbringung von Gitterfehlstellen in den Festkörper, welche - getrieben durch Drift und Diffusion - den periodischen Kollaps des Festkörpers induzieren. Mit diesem Verfahren eröffnet sich die Möglichkeit der Herstellung eines Quanten Festkörpers im Nicht-Gleichgewicht durch die Erhöhung der Fehlstellen-Konzentration überhalb des thermischen Gleichgewichts. Aus dem theoretischen Model ergibt sich, dass die Periodendauer der Oszillationen als Indikator für die Mobilität der Fehlstellen fungiert. Dies erlaubt eine umfassende Studie dieses Quanten-Festkörpers. Das wichtigste Ergebnis ist das Verhalten des Festkörpers als eine ideale Flüssigekeit unterhalb von 1.58 K, welches eindeutige Hinweise auf den experimentellen Nachweis des supersoliden Zustands liefert.

Zukünftige Ziele richten sich auf die Erforschung dieses Nicht-Gleichgewicht Festkörpers bei Temperaturen unter 1.3 K. Es ist interessant herauszufinden, wie die beiden Phasengrenzen $p_u(\mathrm{T})$ und $p_{\mathcal{T}}(\mathrm{T})$ sich bei tieferen Temperaturen verhalten. Ebenso interessant ist die Untersuchung bei höheren Drücken, da die Quanten-Natur des Helium-Festkörpers mit zunehmenden Druck in klassisches Verhalten übergeht.

Weiterhin gilt es, das theoretische Modell in einigen Details zu erweitern. Das oszillierende Verhalten unter 1.58 K ist mit dem vorgestellten theoretischen Ansatz nicht zu reproduzieren. Die kinetische Transportgleichung der Fehlstellen konnte die zeitliche Jet-Intensität über 1.58 K in guter Übereinstimmung wiedergeben. Allerdings treten im Experiment weitere Effekte auf, die eine exakte Reproduktion der Ergebnisse in einigen Fällen erschwerte.

Zukünfige Studien, die zum vollständigen Verständnis des Phänomens beitragen könnten, wären die experimentelle Untersuchungen anderer Quanten-Festkörper wie beispielsweise festen Wasserstoffs. Da jedoch einige Gründe gegen die Beobachtung des periodischen Verhaltens der Jet-Intensität bei der Expansion festem Wasserstoffs sprechen, wäre die Verwendung einer Helium-Wasserstoff Mixtur eine mögliche Alternative. Solche hochporösen Van-der-Waals-Festkörper zeigen sehr interessante Eigenschaften als ein sogenanntes "Quanten-Gel" [74, 79].

Auf der Suche nach dem endgültigen Beweis des Supersolids bieten sich einige Methoden an, die sich aus dem hier vorgestellten Experiment ableiten lassen. Mittels Rotation eines Zylinders gefüllt mit festem Helium-4 wurde beispielsweise von Kim und Chan [75, 75] im Jahre 2004 versucht, den experimentellen Nachweis für den Supersolid zu erbringen. Die Ergebnisse liessen sich jedoch nicht einwandfrei deuten. Vielmehr spricht einiges gegen die Beobachtung des supersoliden Zustands. Als eine Weiterführung der hier vorgestellten Experimente wäre eine Symbiose dieser beiden experimentellen Techniken denkbar. Weiterhin könnte die Verwendung einer Pipette anstatt einer punktförmigen Öffnung direkten optischen Zugang zu den Vorgängen im Festkörper ermöglichen.

Es bleibt zu hoffen, dass die Einzigartigkeit dieses periodischen Effektes und die Möglichkeit der Erzeugung von Quanten Festkörpern im Nicht-Gleichgewicht weiteren Anstoß für die Erforschung von festem Helium geben.

Appendix A

Formation and Mobility of Vacancies

A.1 Vacancy Formation

Because of the minimization of the free enthalpy, or Gibbs energy G for thermodynamic equilibrium at constant temperature and pressure it will be demonstrated that the vacancies in crystals are always present. Furthermore the vacancies concentration at thermal equilibrium is only determined by temperature and the formation energy ϕ_f necessary to create a single vacancy.

The free enthalpy is defined as G = H - TS and has to be minimal for thermodynamical equilibrium, and therefore $\frac{\partial G}{\partial n} = 0$, where n is the number of vacancies. The enthalpy H = U + pV is given by the internal energy U to create vacancies which is the dominant contribution, plus the volume work pV by moving the atoms from the interior site to the surface.

The entropy S is expressed by $S = S_{vib} + S_{mix}$, where the minor component S_{vib} results from the change in the vibrational motion of the atoms around the point defect [127], whereas the entropy of mixture S_{mix} is a measure of randomness, and the presence of point defects reduces the system‘s state of order. This quantity is responsible for the spontaneous existence of point defects at equilibrium. Thus, the free enthalpy is given by:

$$G = (U + pV - TS_{vib}) - TS_{mix} = n \cdot \Phi - TS_{mix}, \tag{A.1}$$

where Φ is the total energy to create a vacancy. The minimization of G demands for an increase of entropy, which is related to the presence of vacancies that violate the perfect crystal geometry. The entropy is given by the Boltzmann equation

$$S_{mix} = k \cdot ln(p), \tag{A.2}$$

where p is the number of different configurations: The change of the entropy is given by the possibilities to distribute n vacancies on N lattice sites:

$$S_{mix} = k \cdot ln\left(\frac{N!}{(N-n)! \cdot N!}\right). \tag{A.3}$$

One obtains for the minimization of the Gibbs free energy:

$$\frac{\partial G}{\partial n} = \frac{\partial}{\partial n}\left[n \cdot \Phi - TS_{mix}\right] = \frac{\partial}{\partial n}\left[n \cdot \Phi - kT \cdot ln\left(\frac{N!}{(N-n)! \cdot N!}\right)\right] \tag{A.4}$$

It follows for the thermodynamical equilibrium that G has to be minimal, and therefore[1]:

$$0 = \frac{\partial G}{\partial n} = \Phi - kT \cdot ln\left(\frac{n}{N}\right). \tag{A.5}$$

Finally, the concentration of vacancies per unit volume [cm^3] is given by:

$$\frac{n}{N} = exp(-\Phi/kT). \tag{A.6}$$

The creation of a vacancy in a perfect lattice causes breaking of bonds between the atom and the neighboring atoms and finally the atom has to vanish by moving to the surface. Therefore, Φ is expressed by:

$$\Phi = \phi_f + pV_a - TS_v, \tag{A.7}$$

where ϕ_f is the formation energy of a single vacancy, V_a the atomic volume. The assumption is permitted that in generating a single vacancy the entropy S_v is negligible [80]. Furthermore, the increase of the volume by introducing an atom at the surface is also negligible. Thus, the total energy of vacancy formation is given only by the formation energy $\Phi = \phi_f$, which leads to the thermally vacancy concentration:

$$\frac{n}{N} = exp(-\phi_f/kT). \tag{A.8}$$

Generally, the unit of vacancy formation energy ϕ_f is Kelvin, so that the Boltzmann constant k can also be neglected.

A.2 Motion of Vacancies

The mechanism of vacancy motion is described in section 2.2.3, whereas this section will give a short introduction into the fundamental mechanism of diffusion and drift.

---

[1] For N » n by applying the Sterling equation ln(n!) ≈ n ln(n) one finds for T$\cdot\frac{\partial S}{\partial n} = kT\cdot ln\left(\frac{n}{N}\right)$

A.2.1 Diffusion

The mechanism of diffusion appears in many different kinds. It describes the distribution of charges in semiconductors and also processes like osmosis that are caused by concentration gradients. Also the development of contact lenses is based on the mechanism of diffusion. Diffusion describes the motion of particles driven by thermal energy as a result of the second law of thermodynamics. The demand on the increase of entropy with time causes that particles move from regions of higher concentrations to regions of lower concentrations, thus going from a state of higher order to a state of lower order.

The intensity of the particles flux is determined by a specific diffusion coefficient D that itself depends on temperature and a distinct activation energy ϕ_a. The process of diffusion was explored and described by Fick [43] in two fundamental laws, whereas the theoretical derivation of Fick‘s laws was given by Einstein [41].

Steady-State Diffusion, Fick‘s 1st Law

The kinetic of diffusion is described by the particle flux in dependence of the concentration gradient. Steady-state diffusion occurs if the incoming flux through a unit volume is equal to the outgoing flux. Therefore, the concentration of particles is constant. As seen in figure A.1 the concentration profile of steady-state diffusion can be approximated by a linear concentration gradient.

The flux which results out of the concentration gradient is determined by Fick‘s first law of diffusion:

$$J = -D_v \frac{\Delta c}{\Delta x}, \tag{A.9}$$

where J is the flux in direction of x given in $[particles/m^2 s]$, D the diffusion coefficient $[m^2 s]$ and $\frac{\Delta c}{\Delta x}$ the concentration gradient $[particles/m^3 m]$. The process of steady state diffusion is a time restricted process, which occurs until the particles are uniformly distributed. Finally, the system is in thermal equilibrium. This time dependent scenario is illustrated in figure A.2.

The diffusion coefficient D itself is depending on temperature and on the activation energy ϕ_a :

$$D = D_0 \cdot e^{-\frac{\phi_a}{T}}. \tag{A.10}$$

Non Steady-State Diffusion, Fick‘s 2nd Law

In a non steady-state diffusion process the initial concentration of particles changes with time. Thus, the incoming flux differs from the outgoing flux. Because of the change in the flux through a volume unit combined with conservation of matter the

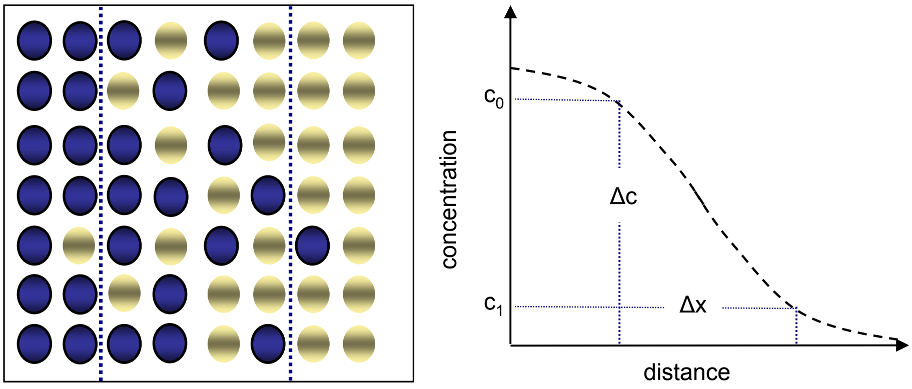

Figure A.1: Diffusion in a uniform concentration gradient. The blue particles change their sites with yellow particles and therefore the particles distribute by diffusion. The concentration gradient is given by a difference in concentration $\Delta c = c_0 - c_1$ over a distance Δx. In a simplified assumption the concentration gradient is linear.

concentration gradient depends on time. Deriving Fick‘s first law in space leads to a time dependence of the concentration profile c(x,t), as to be seen in figure A.3 .

The general solution of the time dependent concentration profile is given by:

$$\frac{c(x,t) - c_0}{c_s - c_0} = 1 - erf(\frac{x}{2\sqrt{Dt}}), \tag{A.11}$$

where c_0 is the final concentration at $t \rightarrow \infty$ and c_s the initial concentration at $t = 0, x = 0$. The expression erf is the so called "error function" that is one solution for the time dependent concentration profile. The "error function" is defined by:

$$erf(x) = \frac{2}{\sqrt{\pi}} \int e^{-u^2} du \ , \tag{A.12}$$

which is plotted in fig A.4

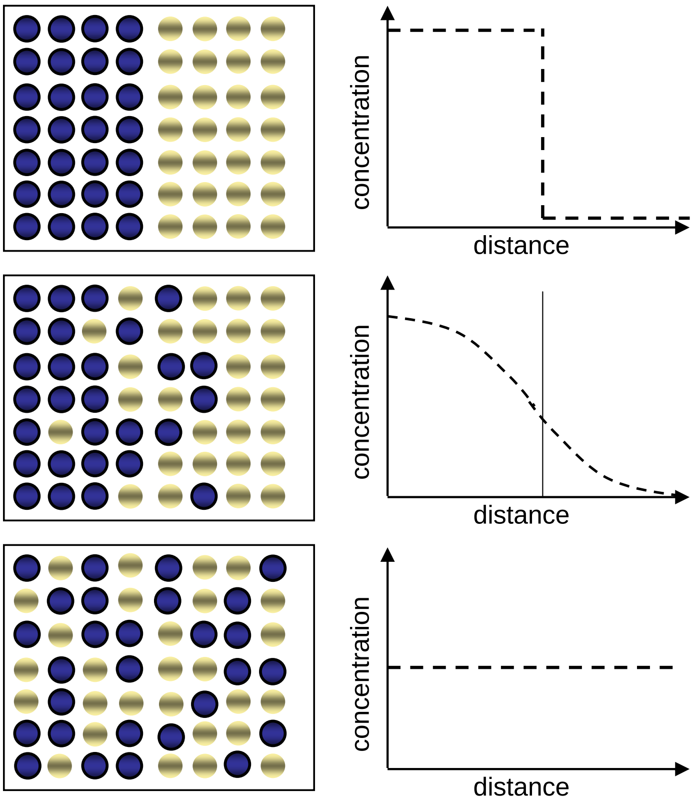

Figure A.2: Following the first law of Fick the concentration profile changes as follows: (Top) By a strict separation of particles the concentration profile is equal to a step function. The particles diffuse (Middle) and the concentration profile changes as long as the concentration is equalized over the whole distance (Bottom). Therefore, steady-state diffusion is a time restricted process caused by the finite number of diffusing particles.

Diffusion of Vacancies

The (self)diffusion of vacancies is describable by atomic diffusion over a vacant lattice site. To change the lattice site the atom requires an activation energy ϕ_a, which allows the atom to overcome the lattice potential, as seen in figure A.5.

An atom jumps into the neighboring vacant lattice site and leaves a vacancy at the former lattice site. This vacant site can be taken by the next atom. Thus, diffusion of atoms and vacancies occurs simultaneously, but in opposite direction.

In quantum crystals the energy to overcome the potential barrier is not a constant value. At low enough temperature the activation energy is determined by an energy band Δ because of the tunnelling probability caused by the large amplitude of the zero-point vibrations. The classical diffusion process changes into quantum diffusion and vacancies turn into delocalized entities (vacanions). The vacancies are highly

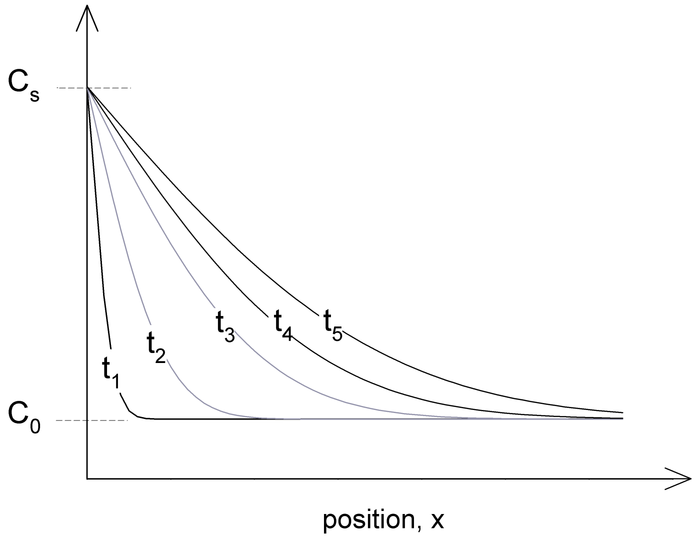

Figure A.3: Non-steady-state diffusion caused by time dependent concentration profile c(x,t). This scenario is related to the second law of Fick. The equalization of the concentration - and the stop of diffusion - does only occur if the concentration reaches c_s for all x.

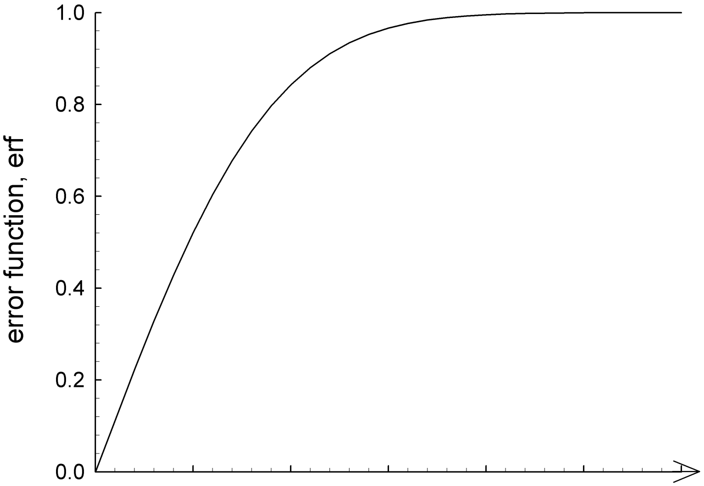

Figure A.4: Error function, erf(x), which is used to describe a concentration profile of non-steady state diffusion.

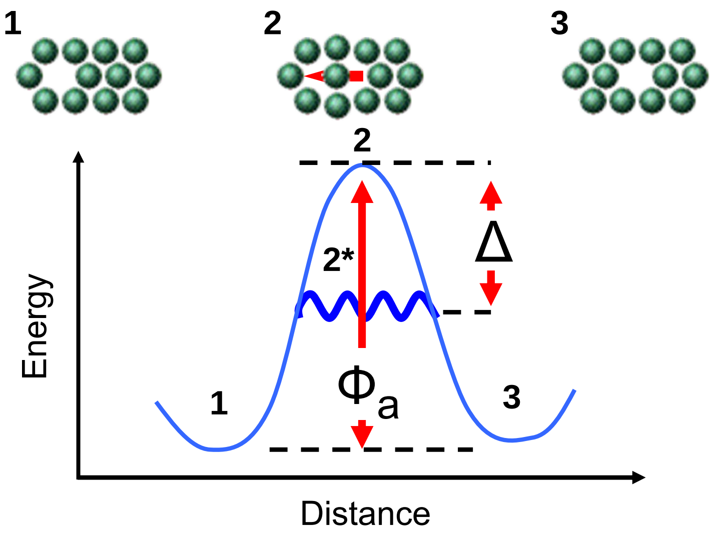

Figure A.5: Atoms move trough the crystal by exchanging the lattice site with vacancies. Therefore, they have to overcome the lattice potential. The vacancies and atoms move in opposite directions. By moving from (1) to (2) the atom displaces the lattice structure which causes a certain amount of energy (activation energy ϕ_a), as seen below. Comparing (1) and (3) the exchange of lattice sites between the atom and the vacancy is obvious. By tunneling (2*) the energy of activation changes into a band of energy states with a bandwidth Δ.

mobile by the decrease of the activation energy by the value of Δ. As a result the vacancies mobility occurs in the energy band $\phi_a \pm \Delta$.

A.2.2 Drift

In 1949 Conyers Herring [68] proposed a theoretical interpretation for the suggestion of Nabarro [94] that any polycrystalline crystal can change its shape by self-diffusion that yield to an applied stress, which influences the behavior in polycrystalline solids close to the melting temperature to appear as a viscous solid. It was found that a vacancy current - and therefore a mass flow of atoms - occurs in whichever direction to relieve the inequality of pressure. This mechanism, known as the Nabarro-Herring mechanism (also Nabarro-Herring creep) causes plastic deformation in solid Helium even at low temperatures. Helium is a highly polycrystalline solid. As a quantum crystal the mobility of defects is about one order of magnitude larger than in ordinary solids so that solid Helium behaves as a polycrystalline solid at high temperatures.

Following the theoretical approach of Herring, vacancies migrate spontaneously from lower to higher pressure to reduce the pressure in the region of higher pressures. In compressing a solid a certain amount of work has to be done which raises the total energy of each atom. Thus, to remove an atom at a higher energy costs less energy than removing it from a lower energy. This difference in energy is obtained at constant temperature and constant lattice sites. The resulting force acting on vacancies is obtained by the derivative minus this difference in energy. Thus, the number of atoms at pressure p is reduced by one unity, whereas it is increased by one unity at p_0. The resulting gain of energy is $-V_a(p-p_0)$, where V_a is the atomic volume. The resulting net force is given by:

$$F = -\nabla[(V^* - V_a)p] = -\triangle V \nabla p, \tag{A.13}$$

where V^* is the vacancy formation volume, which is assumed to be approximately constant. Since vacancies in solid Helium cause inward relaxation the vacancy formation volume is smaller than the atomic volume and therefore the force driving vacancies is directed as the pressure gradient. The resulting flux that is caused by the driving force is is given by:

$$J = u_v \cdot x_v = \mu_v \cdot F \cdot x_v = -\mu_v \cdot \Delta V \nabla p \cdot x_v, \tag{A.14}$$

where u_v is the drift velocity, μ_v the mobility and x_v the concentration of vacancies. Furthermore the flux of drift and diffusion is set up to be equal by the Einstein relation, showing that the mobility and the diffusion coefficient is related by the thermal energy:

$$D_v = kT\mu_v. \tag{A.15}$$

Appendix B

Fit of the Periodical Beam Flux j_{osc}

Following from the theoretical model the observed oscillating beam flux intensity $j_{osc}^{exp}(t)$ can be reproduced by the kinetic transport equation $j_{osc}^{theo}(t)$, as demonstrated in figure 3.9 for source pressure $p_0 = 32$ bar and temperature T = 1.7 K. According to this demonstration the beam flux intensity $j_{osc}^{exp}(t)$ has also been reproduced by the kinetic transport equation $j_{osc}^{theo}(t)$ for source pressures between the melting pressure p_m up to 41 bar and temperatures between 1.6 and 2.1 K, which is presented in this section. An overview of the fitted data is shown in figure B.1.

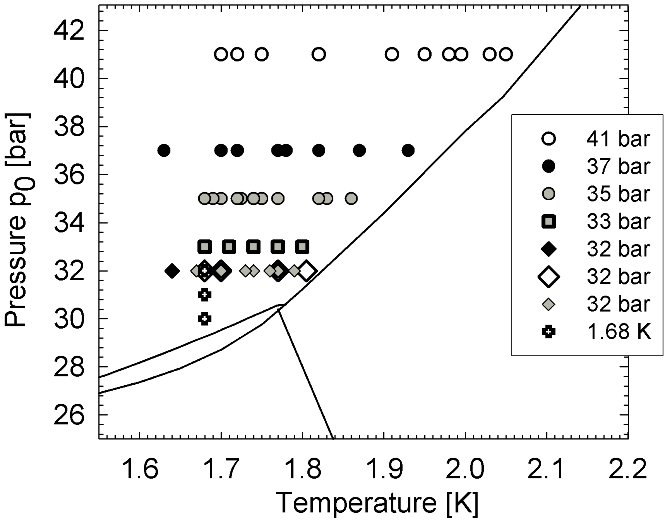

Figure B.1: Overview of the regime of temperatures and pressures at which the Geyser periods have been fitted. Between temperatures T = 2.1 and 1.6 K the oscillating beam flux intensity can be interpreted by the kinetic model. Thus, the fits have been done for temperatures above 1.6 K and corresponding source pressures p_0 between the melting pressure up to 41 bar.

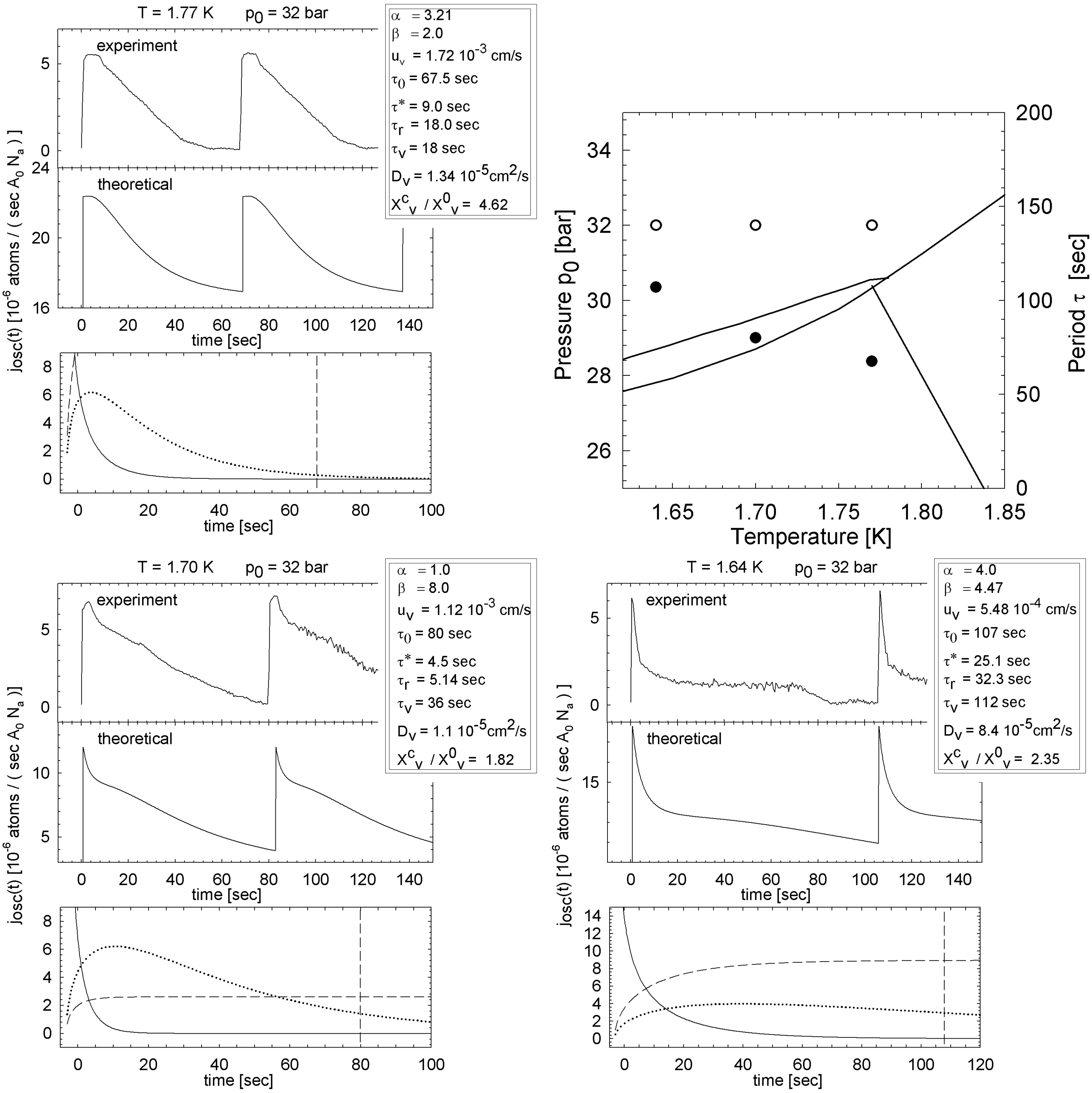

Figure B.2: Theoretical beam flux j_{osc} fitted for constant source pressure $p_0 = 32$ bar. ($d_0(\#17) = 2.28\ \mu$m)

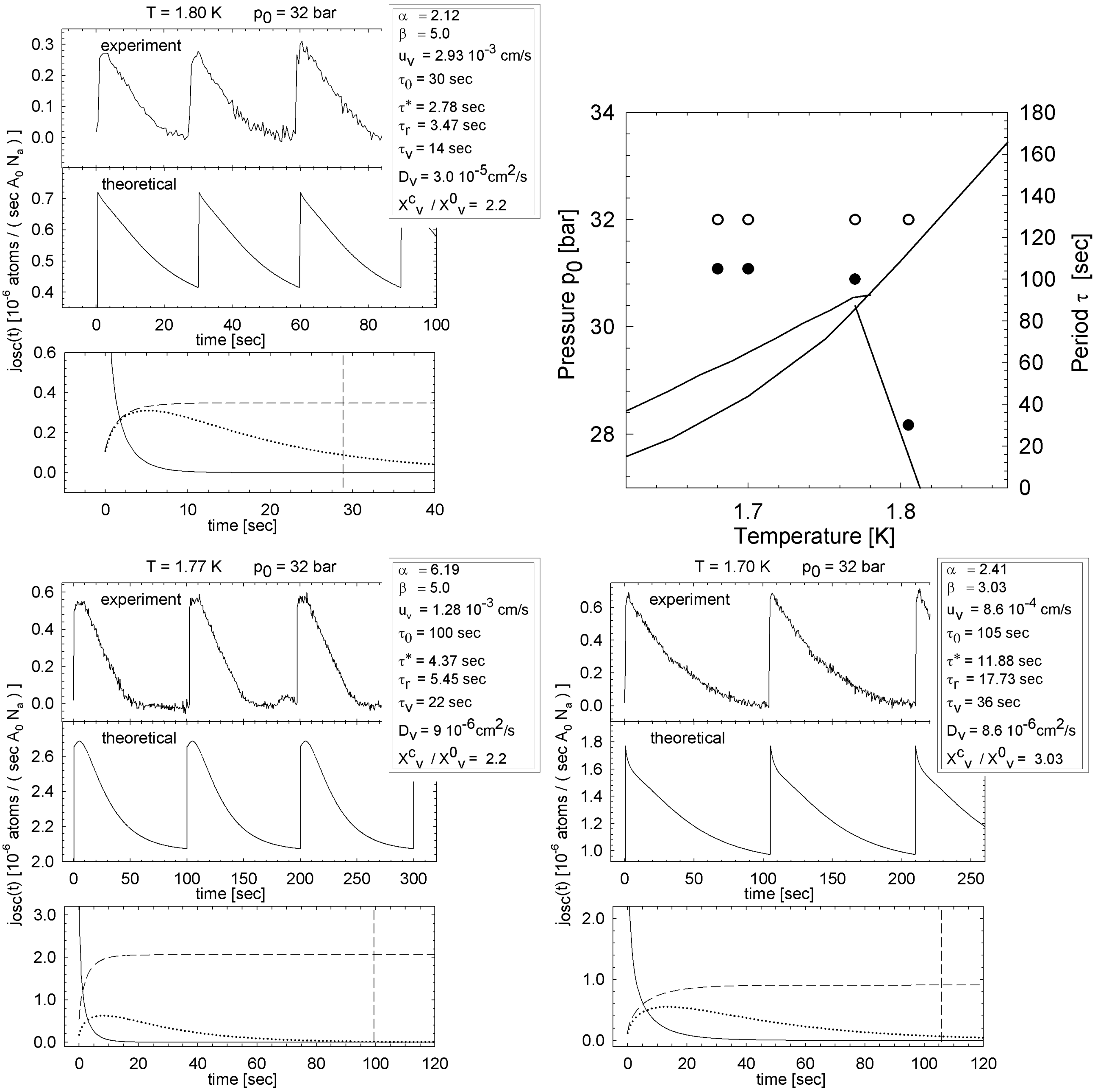

Figure B.3: Theoretical beam flux j_{osc} fitted for constant source pressure p_0 =32 bar. ($d_0(\#17) = 2.28\ \mu$m)

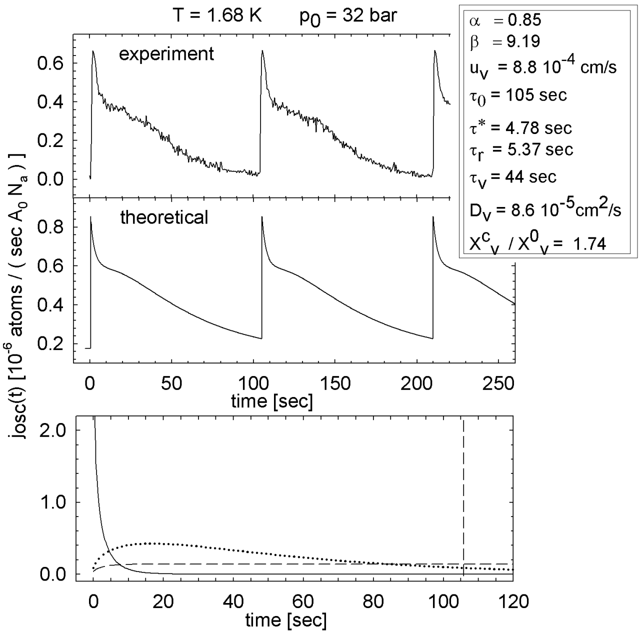

Figure B.4: Theoretical beam flux j_{osc} fitted for constant source pressure p_0 =32 bar. ($d_0(\#17) = 2.28\ \mu$m)

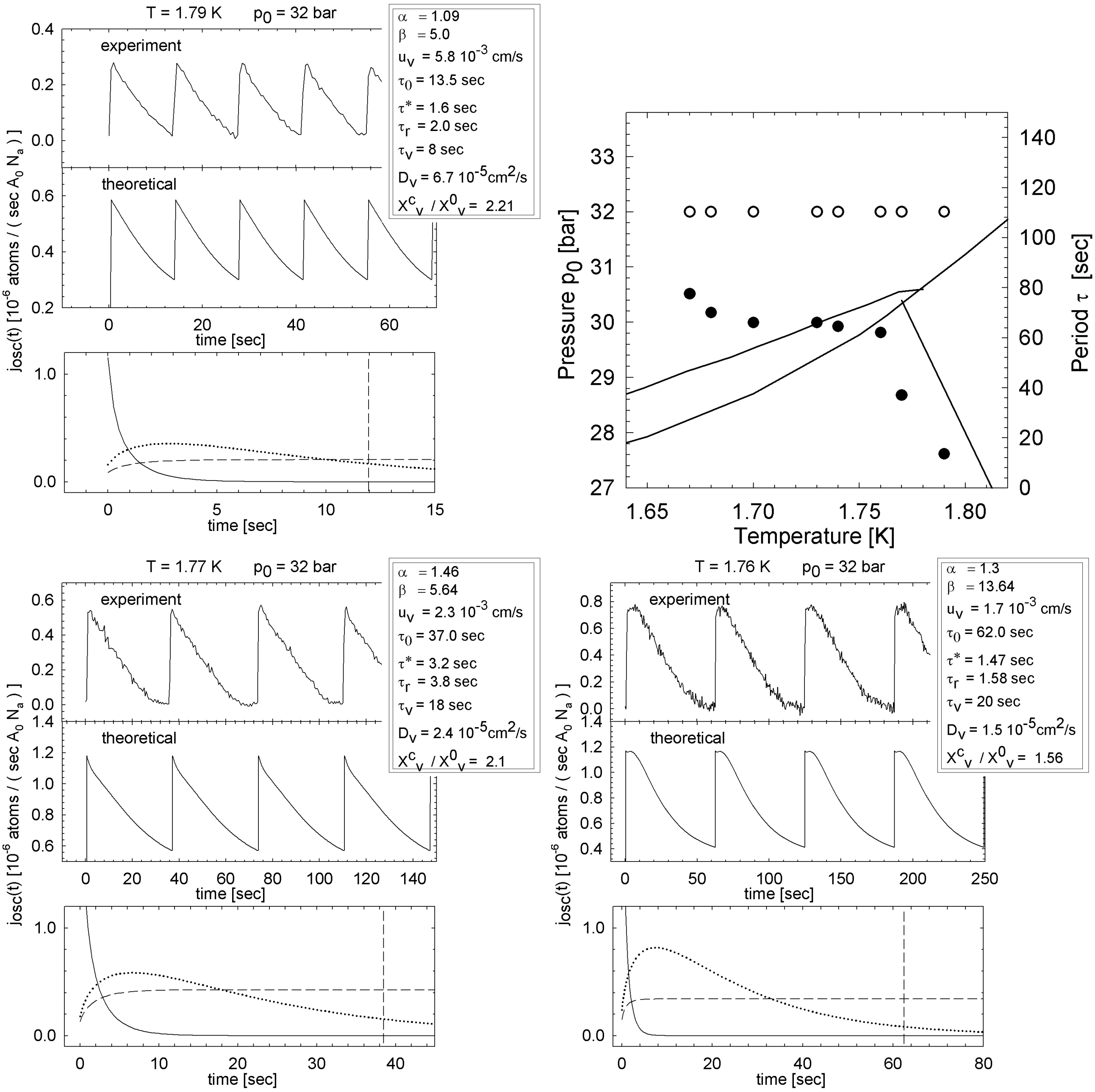

Figure B.5: Theoretical beam flux j_{osc} fitted for constant source pressure $p_0 = 32$ bar. ($d_0(\#17) = 2.28\ \mu$m)

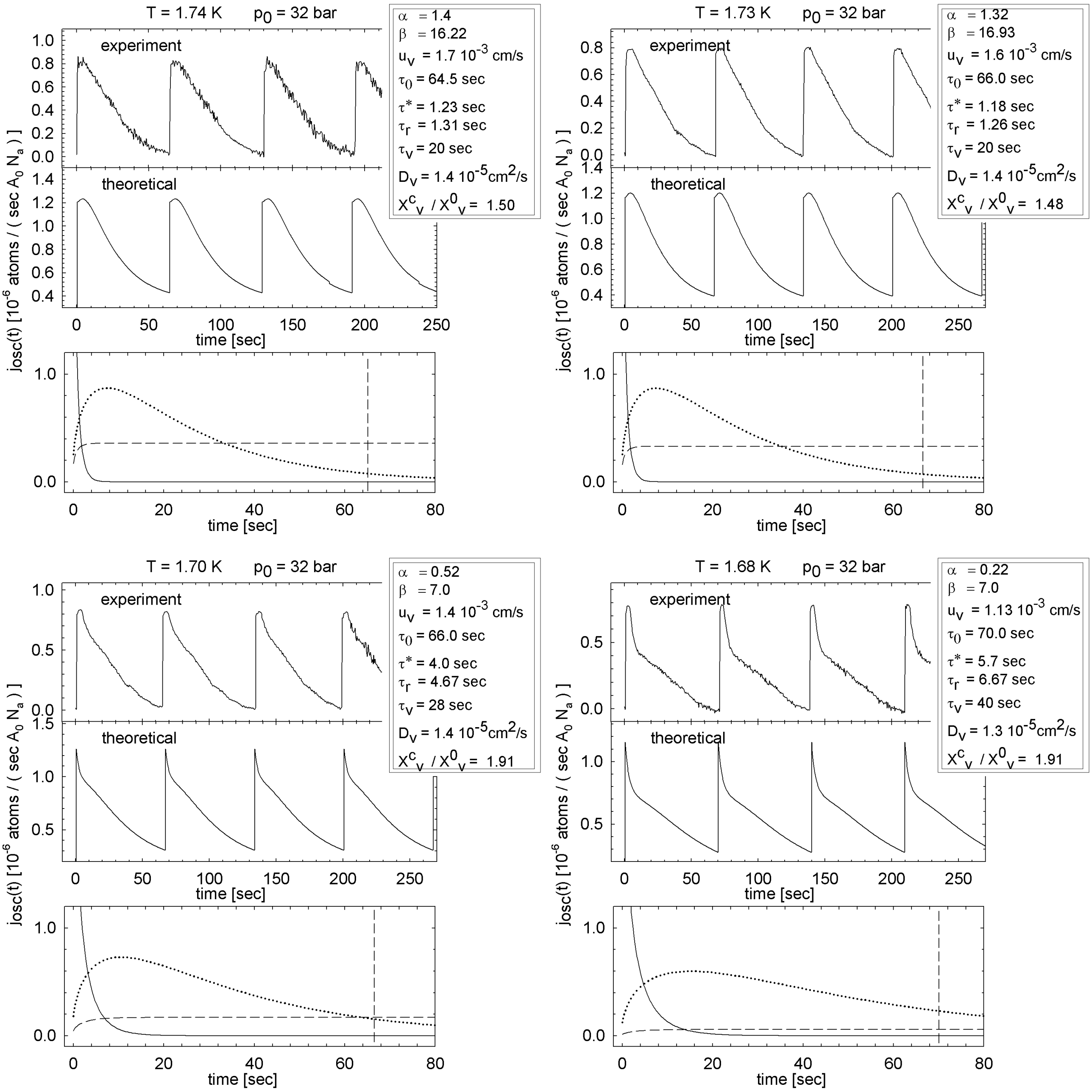

Figure B.6: Theoretical beam flux j_{osc} fitted for constant source pressure p_0 =32 bar. ($d_0(\#17) = 2.28\ \mu$m)

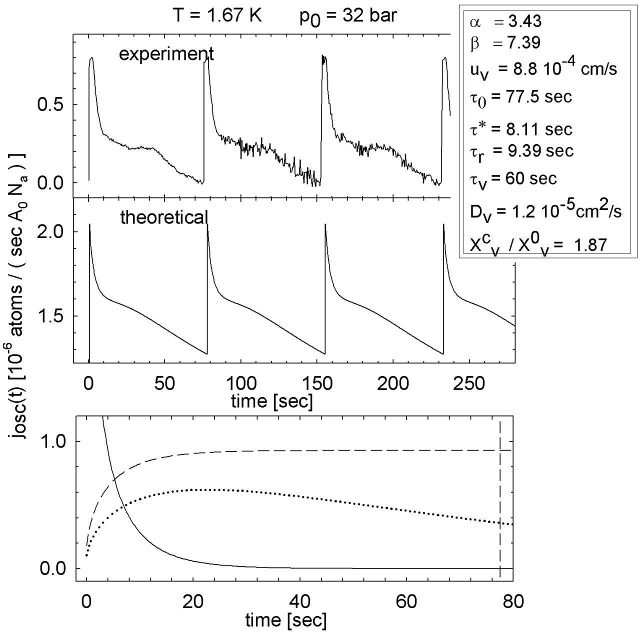

Theoretical beam flux j_{osc} fitted for constant source pressure $p_0 = 32$ bar. ($d_0(\#17) = 2.28\ \mu$m)

Figure B.7:

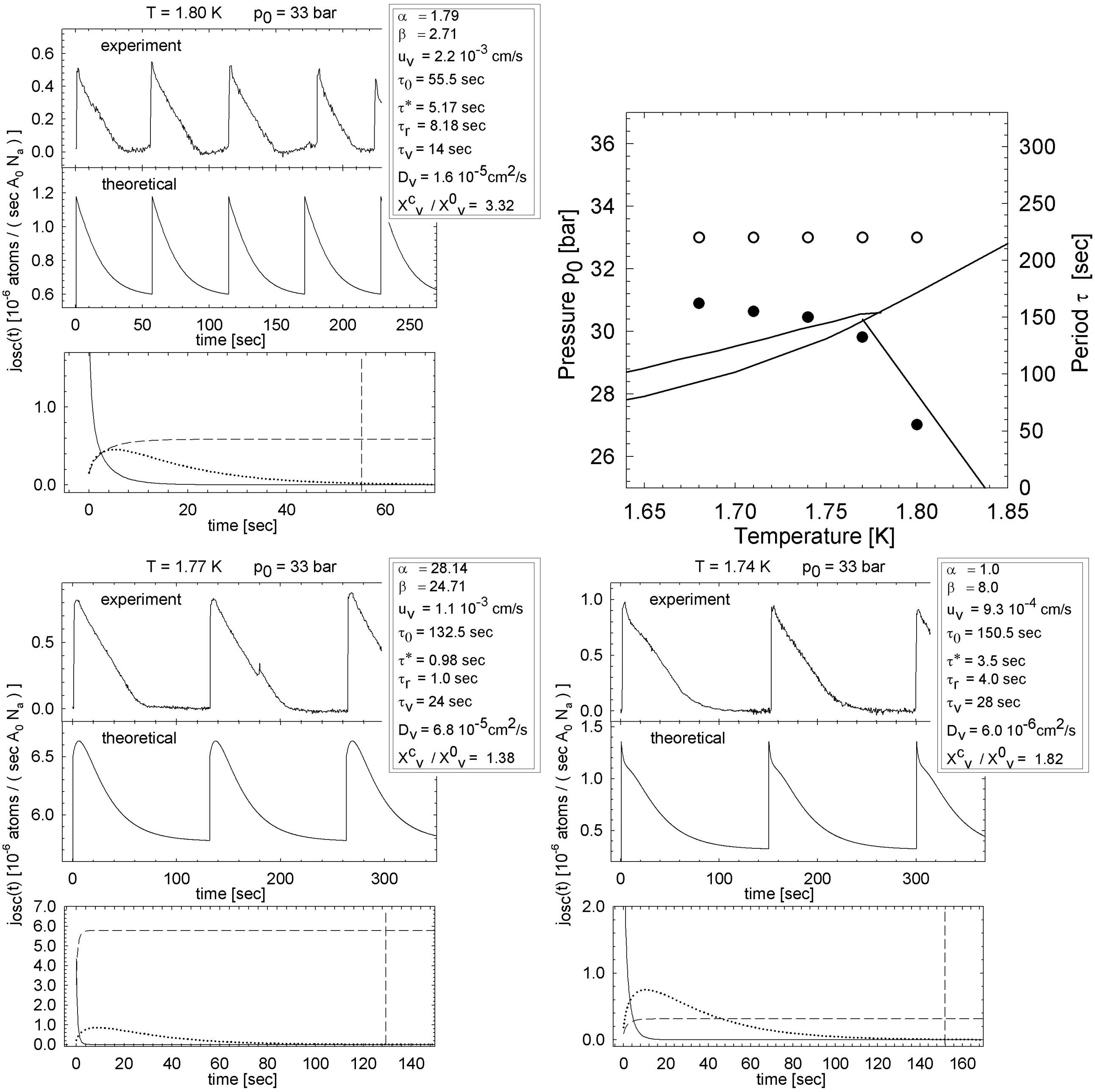

Figure B.8: Theoretical beam flux j_{osc} fitted for constant source pressure $p_0 = 33$ bar. ($d_0(\#17) = 2.28\ \mu$m)

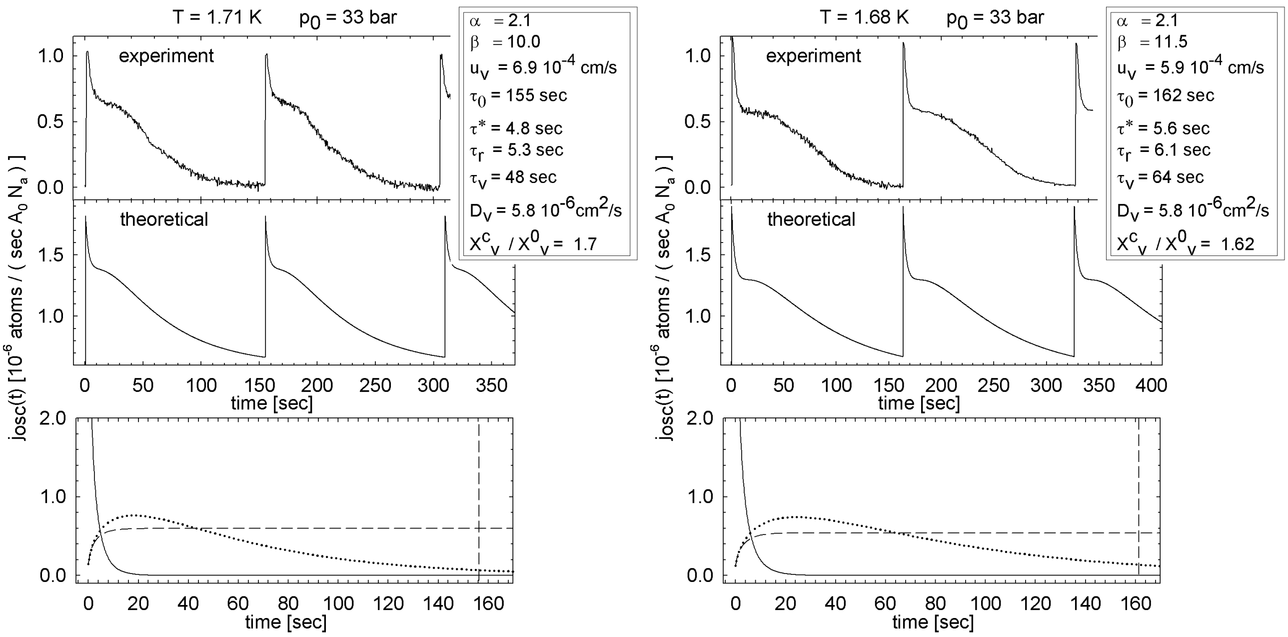

Figure B.9: Theoretical beam flux j_{osc} fitted for constant source pressure $p_0 = 33$ bar. ($d_0(\#17) = 2.28\ \mu$m)

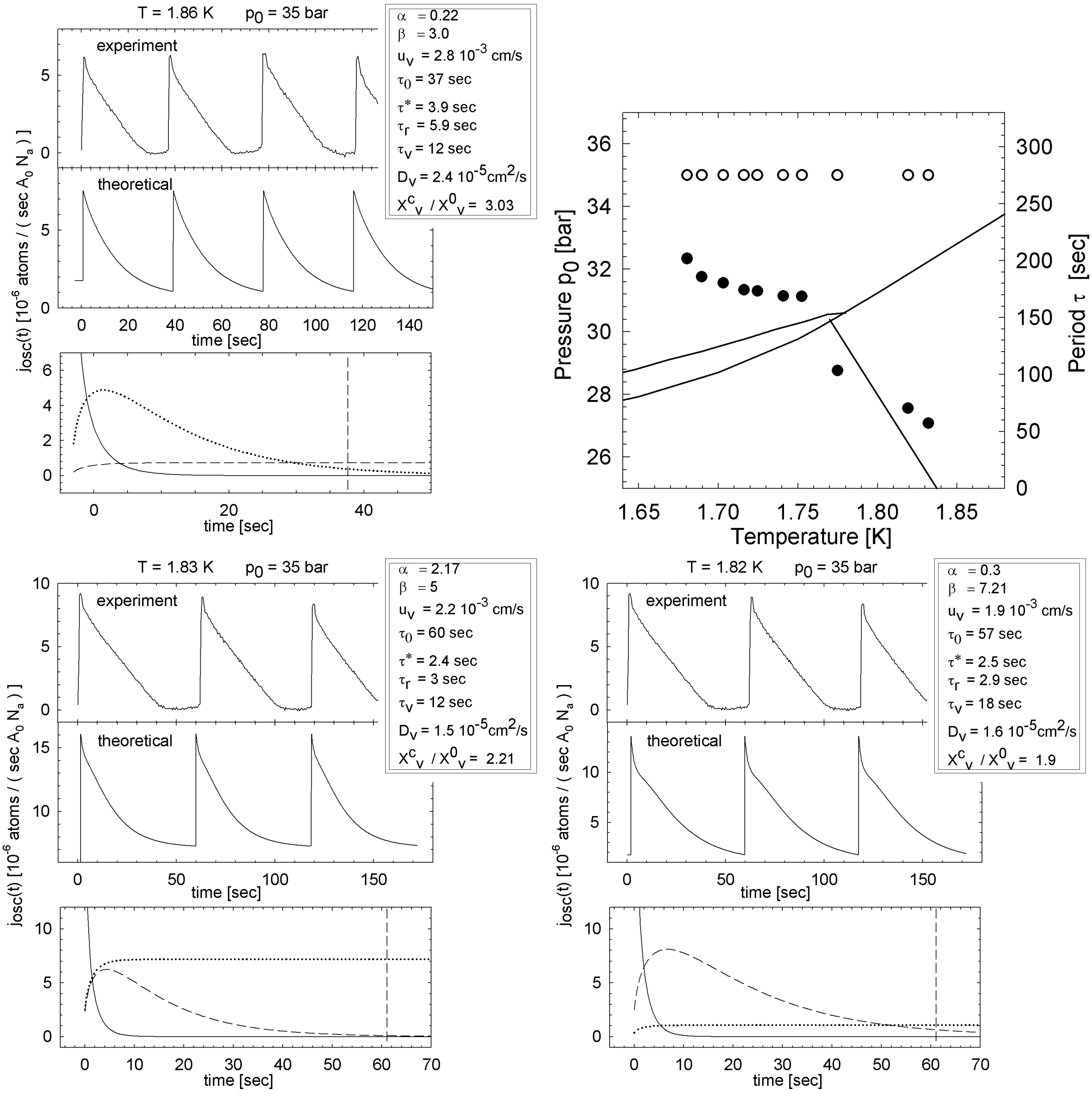

Figure B.10: Theoretical beam flux j_{osc} fitted for constant source pressure $p_0 = 35$ bar. ($d_0(\#17) = 2.28\ \mu$m)

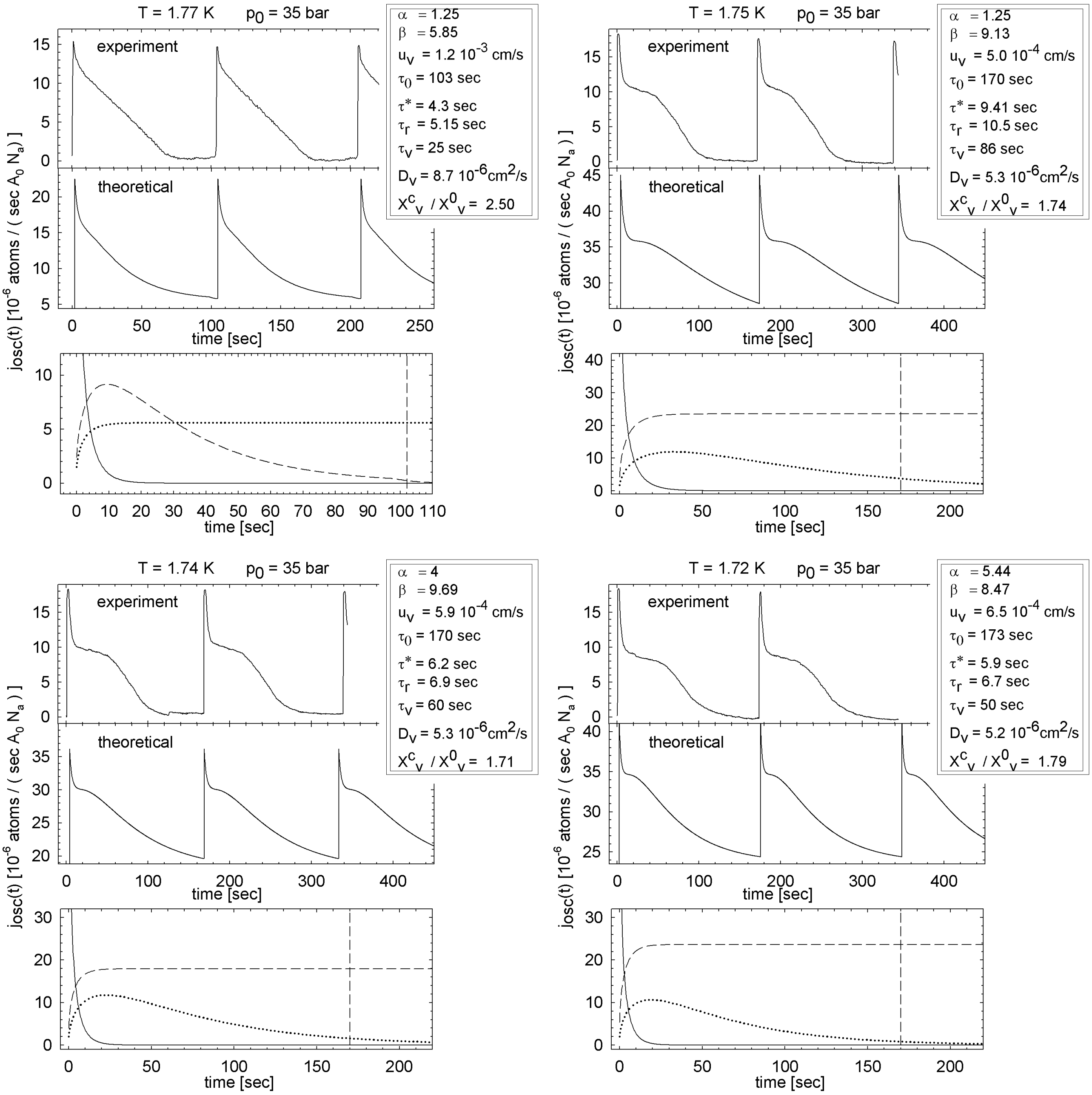

Figure B.11: Theoretical beam flux j_{osc} fitted for constant source pressure $p_0 = 35$ bar. ($d_0(\#17) = 2.28\ \mu$m)

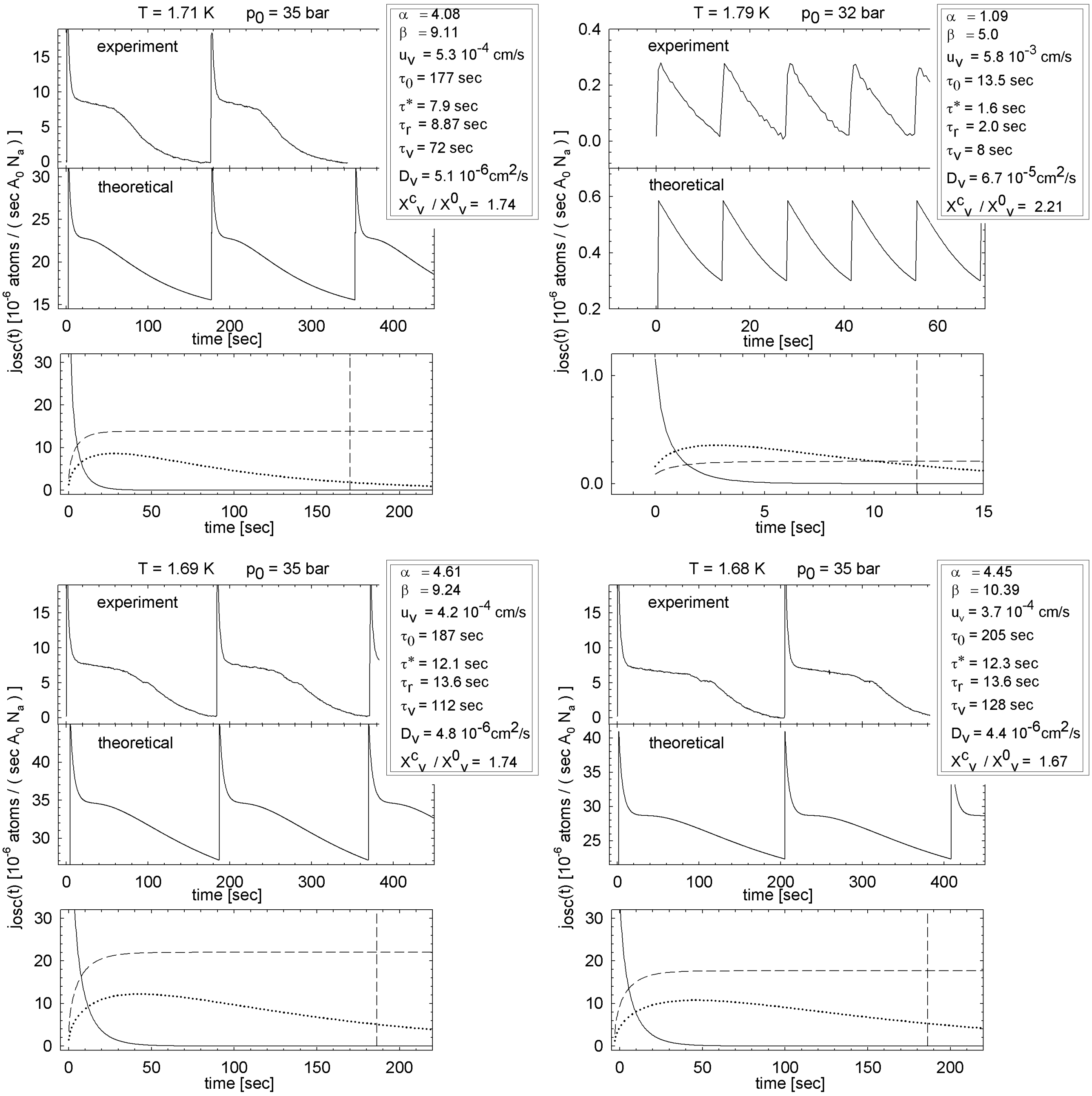

Figure B.12: Theoretical beam flux j_{osc} fitted for constant source pressure $p_0 = 35$ bar. ($d_0(\#17) = 2.28\ \mu$m)

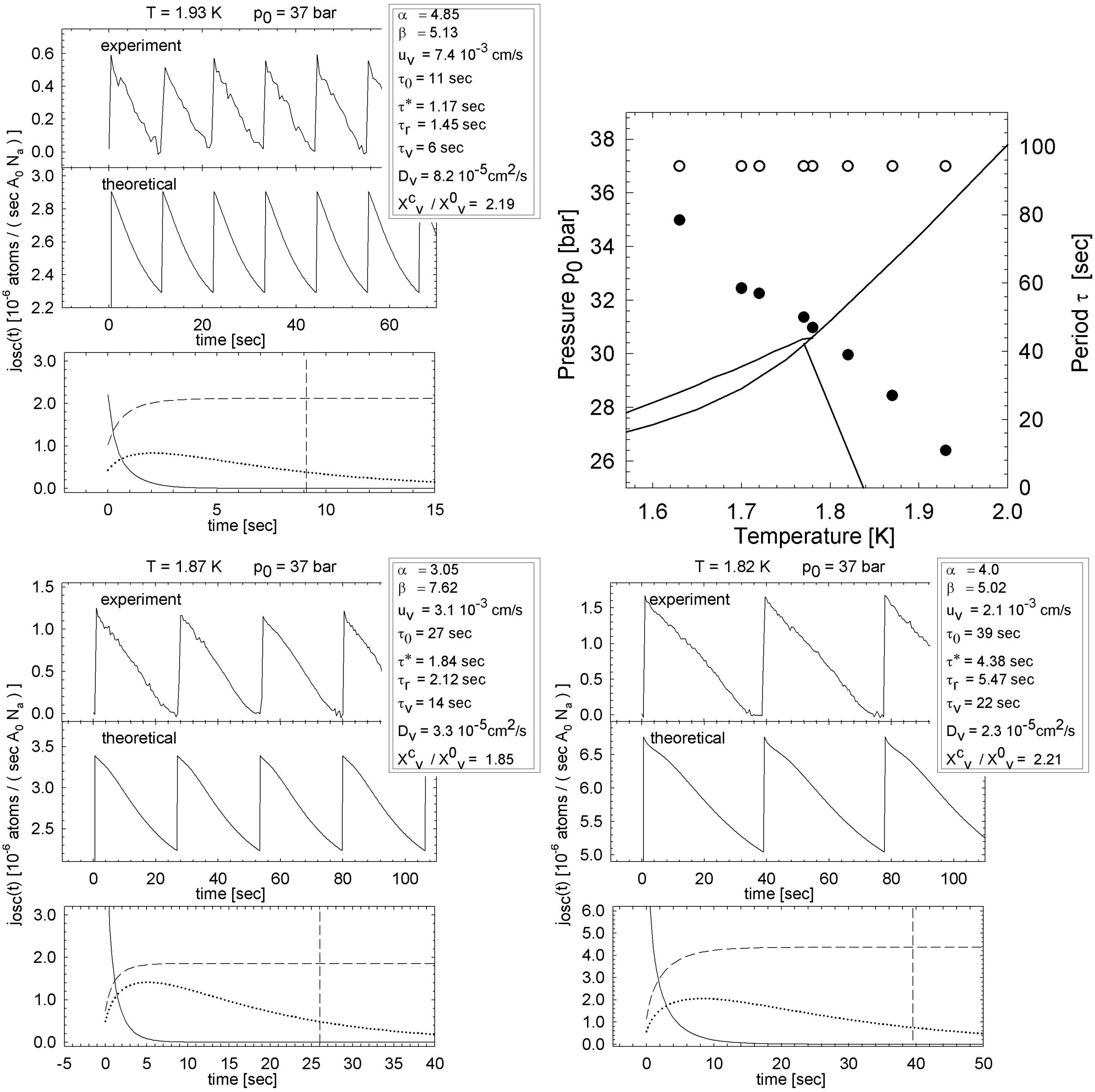

Figure B.13: Theoretical beam flux j_{osc} fitted for constant source pressure $p_0 = 37$ bar. ($d_0(\#18) = 2.9\ \mu$m)

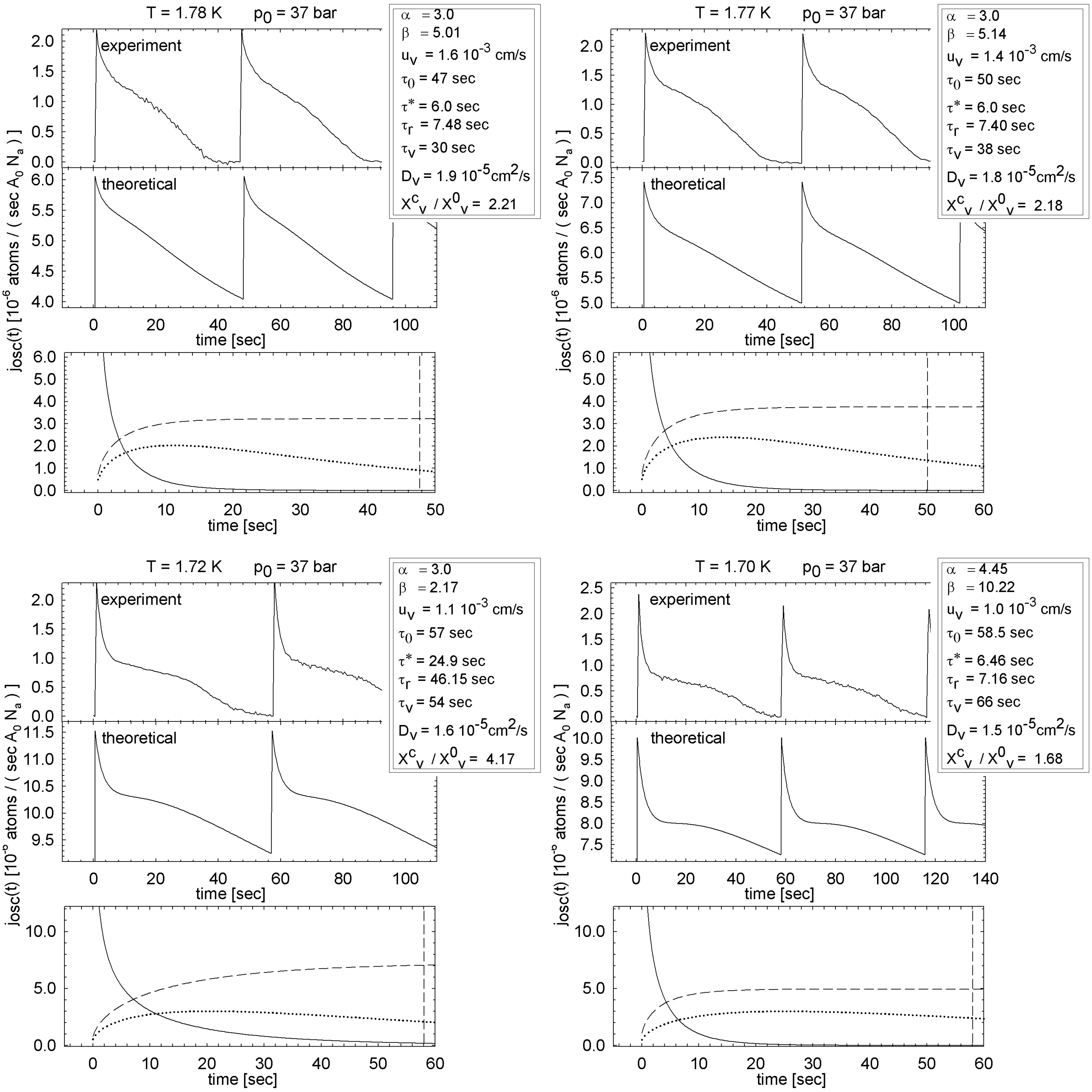

Figure B.14: Theoretical beam flux j_{osc} fitted for constant source pressure $p_0 = 37$ bar. ($d_0(\#18) = 2.9\ \mu$m)

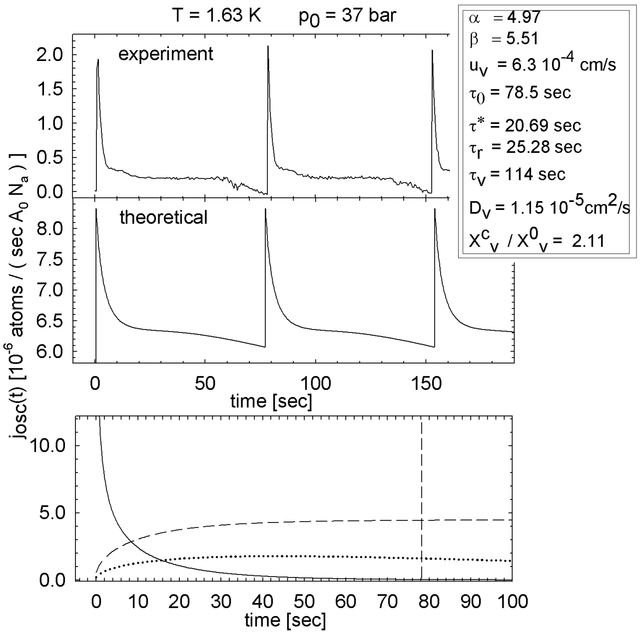

Figure B.15: Theoretical beam flux j_{osc} fitted for constant source pressure $p_0 = 37$ bar. ($d_0(\#18) = 2.9\ \mu$m)

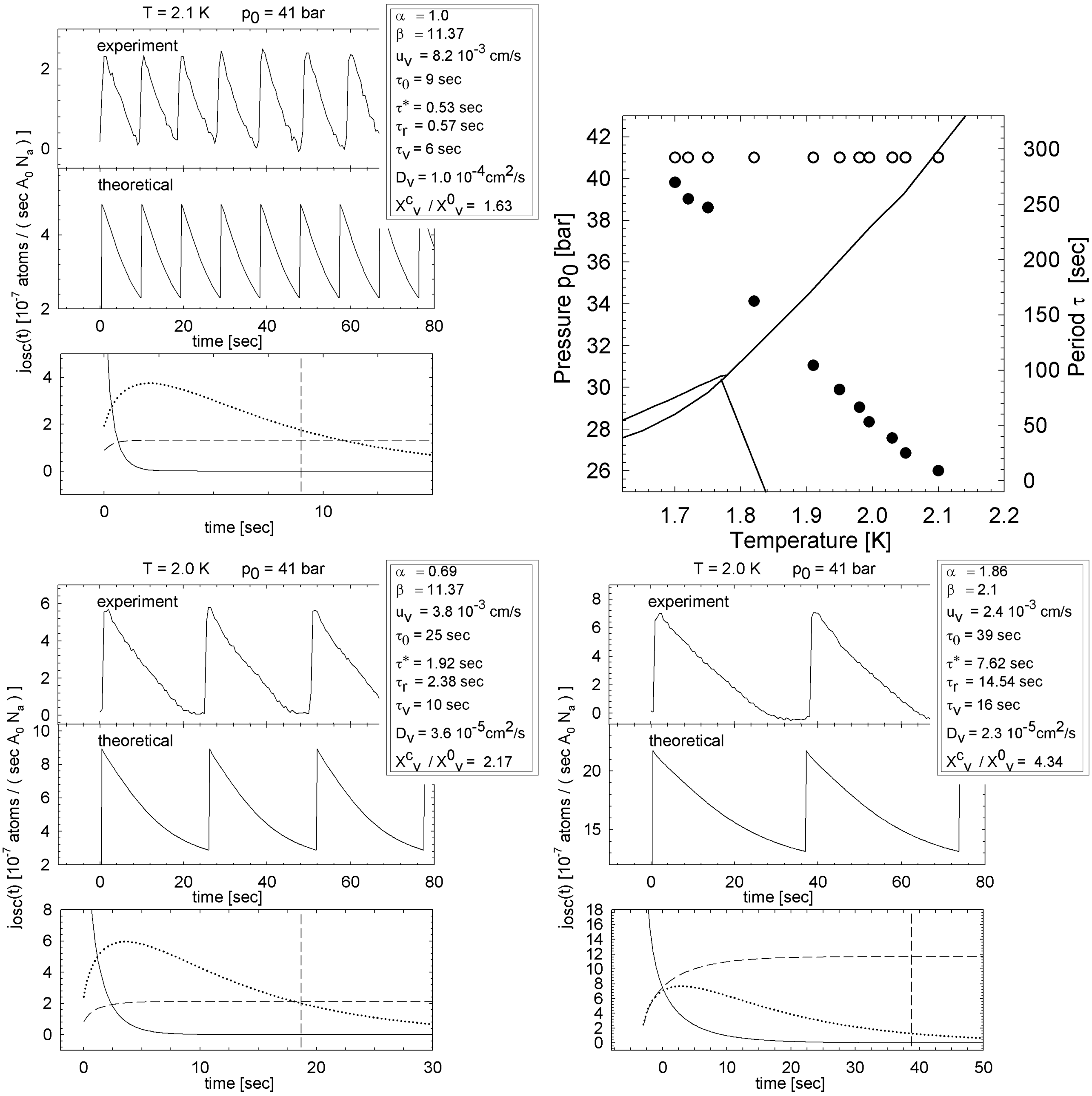

Figure B.16: Theoretical beam flux j_{osc} fitted for constant source pressure $p_0 = 40$ bar. ($d_0(\#17) = 2.28\ \mu$m)

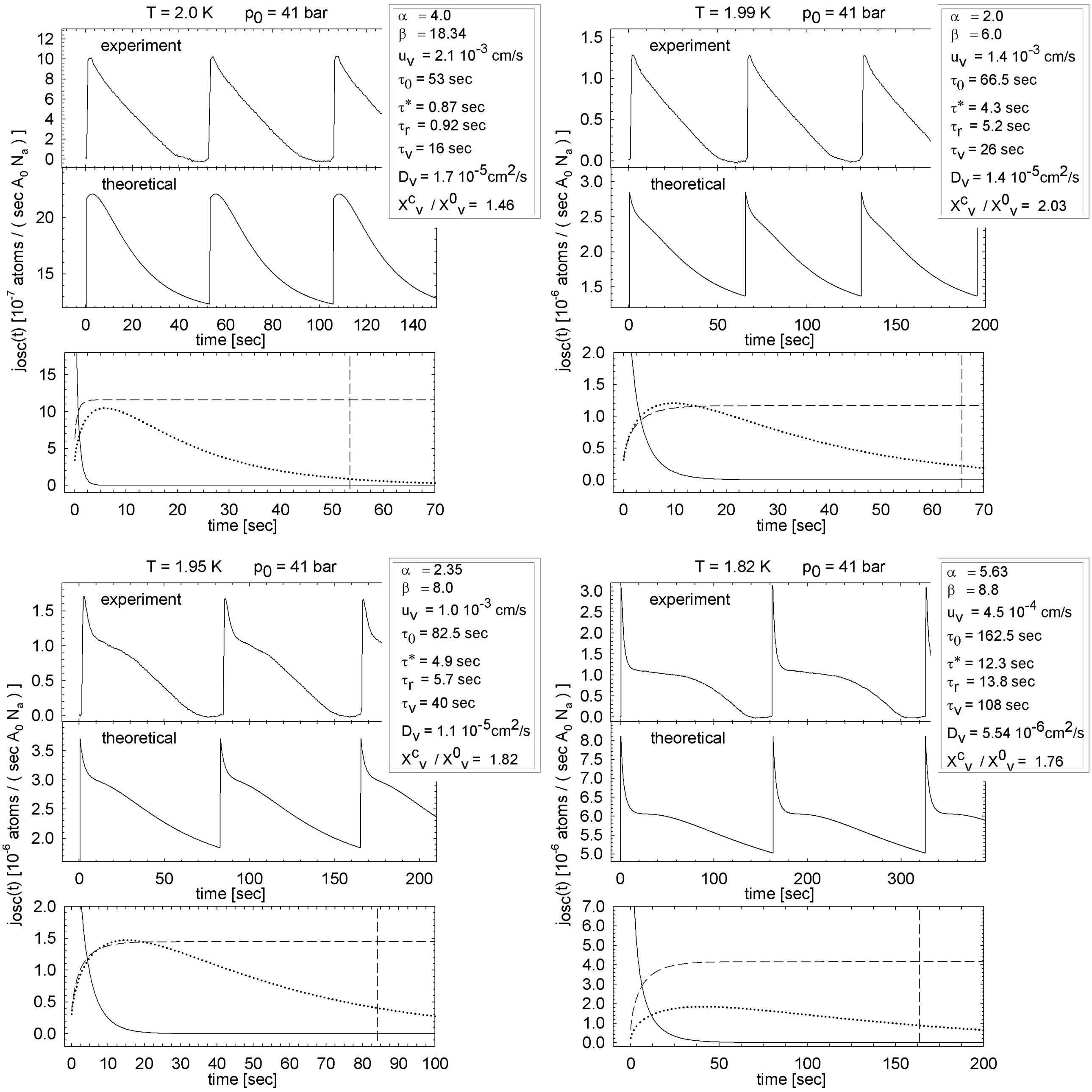

Figure B.17: Theoretical beam flux j_{osc} fitted for constant source pressure $p_0 = 40$ bar. ($d_0(\#17) = 2.28\ \mu$m)

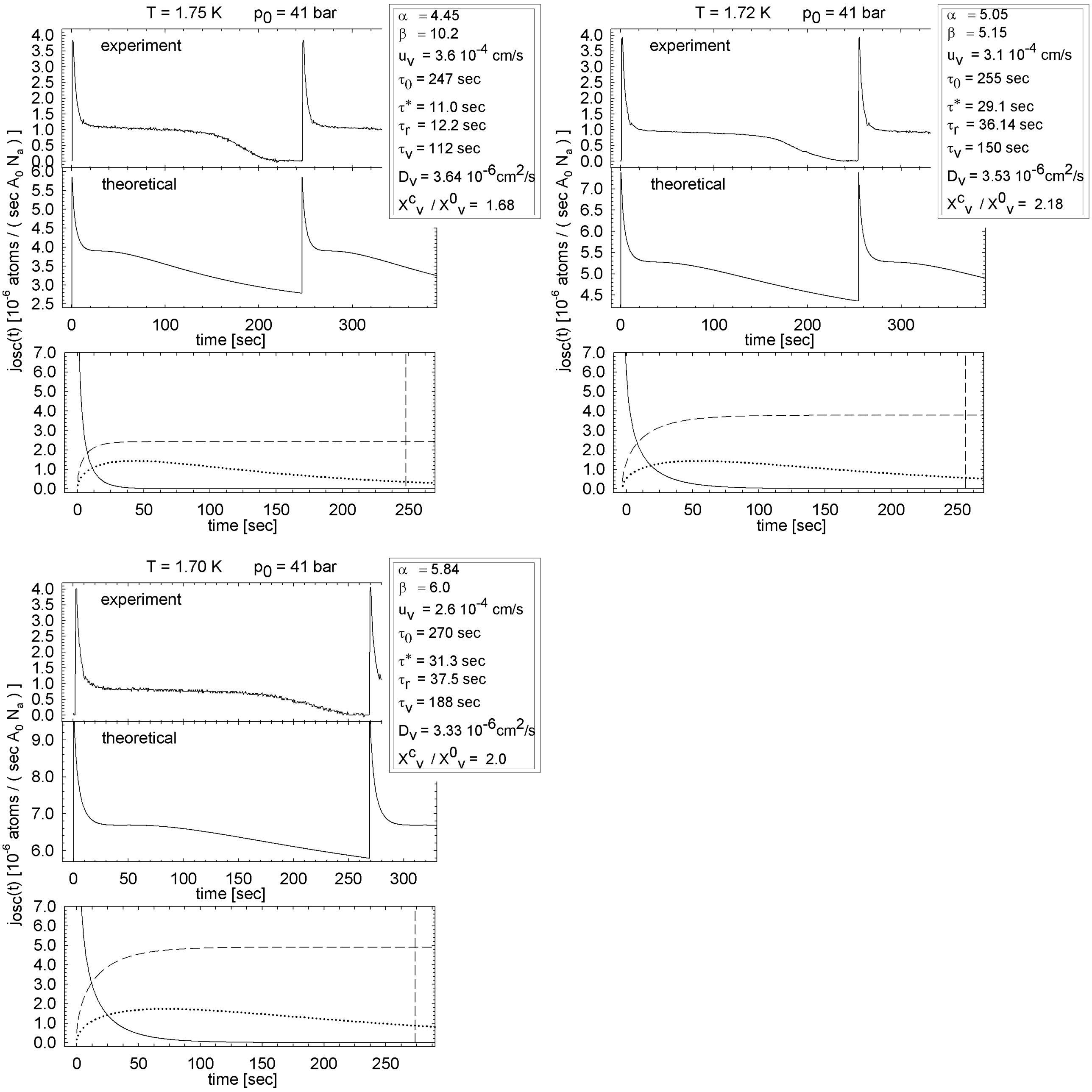

Figure B.18: Theoretical beam flux j_{osc} fitted for constant source pressure $p_0 = 40$ bar. ($d_0(\#17) = 2.28\ \mu$m)

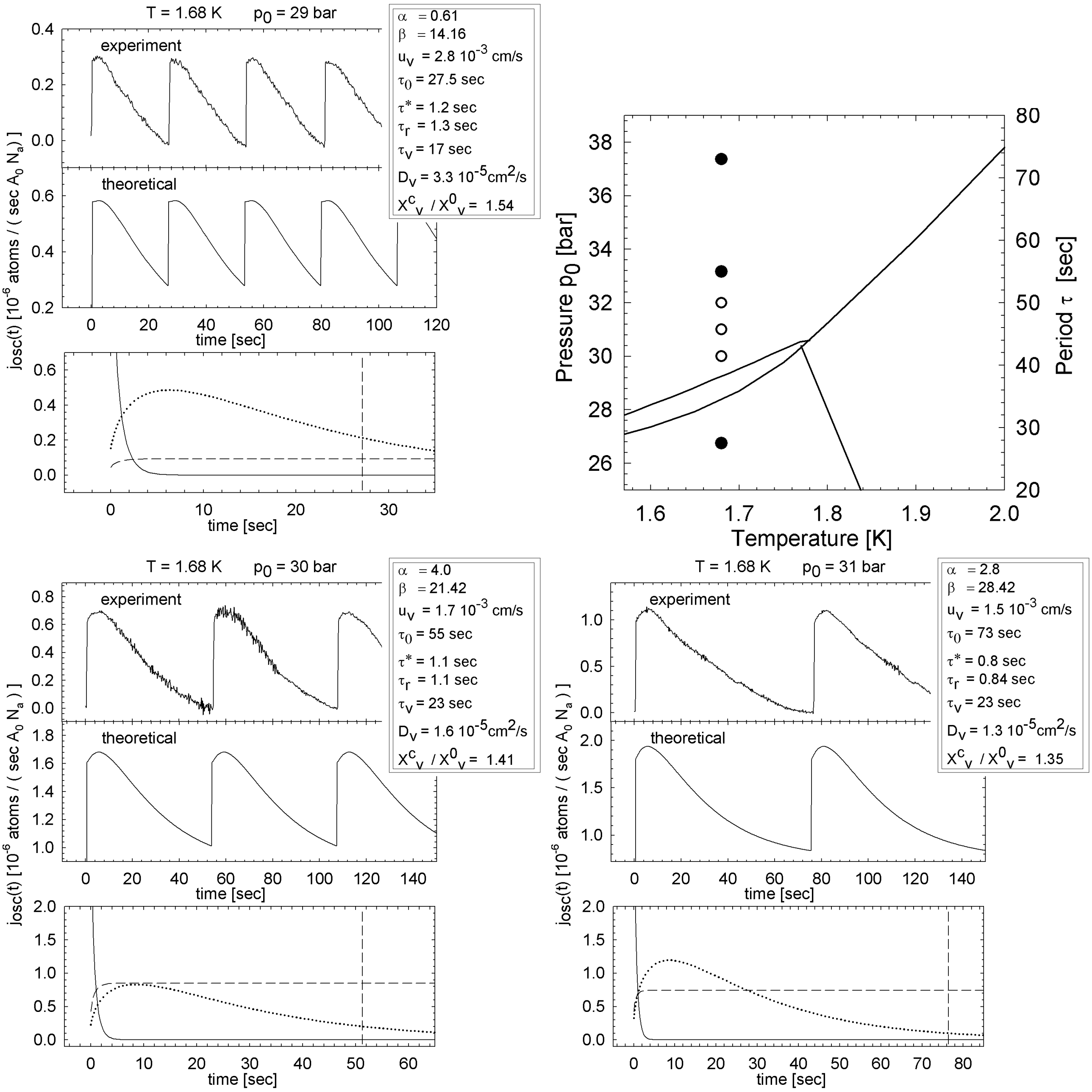

Figure B.19: Theoretical beam flux j_{osc} fitted for constant temperature T = 1.68 K ($d_0(\#22) = 2.2\ \mu$m)

Appendix C

Data

The Geyser effect has mainly been investigated as a function of temperature T at constant source pressure p_0. This section gives a summary of the oscillating detector pressure. An overview is shown in figure C.1: The Geyser oscillations are shown for temperatures between 1.3 K and 2.1 K and pressures between 29.5 and 41 bar. Each measurement of the Geyser effects is labeled with a data filename: (year/month/day) and a consecutive index (e.g. 03012921 measured on 03/01/29 (29th of January 2003) data index 21). Sets of data are summarized as follows: 030129 (19-23).

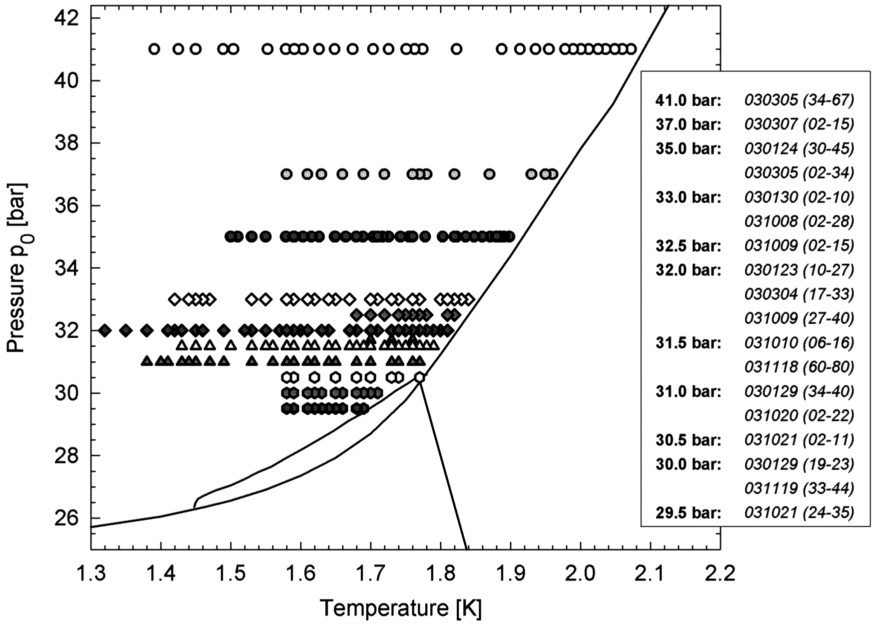

Figure C.1: Overview in the phase diagram, where the oscillating detector pressure has been investigated as a function of temperature T at constant source pressure p_0 with Helium-4.

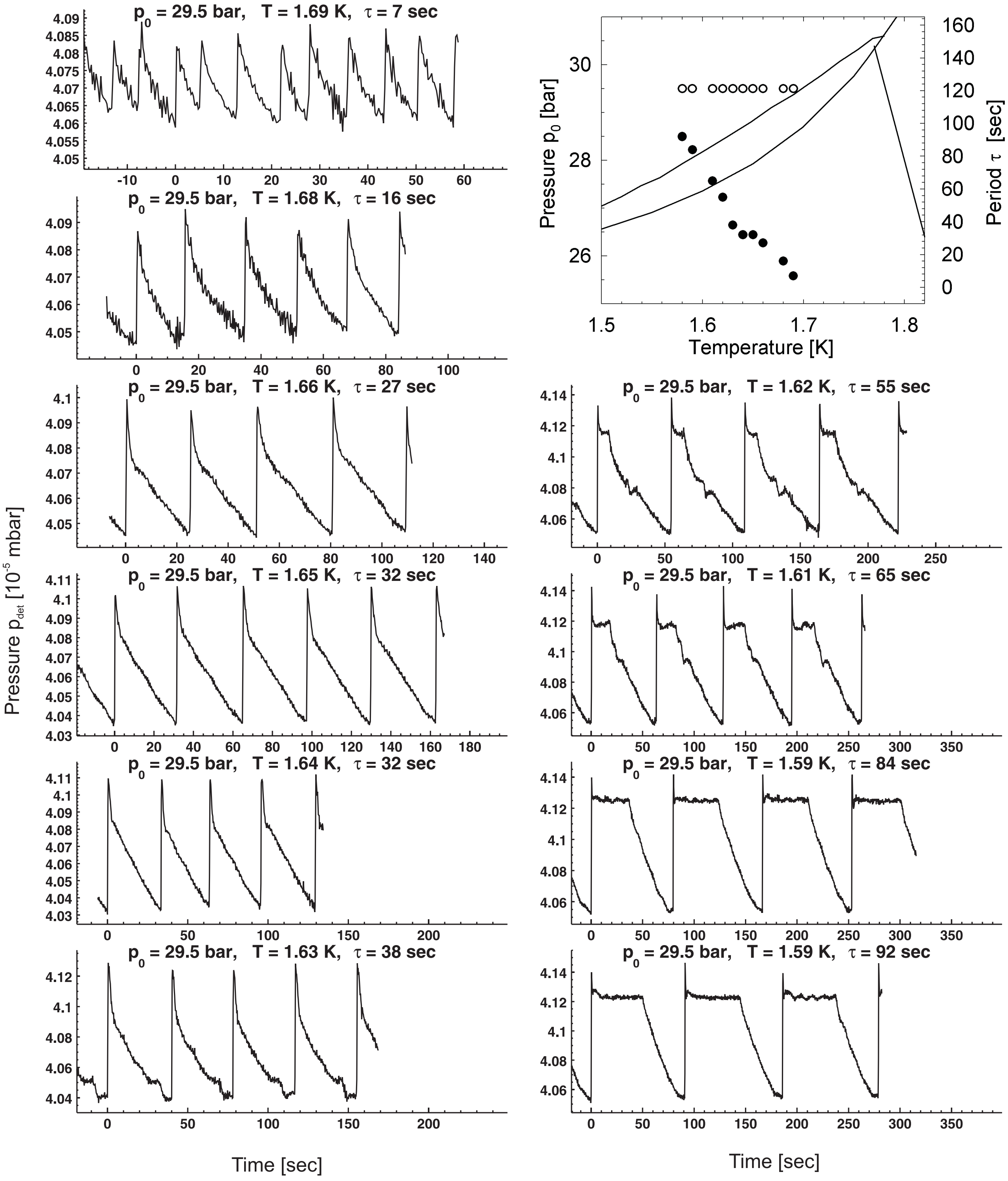

Figure C.2: Oscillating detector pressure p_{det} as a function of time for several temperatures T at constant source pressure p_0 = 29.5 bar. File: 031021 (24-35) ($d_0(\#22) = 2.2\ \mu$m)

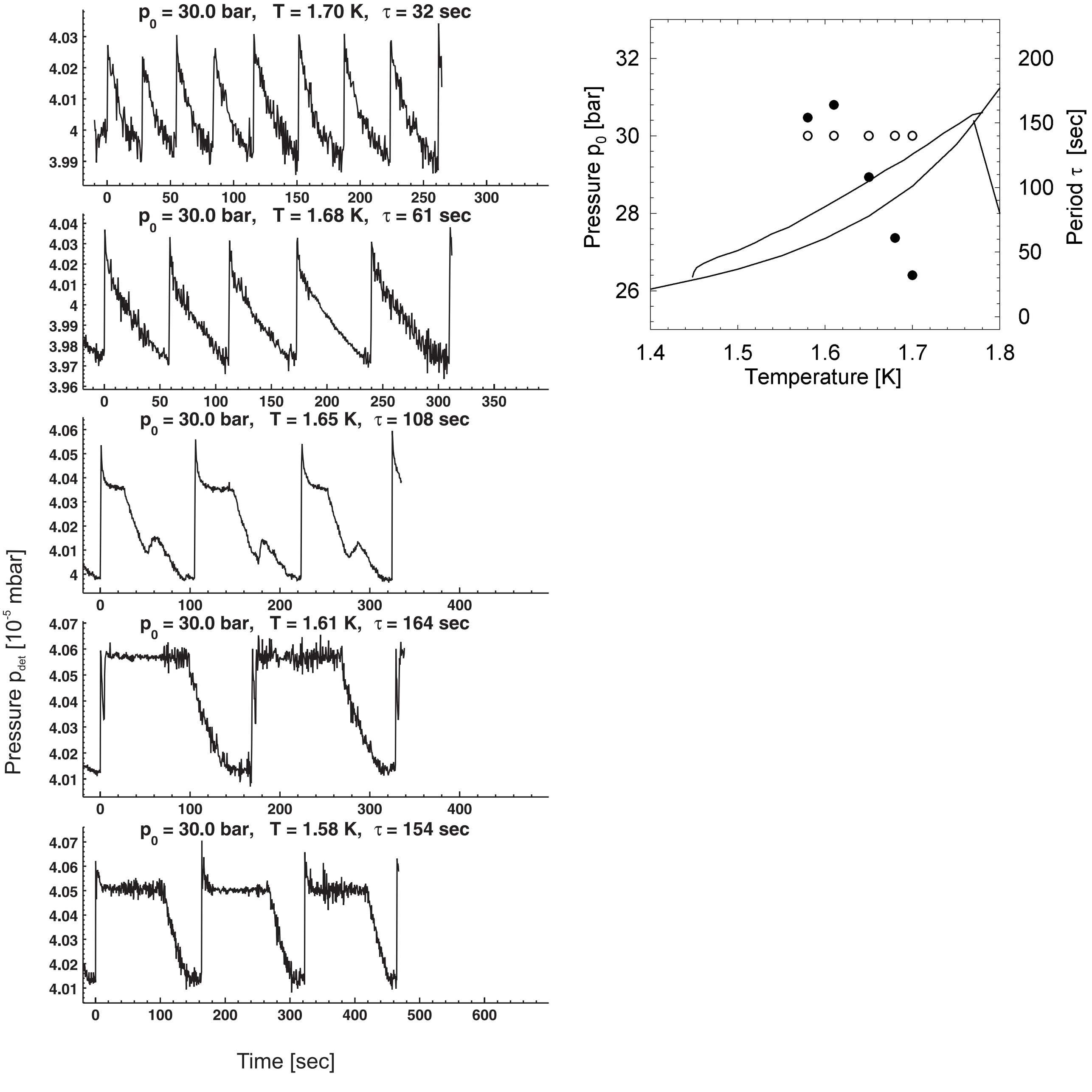

Figure C.3: Oscillating detector pressure p_{det} as a function of time for several temperatures T at constant source pressure $p_0 = 30$ bar. File: 030129 (19-23) ($d_0(\#17) = 2.28\ \mu$m)

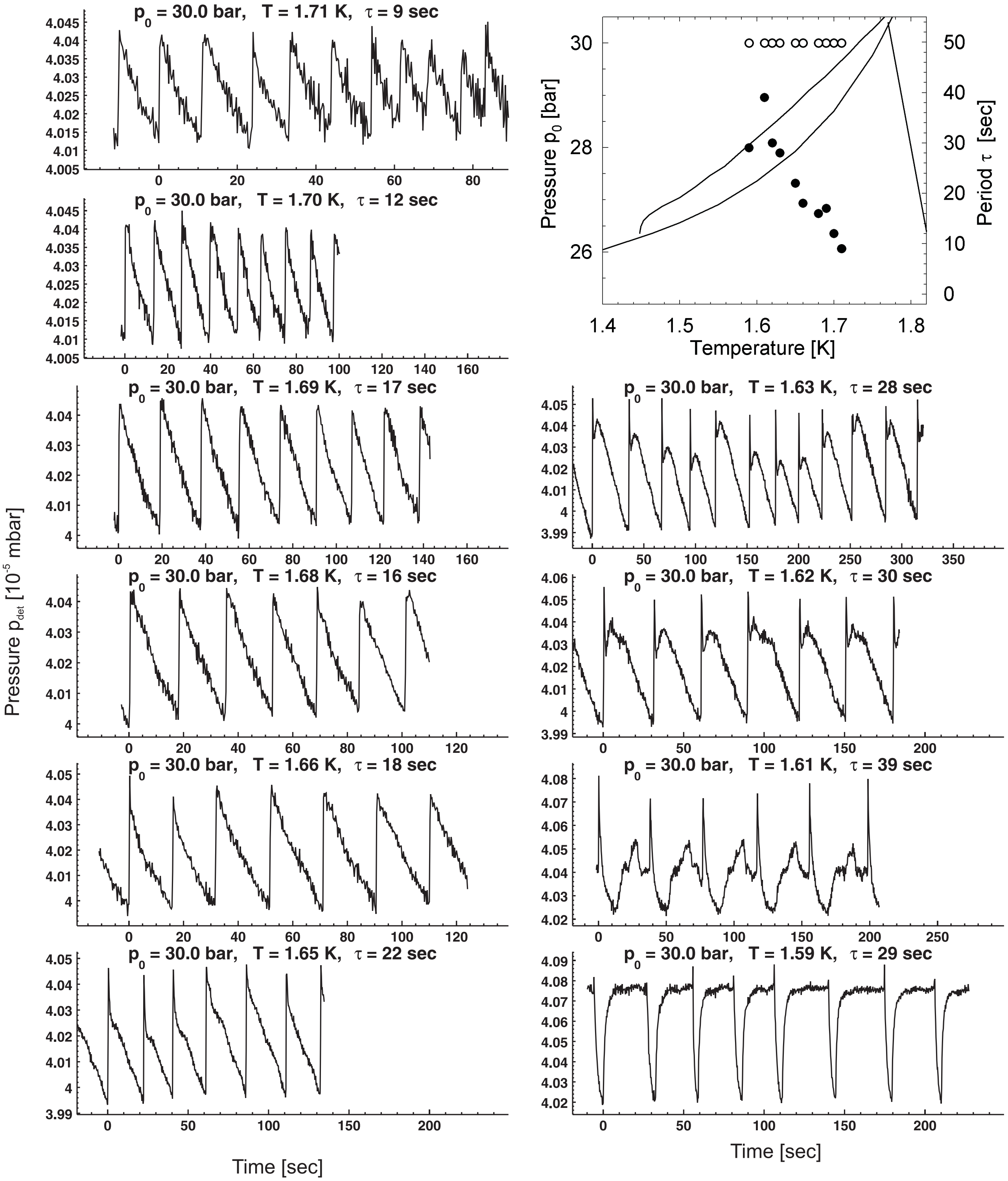

Figure C.4: Oscillating detector pressure p_{det} as a function of time for several temperatures T at constant source pressure $p_0 = 30$ bar. File: 031119 (33-44) ($d_0(\#22) = 2.2\ \mu$m)

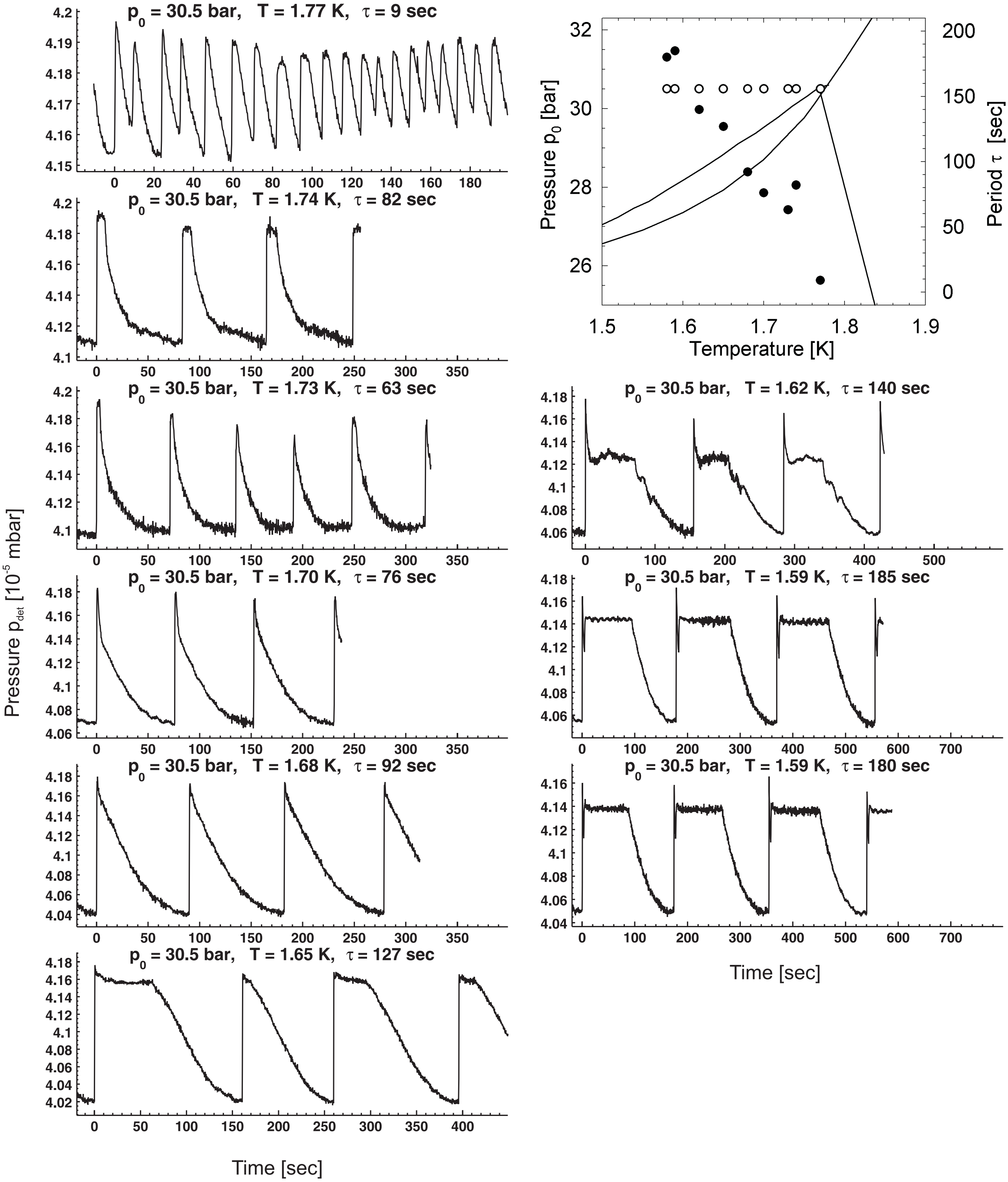

Figure C.5: Oscillating detector pressure p_{det} as a function of time for several temperatures T at constant source pressure p_0 = 30.5 bar. File:031021 (2-11) ($d_0(\#22)$ = 2.2 μm)

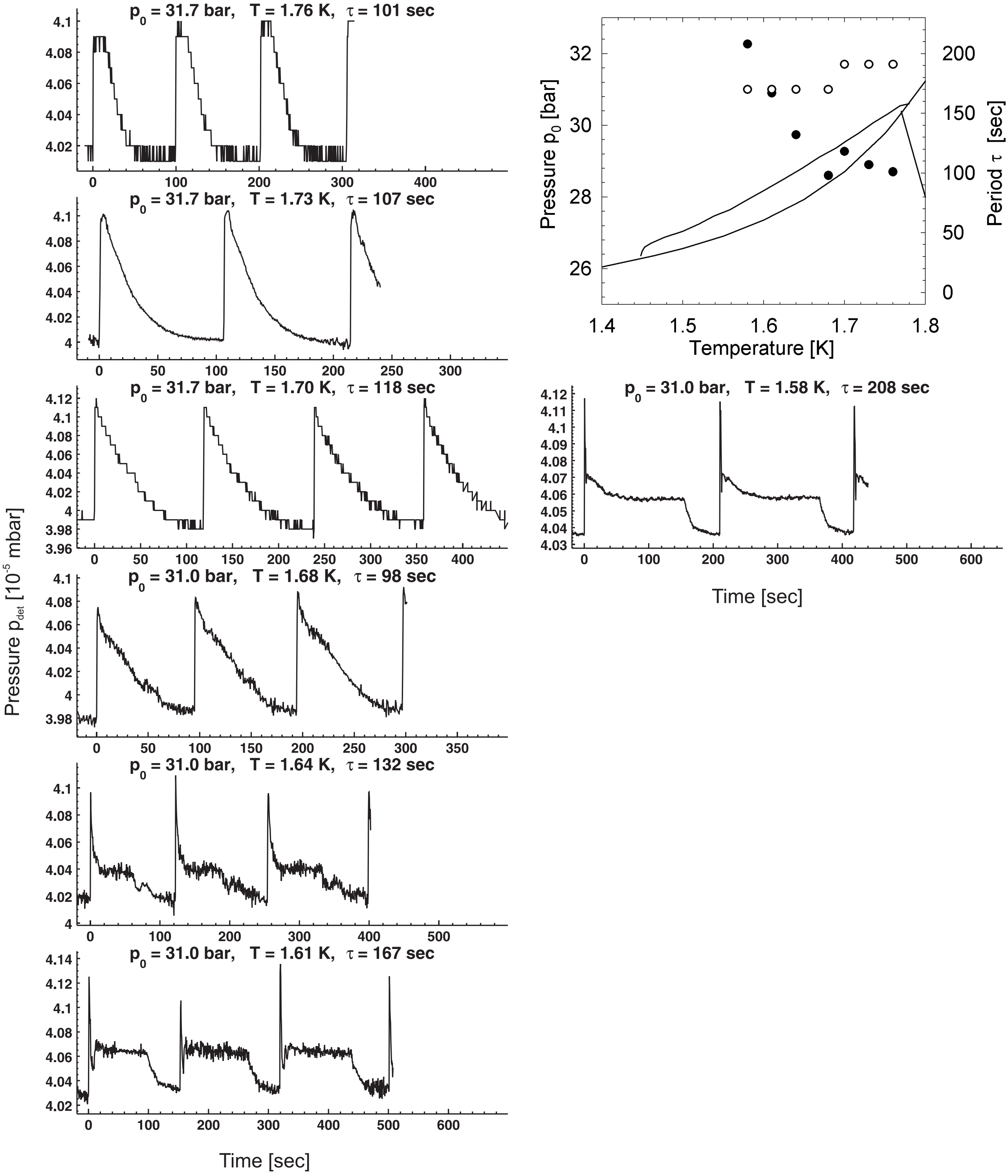

Figure C.6: Oscillating detector pressure p_{det} as a function of time for several temperatures T at constant source pressure p_0 = 31 bar. File: 030129 (34-40) ($d_0(\#17) = 2.28\ \mu$m)

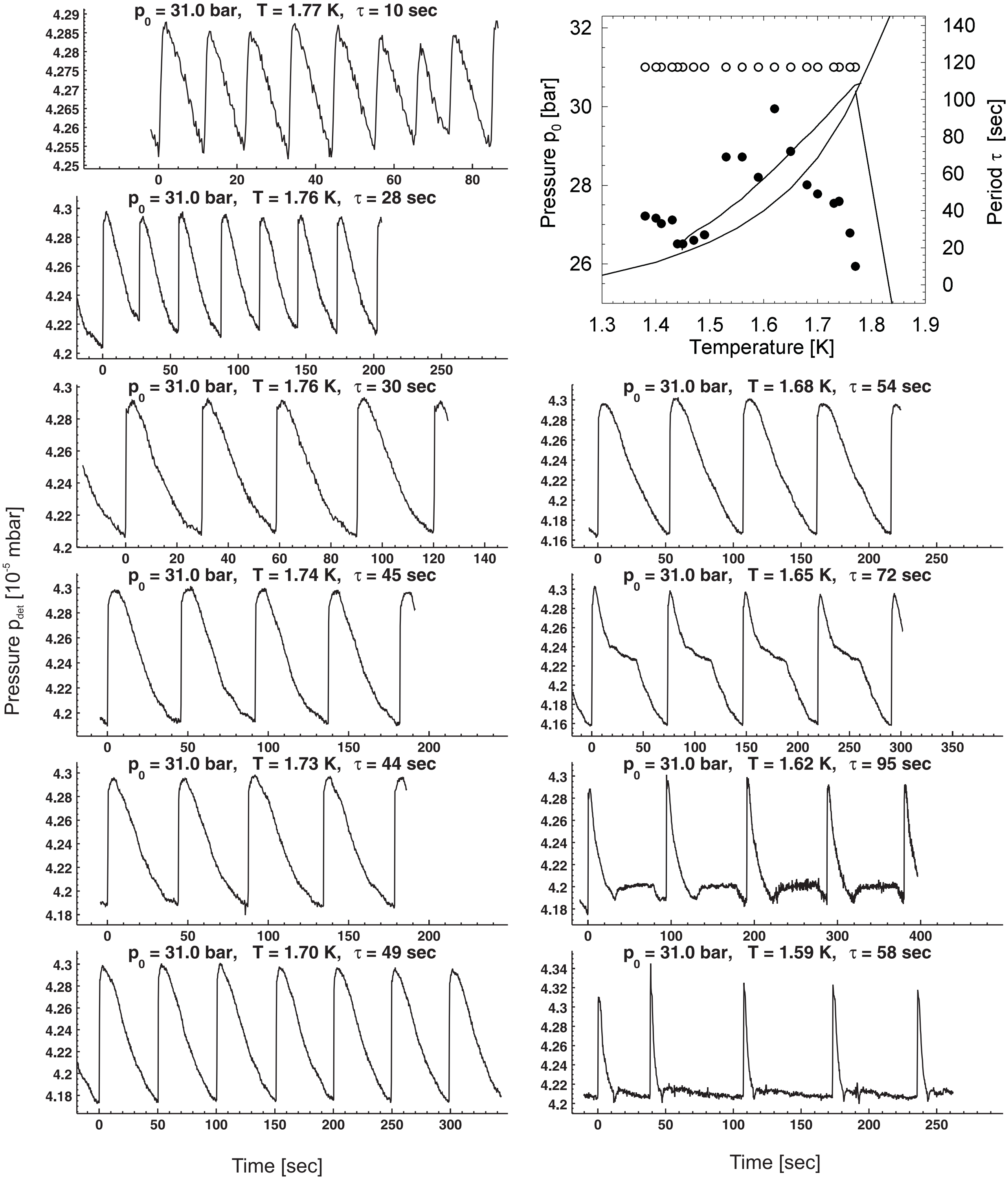

Figure C.7: Oscillating detector pressure p_{det} as a function of time for several temperatures T at constant source pressure $p_0 = 31$ bar. File: 031020 (2-22) ($d_0(\#22) = 2.2\ \mu\text{m}$)

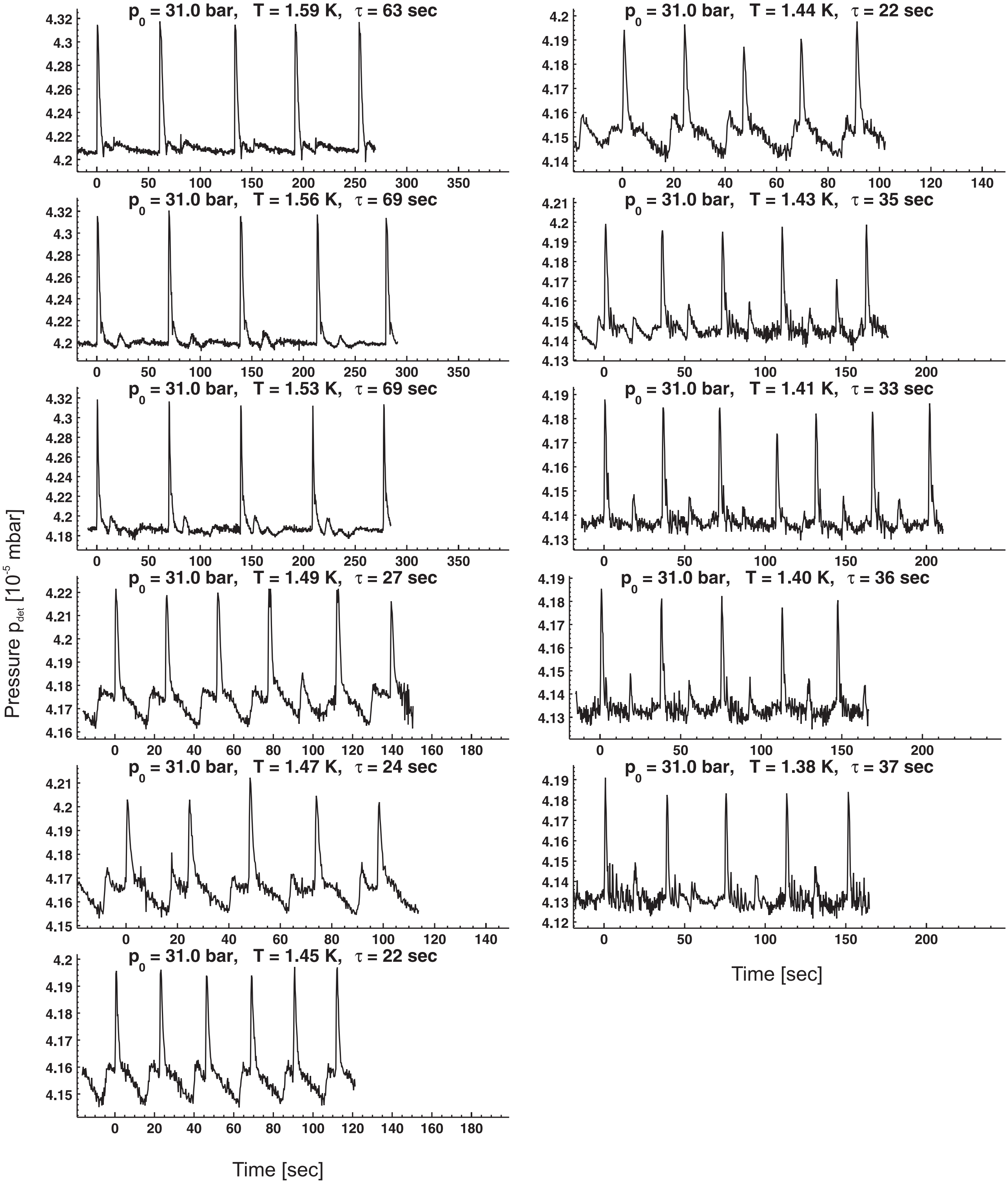

Figure C.8: Oscillating detector pressure p_{det} as a function of time for several temperatures T at constant source pressure $p_0 = 31$ bar. File: 031020 (2-22) ($d_0(\#22) = 2.2\ \mu$m)

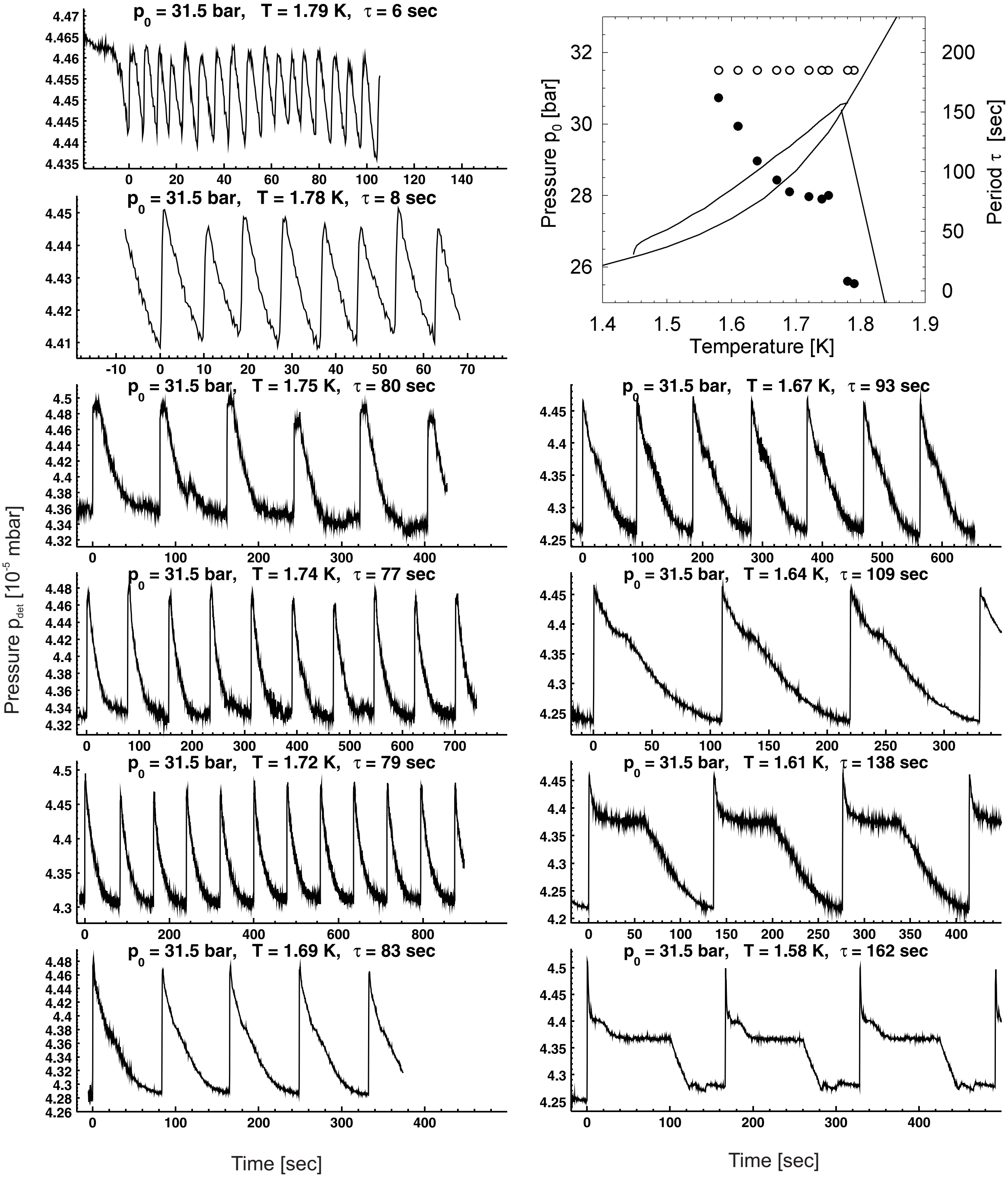

Figure C.9: Oscillating detector pressure p_{det} as a function of time for several temperatures T at constant source pressure p_0 = 31.5 bar. File: 031010 (6-16) ($d_0(\#20) = 2.07\ \mu$m)

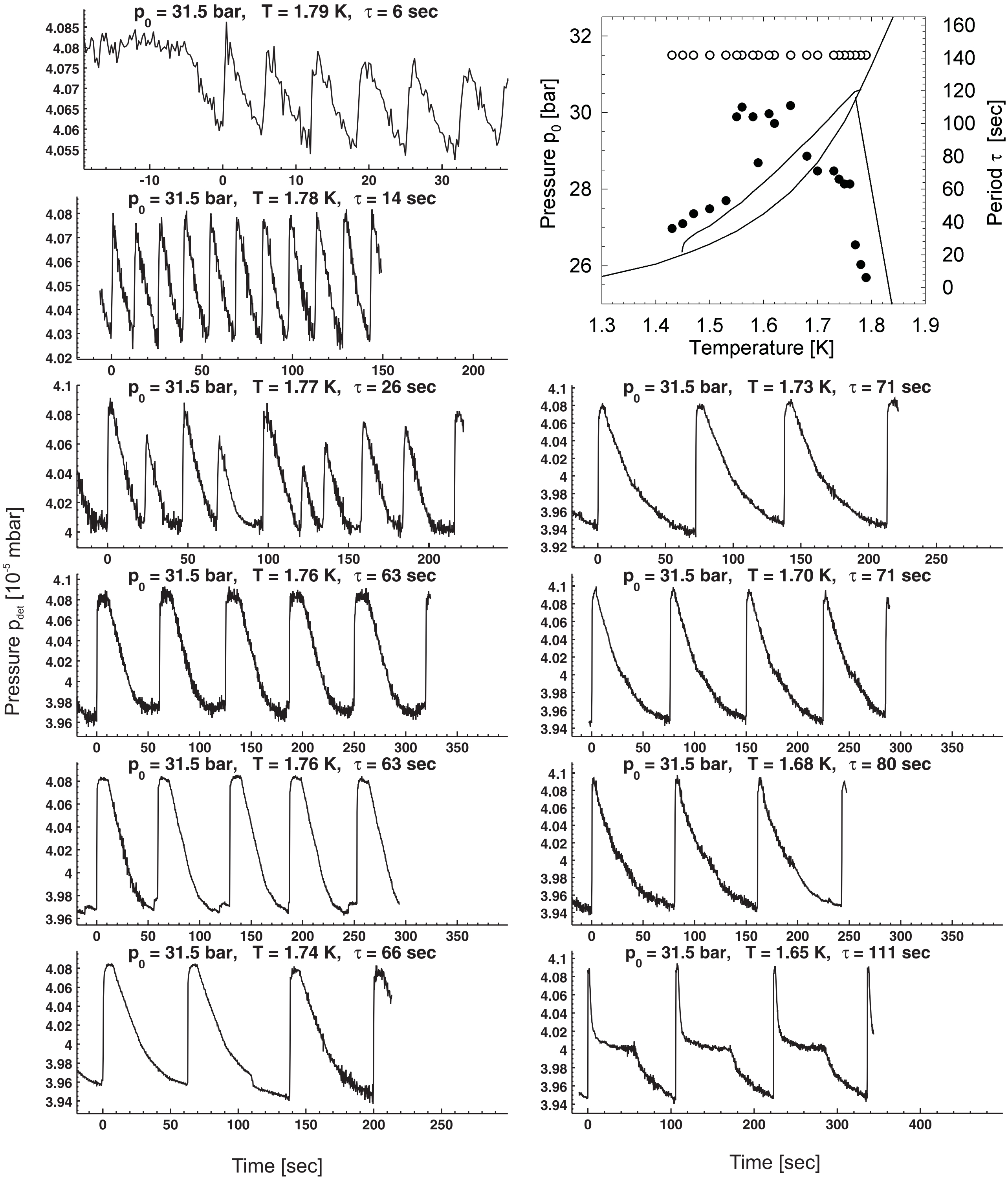

Figure C.10: Oscillating detector pressure p_{det} as a function of time for several temperatures T at constant source pressure p_0 = 31.5 bar. File: 031118 (60-80) ($d_0(\#22) = 2.2\ \mu$m)

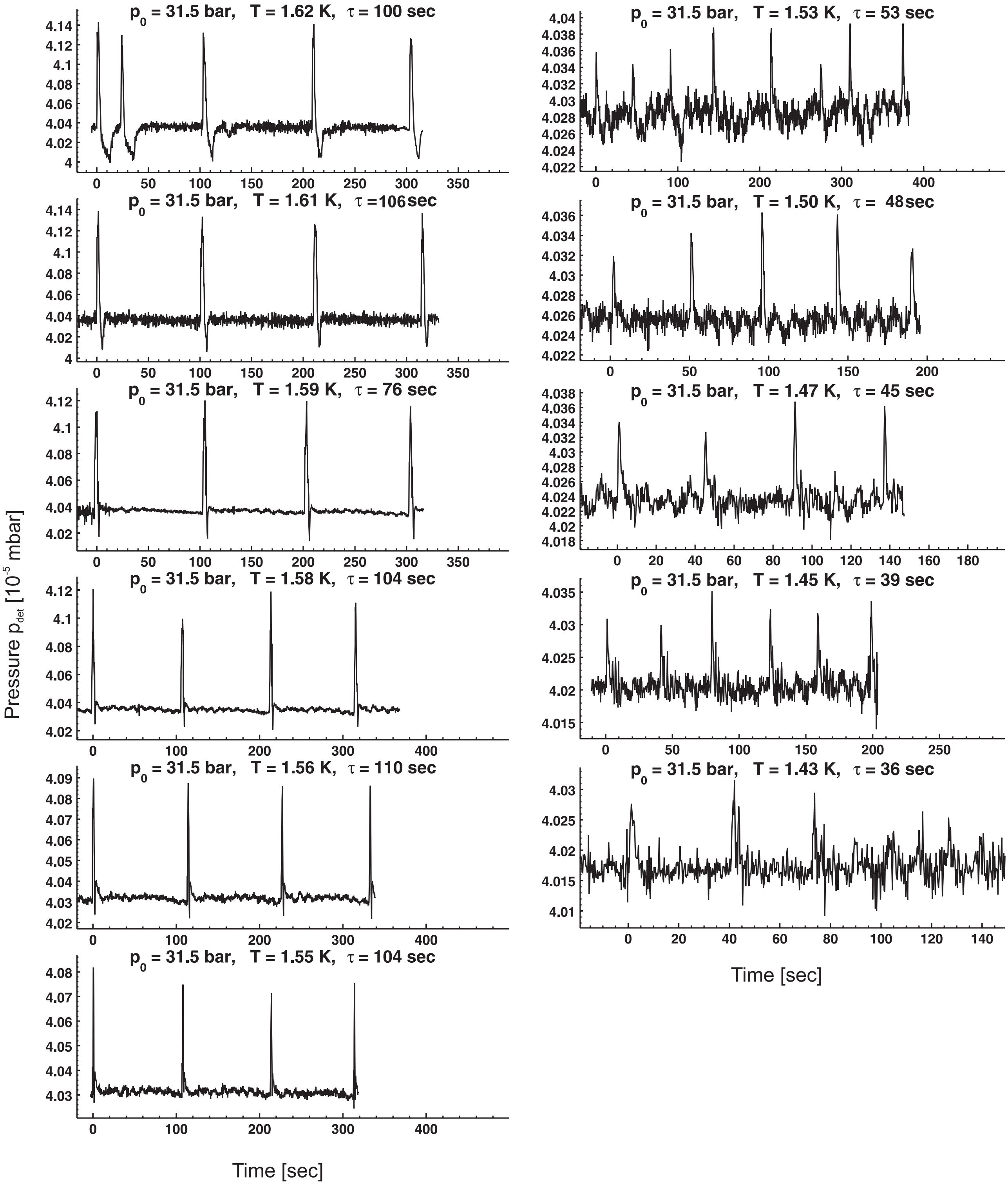

Figure C.11: Oscillating detector pressure p_{det} as a function of time for several temperatures T at constant source pressure $p_0 = 31.5$ bar. File: 031118 (60-80) ($d_0(\#22) = 2.2\ \mu$m)

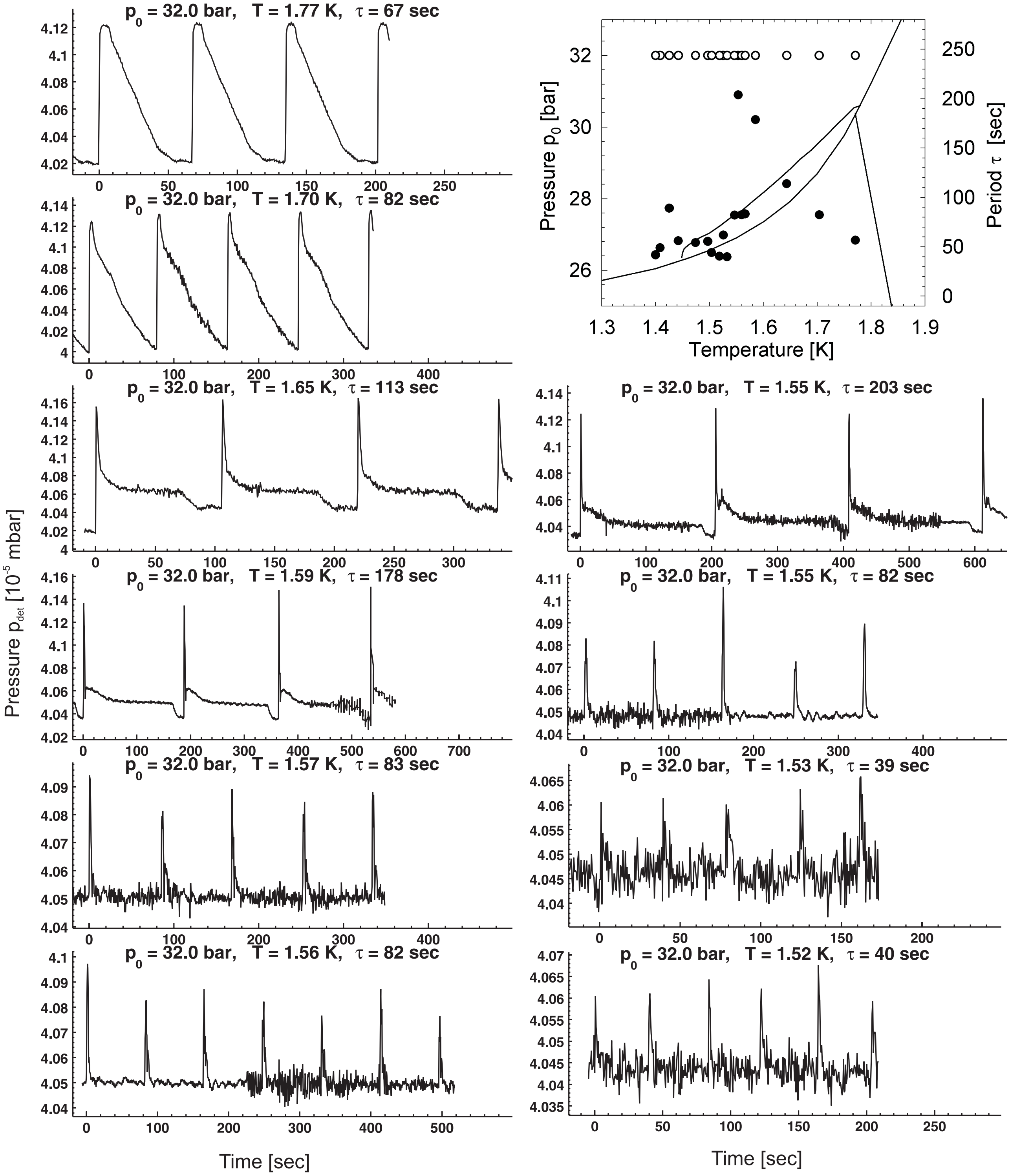

Figure C.12: Oscillating detector pressure p_{det} as a function of time for several temperatures T at constant source pressure $p_0 = 32$ bar. File: 030123 (10-27) ($d_0(\#17) = 2.28\ \mu$m)

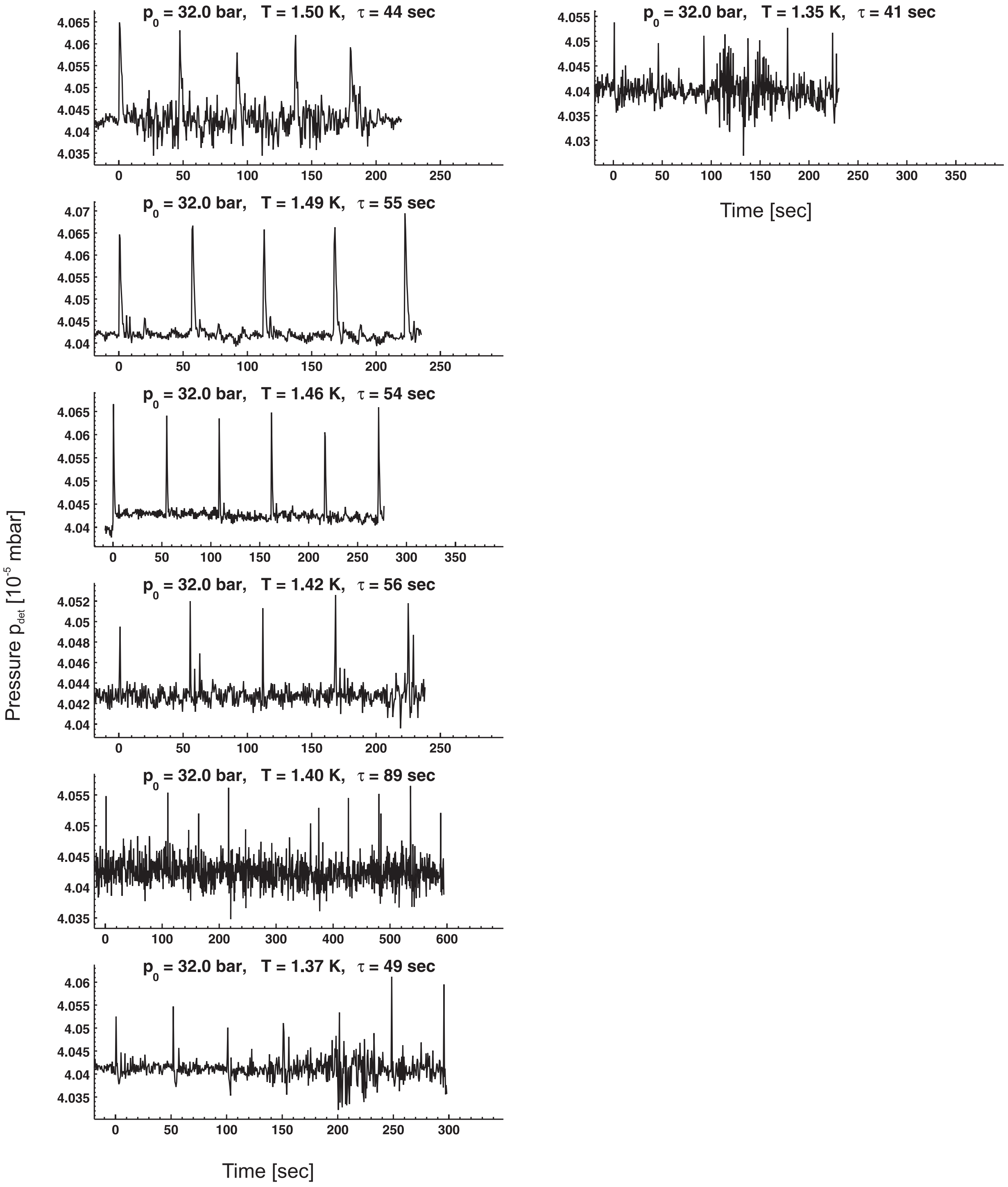

Figure C.13: Oscillating detector pressure p_{det} as a function of time for several temperatures T at constant source pressure $p_0 = 32$ bar. File: 030123 (10-27) ($d_0(\#17) = 2.28\ \mu$m)

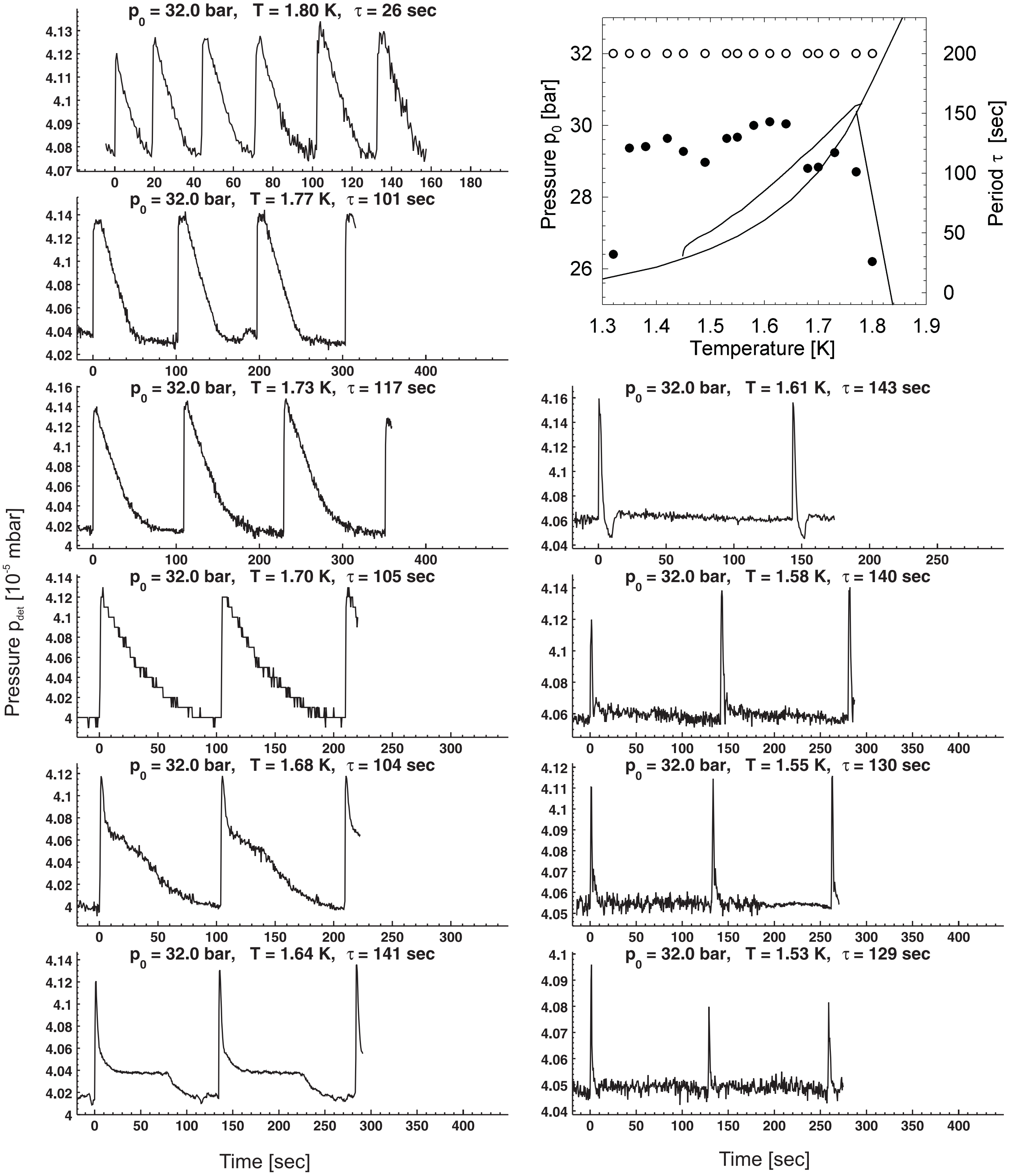

Figure C.14: Oscillating detector pressure p_{det} as a function of time for several temperatures T at constant source pressure p_0 = 32 bar. File: 030129 (49-56) ($d_0(\#17) = 2.28\ \mu$m)

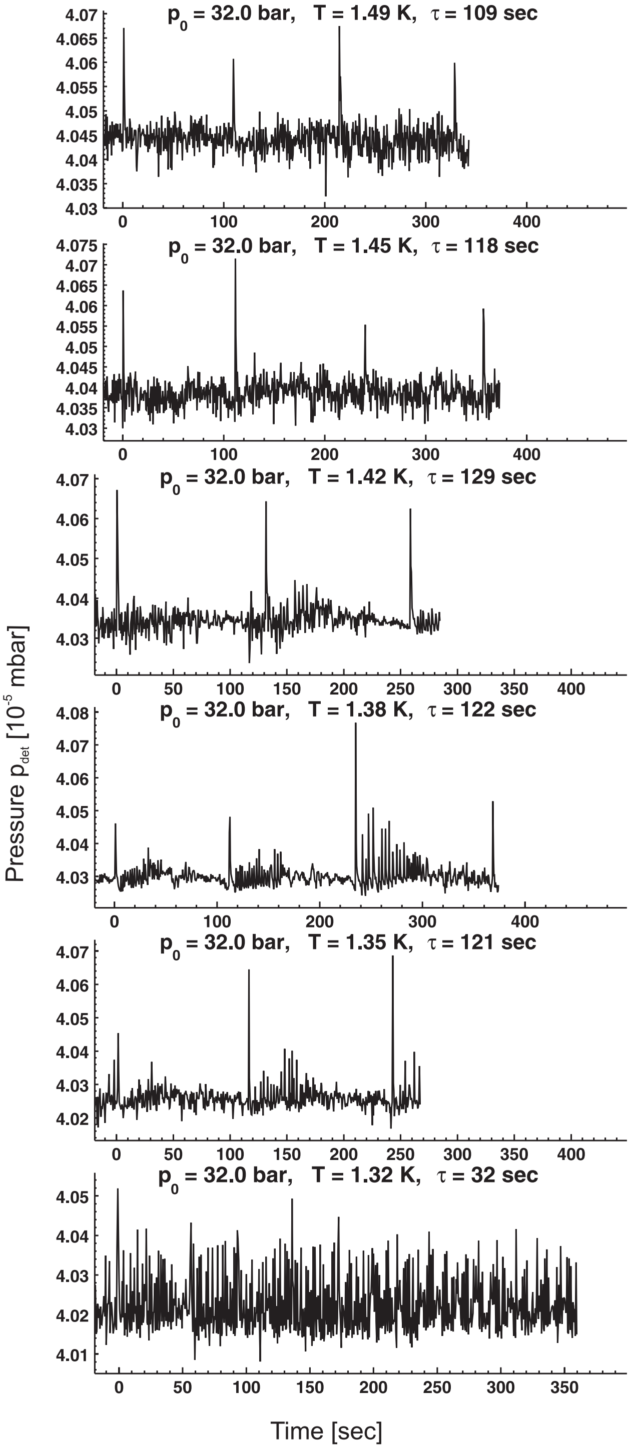

Figure C.15: Oscillating detector pressure p_{det} as a function of time for several temperatures T at constant source pressure $p_0 = 32$ bar. File: 030129 (49-64) ($d_0(\#17) = 2.28\ \mu$m)

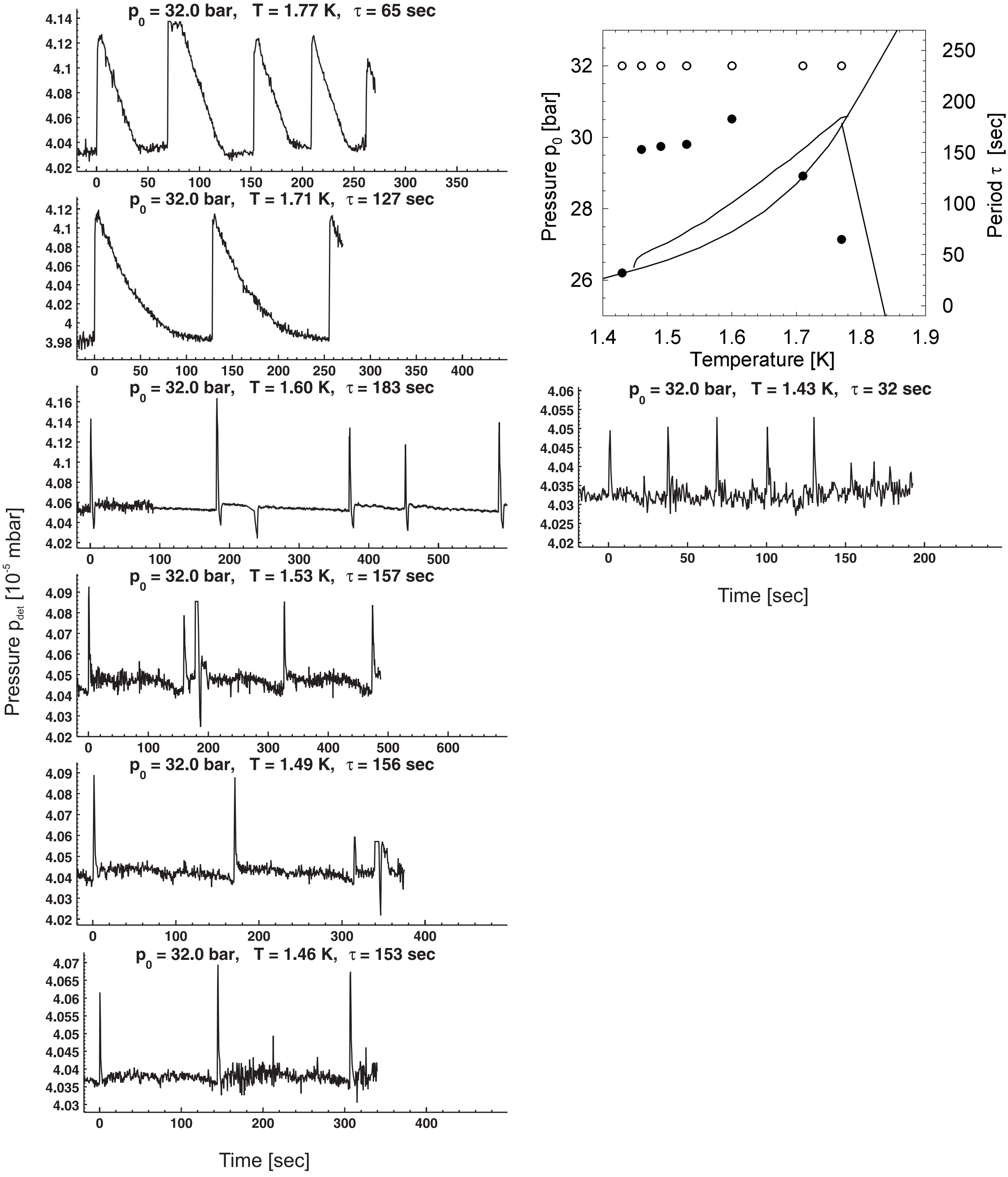

Figure C.16: Oscillating detector pressure p_{det} as a function of time for several temperatures T at constant source pressure p_0 = 32 bar. File: 030130 (31-40) ($d_0(\#17) = 2.28\ \mu$m)

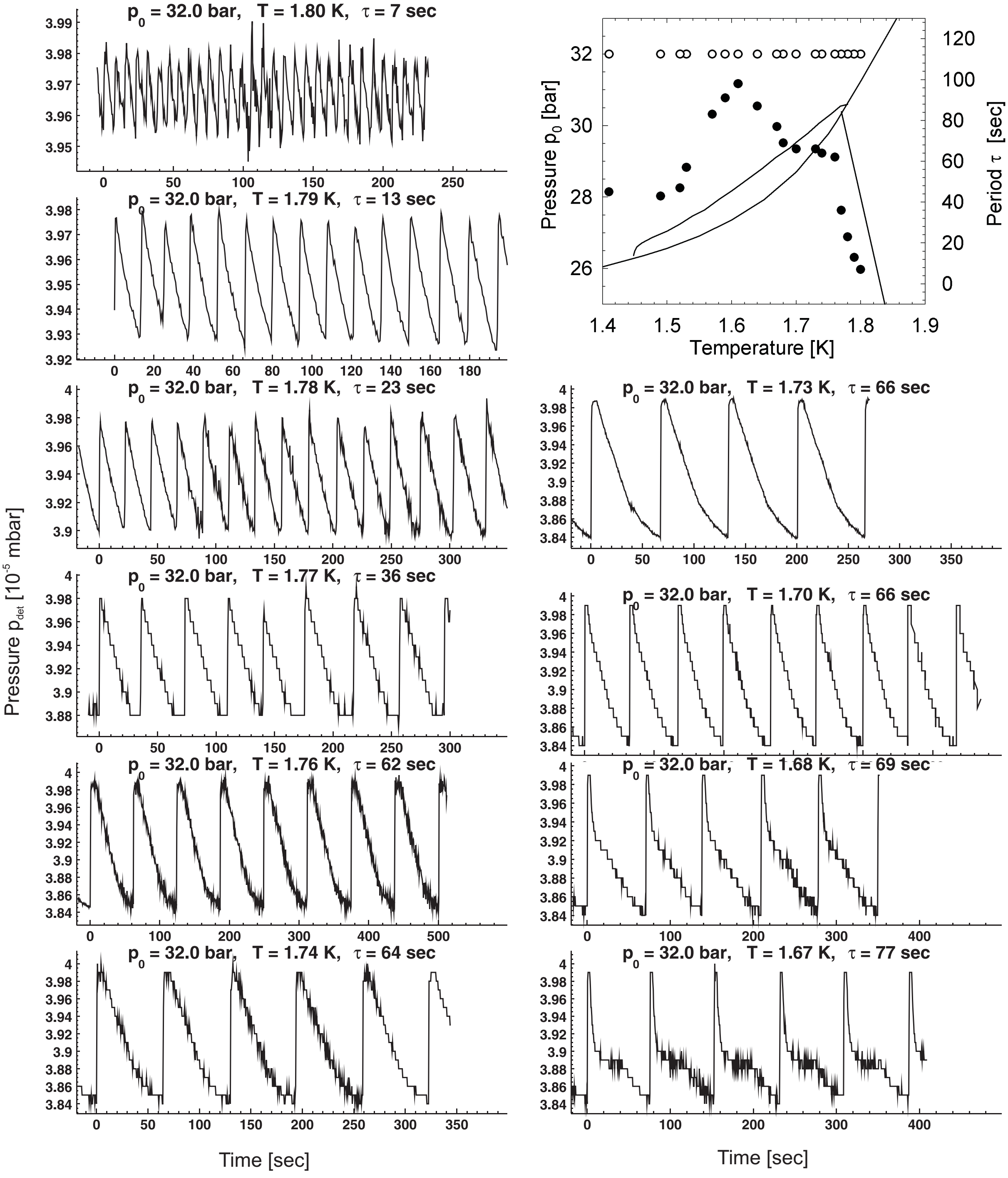

Figure C.17: Oscillating detector pressure p_{det} as a function of time for several temperatures T at constant source pressure $p_0 = 32$ bar. File: 030304 (17-33) ($d_0(\#17) = 2.28\ \mu$m)

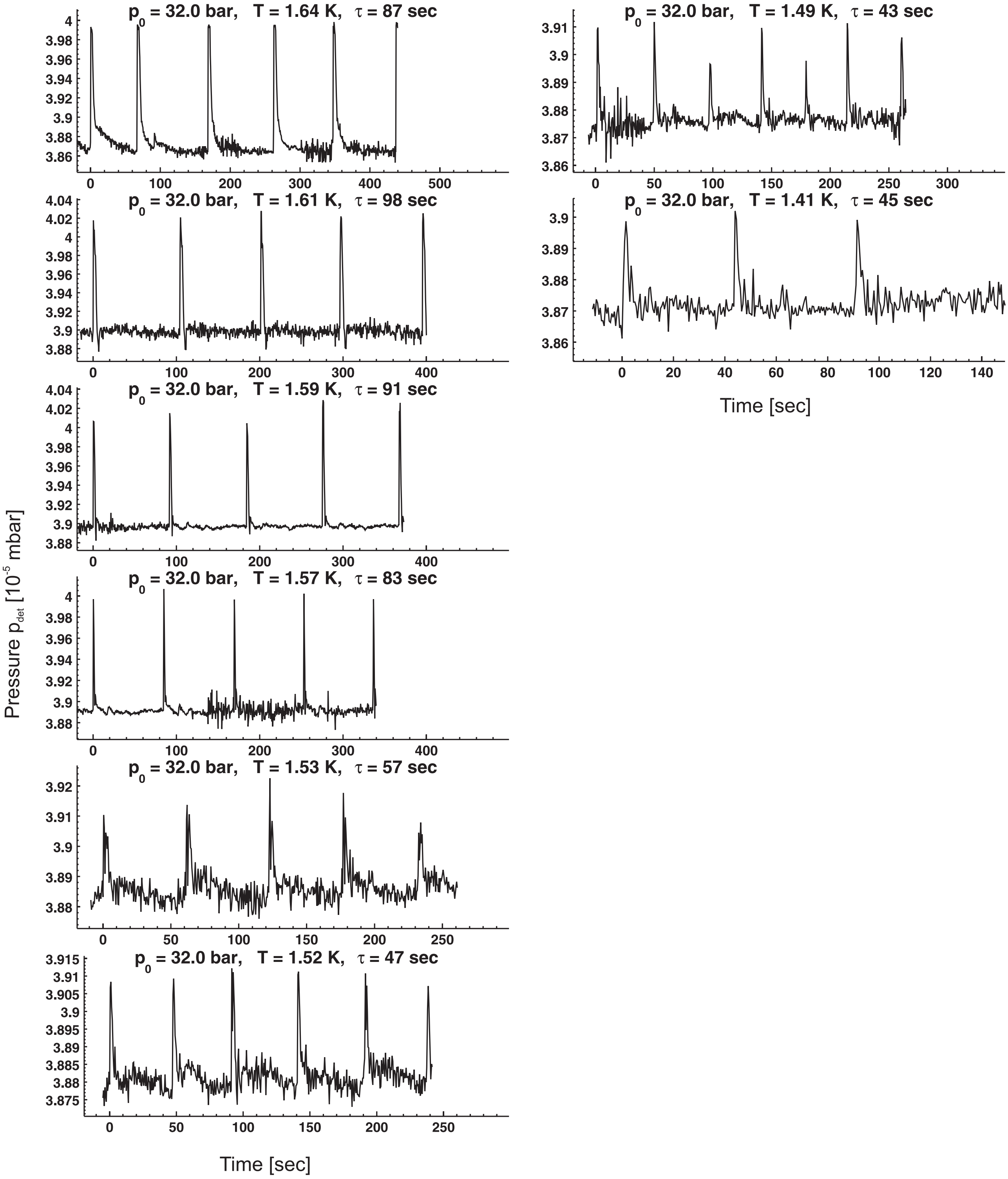

Figure C.18: Oscillating detector pressure p_{det} as a function of time for several temperatures T at constant source pressure p_0 = 32 bar. File: 030304 (17-33) ($d_0(\#17) = 2.28\ \mu$m)

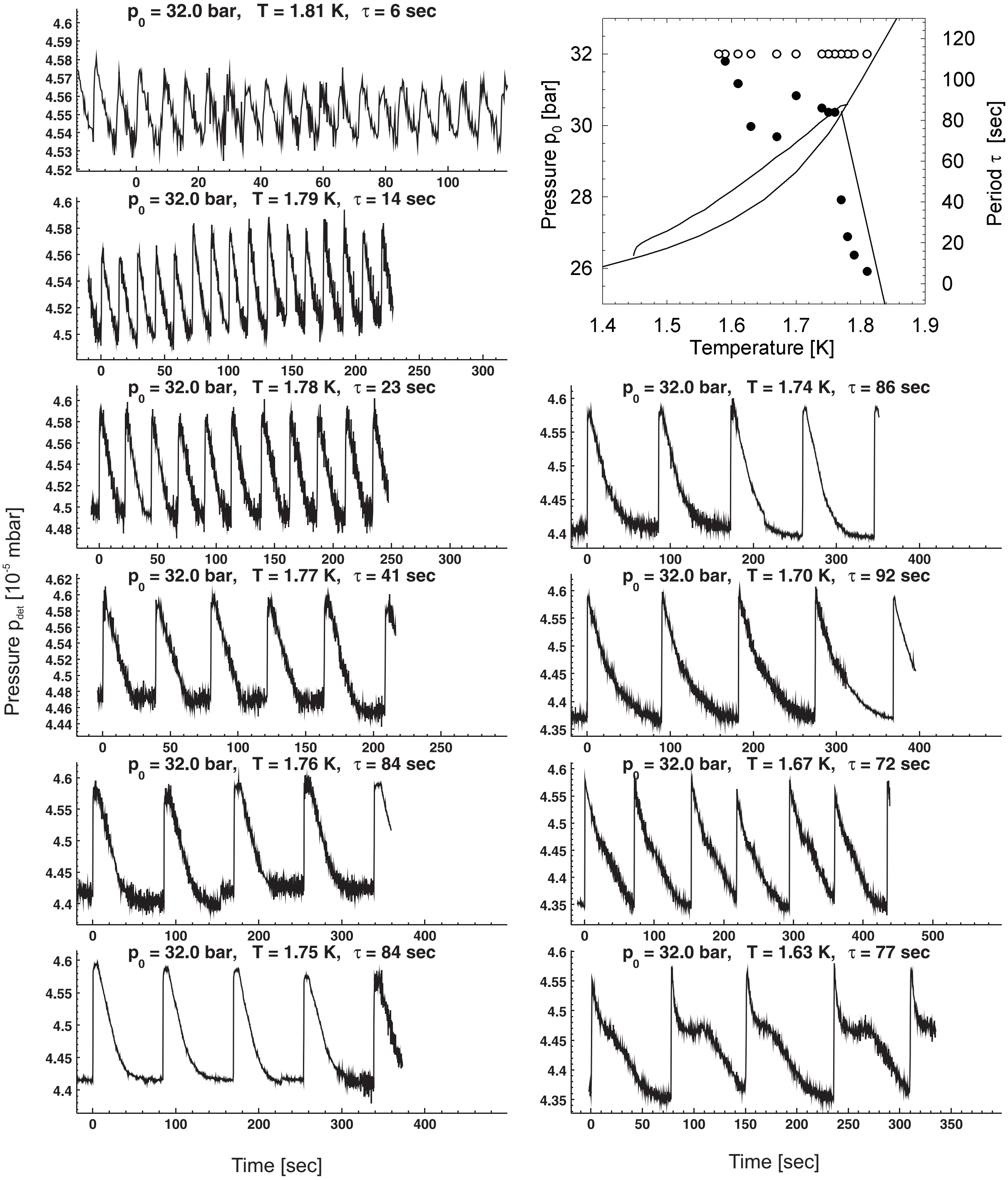

Figure C.19: Oscillating detector pressure p_{det} as a function of time for several temperatures T at constant source pressure p_0 = 32 bar. File: 031009 (27-40) ($d_0(\#20) = 2.07\ \mu$m)

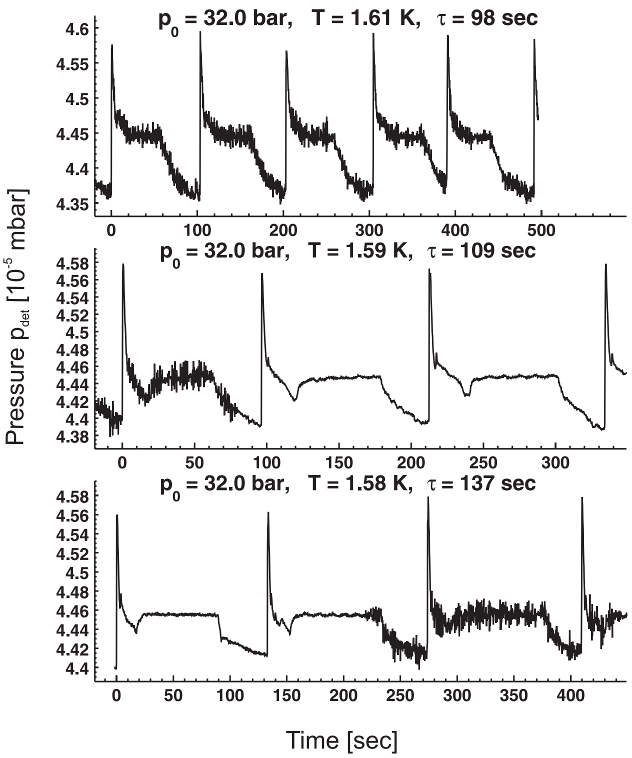

Figure C.20: Oscillating detector pressure p_{det} as a function of time for several temperatures T at constant source pressure p_0 = 32 bar.File: 031009 (27-40) ($d_0(\#20)$ = 2.07 μm)

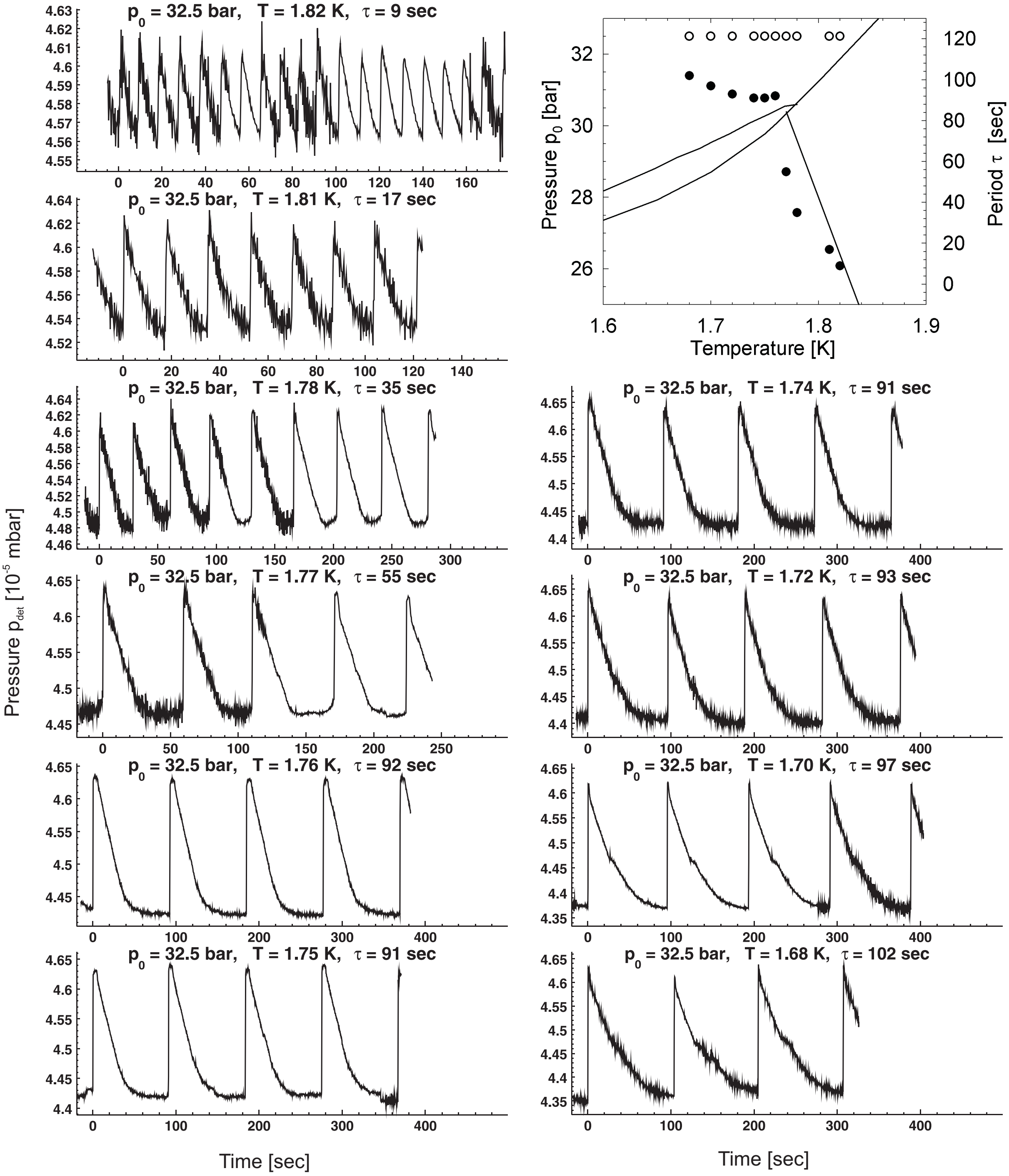

Figure C.21: Oscillating detector pressure p_{det} as a function of time for several temperatures T at constant source pressure p_0 = 32.5 bar. File: 031009 (2-15) ($d_0(\#20) = 2.07\ \mu$m)

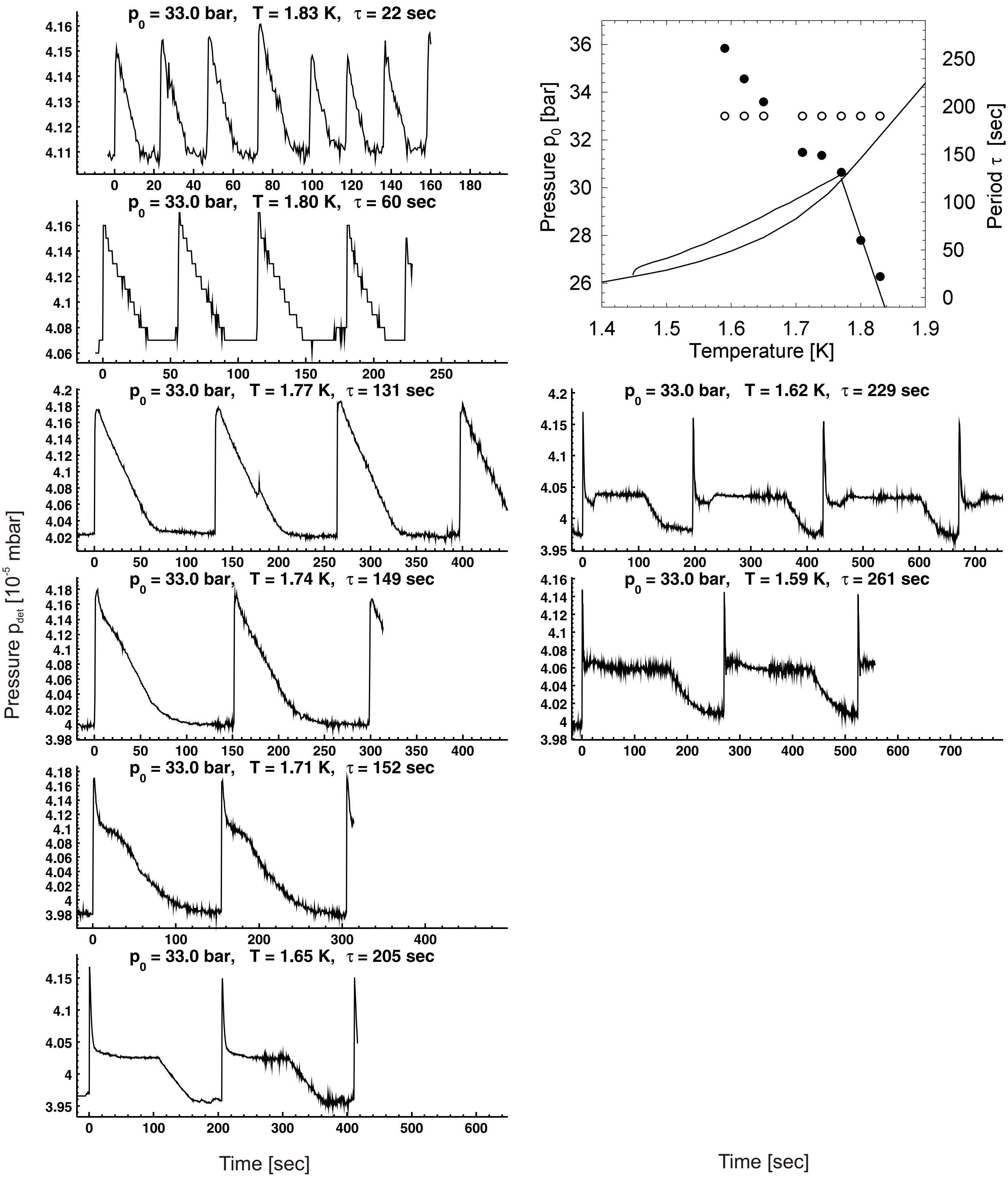

Figure C.22: Oscillating detector pressure p_{det} as a function of time for several temperatures T at constant source pressure p_0 = 33 bar. File: 030130 (2-10) ($d_0(\#17) = 2.28\ \mu$m)

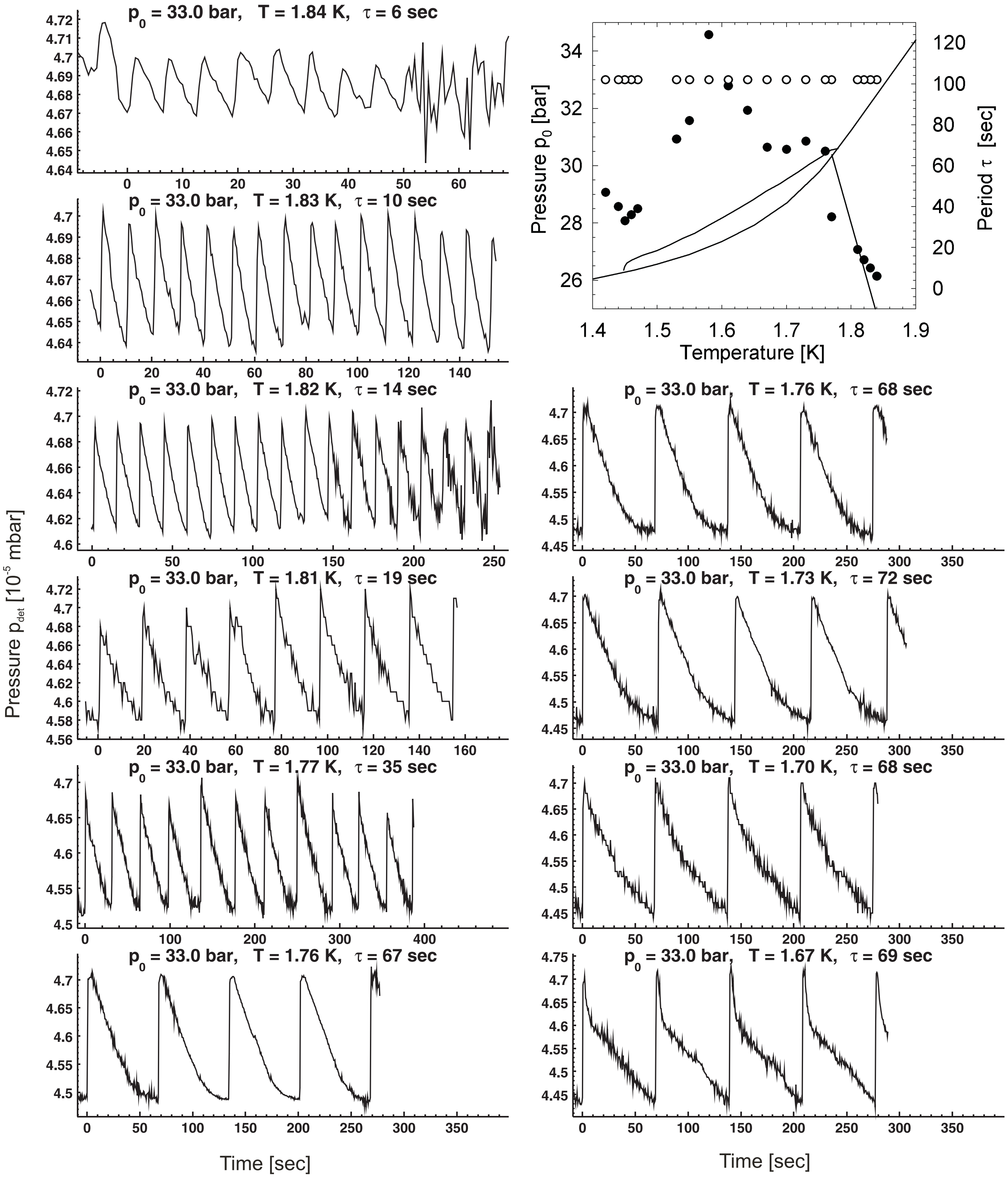

p_0 = 33.0 bar, T = 1.84 K, τ = 6 sec

p_0 = 33.0 bar, T = 1.83 K, τ = 10 sec

p_0 = 33.0 bar, T = 1.82 K, τ = 14 sec

p_0 = 33.0 bar, T = 1.81 K, τ = 19 sec

p_0 = 33.0 bar, T = 1.77 K, τ = 35 sec

p_0 = 33.0 bar, T = 1.76 K, τ = 67 sec

p_0 = 33.0 bar, T = 1.76 K, τ = 68 sec

p_0 = 33.0 bar, T = 1.73 K, τ = 72 sec

p_0 = 33.0 bar, T = 1.70 K, τ = 68 sec

p_0 = 33.0 bar, T = 1.67 K, τ = 69 sec

Figure C.23: Oscillating detector pressure p_{det} as a function of time for several temperatures T at constant source pressure p_0 = 33 bar. File: 031008 (2-28) ($d_0(\#20) = 2.07\ \mu$m)

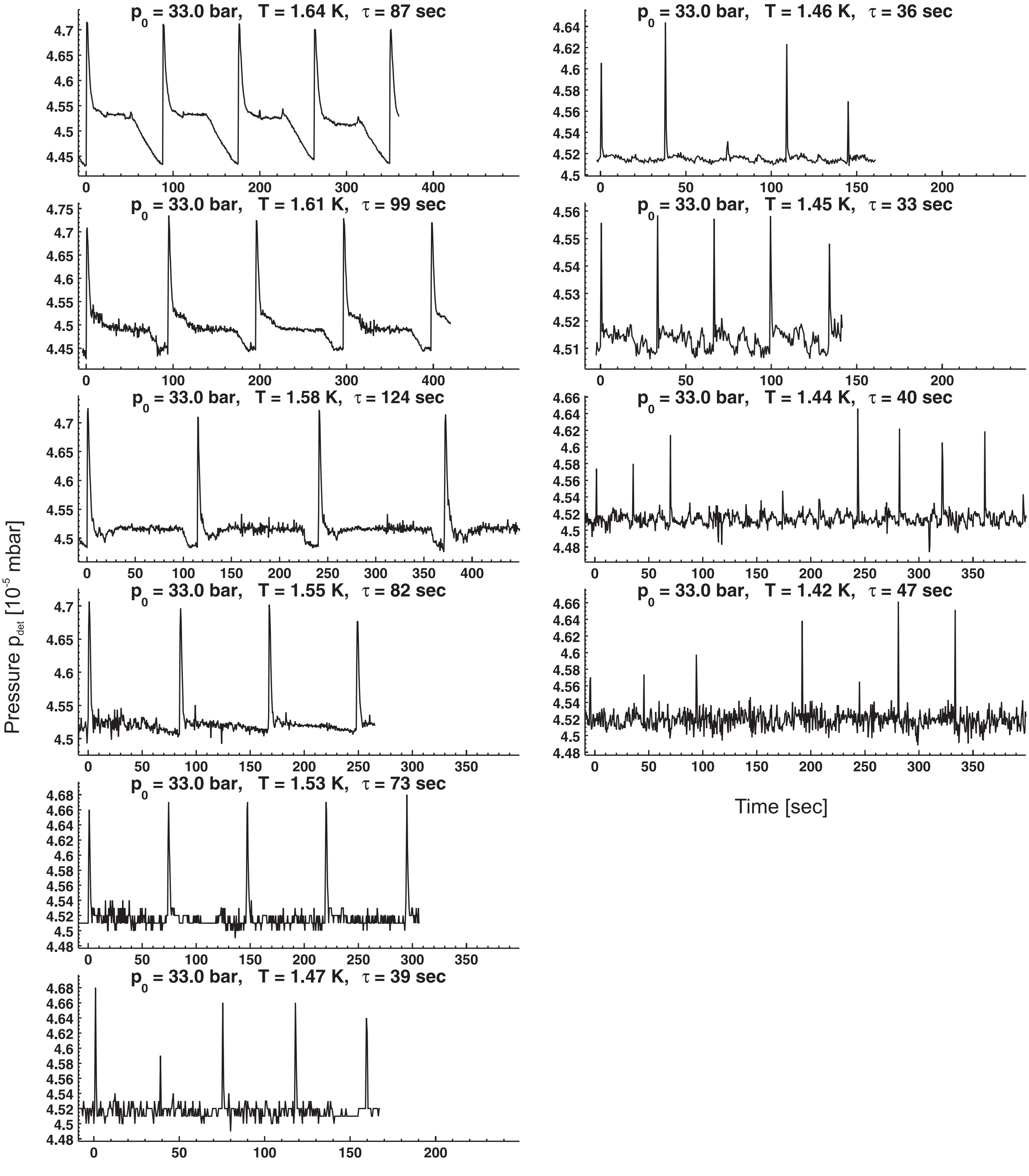

Figure C.24: Oscillating detector pressure p_{det} as a function of time for several temperatures T at constant source pressure $p_0 = 33$ bar. File: 031008 (2-28) ($d_0(\#20) = 2.07\ \mu$m)

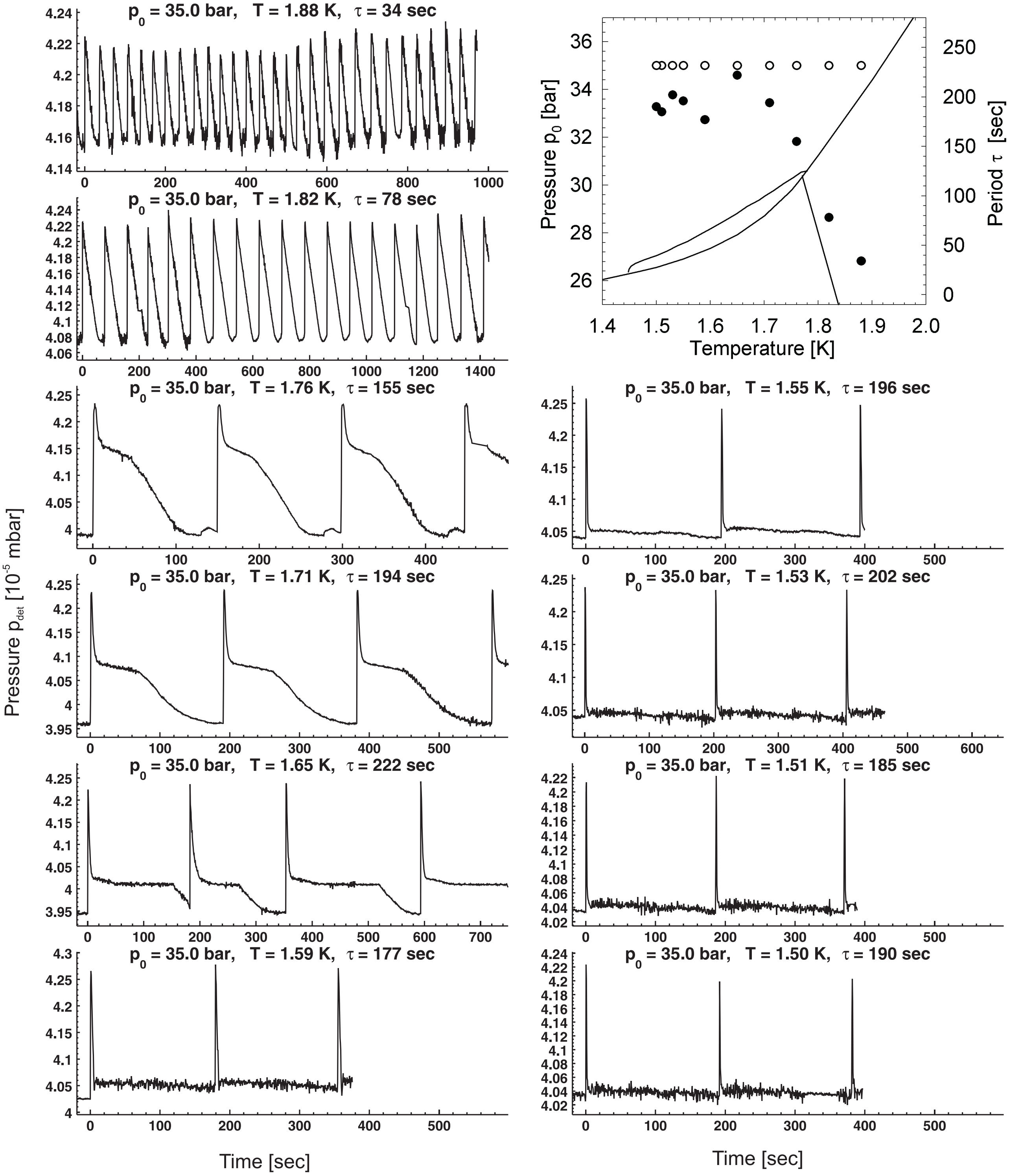

Figure C.25: Oscillating detector pressure p_{det} as a function of time for several temperatures T at constant source pressure p_0 = 35 bar. File: 030124 (30-45) ($d_0(\#17) = 2.28\ \mu$m)

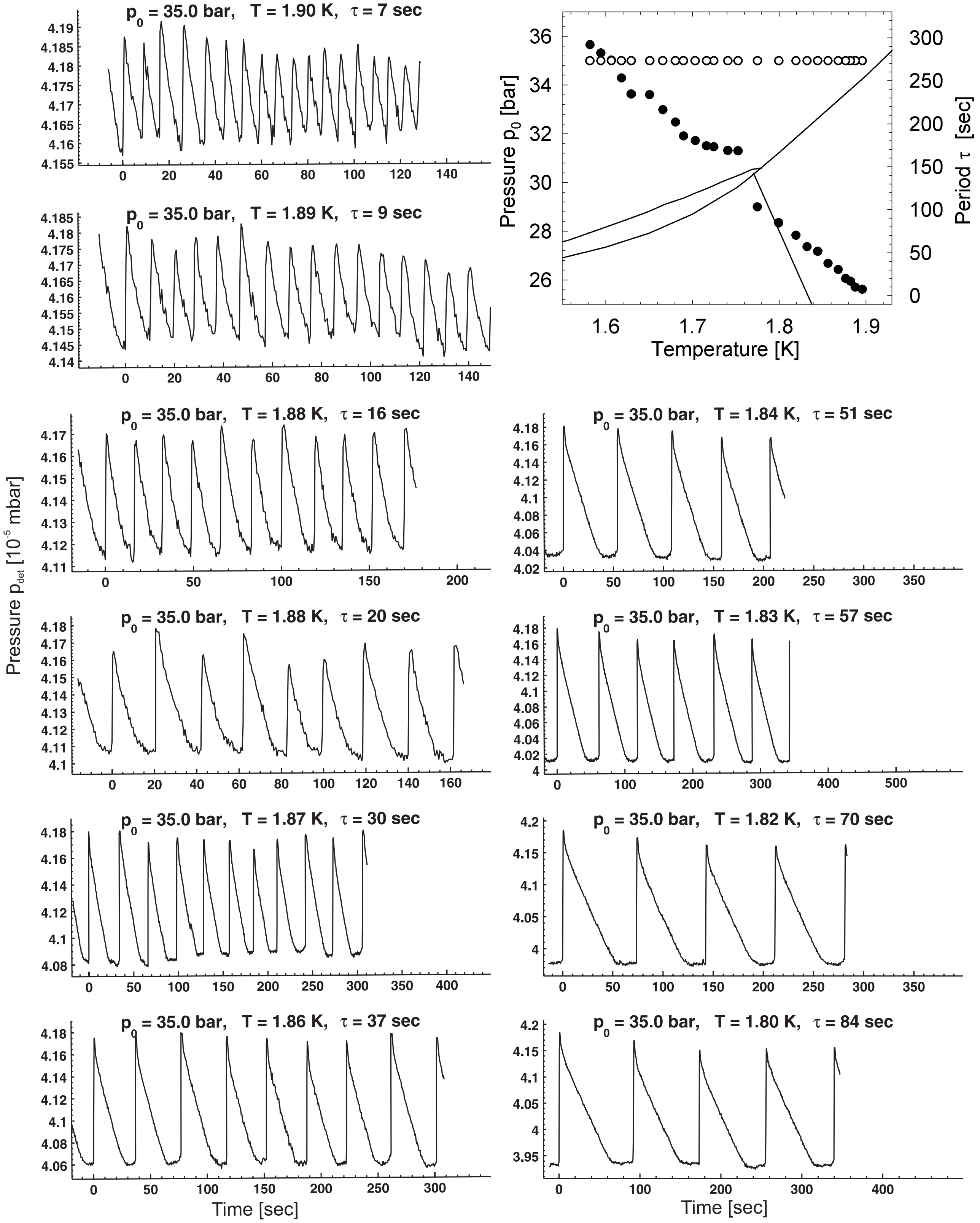

Figure C.26: Oscillating detector pressure p_{det} as a function of time for several temperatures T at constant source pressure $p_0 = 35$ bar. File: 030305 (2-34) ($d_0(\#17) = 2.28\ \mu$m)

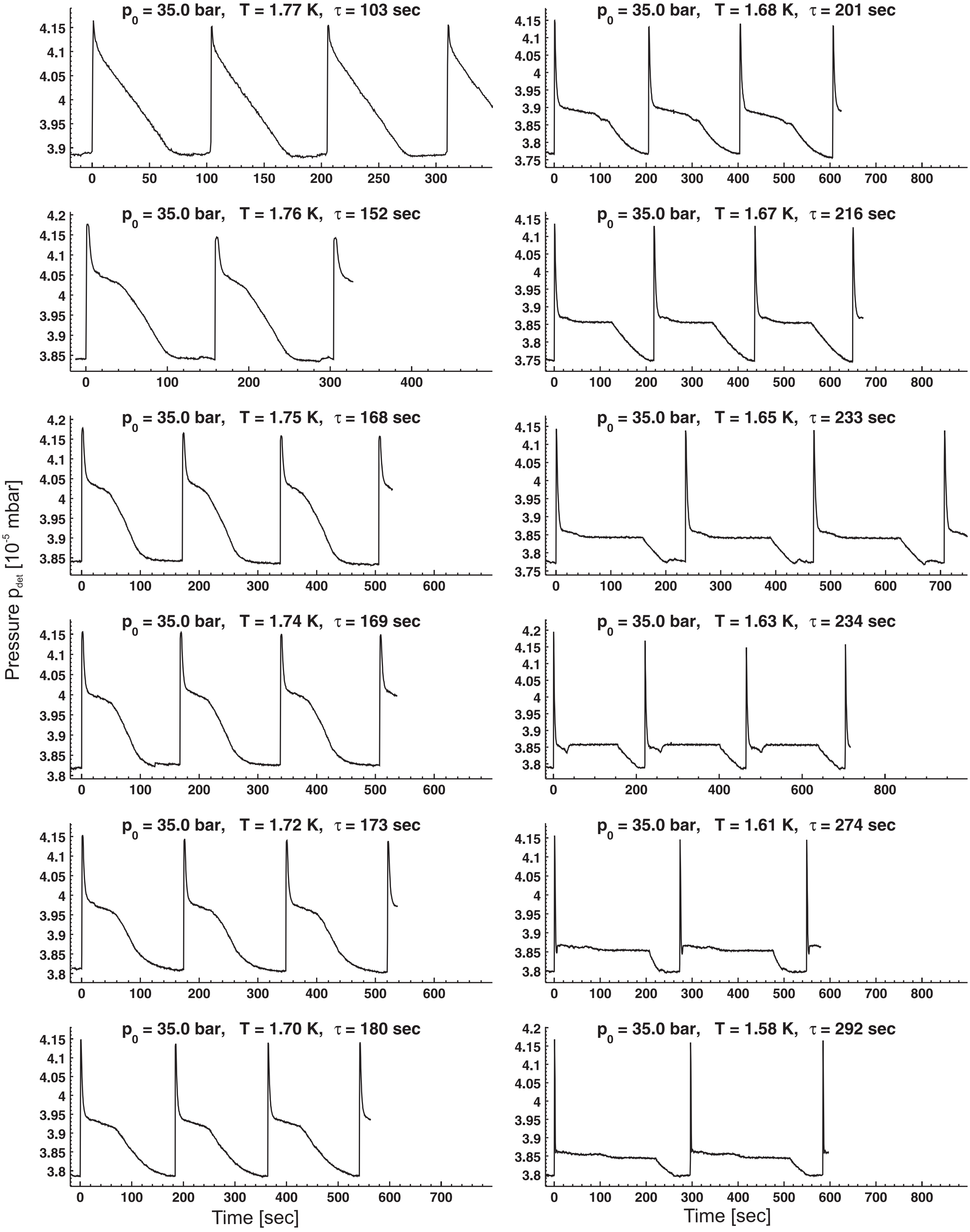

Figure C.27: Oscillating detector pressure p_{det} as a function of time for several temperatures T at constant source pressure p_0 = 35 bar. File: 030305 (2-34) ($d_0(\#17) = 2.28\ \mu$m)

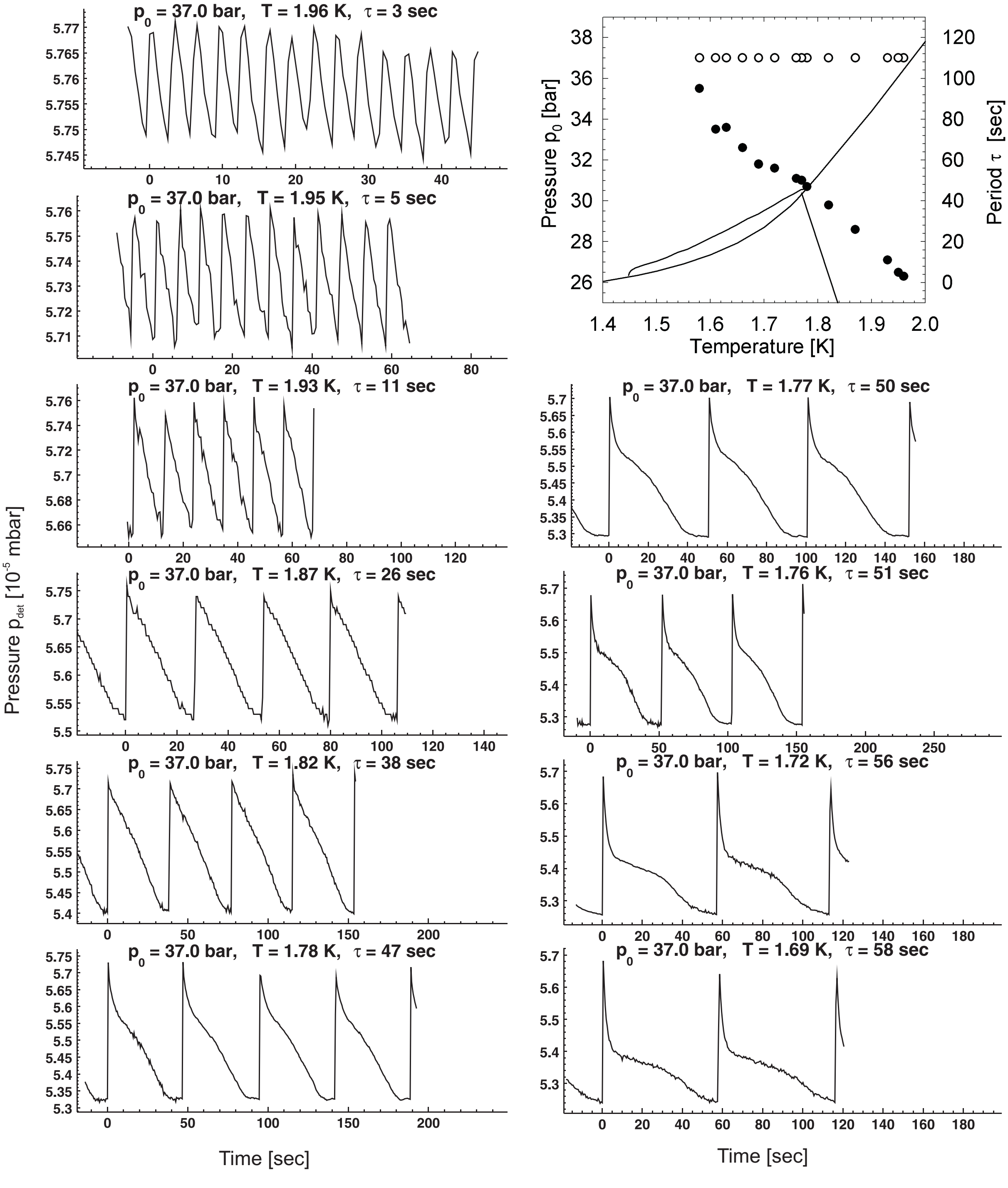

Figure C.28: Oscillating detector pressure p_{det} as a function of time for several temperatures T at constant source pressure p_0 = 37 bar. File: 030307 (2-15) ($d_0(\#18) = 2.9\ \mu$m)

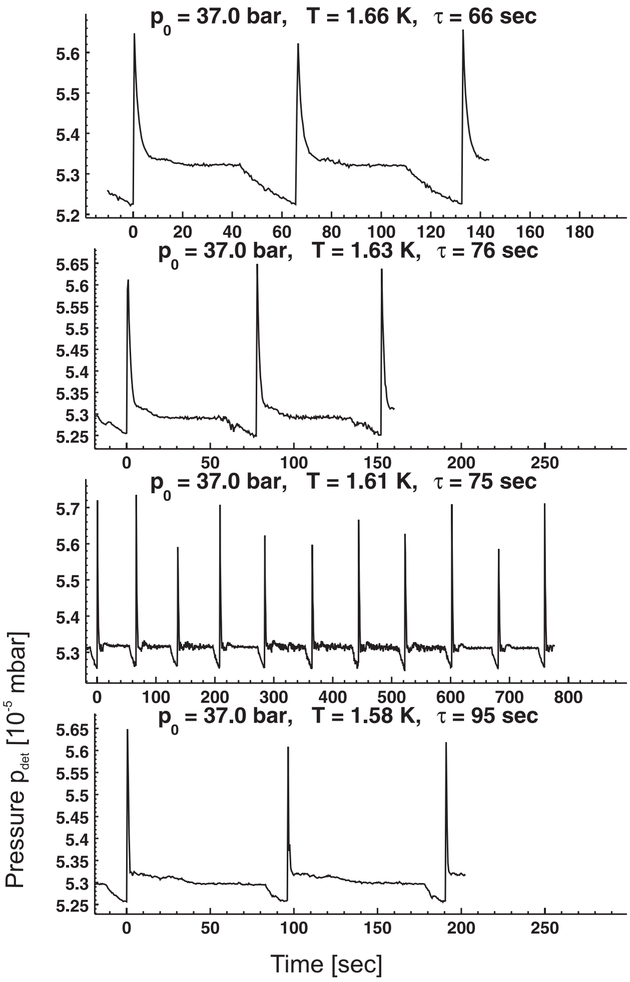

Figure C.29: Oscillating detector pressure p_{det} as a function of time for several temperatures T at constant source pressure p_0 = 37 bar. File: 030307 (2-15) ($d_0(\#17) = 2.28\ \mu$m)

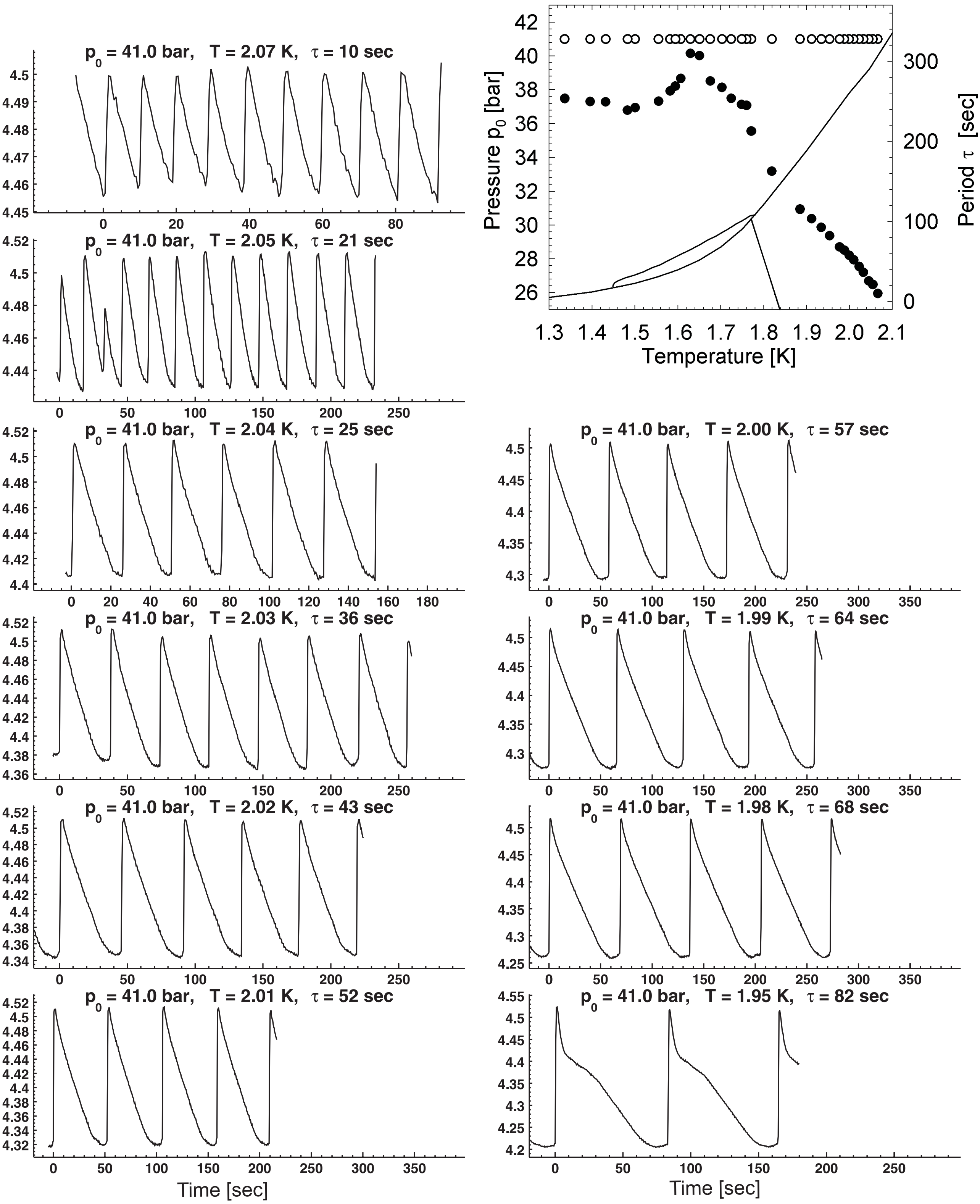

Figure C.30: Oscillating detector pressure p_{det} as a function of time for several temperatures T at constant source pressure p_0 = 41 bar. File: 030305 (34-67) ($d_0(\#17) = 2.28\ \mu$m)

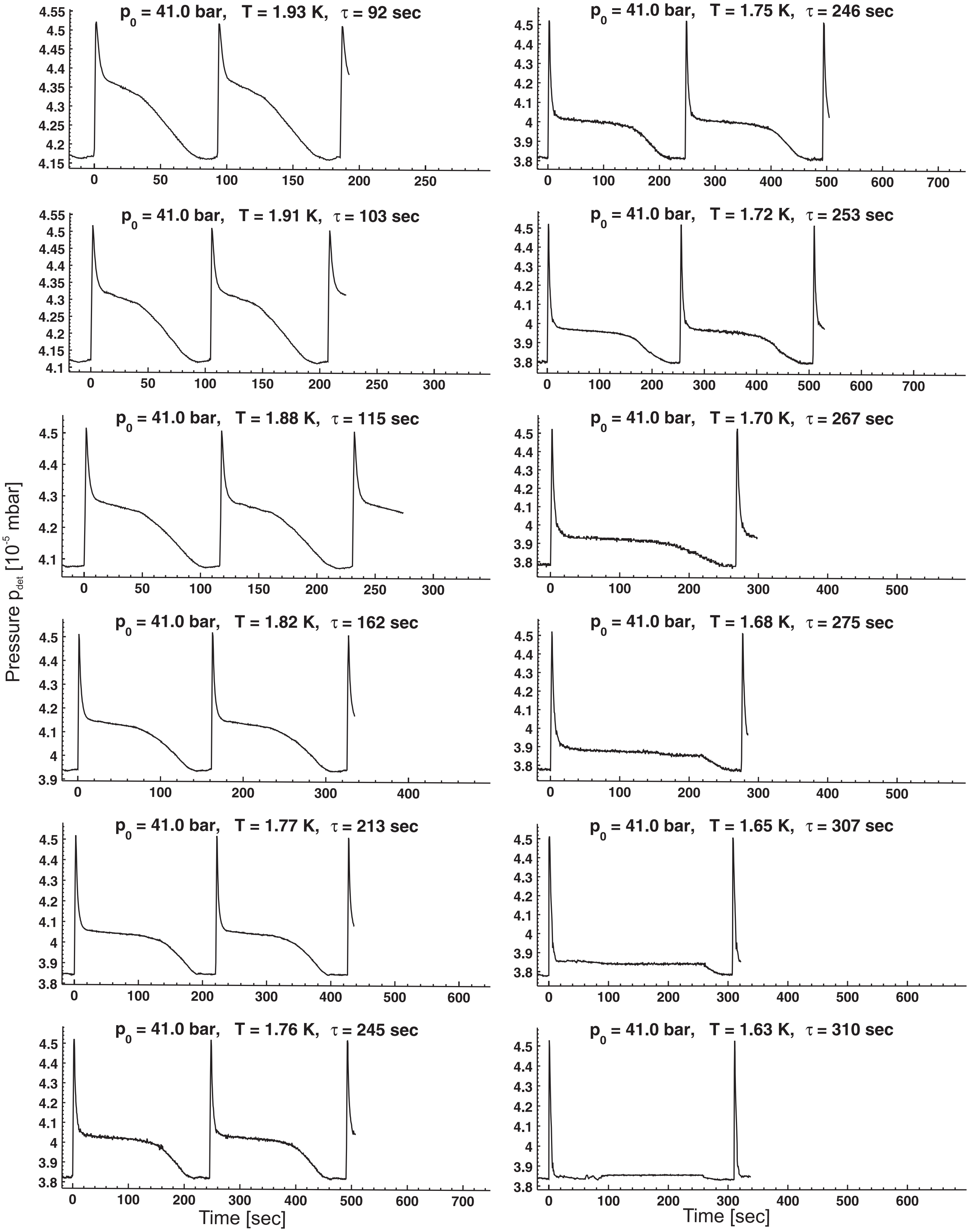

Figure C.31: Oscillating detector pressure p_{det} as a function of time for several temperatures T at constant source pressure $p_0 = 41$ bar. File: 030305 (34-67) ($d_0(\#17) = 2.28\ \mu$m)

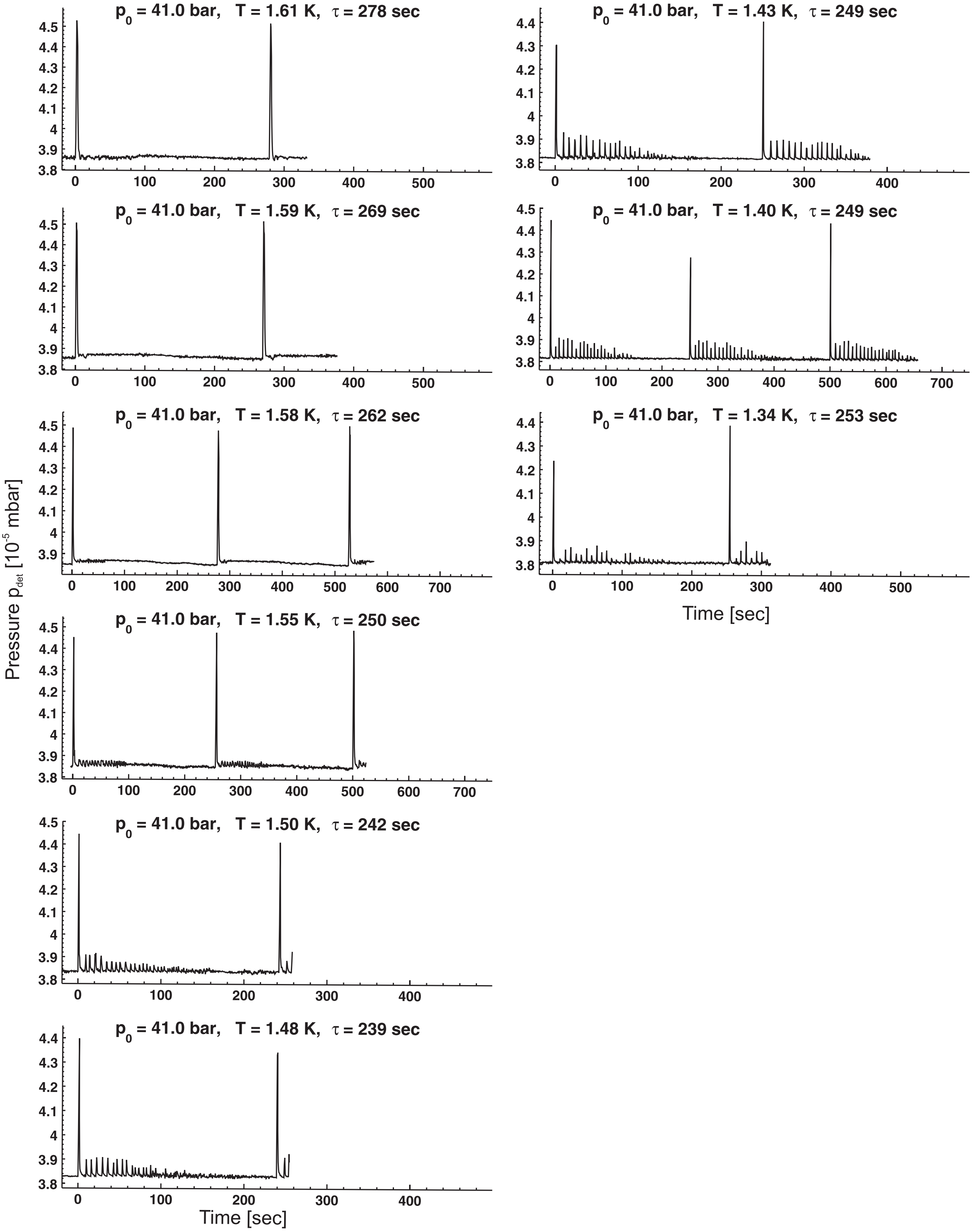

Figure C.32: Oscillating detector pressure p_{det} as a function of time for several temperatures T at constant source pressure $p_0 = 41$ bar. File: 030305 (34-67) ($d_0(\#17) = 2.28\ \mu$m)

Appendix D

Overview of the Used Nozzles

During the experiments nozzles with different diameters d_0 have been used. In table D.1 the corresponding nozzle diameters are summarized. The nozzles are indicated with an consecutive index depending on the date of mounting. Beside the nozzle diameter d_0 given by producers the calibrated nozzle diameter derived with equation 5.7 is shown. The pipettes (#1 - #3) were not used to investigate the Geyser oscillations, but for the investigations of the liquid beam [64] and are included because of completeness. The both nozzles #31 and #32 had a larger aspect ratio with a tube length of ≈ 100 μm. Using this nozzles the periodic effect could be seen, whereas the period behave differently than obtained with the standard nozzles by Rofin.

Index	d_0 [μm]	d_0 [μm] (calibr.)	Type	mounted
01	2	2	Pipette	
02	2	2	Pipette	
03	2	2	Pipette	02.01.2002
04	5	5	Orifice	25.01.2002
05	2	clogged	Orifice	22.05.2002
06	2	2.2	Orifice	26.06.2002
07	2	1.9	Orifice	07.07.2002
08	2	1.86	Orifice	06.08.2002
09	3	3.01	Orifice	12.08.2002
10	3	3.7	Orifice	16.08.2002
11	3	3.47	Orifice	21.08.2002
12	1	0.96	Orifice	01.09.2002
13	2	2	Orifice	11.09.2002
14	2	2	Orifice	16.09.2002

Index	d_0 [μm]	d_0 [μm] (calibr.)	Type	mounted
14a	5	5	Orifice	06.11.2002
15	5	5	Orifice	20.11.2002
16	2	2	Orifice	26.11.2002
17	2	2.28	Orifice	23.01.2003
18	2	2.9	Orifice	07.03.2003
19	5	5	Orifice	12.03.2003
20	2	2.07	Orifice	02.10.2003
21	2	2.31	Orifice	13.10.2003
22	2	2.2	Orifice	16.10.2003
23	1	1.52	Orifice	26.01.2004
24	3	3.63	Orifice	09.02.2004
25	3	2.92	Orifice	11.02.2004
25a	1	1.4	Orifice	29.03.2004
26	1	1.3	Orifice	02.04.2004
27	2	1.81	Orifice	06.04.2004
28	2	1.78	Orifice	20.07.2004
29	2	2.75	Orifice	26.07.2004
30	2	2.4	Orifice	28.07.2004
31	2	3.1	Tube	17.08.2004
32	1	1.4	Tube	18.08.2004
33	3	3.4	Orifice	19.08.2004
34	3	3.4	Orifice	25.08.2004
34a	2	2.4	Orifice	26.08.2004
35	1	1.39	Orifice	27.08.2004

Table D.1: Overview of the mounted nozzles during the experiments. The nozzles are indicated with an consecutive index. The Geyser effect was not investigated with pipettes #1-#3. The used nozzles #31 and #32 had a larger aspect ratio with a tube length of ≈ 100 μm. The periodic effect was observable whereas the period τ did not match with the period obtained with the other nozzles.

Bibliography

[1] A.R. Allen, M.G. Richards, *Int. Quant. Cryst. Conf. Fort Collins, Colorado* p. C-83.

[2] A.F. Andreev, Keshishev, L. Mezhov-Deglin, A. Shal'nikov, *Soviet Physics JETP. Lett.* Vol. **9** , 309 (1969)

[3] A.F. Andreev, I.E. Lifshitz: Quantum theory of defects in crystals, *Zh. Eksp. Teor. Fiz.* Vol. **29**, 6 (1969)

[4] A.F. Andreev: Quantum crystals, *Progress in Low Temp Physics* Vol. **8** Chap. 2 (1982)

[5] G. Baskaran: A quiet flow in supersolid Helium-4, *ArXiv:cond-mat.* No. **0505160 v1** (2005)

[6] J. Beamish: Supersolid Helium, *Nature*, Vol. **427**, 204-205 (2004)

[7] J.R. Hikata, A. Hikata, L. Tell, C. Elbaum: Solidifaction and superfluidity of Helium-4 in porpous vycor glass, *Phys. Rev. Lett.* Vol. **50**, 425-428 (1983)

[8] G. Benedek: private communication (2002)

[9] G. Benedek: private communication (2004)

[10] G. Benedek, F. Dalfovo, R.E. Grisenti, M. Käsz, J.P. Toennies: Oscillations in the expansion of solid ^{4}He into vacuum *Phys. Rev. Lett.* Vol. **95**, 095301 (2005)

[11] G. Benedek, R.E. Grisenti, M. Käsz, J.P. Toennies: In Search of ^{4}He Supersolid, *Bull. Cl. Sci. Acad. Royal Belg.* Vol. **101**, 35 (2005)

[12] I. Berent, E. Polturak: Critical behavior of the shear resistance of solid Helium-4 near a structural phase transition, *Phys. Rev. Lett.* Vol. **81**, 4 (1998)

[13] I. Berent, E. Polturak: Self diffusion in solid Helium-4 and ^3He-Helium-4-mixtures near the bcc-hcp phase transition, *J. Low Temp. Phys.* Vol. **112**, 5/6 (1998)

[14] B. Bernu, D.M. Ceperley: Path Integral Calculations of exchange in solid ^{4}He, ISSP9 conference proceedings, ed. H. Ishimoto, Elsevier (2005) and *ArXiv:cond-mat.* No. **0502486** (2005)

[15] M. Bijsma, H. Stoof: Collective Modes in Supersolid ^4He, *Phys. Rev. B* Vol. **56**, 14631 (1997)

[16] D.J. Bishop, M.A. Paalanen, J.D. Reppy: Search for superfluidity in hcp ^{4}He, *Phys. Rev. B* Vol. **24**, 2844-2845 (1981)

[17] D.J. Bukmann, J.M.J. van Leeuwen: Pressure and density of vacancies in solid Helium-4, *Phys. Rev. B* Vol. **49**, 1 (1994)

[18] C.A. Burns, J.M. Goodkind: Search for evidence of the influence of vacancies on the thermal conductivity of solid Helium-4, *J. Low Temp. Phys.* Vol. **93**, 1/2 (1993)

[19] C.A. Burns, J.M. Goodkind: The role of vacancies in solid Helium-4, *Physica B.* Vol. **194-196** (1994)

[20] E. Burovski, E. Kozik, A. Kuklov, N. Prokof'ev, B. Svistunov: Superfluid Interfaces in Quantum Solids, *Phys. Rev. Lett.* Vol. **94**, 165301 (2005)

[21] M. Boninsegni, N. Prokof'ev: Supersolid phase of hardcore bosons on triangular lattice, *Phys. Rev. Lett.* Vol. **95**, 237204 (2005)

[22] M. Boninsegni, N. Prokof'ev, B. Sustinov: Superglass Phase of ^{4}He,*Phys. Rev. Lett.* Vol. **96**, 105301 (2006)

[23] D.M. Ceperly, B. Bernu: Ring exchanges and the supersolid phase of Helium-4, *Phys. Rev. Lett.* Vol. **93**, 155303 (2004)

[24] B. Chaudhuri, F. Pederiva, G.V. Chester: Monte Carlo study of vacancies in the bcc and hcp phasese of ^{4}He, *Phys. Revi. B* Vol. **60**, 5 (2000)

[25] G.V. Chester: Speculations on Bose-Einstein condensation and quantum crystals, *Phys. Rev. A* Vol. **2**, 256–258 (1970)

[26] B.K. Clark, D.M. Ceperly: Off-Diagonal Long-Range Order in Solid ^{4}He, *Phys. Rev. Lett.* Vol. **96**, 105302 (2006)

[27] G.P. Collins: A Glimpse of Supersolid, *Scientific American* Jan.05 (2005)

[28] http://www.public.asu.edu/ scottv/Materials/Materials.html

[29] X. Dai, M. Ma, F.C. Zhang: Theory for supersolid Helium-4,*Phys. Rev. B* Vol. **72**, 132504 (2005)

[30] J. Day, T. Herman, J. Beamish: Freezing and Pressure-Driven Flow of Solid Helium in Vycor,*Phys. Rev. Lett.* Vol. **95**, 035301 (2005)

[31] J. Day, J. Beamish: Pressure-driven flow of solid Helium, *Phys. Rev. Lett.* Vol. **96**, 105304 (2006)

[32] J. de Boer, *Physica* Vol. **14**, 139 (1948)

[33] http://www.cartage.org.lb/en/themes/Sciences/Physics/SolidStatePhysics/AtomicBonding/CrystalStructure/Crystalline/Crystalline.htm

[34] http://www.tf.uni-kiel.de/matwis/amat/def_en/kap_5/illustr/dislocation_3dim.jpg

[35] A.T. Dorsay, P.M. Goldbart, J. Toner: Squeezing superfluid from a stone: Coupling superfluidity and elasticity in a supersolid,*ArXiv:cond-mat.* No. **0508271 v2** (2005)

[36] N.E. Dyumin, N.V. Zuev, S.V. Svatko, V.N.Grigor'ev: Rate of flow of bcc crystals of ^{4}He through a porous membrane , *Fiz. Nizk. Temp.* Vol. **17**, 895-898 (1991)

[37] N.E. Dyumin, N.H. Zuev, V.V. Boiko, and V.N. Grigor´ev,*Fiz. Nizk. Temp.* **19**, 980 (1993) [Engl. transl.: *J. Low Temp. Phys.* Vol. **19**, 696 (1993)]

[38] N.E. Dyumin, S.V. Svatko, N.V. Grigor´ev *Soviet Physics JETP* Vol. **15**, 295 (1998)

[39] C. Ebner, C.C. Sung: Vacancies and diffusion in solid hydrogen, *Phys. Rev. A* Vol. **5**, 6 (1972)

[40] http://www.engr.ku.edu/r̃hale/ae510/lecture2/sld029.htm

[41] A. Einstein: Von der molekulärkinetischen Theorie der Wärme gefordete Bewegung von in ruhenden Flüssigkeiten suspendierten Teilchen. *Annalen der Physik* Vol. **17**, 549–554 (1905)

[42] A. Einstein: Quantentheorie des einatomigen idealen Gases. Zweite Abhandlung. *Sitzungsber. Kgl. Preuss. Akad. Wiss.* Vol. **1925**, 3 (1925)

[43] A.E. Fick: Über Diffusion. *Annalen der Physik, Leipzig* Vol. **94**, 59–86 (1855)

[44] C.P. Flynn, A.M. Stonecham: Quantum Theory of Diffusion with Application to Light Interstitials in Metals, *Phys. Rev. B* Vol. **1**, 3966 (1970)

[45] B.A. Fraas, P.R. Granfors, R.O. Simmons: X-ray measurements of thermal vacancies in hcp Helium-4, *Phys. Rev. B* Vol. **39**, 1 (1989)

[46] A. Frohn, N. Roth: Dynamics of Droplets, *Springer* (2000)

[47] D.E. Galli, L. Reatto: Vacancies in solid Helium-4 and Bose Einstein condensation , *J. Low Temp. Phys.* Vol. **124**, 1/2, pp. 197-207(11) (2001)

[48] D.E. Galli, L. Reatto: Vacancy excitation spectrum in solid Helium-4 and longitudinal phonons , *Phys. Rev. Lett.* Vol. **90**, 17 (2003)

[49] D.E. Galli, L. Reatto: Bose-Einstein condensation in solid ^4He,*Phys. Rev. B* Vol. **71**, 140506(R) (2005)

[50] D.E. Galli, L. Reatto: Bose Einstein Condensation of incommensurate solid ^{4}He, *ArXiv:cond-mat.* No. **0602055 v1** (2006)

[51] V.Ginzburg, A. Sobyanin: Can liquid molecular hydrogen be superfluid?, *JETP Lett.* Vol. **15** , 242 (1972)

[52] H.R. Glyde: Excitations in liquid and solid Helium, *Clarendon Press, Oxford* (1994)

[53] H.A. Goldberg, R.A. Guyer: Vacancy motion in solid Helium ,*J. Low Temp. Phys.* Vol. **28**, 5/6 (1977)

[54] E. B. Gordon, A. Usenko, G. Frossati: Embedding Impurities Into Solid Helium, *J. Low Temp. Phys.* Vol. **130**, 15 (2003)

[55] N. Gov, E. Polturak: Local modes, phonons, and mass transport in sold Helium-4, *Phys. Rev. B* Vol. **60**, 2 (1999)

[56] M.P. Grams: Novel cryogenic sources for liquid droplet and solid filament beams, *Thesis work* (2005)

[57] M.P. Grams, B. Stasicki, J.P. Toennies: Production and characterization of micron-sized filaments of solid argon,*Review of Scientific Instruments* Vol. **76**(12), 23904 (2005)

[58] M.P. Grams, J. Turner, A.M. Cook, R.B. Doak: Microscopic Fused Silica Capillary Nozzles as Supersonic Molecular Beam Sources, Vol. **Journal of Physics D: Applied Physics** Vol.**39** 930-936 (2006)

[59] P.R. Granfors, B.A. Fraass, R.O. Simmons: Direct measurements of thermal vacancies in bcc Helium-4, *J. Low Temp. Phys.* Vol. **11167**, 5/6 (1987)

[60] S. Grebenev, B. Sartakov, J.P. Toennies, A.F. Vilesov: Evidence for Superfluidity in Para-Hydrogen Clusters Inside Helium-4 Droplets at 0.15 Kelvin, *Science* Vol. **289** (5484), 1532–1535 (2000)

[61] D.S. Greywall: Search for superfluidity in solid Helium-4, *Phys. Rev. B* Vol. **16** , 3 (1977)

[62] V.V. Grigorev, B.N. Eselson, V.A. Mikheev, *Sov. Phys. JEPT* Vol. **39**, 153 (1974)

[63] R.E. Grisenti: Estimation of the nozzle orifice diameter, unpublished (2003)

[64] R.E. Grisenti, J.P. Toennies: Cryogenic microjet source for orthotropic beams of ultralarge superfluid helium droplets, *Phys. Rev. Lett.* Vol. **90**, 234501 (2003)

[65] R.E. Grisenti, private communication (2004)

[66] R.E. Grisenti, R.A. Costa Fraga, N. Petridis, R. Dörner, J. Deppe: Cryogenic microjet for exploration of superfluidity in highly supercooled molecular hydrogen, *Europhys. Lett.* Vol. **73 (4)**, pp. 540-546 (2006)

[67] R.A. Guyer: Vacancy waves, *J. Low Temp. Phys.* Vol. **8**, 5/6 (1972)

[68] C. Herring: Diffusional viscosity of a polycrystalline solid, *J. Appl. Phys.* Vol. **21**, 437 (1950)

[69] Th. Hehenkamp, W. Berger, J.–E. Kluin, Ch. Lüdecke, and J. Wolff: Equilibrium vacancy concentrations in copper investigated with the absolute technique, *Phys. Rev. B* Vol. **45**, 1998–2003 (1992)

[70] V. Hyzhnyakov, G. Benedek: Quantum diffusion: effect of defect-localized phonon dynamics, *Eur. Phys. Journ. B* Vol. **43**, 431-438 (2005)

[71] P. Kapitza: The study of heat transfer in helium II, *J. Phys. (USSR)* Vol. **4** 181-210 (1941)

[72] W.E. Keller: Helium-3 and Helium-4, *Plenum Press New York* (1969)

[73] S.A. Khairallah, D.M. Ceperley: Superfluidity of Dense ^{4}He in Vycor, *Phys. Rev. Lett.* Vol. **95**, 185301 (2005)

[74] V.V. Khmelenko, S.I. Kiselev, D.M. Lee, C.Y. Lee: Impurity-Helium solids - Quantum Gels? *Physica Scripta* Vol. **102**, 118-127 (2002)

[75] E. Kim, H.W. Chan: Probable observation of a supersolid Helium phase , *Nature* Vol. **427**, 225 (2004)

[76] E. Kim, H.W. Chan: Observation of superflow in solid Helium, *Science* Vol. **305**, 5692 (2004)

[77] E. Kim, H.W. Chan, talk at the March 2005 Meeting of the American Physical Society. Also reported in *Science* Vol. **308**, 190 (2005)

[78] http://www.sciam.com/media/inline/000D26B6-0A03-11BF-AD0683414B7F0000_1.jpg

[79] S.I. Kiselev, V.V. Khmelenko, D.M. Lee: Structural studies of impurity-helium solids, *Phys. Rev. B* , Vol. **65**, 024517 (2001)

[80] E.G. Kisvarsanyi, N.S. Sullivan: Quantum diffusion of ^{3}He impurities in solid ^{4}He *Phys. Rev. B* Vol. **48**, 22 (1993)

[81] E.G. Kisvarsanyi, N.S. Sullivan: Quantum tunneling in solid D_2 and solid H_2 *Phys. Rev. B* Vol. **51**, 6 (1995)

[82] S. Koh: Non-classical rotational intertia in the supersolid state, *ArXiv:cond-mat.* No. **0411713 v1** (2004)

[83] D. L. Kovrizhin, G. Venketeswara, S. Sinha: Density wave and supersolid phases of correlated bosons in an optical lattice,*EPL* Vol. **72**, 162 (2005)

[84] N. Kumar: Supersolid and the non-uniform condensate, *ArXiv:cond-mat.* No. **0507553** (2005)

[85] Labview software by National instruments, *http://www.ni.com/labview/*

[86] T. Leggett: Superfluidity in a Crystal? *Science* Vol. **305**, 5692, pp. 1921 - 1922 (2004)

[87] A.J. Leggett: Can a solid be a "superfluid"? *Phys. Rev. Lett.* Vol. **25**, 22 (1970)

[88] G.A. Lengua, J.M. Goodkind: Elementary excitations and a collective mode in hcp ^{4}He, *J. Low Temp. Phys.* Vol. **79**, 251 (1990)

[89] V. Lubchenko: Can a Solid be a Superfluid? *Term Paper for physics* Vol. **463** (1999)

[90] A.T. Macrander: Constant-volume x-ray study of solid argon and solid krypton, *Phys. Rev. B* Vol. **21**, 6 (1980)

[91] T. Markovich, E.Polturak, J.Bossy, E.Fahri: Observation of a new excitation in bcc Helium-4 by inelastic neutron scattering, *Phys. Rev. Lett.* Vol. **88**, 19 (2002)

[92] V.A. Mikheev, B.N. Esel´son, V.N. Grigorev, N.P. Mikhin, *Fiz. Nizk. Temp.* Vol. **3**, 385 (1977)

[93] D, S, Miyosho, R.M. Otts, A.S. Greenberg, R.C. Richardson: Nuclear Magnetic Resonance in Solid Helium-3—Helium-4 Mixtures between 0.3 and 2.0 °K, *Phys. Rev. A* Vol. **2**, 870 (1970)

[94] F.R.N. Nabarro, Report of a conference on the strenght of solids, *Physical Society London*, page **75** (1948)

[95] J.V. Pearce, J. Bossy, H. Schober, H.R. Glyde, D.R. Daughton, N. Mulders: Excitations of metastable superfluid ^{4}He at pressures up to 40 bar, *Phys. Rev. Lett.* Vol. **93**, 145303 (2004)

[96] O. Penrose, L. Onsager: Bose-Einstein Condensation and Liquid Helium, *Phys. Rev.* Vol. **104**, 576 (1956)

[97] E. Polturak, I. Schuster, I. Berent, Y. Carmi, S. Lipson, B. Chabaud: NMR, Optical, and Plastic flow Experiments in bcc ^{3}He-^{4}He Mixture Crystals - in Pursuit of Vacancy Fluid, *J. Low Temp. Phys.* Vol. **101**, 1/2 (1995)

[98] E. Polturak, A. Kanigel, N. Gov, T. Markovich, J. Adler: The role of point defects in melting of solid He, *Physica B* Vol. **280**, 142-145 (2000)

[99] E. Polturak, N. Gov: Inside a quantum solid, *Contemporary Physics* Vol. **44**, 2 (2003)

[100] N. Prokof'ev and B. Svistunov: On the Supersolid State of Matter, *ArXiv:cond-mat.* No. **409472** (2004)

[101] D. I. Pushkarov: Quantum diffusion, *ArXiv:cond-mat.* No. **0310283 v1** (2003)

[102] R.C. Reid,J.M. Prausnitz, B.E. Poling: Diffusion coefficients. The Properties of Gases and Liquids *New York: McGraw-Hill, Fourth Edition*, p. **577-631** (1987)

[103] Rofin-Sinar Technologies Inc. , MI 48170, USA, *http://www.rofin.com/index-e.htm*

[104] M. Rossi, D. E. Galli, L. Reatto: Layer by layer solidification of ^{4}He in narrow porous media, *Phys. Rev. B* Vol. **72**, 064516 (2005)

[105] M.G. Rozman, M. Urbakh, J. Klafter, *Phys. Rev. Lett.* Vol. **77**, 683 (1996)

[106] D.J. Sanders, H. Kwun, A. Hikata, C. Elbaum: Plastic deformation of bcc Helium-4, *Phys. Rev. Lett.* Vol. **40**, 7 (1977)

[107] W.M. Saslow: Superflow in Solid Helium-4, *ArXiv:cond-mat.* No. **0407166 v1** (2004)

[108] W.M. Saslow: Superfluidity of periodic solids, *Phys. Rev. Lett.* Vol. **36**, 19 (1976)

[109] W.M. Saslow, S. Jolad: Supersolid ^{4}He Likely Has Nearly Isotropic Superflow, *ArXiv:cond-mat.* No. **0511214 v1** (2005)

[110] I. Schuster, Y. Swirsky, E.J. Schmidt, E.Polturak, S.G. Lipson: Observation of rapid atomic motion in solid ^{3}He-^{4}He mixtures using NMR, *Europhys. Lett.* Vol. **33**, pp. 623-628 (1998)

[111] L.A. Schwalbe: Equilibrium vacancy concentration measurement in solid argon, *Phys. Rev. B* Vol. **14**, 4 (1975)

[112] K. Shirahama: Observation of NCRI in bulk solid ^{4}He confined to a cylindrical cavity, *talk at the KITP Miniprogram: The Supersolid State of Matter* (2006)

[113] R.O. Simmons: Thermal vacancies in quantum solid Helium, *J. Phys. Chem. Solids* Vol. **55** , 10, 895-906 (1994)

[114] R.O. Simmons: Defects in noble gas crystals, *Material chemistry and physics* Vol. **50**, 124-132 (1997)

[115] D.T. Son: Effective Lagrangian and Topological Interactions in Supersolids, *Phys.Rev.Lett.* Vol. **94**, 175301 (2005)

[116] B. Sustinov: From Superfluid Interfaces to Superglass, *talk at the KITP Miniprogram: The Supersolid State of Matter* (2006)

[117] H. Suzuki: Plastic flow in solid Helium, *Journ. phys. soc. Japan* Vol. **35**, 5 (1973)

[118] K.T. Tang, J.P. Toennies: The van der Waals potentials between all the rare gas atoms from He to Rn, *Journal of Chemical Physics* Vol. **118**, 11 (2002)

[119] D.R. Tilley, J. Tilley: Superfluidity and superconductivity, third edition, *Institute of physics publishing Bristol and Philadelphia* (1990)

[120] M. Tiwari, A. Datta: Supersolid Phase in Helium-4,*ArXiv:cond-mat.* No. **0406124 v1** (2004)

[121] J.P. Toennies: Flow of solid Helium through narrow constrictions, *talk at the KITP Miniprogram: The Supersolid State of Matter* (2006)

[122] http://www.jlab.org/c̃keith/TOOLS/HeVaporTable.html

[123] J.H. Vignos, H.A. Fairbank: New solid phase in Helium-4, *Phys. Rev. Lett.* Vol. **6**, 6 (1961)

[124] D.S. Weiss: A new framework for understanding supersolidity in Helium-4, *ArXiv:cond-mat.* No. **0407043** (2004)

[125] S. Wessel, M. Troyer: Supersolid hardcore bosons on the triangular lattice, *Phys. Rev. Lett.* Vol. **97**, 127205 (2005)

[126] J.S. Wettlaufer: Supersolid or melted superfluid film?, http://www.physorg.com/news4562.html (2005)

[127] B.D. Wirth: Point defects, *Nuclear engineering, lecture script* Chapter **3** Department of Nuclear Engineering, Berkeley (2004/2005)

[128] H. Zhai, Y.S. Wu: Condensation of Zero-Point Lattice vibrations and superfluidity in perfect crystals , *J. Stat. Mech.* No. **P07003** (2005)

[129] E. Zhao, A. Paramekanti: Excitations in correlated superfluids near a continuous transition into a supersolid, *Phys. Rev. Lett.* Vol. **96**, 105303 (2006)

[130] D. Zhou, C.M. Edwards, N.S. Sullivan: Quantum diffusion of vacancies and impurities in solid Hydrogen, *Phys. Rev.Lett.* Vol. **62**, 13 (1989)

[131] N.V. Zuev, V.V. Boiko, N.E. Dyumin, V.N. Grigorev: Investigation of vacancy diffusion in solid Helium, *J. Low Temp. Phys.* Vol. **111**, 3/4 (1998)

Index

Danksagung

Geschafft! Da steht es nun, mein Eigenheim! Was braucht es für ein wissenschaftliches Eigenheim? Eine Forschungsrichtung, sei es theoretischer oder experimenteller Natur. Dies wäre wohl der Bauplatz. Dann wäre eine Theorie wohl das nötige Kapital, der Architekt der Doktorvater, ein Kapitel wäre ein Zimmer und die Bilder der Arbeit zweifelsohne die Fenster.

Da stand ich nun also vor drei Jahren und träumte von einem Eigenheim. Also suchte ich mir ein Unternehmen, mit der ich dieses Vorhaben in die Tat umsetzen wollte. Und schließlich wurde ich am Institut für Kernphysik in der Gruppe von Reinhard Dörner fündig. Diese Firma schuf während meiner Zeit eindrucksvolle Gebilde, sei es die ICD-Arena oder den ersten Glockenturm mit Attosekundenzeiger!

Ein Bauplatz für mein Eigenheimprojekt war in Göttingen schnell gefunden, der sich als sehr fruchtbarer Boden herausstellte. Und in diesem Boden, da fand ich wahre Schätze! Aus diesem Grund brachte mich dort niemand mehr weg! Nun stehe ich vor diesem Haus und betrachte es zufrieden. Mit den letzten Handgriffen enststeht nun eine Gedenktafel, auf der ich mich bei Allen bedanken möchte, die mir beim Bau dieses Eigenheim geholfen haben:

Prof. Reinhard Dörner: Wenn es eine Arbeitsgruppe gab, in der ich wirklich doktorieren wollte, so war dies Deine Gruppe. Und obwohl ich von Delaylineanoden oder Ähnlichem gar keine Ahnung hatte, holtest Du mich an Bord, um mich verrückte Sachen erforschen zu lassen! Danke, dass Du mir das ermöglichst hast! Es heißt: Begeistern kann nur der, der selbst begeistert ist! Und nach diesen knapp vier Jahren bin ich begeistert!

Robert Grisenti: Wenn jemand eine verrückte Eissorte entdecken kann, dann wohl nur ein Italiener! Ich möchte Dir für die viele Geduld und die sehr impulsiven Gespräche danken, die mich immer wieder von Neuem für die Helium-Eiscreme haben begeistern können. Mehr noch! Danke für die schöne Zeit als Doktorrand und die gute Freundschaft! Robert: Dein Weg liegt ganz klar vor Dir, jetzt mußt Du ihn nur noch gehen!

I have to thank Prof. Giorgio Benedek, the most incredible and definitely kindest theoretician I‘ve ever met. I have to mention the remarkable achievement of Giorgio[1], to understand the complex mechanism of Helium-Icecream and to develop a model that works more than properly! For those who don‘t understand the background: One should try the following: Sniff on an exhaust of a car and explain, how such an combustion engine works without lifting the engine hood. Thanks for all the patience to introduce me into the world of the Geyser effect and your full-time hospitality in Milano!

Prof. J. Peter Toennies: Vielen Dank für die Möglichkeit im alteehrwürdigsten aller Max-Plack-Institute in Göttingen, der deutschen Hauptstadt der Physik, in die wun-

---

[1] (together with Franco Dalfovo : Unfortunetely, I‘v never met him. But we share the place on the authors list of the paper. Thus, Hi to Franco Dalfovo, my name is Manuel!)

derbare Welt der Physik zu erforschen. Hätten junge Menschen auch nur 10 Prozent ihres Forscherdrangs, so wären die Geheimnisse in der Natur Mangelware!

Prof. Horst Schmidt-Böcking: Dein Prinzip von "Geht nicht-Gibt's nicht" beeindruckt die Menschen immer wieder. Dabei schaffen sich die Menschen doch nur ihre eigenen Grenzen. Und Du reißt diese Grenzen immer wieder ein! Davon kann ich lernen! Es würde mich nicht wundern, wenn einmal jemand in Stockholm mit den Worten beginnt: Mein ganz besonderer Dank gilt Prof. Horst Schmidt-Böcking.

Jens Pick-Nowack: Dein Engagement und Deine Hilfsbereitschaft haben im ganz großen Maße zum Gelingen dieses Experiments beigetragen. Du warst ein ganz großer Grund dafür, dass ich mich in Göttingen immer sehr wohl gefühlt habe. Dafür, und für Vieles mehr möchte ich mich bei Dir ganz herzlich bedanken!

Achim Czasch: Du hast in jeder Hinsicht meinen tiefen Dank verdienst, sei es die spontane Aufopferung, mein Leid bei der Konfrontation mit meinem Laptop zu lindern, oder aber für die Korrekturen meiner Arbeit. Für eines aber bin ich besonders dankbar: Die Freundschaft und die gnadenlos gute Stimmung in unserem Zimmer! Ganz besonders möchte ich mich auch bei Tanja bedanken, die mir mit vollem Bauch und viel Gedult über die letzten Hürden der Arbeit geholfen hat. Euch Beiden wünsche ich alles erdenklich Gute, auch zum Quadrat!

Sven Schössler: Ich warte immer noch auf ein Problem, welches Du nicht lösen kannst! Deine Hilfsbereitschaft ist schon legendär! Sven, ohne Dich - und das können ganz sicher Viele sagen - hätte ich besonders in den letzten Zügen der Arbeit vor einem tiefen Abgrund gestanden! Neben Deinem bedingungslosen Einsatz zur Rettung unseres Planeten und Deiner helfenden Hand schätze ich in keinem geringeren Maße die vielen lustigen Smalltalks zwischendurch!

Markus Schöffler: Gemeinsam kommt man auch bei langen und sich windenden Strassen irgendwann ans Ziel! Auch wenn sich das Ziel manchmal mit rasender Geschwindigkeit von uns wegbewegt hat, so haben sich unsere gegenseitigen Motivationsausbrüche doch gelohnt! Und wie schnell kann Euphorie auch in völliger Verzweiflung enden...

November 2005: *... Meine Arbeit ist irgendwie noch eine einzige Baustelle! Und ich träume noch davon, in diesem Jahr einziehen zu können. Kein einziger Raum (Kapitel) ist wirklich bezugsfertig. Ok, Fenster (Bilder) sind schon eingesetzt, Strom und Wasser fließen mehr schlecht als recht (roter Faden). Aber es pfeift noch durch alle Ritzen hindurch (Sprache), und das Dach ist auch noch nicht fertig (Auswertung, Zusammenfassung und Anhang). Und wenn der Architekt erst mal das Bauwerk inspiziert, dann rollen die Bagger wieder. Aber dieses mal kommen sie nicht mit der Schaufel, sondern mit der Abrißbirne! Ich brenne die Bruchbude ab! Dann wärme ich mich, und denke an meine kleine Wohnung (Diplom) in der andere auch glücklich geworden sind! Wer braucht schon ein Eigenheim? Aber kennst Du unseren Ansporn? Ab nächstem Jahr fällt die Eigenheimzulage weg! Also weiter Markus! ...*

Durch die Fenster habe ich einen fantastischen Blick auf die Natur. Und ich kann Dir sagen, der Ausblick ist wunderschön! Und ich stehe hier nun am Ende einer langen Reise und erwarte ungeduldig Deinen Zieleinlauf!

Mehr als ein Dankeschön geht an unsere Arbeitsgruppe: Ok, machen wir es kurz: Ohne Euch wäre meine Arbeit - wäre unsere ganze Forschung - gar nicht möglich. "Wenn doktorieren, dann aber im IKF!", so sprach ich im Jahre 2002. Und während all der Zeit bin ich immer mehr davon überzeugt, dass ich mich nicht geirrt habe! Vielen Dank für eine wunderschöne Zeit, sowohl in unserer alten IKF-Herberge, als auch hier am Riedberg!

Danke an Lutz, Nadine, Maciek, Rui und Nikos, weiterhin an André (Viele liebe Grüsse nach Ottawa!), Katharina, Tilo, das SK**IKF**-Racing Team, Odi, Martin, Robert W., Totti - the Godfather of Smartness, Till[2] - The Godfather of Coolness, Birte, Stefan, Lothar, Klaus[3], Daniel, Ottmar... na ja, alle eben!

Zwei von Euch muß ich auf die Seite nehmen: Jasmin und Ralf! Ich würde Euch gerne in einem Wort sagen, dass Ihr mir schwer ans Herz gewachsen seid. Kann ich aber nicht! Ich würde es gerne in vielen Worten tun... dafür reicht der Platz nicht! Was soll ich also sagen, ausser, dass es so ist! Wenn eine(r) von uns Dreien richtig Karriere macht[4], dann wird es sehr sehr teuer, die Rechte an den vielen Bildern unter **Voll**last zu erwerben!

Mike Grams: Thanks for a great time we had in Göttingen, especially during the incredible moments in which you discovered the solid Argon stuff! Moreover, after we packed up work we explored something also very important: The Göttingen night life! Thanks for so much fun!

Ebenso danke ich den guten Seelen des Hauses, Frau Frey, Frau Lang und Frau Kömpel, sowie Herrn Köpf und Herrn Eschenbrenner. Bei vielen kleinen oder großen nicht-physikalischen Problemen bekommen wir stets Hilfe. Vielen Dank!

Auf die immerwährende Unterstützung einer Familie kann sicherlich ein jedermann bauen. Gerade in Ausnahmesituationen ist es vielleicht nur ein Anruf, oder einige liebe Worte, die weiterhelfen. Vielen Dank Euch allen! Nicht ich alleine werde Doktor, sondern WIR holen den Titel!

Den Streß und die geistige Abwesenheit bekommen ebenso die guten Freunde zu spüren - gerade die Guten! Sollte es so sein - ach Quatsch... es war so! -, dass ich manches Mal mit Tunnelblick und Desinteresse, mit gereizten Äußerungen und hektischem Geplappere auf mich aufmerksam gemacht habe: Es war mir bewußt, und gerade deswegen tut es weh, nicht derjenige sein zu können, den ihr kennt! Auch ihr habt Euren Beitrag zum Gelingen dieser Arbeit geleistet, wahrscheinlich mehr, als es Euch bewußt war!

Finally I would like to thank all the people who contributed to facilitate the writing of this work. The knowledge that results out of their investigations gives their work importance. This underlines that research has the unrestricted entitlement to be done, because the impact of scientific research can't be estimated.

---

[2] Is klar: Ohne Till, kein Manuel auf Strahlzeit! War super, Danke! Habe gerne für Euch gekocht!

[3] Fange nie an, das Verhältnis zwischen Computerabstürzen und virtuellen 747-Abstürzen zu bestimmen... Führt zu Nichts! Und Microsoft ist auch nicht Schuld, eher das pixellige Wetter! Wir sehen uns über den Wolken!

[4] Nein Ralf! ... Fan der schwedischen Frauen- Volleyball-Nationalmannschaft ist kein Beruf!

Curriculum vitae

Name	Manuel Käsz
Home adress	Oskar Müller Str. 7 65510 Idstein 2
Date of birth	March 29th, 1976 in Wiesbaden / Germany
Family status	unmarried
1982-1988	School education (Elementary school, basic education)
1988-1995	Pestalozzischule Idstein (Comprehensive secondary school) Graduation: general qualification for university entrance
1995-1996	Community service: Feldbergschule Idstein (school for mentally handicaped children)
1996-2002	Study of physics at the JWG University of Frankfurt/Main - Emphasis: Digital signal processing, speech signal processing - 03/2000 - 09/2000 Investigation residence at the technical University of Budapest (BME), Hungary - Diploma thesis: Investigation of concatenative speechsynthesis with non-uniform units
08/2002	Diploma graduation
09/2002 - 02/2006	Scientific employee at the JWG University Frankfurt/Main, department of physics
09/2002 - 03/2006	Ph.D. thesis JWG University of Frankfurt, Institute of Nuclear Physics (IKF)
foreign language	english hungarian (developable)

Research period

03/2000	-09/2000	(6 month)	Technical University of Budapest, (Hungary)
09/2002	-12/2002	(7 weeks)	MPI für Strömungsforschung, Göttingen
01/2003	-03/2003	(3 weeks)	MPI für Strömungsforschung, Göttingen
10/2003	-11/2003	(6 weeks)	MPI für Strömungsforschung, Göttingen
11/2003		(1 week)	Bessy, Berlin
11/2003		(1 week)	Universita degli Studi di Milano - Bicocca, (Italy)
01/2004	-02/2004	(3 weeks)	MPI für Strömungsforschung, Göttingen
02/2004	-03/2004	(3 weeks)	Universita degli Studi di Milano - Bicocca, (Italy)
04/2004		(2 weeks)	MPI für Strömungsforschung, Göttingen
04/2004		(1 week)	Universita degli Studi di Milano - Bicocca, (Italy)
06/2004	-08/2004	(6 weeks)	MPI für Strömungsforschung, Göttingen
10/2004		(1 week)	MPI für Strömungsforschung, Göttingen
05/2005		(1 week)	MPI für Strömungsforschung, Göttingen
09/2005		(1 week)	Universita degli Studi di Milano - Bicocca, (Italy)
01/2006		(1 week)	MPI für Strömungsforschung, Göttingen

Fellowships

11/2003	-04/2004	(6 month)	Marie Curie Fellowships, N.5 Fellowships for Doctoral Students Material and Plasma Science, No. HPMT-CT-2001-00242, INFM Unit-Milano Bicocca, Dept. of Material Science.